Developing Target Identification Platforms Using Profiled Kinase Inhibitors

by

Eric Joseph Lachacz

A dissertation submitted in partial fulfillment
of the requirements for the degree of
Doctor of Philosophy
(Medicinal Chemistry)
in the University of Michigan
2017

Doctoral Committee:

Assistant Professor Matthew B. Soellner, Chair
Assistant Professor Amanda L. Garner
Professor Elizabeth R. Lawlor
Professor Henry I. Mosberg
Professor Nouri Neamati

Eric Joseph Lachacz

elachacz@umich.edu

ORCID iD: 0000-0003-1081-6962

DEDICATION

To my family

ACKNOWLEDGEMENTS

As I reflect on the path of my degree I realize that I would not have made it this far without the support of many key individuals. The list of people and organizations who have contributed to my education is long. At the top of that list is Prof. Matthew Soellner, who has supported me during the last five years. As my mentor, Matt took an intense and aggressive path to my education. Matt may have been a "different" kind of mentor, with a "pressure makes diamonds" approach, but I really cannot imagine my time at Michigan without his guidance. On second thought... I can. And it's a reality where I have more free time, less sleepless nights, no vacation day calendar, but also significantly less scientific capability. They say that unlike your family you can pick your mentor, but all joking aside I would still pick Matt every time and have never thought otherwise. While I may have driven him crazy (really), Matt has consistently led by example and has set the standard of how I want to think scientifically. While I still have a way to go, he has given me the tools to one day get there and I cannot thank him enough.

I would like to thank Profs. Hank Mosberg, Amanda Garner, Nouri Neamati, and Elizabeth Lawlor for serving on my committee. Their input during the various committee meetings has been useful as I have progressed through my projects. I would also like to thank the Medicinal Chemistry department at large. The faculty members have been readily available for any questions I had about classes or topics outside my own projects. I am indebted to Dr. Hassan Al-Ali (University of Miami) who performed work critical to this thesis.

I need to thank all the members of Soellner lab that I have overlapped with during my time at Michigan: Christel Fox, Michael Steffey, Dr. Kris Brandvold, Dr. Shana Santos, Dr. Meghan Breen, Dr. Sameer Phadke, Dr. Frank Kwarcinski, Dr. Kristin Ko, Dr. Taylor Johnson, Dr. Michael Agius, and Omar Beleh. Specifically, I must mention Mike Steffey who prepared me for taking over all of the cell work in our lab. I also need

to mention Mike Agius with whom I “grew up” in the lab with, and who was always ready to share his knowledge of kinase structure nuances. Discussions with Sameer about various aspects of my projects (and life) were also meaningful, with his best advice often occurring at the Jug. Sameer’s value as an audience member to Matt’s antics towards me also needs mention. As a group I have to mention Mike, Taylor, and Sameer who really have been supportive in the late stages of my education. These three have made the toughest times in the lab not just bearable but fun.

I need to also mention Prof. Sofia Merajver and her group. Sofia has provided some excellent insight into some of my projects with her expertise. The members of her group have also contributed to this work. I need to specifically mention Dr. Rabia Gilani who has always been available for any question about breast cancer I would have, as well as teaching me some of the cellular biology techniques that I have implemented in this work. Dr. Zhi-Fen Wu, Dr. Li Wei Bao, and Dr. Xu Cheng have also contributed to this thesis, especially during its writing which took place while we moved our lab. Some of the experiments herein would not have been completed in time without their help.

I also need to mention Prof. Torsten Nielsen at the University of British Colombia. During a sabbatical, Torsten took me in to pursue some leads in one of my projects. Torsten made some substantial suggestions to my sarcoma work which were invaluable as he is one of the leading experts of synovial sarcoma. While I could not include some of the interesting findings from my sabbatical in this work, the wider scope of knowledge I gained from my time in Vancouver helped to shape this thesis.

I would never have found an interest in research if it was not for my education from the Chemistry Department at Saint John Fisher College. Specifically, I need to thank Dr. Daniel Piccolo. Dr. Piccolo, as my research advisor, really taught me the value of hard work in the budding years in my career. I credit his (very) old-school, blue collar approach to mentorship as to what gave me the tools to take constructive criticism and use it to my advantage. I would not have been equipped for my time at Michigan otherwise.

I would also like to acknowledge the organizations that have provided financial support during my graduate studies. The work here has been funded by the University of Michigan College of Pharmacy, and the Rackham Graduate Student Research Grant. I am

also grateful for the support provided by the Fred W. Lyons Fellowship, the Edward S. Blake Fellowship, the Lilly Endowment Fellowship, American Foundation of Pharmaceutical Education Pre-Doctoral Fellowship, and the University of Michigan Chemistry Biology Training Program, the latter of which provided additional professional training in my education including my sabbatical to Vancouver.

On a more personal level I would like to thank all of my friends I made here at the department, which are actually too many to list. From tailgating, to holiday parties, to just hanging out, it has been a blast. I need to thank my family: Mom, Dad, Stephanie, Ryan, Nana, Dziadzi, Grandma, and Papa. Without their love and support I would not be where I am today. I consider myself incredibly lucky to have them as my foundation. Lastly, I need to thank my fiancée Kellisa Hansen. How she puts up with me I really do not know. Her patience with me as we progressed through graduate school has been amazing, especially at times when my mind was sometimes elsewhere worrying about experiments that in the end pale in comparison to what really matters. Our time apart has really put into perspective what is important in life. With true friends and family, what else do you need?

TABLE OF CONTENTS

LIST OF TABLES

LIST OF FIGURES

LIST OF SCHEMES

LIST OF APPENDICES

ABSTRACT

Kinases are important enzymes in cellular signaling with their expression and activity tightly regulated. Dysregulated kinase activity can lead to numerous disease states such as cancer. Inhibiting aberrant kinase activity can slow cancer cell growth or cause cancer cell death. Thus, kinase inhibitors are well-validated drugs for cancer treatment. To date, nearly all kinase inhibitors approved for cancer treatment have been discovered using hypothesis driven target-based approaches. This is in sharp contrast to other cancer drug classes which have recently seen an increase in approvals and new chemical entities whose leads were discovered through phenotypic-based approaches. Phenotypic screening enables the discovery of novel mechanisms of action. Furthermore, cancer drug discovery is steadily moving toward strategically combining target- and phenotypic-based approaches with success in multiple drug classes. Kinase inhibitor cancer drugs lag behind other drug classes in this regard due, in part, to the use of poor phenotypic models. Cancer cell lines, the most common model, do not recapitulate cells found in tumors, and kinase signaling pathways are very sensitive to the context of cellular environment. For kinase inhibitor drugs to benefit from integrating target- and phenotypic-based approaches, creative strategies combining kinase target data with clinically relevant models will be needed. Versatile small molecule probes will be needed to investigate kinase targets identified from such approaches.

Herein, I describe a library of profiled kinase inhibitors with diverse chemistries and biochemical activities for use in phenotypic assays. I use a machine learning-based algorithm to relate the compound inhibition profiles across 237 kinases to their cell-based activities. This approach enables the identification of important kinases in multiple cell lines of sarcoma, a class of rare and understudied cancers. In these screens I identified Protein Kinase D (PRKD) as a putative novel target in synovial sarcoma. A synergy

screen of a synovial sarcoma cell line in the presence of a PRKD inhibitor vastly changed the targets identified. These new targets, such as Cyclin Dependent Kinase (CDK) and AKT, displayed synergism when inhibited along with PRKD. I then apply this framework in advanced models of triple negative breast cancer (TNBC). Here, I use ten TNBC patient-derived xenografts (PDXs) to create short-term *ex vivo* 3D cell cultures from harvested tumors that are amenable for high-throughput screening. The profiled kinase inhibitor screen of these cultures identified multiple kinases broadly important in TNBC. Two identified kinase groups, FES/FER and MARK/SIK, have early emergent genomic evidence as potential targets in TNBC. My pharmacologically-based findings suggest these kinases as actionable targets. Also, I cluster these PDXs using the kinase target scores obtained. Lastly, I describe the development of an irreversible small molecule fluorescent probe for use in localization studies. This probe was found to exhibit a signal in fluorescent microscopy specific to c-SRC, a kinase shown to be a TNBC target in previous studies and in the above PDX screens. I found that this probe displayed turn-on fluorescence, could be used in live-cell microscopy, did not require washing, and was compatible with live-cell super-resolution stimulated emission depletion (STED) microscopy. I then use this probe to interrogate c-SRC localization in multiple TNBC cell lines and track localization changes in response to drug treatment. This work highlights that understanding kinase chemical biology on both molecular and global levels will be needed to continue investigating these *bona fide* cancer targets.

CHAPTER I

Small Molecule Kinase Inhibitors in Target- and Phenotypic-Based Cancer Drug Discovery

Abstract

Kinases are important enzymes in cellular signaling with their expression and activity tightly regulated. Dysregulated kinases can lead to numerous disease states such as cancer. Kinase inhibitors have emerged as a well-validated means of cancer treatment by inhibiting aberrant kinase activity, slowing cancer cell growth, or causing cancer cell death. To date, nearly all kinase inhibitors approved for cancer treatment have been discovered using target-based approaches. This chapter briefly details the limitations of target-based approaches, especially as they pertain to kinase inhibitors in cancer. I then discuss how, despite its promise, phenotypic-based drug discovery has failed to significantly predict clinical success of these drugs in cancer. I then describe how combining target- and phenotypic-based approaches has recently led to increased approval of drugs and how kinase inhibitor drug discovery can stand to benefit. Lastly, I briefly touch on how small molecule kinase inhibitor probes are used to understand the role of these targets in cancer.

Kinases in Cellular Signaling and Disease

Post-translational phosphorylation of proteins, lipids, or other cellular components, has long been established as a pillar of cellular signaling.[1, 2] These events are regulated by kinases, enzymes which catalyze the transfer of the γ-phosphate of adenosine triphosphate (ATP) to a given substrate (**Figure 1.1A**).[3] The phosphorylation status of a these substrates can then alter their function and/or activity which can propagate a signal. The fate of these signals can have a wide range of effects on the cell (**Figure 1.1B**) The most obvious examples are kinases phosphorylating other kinases, increasing or decreasing their catalytic activity which then alters the flux of a given

cellular signaling pathway.[3] This phospho-signaling network is tightly regulated by 518 protein kinases and 156 phosphatases.[1, 3, 4] Despite this, kinases can become dysregulated through activating mutations, overexpression, or absence of negative regulators. Such events can result in dysregulated cellular signaling which can lead to disease states.[5] With dysregulated cellular signaling often tied to cancer, the role of kinases has been a focus of research in these diseases.[5] Often, this research will tie a specific kinase, or group of kinases, as important in progression of a given cancer subtype.[6, 7] As such, considerable effort has been invested into developing drugs that target such kinases.

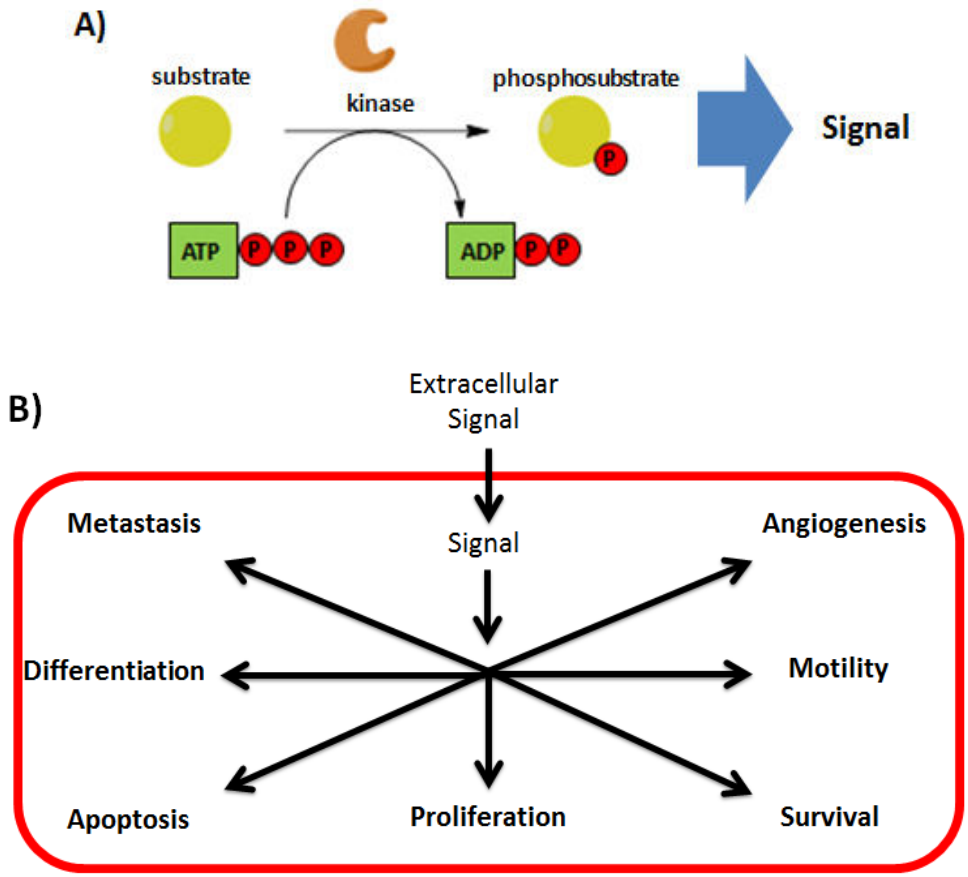

Figure 1.1: Overview of kinases in cellular signaling. **A)** Cartoon depicting a kinase phosphorylating substrate to propagate a cellular signal. **B)** End results of cellular signaling pathways propagated by kinases. Dysregulation of these pathways result in disease states such as cancer.

Kinase Inhibitors in Target-Based Cancer Drug Discovery

In many ways, kinases are an ideal target for cancer drug development. They have a well-defined ATP-binding pocket where small molecules can tightly bind, are amenable for crystal structures with bound inhibitors, and inhibition/binding assays are relatively easy to perform. For these reasons and others, most therapeutic kinase inhibitors have been developed using target-based approaches (**Figure 1.2**).[8, 9] In target-based screening, a target of a disease is known, and biochemical assays of this purified target can be performed to identify and optimize lead drug compounds. This often leads to potent drugs for the target in question. The case of imatinib (Gleevec) is only one example of successful targeted-based kinase inhibitor drug discovery.[10, 11] Imatinib was FDA-approved in 2001 for the treatment of chronic myelogenous leukemia (CML), a disease in which a chromosomal translocation results in the BCR-ABL fusion protein with the constitutively active kinase domain of c-ABL.[10, 11] Optimized to potently and selectively inhibit BCR-ABL in an ATP-competitive manner, imatinib was one of the first rationally designed small molecule molecularly targeted cancer therapies.[11] This success has led to target-based screening as the dominant strategy for developing therapeutic kinase inhibitors.[9, 12] Indeed, 26/27 approved kinase inhibitors are the result of target-based cancer drug development.[8]

Despite this success, developing kinase inhibitor cancer drugs with target-based screening is not without challenges and limitations. First, the biochemical assays of a target may not accurately model the target's behavior in the cell, where the presence of cofactors or post-translational modifications can affect inhibitor binding.[13, 14] Also, many of these biochemical assays only use a single domain of multi-domain complexes due to the difficulty in purification of many full length proteins.[13] In the case of kinase biochemical assays, usually only the kinase domain is used despite many kinases possessing autoregulatory domains.[13, 15] To account for these limitations, cell-based assays have been used. A recent review details the available cell-based assays for kinase drug discovery.[14]

Cases where a single kinase drives a cancer in which an inhibitor of said kinase results in effective treatment (i.e. imatinib treatment of CML) are few and far between.[9, 12] Instead, target kinases in cancer are often nodes of complex signaling networks in

which their inhibition can be compensated through crosstalk signaling, feedback, or redundancy.[9, 16] As such, highly selective kinase inhibitors often have less of an effect than predicted in a given disease.[17] In fact, it may be more beneficial to use multi-targeted kinase inhibitor therapies for cancer treatment to overcome these obstacles.[17] Additionally, the efficacy of some approved kinase inhibitors developed with target-based approaches was found to be due to cryptic off-targets. For example, sorafenib (Nexavar) was developed as a RAF inhibitor but was found to be most efficacious in some cancers by inhibiting VEGFR2, independent of RAF mutation status.[3, 18] Elucidating the kinase, or collection of kinases, important in the efficacy of an inhibitor is a blind spot of target-based approaches which rely entirely on the strength of the disease-target hypothesis.

Figure 1.2: Timeline of FDA approval small molecule kinase inhibitor drugs for cancer treatment. In green are inhibitors discovered using primarily target-based approaches. In red are inhibitors discovered using phenotypic-based approaches.

In practice, target-based drug discovery is rationally informed by phenotypic assays as a means to form hypotheses. This requires appropriate selection of phenotypic models used to establish rationale for pursuit of a given target(s). A recent review identified that lack of a clear link between pursued nominal targets and mechanism-based phenotypic models was a common trait amongst failed drugs stemming from target-based drug discovery.[9] Despite target-based discovery being a hypothesis-driven and logical approach it may be oversimplified in many cases. This is especially true with drugs of kinases, due to their compensatory signaling pathways.

Phenotypic Screens in Cancer Drug Discovery

In light of the above there has been growing interest in phenotypic screening, where leads and/or targets are initially identified on the basis of a desired functional effect without regard for mechanism of action.[9, 17] Also, phenotypic screens with target-agnostic approaches can benefit from the potential of novel target discoveries that might not be found otherwise. In 2011, Swinney and Anthony found that phenotypic screening resulted in higher rates in the approval of new chemical entities compared to the more prevalent target-based screening approaches.[19]

The MEK inhibitor trametinib (Mekinist) emerged as the first approved kinase inhibitor for cancer discovered in a *de novo* phenotypic screen.[20] However, phenotypic screening has not impacted the number of approved kinase inhibitor cancer drugs, in contrast to other cancer drug classes. Indeed, trametinib is the only example. Excluding kinase inhibitors, from 1999-2013 there were more approved cancer drugs originating from phenotypic-based approaches than target-based approaches (**Figure 1.3**).[9] However, considering all cancer drug classes, targeted-based drug discovery was still by far the dominant origin of new chemical entities in phase II/III clinical cancer trials in 2013 (**Figure 1.3**).[9] This highlights that despite the success of phenotypic screening, there is still a large focus in target-based screening in cancer drug discovery.

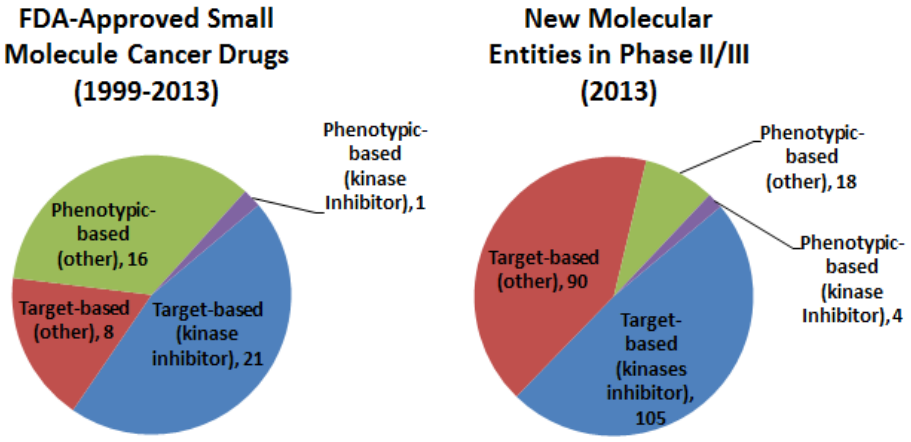

Figure 1.3: Clinical cancer drugs categorized by the approach in their lead discovery. **Left)** FDA-approved small molecule cancer drugs (from 1999-2013). **Right)** New chemical entities in phase II/III clinical trials (in 2013) as categorized in a cancer drug analysis by Moffat et al.[9] Numbers indicate the number of drugs in a given category.

Phenotypic-based drug discovery, despite its promise, has some serious limitations in cancer. Phenotypic screens in cancer often utilize cancer cell lines as the systems in which these studies are performed.[9] This is mostly due to the fact that cancer cell lines are easy to handle and readily amenable for high-throughput screening. However, cancer cell lines in culture are themselves limited in their ability to model cells found in tumors.[9] Cancer cell lines have shown to be poor predictors of clinical efficacy based on results in both *in vitro* as well as *in vivo* preclinical studies.[9, 21, 22] These concerns have likely delayed the wide scale adoption of phenotypic screening in the field of cancer drug discovery. Despite these obstacles, incremental improvements in the modeling of the tumor microenvironment have been made.[21, 23, 24] Improvements such as 3D culture and patient-derived xenografts, are described and utilized in my work described in **Chapter III**.

Another obstacle inherent to phenotypic screening is the identification of the target or combination of targets through which a lead compound exerts its effect. Failing to identify the targets of a lead compound makes it extremely difficult to chemically optimize that lead. The difficulty of this identification has thus limited the potential of phenotypic screening in cancer, as well as in other disease types.[12] Much effort has been spent in developing methodologies to identify the targets of hits from phenotypic approaches.

One strategy is to directly detect the target(s) through the use of affinity purification.[12] In one example, the identified lead is immobilized via a covalent linker attached to a solid scaffold material which is then exposed to whole-cell lysate.[25] The target(s) then bind the lead drug, is eluted, and then identified through mass spectrometry and/or sequencing. This approach was used in the discovery of the target of trametinib, MEK, and was done so in a purely target agnostic manner.[20] One problem with this strategy is that it can be difficult to detect low abundance targets and targets with weak binding affinity for the lead.[26] A systems-based interference approach can also be used. In these cases, treatment of a phenotypic model, i.e. a cancer cell line, will bring about changes such as alterations in cellular signaling pathways through changes in protein levels or post-translational modifications.[27, 28] These changes, which can be detected at the proteome level using mass spectrometry or at the gene level using RNA sequencing,

can provide clues to a lead compound's mechanism of action. In the case of RNA sequencing, care must be taken in interpreting the results as mRNA expression is not always a function of protein level and activity.[29] This is especially true of kinases, whose activity can widely change depending on multiple phosphorylation states. Alternative strategies in identifying targets in phenotypic screening will help to push forward the potential of this screening approach. In **Chapter II**, I describe the use of a recently described machine learning methodology to identify targets of lead compounds in phenotypic screening, and use this strategy in cancer.[17]

Selecting Readouts for Phenotypic Screening in Cancer

Selection of the phenotypic model used in phenotypic screening is *the* most important part in the experimental design of these campaigns. An inappropriate model and readout can doom a screening study before it even begins. As described above, cancer cell lines, despite their disadvantages, have been the model of choice for drug screening in cancer. In most screens with cancer cell lines, the most common phenotypic output is cell viability or cell cytotoxicity.[9] The widespread use of these readouts is due to the ease in performing their respective assays. While these outputs have resulted in successful discovery of several cancer drugs, they likely cause a bias toward highly druggable mechanisms of action, i.e. DNA modulators or microtubule-targeting drugs.[9] Thus, many mechanisms of action are constantly being rediscovered using phenotypic screening despite its inherent ability to discover novel mechanisms of action. Furthermore, there are many cancer specific activities that can be altered via drugs beyond simple cancer cell viability, such as metastasis or invasion.

To break from this pattern, alternative phenotypic readouts can be used. In the example of invasion, high throughput three-dimensional invasion assays have been leveraged to identify potential drugs that modulate this activity.[30-32] In terms of cancer cell motility, simple scratch-wound healing assays can be used in a high throughput manner as well.[30, 32] These readouts, which are widely used, add new dimensions to phenotypic screening efforts by identifying leads that would not be discovered strictly using cell viability.

Ideally, the phenotypic readout of a phenotypic screen should be mechanistically tied to the disease state in question.[9] For example, if a specific signaling pathway is known to be tightly correlated to the progression of a cancer subtype, a phenotypic readout which measures the flux of that pathway is extremely valuable in identifying the most promising leads.[9] The same can be said for phenotypic readouts which evaluate gene expression or protein phosphorylation that are integral to the progression of a given cancer.[9] For example, trametinib was discovered through phenotypic screening using expression of CDK4/6 inhibitor $p15^{INK4b}$, a negative regulator in cancer cell cycle progression, as the readout.[33] In another example of screening mechanistically relevant cancer phenotypes, one group used an assay that measures the disruption of a fusion oncoprotein complex responsible for synovial sarcoma tumorigenesis for phenotypic screening.[34] Examples of drugs discovered using these mechanistically informed and relevant phenotypic outputs can be found in a recent review.[9]

Combining Target and Phenotypic-based Screening

Moffat et al. recently reviewed the roles of target-based and phenotypic-based cancer drug discovery in newly approved drugs, including kinase inhibitors.[9] One major conclusion drawn from the authors was that despite early success, the approval rates of new molecular entity cancer drugs from pure target-based approaches have decreased. This was also found in an earlier review by Swinney and Anthony for drugs as a whole.[19] Also, despite the promise of phenotypic-based strategies only a handful of drugs have been discovered using them in the purest sense in target-agnostic studies.[9] Although pure-phenotypic screening can directly identify the most efficacious compounds, figuring out how these compounds exert their effects is a challenge. Instead, Moffat et al. found that recently approved cancer drugs have been discovered using a combination of the two approaches in ways that complement each other.[9] They concluded that the future of cancer drug discovery will continue to move, and should, toward "mechanistically-informed phenotypic drug discovery."[9] In other words, screens of compounds with known mechanisms of action are assessed and optimized using clinically relevant phenotypic models. These mechanisms of action can then be directly tied to the observed phenotype. As described above, the phenotypic output should ideally be mechanistically

tied to the disease state in question. Comparison of the two approaches can show how strategic combination can have a synergistic effect on cancer drug discovery (**Figure 1.4**).

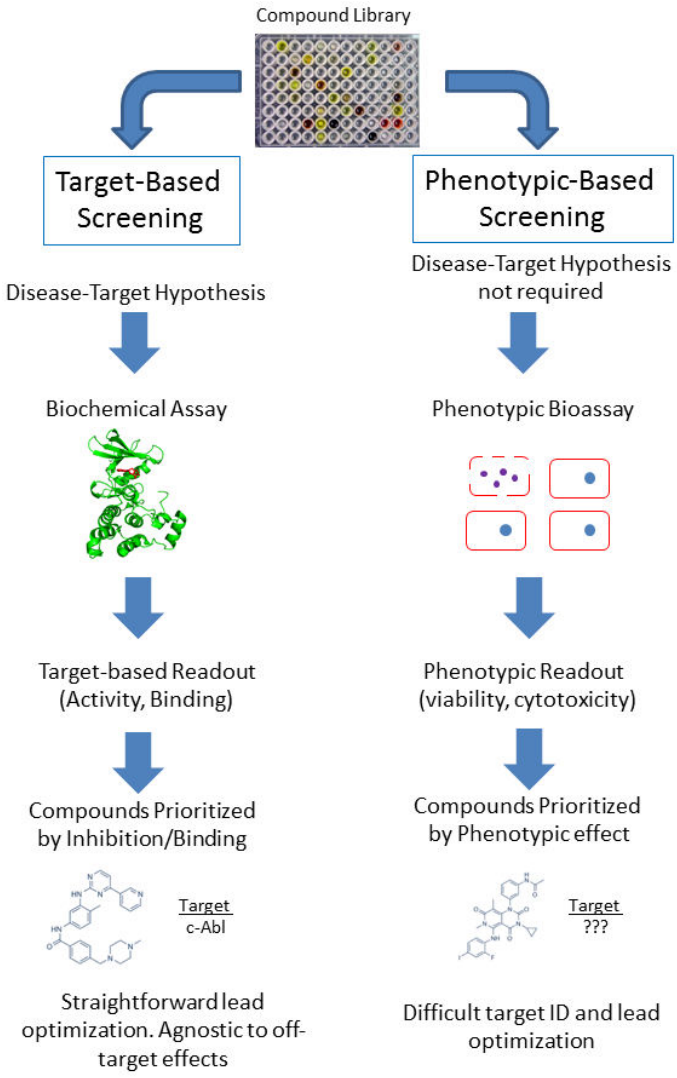

Figure 1.4: Overview of target-based and phenotypic-based approaches in drug discovery screening.

Despite continuing trends of combined target- and phenotypic-based approaches in cancer drug discovery, recently approved kinase inhibitors have still been the result of strictly target-based lead discovery (**Figure 1.2**).[8] This may be limiting the discovery of approved kinase inhibitors with novel mechanisms of action. Encouragingly, a number of kinase inhibitors using phenotypic or partial-phenotypic approaches have made it to late

clinical trials (**Figure 1.3**).[9] With multiple kinase profiling services available and the plethora of kinase inhibition data in the literature, kinase inhibitors are primed for this integrative approach. Strategically combining kinase inhibitor target data with clinically relevant phenotypes could be a boon for the field. Recently, Al-Ali et al. used such an approach to identify new kinase targets and lead compounds that promote neuron growth in a proof-of-concept study.[17] It is easy to envision how kinase inhibitors may benefit using such an approach in cancer. I describe an approach inspired by this study in **Chapter II**.

Investigating Kinase Targets using Small Molecule Kinase Inhibitors as Chemical Probes

Small molecule inhibitors are almost invariably used to assess the potential of kinase cancer targets identified with the above described approaches.[3, 15] Aside from demonstrating how actionable a given kinase is as a therapeutic target, small molecule kinase inhibitors are widely used in basic chemical biology studies in drug discovery. Small molecules as kinase probes are important as they can inhibit the catalytic domain of multi-domain kinases without interfering with the other domains, as would be the case with genetic techniques such as RNAi.[1] Based on the type of studies undertaken in drug discovery projects, the needs for the type of kinase inhibitors may vary. These needs can range from inhibitors that are selective or promiscuous, to inhibitors that bind a certain combination of kinases, or inhibit a particular kinase family.[35, 36]

With respect to using inhibitors selective for a given kinase, or group of kinases, there are significant challenges. Many kinase inhibitors bind competitively in the ATP-binding site, which is highly conserved across the kinome (**Figure 1.5A**).[3, 37] This high conservation makes the use of small molecules to inhibit target kinases, and only target kinases, difficult. These ATP-competitive kinase inhibitors often bind to the conserved hinge region, which connects the N-terminal and C-terminal kinase lobes, forming tight hydrogen bonds with the inhibitor.[37] Through these hydrogen bonds and utilizing van der Waals interactions within the pocket, many ATP-competitive inhibitors can bind potently.[37] However, as our understanding of kinase chemical biology has increased so too has our ability to develop inhibitors with desired selectivities. Selective inhibitors of

kinases will often take advantage of variable features within the kinase domain (**Figure 1.5B**). These features include the position of the activation loop, αC-helix, and phosphate-binding loop (P-loop), which can allow for differing inhibitor binding modes (i.e. binding of active or inactive kinase conformations).[35, 37-39] Other strategies can range from inhibitors that are allosteric, bivalent, bind the substrate site, and bind covalently through non-conserved cysteines. [20, 40-42]

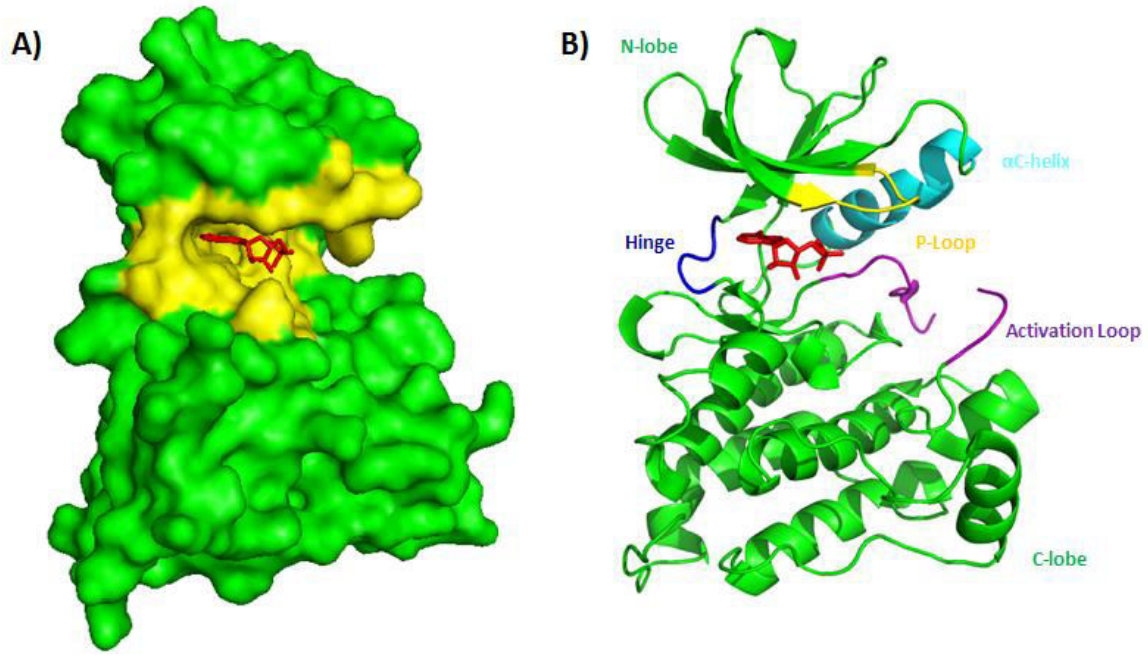

Figure 1.5: A representative kinase domain bound to ATP-γ-S (red). **A)** A surface depiction highlighting the highly conserved ATP-binding pocket in yellow. **B)** A cartoon depiction of key features the representative kinase domain. The hinge region (blue), activation loop (purple), P-loop (yellow), and αC-helix (cyan) are highlighted as structural features used confer kinase selectivity on small molecule inhibitors. (PDB: 3DQX) [43]

Understanding these nuances of small molecule kinase inhibitor probes go beyond use of simply perturbing target kinase catalytic function.[44] These strategies can be applied for other types of probes that aid in understanding kinase chemical biology in a given context. For example, synthesis of a selective kinase probe with an attached azide can be used in click chemistry experiments for capture and identification of kinase substrates in the cell.[45] Another example is the design of small molecule fluorescent probes for live-cell cellular localization studies of a particular kinase.[46] In latter case,

achieving selectivity is extremely important so that any fluorescent signal can be attributed to the kinase in question. Strategic and/or alternative strategies are needed to achieve the selectivity required and to enhance the scope of fluorescent kinase probes in microscopy. In **Chapter IV**, I describe such alternative strategies for designing new irreversible fluorescent kinase probes and their use. Expanding the scope of kinase probes, both fluorescent and otherwise, will continue to further our understanding of these *bona fide* cancer targets.

Conclusions

The kinase inhibitor class of cancer drugs has overwhelmingly been the result of target-based drug discovery. While this has given medicine a myriad of cancer drugs this has likely limited the discovery kinase inhibitors with novel mechanisms of action. Indeed, only one kinase inhibitor has been approved whose lead was discovered in a phenotypic screen. This is in sharp contrast to other cancer drug classes in which the number of approvals resulting from phenotypic and phenotypic/target hybrid approaches have increased in recent years. Strategic ways to combine kinase target data with clinically relevant cancer phenotype models and readouts would aid in identifying novel targets and lead compounds. Phenotypes that are directly related to the progression of a specific cancer subtype, if appropriately modeled, will enable phenotypic screening to identify more clinically relevant targets. These novel targets that would be identified will then need to be further explored using small molecule kinase inhibitors as chemical probes. Expanding the scope of such probes by demonstrating new methods of achieving desired selectivity will always be beneficial to basic science research of kinases in general. A clear understanding of individual kinase chemical biology as well as the kinome at large will be valuable in continuing kinase inhibitors as an important class of cancer therapeutics.

References

1. Manning, G.; Whyte, D. B.; Martinez, R.; Hunter, T.; Sudarsanam, S., The protein kinase complement of the human genome. *Science* **2002,** *298* (5600), 1912-34.
2. Marshall, C. J., Specificity of receptor tyrosine kinase signaling: transient versus sustained extracellular signal-regulated kinase activation. *Cell* **1995,** *80* (2), 179-85.
3. Zhang, J.; Yang, P. L.; Gray, N. S., Targeting cancer with small molecule kinase inhibitors. *Nature Reviews Cancer* **2009,** *9* (1), 28-39.
4. Kholodenko, B. N., Cell signaling dynamics in time and space. *Nat Rev Mol Cell Biol* **2006,** *7* (3), 165-76.
5. Giancotti, F. G., Deregulation of cell signaling in cancer. *FEBS Lett* **2014,** *588* (16), 2558-70.
6. Salesse, S.; Verfaillie, C. M., BCR/ABL: from molecular mechanisms of leukemia induction to treatment of chronic myelogenous leukemia. *Oncogene* **2002,** *21* (56), 8547-8559.
7. Siehl, J.; Thiel, E., C-kit, GIST, and imatinib. *Recent Results Cancer Res* **2007,** *176*, 145-51.
8. Wu, P.; Nielsen, T. E.; Clausen, M. H., Small-molecule kinase inhibitors: an analysis of FDA-approved drugs. *Drug Discov Today* **2016,** *21* (1), 5-10.
9. Moffat, J. G.; Rudolph, J.; Bailey, D., Phenotypic screening in cancer drug discovery [mdash] past, present and future. *Nature Reviews Drug Discovery* **2014,** *13*, 588-602.
10. Druker, B. J.; Sawyers, C. L.; Kantarjian, H.; Resta, D. J.; Reese, S. F.; Ford, J. M.; Capdeville, R.; Talpaz, M., Activity of a specific inhibitor of the BCR-ABL tyrosine kinase in the blast crisis of chronic myeloid leukemia and acute lymphoblastic leukemia with the Philadelphia chromosome. *N Engl J Med* **2001,** *344* (14), 1038-42.
11. Capdeville, R.; Buchdunger, E.; Zimmermann, J.; Matter, A., Glivec (STI571, imatinib), a rationally developed, targeted anticancer drug. *Nat Rev Drug Discov* **2002,** *1* (7), 493-502.
12. Al-Ali, H., The evolution of drug discovery: from phenotypes to targets, and back. *Med. Chem. Commun.* **2016,** *7*, 788-798.
13. Glickman, J. F., *Assay Development for Protein Kinase Enzymes*. Eli Lilly & Company and the National Center for Advancing Translational Sciences: 2012.
14. Smith, G. K.; Wood, E. R., Cell-based assays for kinase drug discovery - ScienceDirec. *Drug Discovery Today: Technologies* **2017,** *7* (1), e13-e19.
15. Davis, M. I.; Hunt, J. P.; Herrgard, S.; Ciceri, P.; Wodicka, L. M.; Pallares, G.; Hocker, M.; Treiber, D. K.; Zarrinkar, P. P., Comprehensive analysis of kinase inhibitor selectivity. *Nat Biotechnol* **2011,** *29* (11), 1046-51.
16. Williams, R., Discontinued drugs in 2012: oncology drugs. *Expert Opin Investig Drugs* **2013,** *22* (12), 1627-44.
17. Al-Ali, H.; Lee, D. H.; Danzi, M. C.; Nassif, H.; Gautam, P.; Wennerberg, K.; Zuercher, B.; Drewry, D. H.; Lee, J. K.; Lemmon, V. P.; Bixby, J. L., Rational Polypharmacology: Systematically Identifying and Engaging Multiple Drug Targets To Promote Axon Growth. *ACS Chem Biol* **2015,** *10* (8), 1939-51.
18. Mangana, J.; Levesque, M. P.; Karpova, M. B.; Dummer, R., Sorafenib in melanoma. *Expert Opin Investig Drugs* **2012,** *21* (4), 557-68.

19. Swinney, D. C.; Anthony, J., How were new medicines discovered? *Nat Rev Drug Discov* **2011,** *10* (7), 507-19.
20. Yoshida, T.; Kakegawa, J.; Yamaguchi, T.; Hantani, Y.; Okajima, N.; Sakai, T.; Watanabe, Y.; Nakamura, M., Identification and characterization of a novel chemotype MEK inhibitor able to alter the phosphorylation state of MEK1/2. *Oncotarget* **2012,** *3* (12), 1533-45.
21. Bruna, A.; Rueda, O.; Greenwood, W.; Batra, A.; Callari, M.; Batra, R.; Pogrebniak, K.; Sandoval, J.; Cassidy, J.; Tufegdzic-Vidakovic, A.; Sammut, S. J.; Jones, L.; Provenzano, E.; Baird, R.; Eirew, P.; Hadfield, J.; Eldridge, M.; McLaren-Douglas, A.; Barthorpe, A.; Lightfoot, H.; O'Connor, M.; Gray, J.; Cortes, J.; Baselga, J.; Marangoni, E.; Welm, A.; Aparicio, S.; Serra, V.; Garnett, M.; Caldas, C., A Biobank of Breast Cancer Explants with Preserved Intra-tumor Heterogeneity to Screen Anticancer Compounds. *Cell* **2016,** *167* (1), 260-274 e22.
22. Gillet, J. P.; Varma, S.; Gottesman, M. M., The Clinical Relevance of Cancer Cell Lines. *J Natl Cancer Inst* **2013,** *105* (7), 452-8.
23. Edmondson, R.; Broglie, J. J.; Adcock, A. F.; Yang, L., Three-dimensional cell culture systems and their applications in drug discovery and cell-based biosensors. *Assay Drug Dev Technol* **2014,** *12* (4), 207-18.
24. Gao, H.; Korn, J. M.; Ferretti, S.; Monahan, J. E.; Wang, Y.; Singh, M.; Zhang, C.; Schnell, C.; Yang, G.; Zhang, Y.; Balbin, O. A.; Barbe, S.; Cai, H.; Casey, F.; Chatterjee, S.; Chiang, D. Y.; Chuai, S.; Cogan, S. M.; Collins, S. D.; Dammassa, E.; Ebel, N.; Embry, M.; Green, J.; Kauffmann, A.; Kowal, C.; Leary, R. J.; Lehar, J.; Liang, Y.; Loo, A.; Lorenzana, E.; Robert McDonald, E., 3rd; McLaughlin, M. E.; Merkin, J.; Meyer, R.; Naylor, T. L.; Patawaran, M.; Reddy, A.; Roelli, C.; Ruddy, D. A.; Salangsang, F.; Santacroce, F.; Singh, A. P.; Tang, Y.; Tinetto, W.; Tobler, S.; Velazquez, R.; Venkatesan, K.; Von Arx, F.; Wang, H. Q.; Wang, Z.; Wiesmann, M.; Wyss, D.; Xu, F.; Bitter, H.; Atadja, P.; Lees, E.; Hofmann, F.; Li, E.; Keen, N.; Cozens, R.; Jensen, M. R.; Pryer, N. K.; Williams, J. A.; Sellers, W. R., High-throughput screening using patient-derived tumor xenografts to predict clinical trial drug response. *Nat Med* **2015,** *21* (11), 1318-25.
25. Guiffant, D.; Tribouillard, D.; Gug, F.; Galons, H.; Meijer, L.; Blondel, M.; Bach, S., Identification of intracellular targets of small molecular weight chemical compounds using affinity chromatography. *Biotechnol J* **2007,** *2* (1), 68-75.
26. Terstappen, G. C.; Schlupen, C.; Raggiaschi, R.; Gaviraghi, G., Target deconvolution strategies in drug discovery. *Nat Rev Drug Discov* **2007,** *6* (11), 891-903.
27. Butcher, R. A.; Schreiber, S. L., Using genome-wide transcriptional profiling to elucidate small-molecule mechanism. *Curr Opin Chem Biol* **2005,** *9* (1), 25-30.
28. Rix, U.; Superti-Furga, G., Target profiling of small molecules by chemical proteomics. *Nat Chem Biol* **2009,** *5* (9), 616-24.
29. Gygi, S. P.; Rochon, Y.; Franza, B. R.; Aebersold, R., Correlation between protein and mRNA abundance in yeast. *Mol Cell Biol* **1999,** *19* (3), 1720-30.
30. Evensen, N. A.; Li, J.; Yang, J.; Yu, X.; Sampson, N. S.; Zucker, S.; Cao, J., Development of a High-Throughput Three-Dimensional Invasion Assay for Anti-Cancer Drug Discovery. *PLoS One* **2013,** *8* (12), e82811.
31. Lovitt, C. J.; Shelper, T. B.; Avery, V. M., Advanced Cell Culture Techniques for Cancer Drug Discovery. *Biology (Basel)* **2014,** *3* (2), 345-67.

32. Hulkower, K. I.; Herber, R. L., Cell Migration and Invasion Assays as Tools for Drug Discovery. *Pharmaceutics* **2011,** *3* (1), 107-24.
33. Yamaguchi, T.; Yoshida, T.; Kurachi, R.; Kakegawa, J.; Hori, Y.; Nanayama, T.; Hayakawa, K.; Abe, H.; Takagi, K.; Matsuzaki, Y.; Koyama, M.; Yogosawa, S.; Sowa, Y.; Yamori, T.; Tajima, N.; Sakai, T., Identification of JTP-70902, a p15(INK4b)-inductive compound, as a novel MEK1/2 inhibitor. *Cancer Sci* **2007,** *98* (11), 1809-16.
34. Nielsen, T. O.; Andrews, H. N.; Cheang, M.; Kucab, J. E.; Hsu, F. D.; Ragaz, J.; Gilks, C. B.; Makretsov, N.; Bajdik, C. D.; Brookes, C.; Neckers, L. M.; Evdokimova, V.; Huntsman, D. G.; Dunn, S. E., Expression of the insulin-like growth factor I receptor and urokinase plasminogen activator in breast cancer is associated with poor survival: potential for intervention with 17-allylamino geldanamycin. *Cancer Res* **2004,** *64* (1), 286-91.
35. Brandvold, K. R.; Steffey, M. E.; Fox, C. C.; Soellner, M. B., Development of a highly selective c-Src kinase inhibitor. *ACS Chem Biol* **2012,** *7* (8), 1393-8.
36. A., G. J.; Roth , B. L., Developing selectively nonselective drugs for treating CNS disorders. *Drug Discovery Today: Therapeutic Strategies* **2006,** *3* (4), 413-419.
37. Knight, Z. A.; Shokat, K. M., Features of selective kinase inhibitors. *Chem Biol* **2005,** *12* (6), 621-37.
38. Gilani, R. A.; Phadke, S.; Bao, L. W.; Lachacz, E. J.; Dziubinski, M. L.; Brandvold, K. R.; Steffey, M. E.; Kwarcinski, F. E.; Graveel, C. R.; Kidwell, K. M.; Merajver, S. D.; Soellner, M. B., UM-164: A Potent c-Src/p38 Kinase Inhibitor with In Vivo Activity against Triple-Negative Breast Cancer. *Clin Cancer Res* **2016,** *22* (20), 5087-5096.
39. Kwarcinski, F. E.; Brandvold, K. R.; Phadke, S.; Beleh, O. M.; Johnson, T. K.; Meagher, J. L.; Seeliger, M. A.; Stuckey, J. A.; Soellner, M. B., Conformation-Selective Analogues of Dasatinib Reveal Insight into Kinase Inhibitor Binding and Selectivity. *ACS Chem Biol* **2016,** *11* (5), 1296-304.
40. Kwarcinski, F. E.; Fox, C. C.; Steffey, M. E.; Soellner, M. B., Irreversible inhibitors of c-Src kinase that target a nonconserved cysteine. *ACS Chem Biol* **2012,** *7* (11), 1910-7.
41. Breen, M. E.; Steffey, M. E.; Lachacz, E. J.; Kwarcinski, F. E.; Fox, C. C.; Soellner, M. B., Substrate Activity Screening with Kinases: Discovery of Small-Molecule Substrate-Competitive c-Src Inhibitors. *Angewandte Chemie International Edition* **2017,** *53* (27), 7010-7013.
42. Johnson, T. K.; Soellner, M. B., Bivalent Inhibitors of c-Src Tyrosine Kinase That Bind a Regulatory Domain. **2016,** *27* (7), 745–1749.
43. Azam, M.; Seeliger, M. A.; Gray, N. S.; Kuriyan, J.; Daley, G. Q., Activation of tyrosine kinases by mutation of the gatekeeper threonine. *Nat Struct Mol Biol* **2008,** *15* (10), 1109-18.
44. Agius, M. P.; Soellner, M. B., Modulating noncatalytic function with kinase inhibitors. *Chem Biol* **2014,** *21* (5), 569-71.
45. Su, Y.; Pan, S.; Li, Z.; Li, L.; Wu, X.; Hao, P.; Sze, S. K.; Yao, S. Q., Multiplex Imaging and Cellular Target Identification of Kinase Inhibitors. *Scientific Reports* **2015,** *5*, Article number: 7724.

46. Vetter, M. L.; Zhang, Z.; Liu, S.; Wang, J.; Cho, H.; Zhang, J.; Zhang, W.; Gray, N. S.; Yang, P. L., Fluorescent visualization of Src by using dasatinib-BODIPY. *Chembiochem* **2014,** *15* (9), 1317-24.

CHAPTER II

Target Identification in Sarcomas using Machine Learning and a Profiled Kinase Inhibitor Library

Abstract

Protein kinases are established and attractive therapeutic targets in oncology. Sarcomas are mesenchymal cancers for which few therapeutic targets are known. Here, I screen a library of kinase inhibitors with diverse chemistries and biochemical activities in a phenotypic assay using a variety of sarcoma cell lines. I use a previously described machine learning-based algorithm to relate the compound inhibition profiles across 237 kinases to their cell-based activities. Using this method, I identified Protein Kinase D (PRKD) as a putative novel target kinase in synovial sarcoma cell lines whereby its inhibition leads to a decrease in cell proliferation. I perform a synergy screen of synovial sarcoma cells in presence of a PRKD inhibitor to identify kinases whose co-inhibition with PRKD may synergistically inhibit synovial sarcoma cell proliferation. In this second screen, I identified Cyclin Dependent Kinase (CDK) and AKT kinase as targets with increased target scoring in the machine learning algorithm. Using selective clinical inhibitors of these kinases, I confirmed that their inhibition with PRKD synergistically reduced synovial sarcoma cell proliferation as defined by Chou-Talalay. Together, this approach provides a promising framework to identify new targets of rare cancers and a novel methodology to identify new combinational strategies for treatment. This chapter is part of my overarching work in strategically combining phenotypic- and target-based screening for investigating cancer.[†‡]

[†] Curation of inhibitor profiling data, kinase grouping, and kinase scoring using a machine learning algorithm was performed by Hassan Al-Ali (University of Miami).
[‡] Western blots were obtained with the help of Zhi Fen Wu (University of Miami).

Introduction

Phenotypic screening is a promising approach for drug discovery, in part due to its ability to identify promising leads without *a priori* knowledge of drug targets.[1] Identifying targets is a challenging task, particularly in cancer, where drug sensitivities consistently show poor correlation with gene expression and genomic mutational analyses.[2] Nevertheless, target-centric approaches are important for drug development activities, including lead optimization, mechanistic investigation, and development of biomarkers for clinical studies. As discussed in **Chapter I**, strategies that combine both approaches may thus be warranted for efficient identification of both promising lead compounds and effective targets.

A small molecule library with comprehensive target binding and/or inhibition data would prove instrumental in combining phenotypic- and target-screening to identify targets in diseases. The published kinase inhibitor set 1 (PKIS1) is a publically available collection of 360 small molecule kinase inhibitors that have been previously published by scientists at GlaxoSmithKline.[3, 4] The PKIS compound collection is an open source drug discovery effort with publically available biochemical and cellular screening data. Significantly, each of the 360 inhibitors within the PKIS has been profiled against a panel of 220 kinases at two concentrations (0.1 and 1 μM).[3, 4] The small molecule kinase inhibitors consist of >20 diverse chemotypes that have activity for 217 of the 220 kinases profiled.[3, 4] The public availability of the profiling data matrix enables use of this library to identify druggable targets using phenotypic screens. An extension of the PKIS1, the PKIS2, was also briefly made available, and was comprised of 523 kinase inhibitors profiled against the entire kinome at 1 μM. Additionally, several kinase inhibitor libraries are commercially available which contain a number of compounds with published kinase binding and/or inhibition data. Curating the published data of the inhibitors in these commercial libraries could be combined with open source libraries like the PKIS. This would form a broad kinase inhibitor library with comprehensive kinase inhibition data. Based on previous success of target identification in axon repair studies using only the PKIS1 data set with this strategy, an expanded profiled library such as the one proposed could be useful in target identification in cancer.[5]

Sarcomas are cancers of mesenchymal origin that, while common in animals, account for less than one percent of human cancer diagnoses yearly; however, over 20% of pediatric cancers are sarcomas.[6-10] Protein kinases have emerged as a promising target for cancer drug discovery as many tumors, including sarcomas, exhibit aberrant kinase signaling.[11] Many kinase inhibitors approved for other cancers have been studied in sarcoma clinical and pre-clinical experiments.[12-16] As an encouraging example, imatinib (Gleevec), a BCR-ABL tyrosine kinase inhibitor that was originally developed by Novartis to treat chronic myeloid leukemia, was approved in 2002 for the treatment of metastatic gastrointestinal stromal tumor (GIST).[17] This successful repurposing was possible because imatinib was known to also inhibit c-KIT tyrosine kinase.[18] Prior research had identified c-KIT activation through a gain-of-function mutation as crucial to the tumorigenesis of GIST and led to the study of imatinib for anti-GIST activity.[19] Unfortunately, other sarcomas have not been as extensively studied due to their rarity and kinase target validation has been limited. Indeed, for many sarcomas, clinical trials are often performed using kinase inhibitors approved for other cancers without extensive pre-clinical justification for their use. Sarcomas thus make a good candidate to demonstrate the impact a profiled kinase inhibitor-based target discovery approach could have on specific cancer subtypes.

I chose to apply the comprehensive profiled kinase inhibitor library toward the study of three sarcomas without promising targeted therapies; osteosarcoma, Ewing's sarcoma, and synovial sarcoma. Osteosarcoma is a malignant tumor of the bone and arises primarily in children and adolescents.[20, 21] Current therapy combines surgery with conventional cytotoxic chemotherapy, however, the 5-year survival rate survival has remained unchanged at 20% in metastatic and relapse cases.[20] Characterized by chromosomal instability resulting in multiple complex karyotypes, osteosarcoma is a heterogeneous disease.[20, 22] As a result of this heterogeneity and a lack of pathognomonic mutations, targeted therapies have not been realized.[20, 22] Conversely, Ewing's sarcoma and synovial sarcoma are tumors whose malignancy are driven by pathognomonic fusion oncoproteins, EWS-FLI1 and SS18-SSX respectively.[7] Ewing's sarcoma is a tumor of the bone or soft tissue and synovial sarcoma is a soft-tissue sarcoma with both having a high occurrence in adolescents and young adults.[21, 23] For Ewing's sarcoma, intense

chemotherapy with localized tumors has improved survival rates to more than 70%, but survival rates of metastatic disease has remained at 20%.[24, 25] For synovial sarcoma, current treatment of this disease involves surgical removal of the tumor followed by adjuvant or neo adjuvant radiotherapy or chemotherapy to cure local disease.[26-28] Late recurrence and metastasis usually results in synovial sarcoma patient mortality with conventional chemotherapy only giving a temporary response.[29] Despite the presence of pathognomonic mutations, Ewing's sarcoma and synovial sarcoma, like osteosarcoma, have not benefited from molecularly target therapy. The number of validated and druggable targets has been a hindrance to the development of targeted therapies for these sarcomas. Herein, I describe a profiled kinase inhibitor-based target deconvolution platform. This approach combines phenotypic- and target-screening (as described in **Chapter I**), to identify kinase targets and combinational strategies for these sarcomas, with particular success in synovial sarcoma.

Phenotypic Screens of Sarcoma Cell Lines with a Profiled Kinase Inhibitor Library

To identify kinase targets for sarcomas, I performed a phenotypic screen (cell viability) using a collection of profiled kinase inhibitor libraries (**Table 2.1**). This collection comprised the PKIS1, PKIS2, commercial kinase inhibitor libraries obtained from EMD Millipore, Enzo Life Sciences, Cayman Chemical, and an in house collection consisting of kinase inhibitors profiled in previous studies. As described above, the PKIS libraries have extensive kinase profiling available. The commercial libraries contain many kinase inhibitors with published profiling data. This data was curated from the ChEMBL database by Hassan Al-Ali (University of Miami) for use.[†]

The panel of sarcoma cell lines consisted of three sarcoma subtypes: MG63, SAOS2, and U2OS cell lines for osteosarcoma; A673 and TC32 cell lines for Ewing's sarcoma; SYO1 and MOJO cell lines for synovial sarcoma; and the SW982 cell line derived from a surgical specimen described as a biphasic synovial sarcoma lacking the SS18-SSX translocation pathognomonic of this disease. The profiled kinase inhibitor collection was screened at 1 μM (n=2) against the sarcoma cell line panel, the concentration at which a majority of compounds were profiled against the kinome. Percent viability values relative to vehicle control were converted to z-scores (z-score =

(x - vehicle)/(stdev.)). For future analysis, the data of each cell line was stratified into hits (Z-score ≤ -4 or -6) and non-hits (Z-score ≥ -1). A representative screen with stratified data is shown in **Figure 2.1**. In **Chapter I**, it was discussed in detail that cancer cell lines with viability outputs are not always ideal for phenotypic screening. In this case, where I am evaluating the utility of a methodology for target deconvolution in cancer, these simple models and outputs are sufficient.

Table 2.1: Profiled kinase inhibitor library overview.

Library	# of Inhibitors (1342 Total)	Profiling Data
GSK Publish Kinase Inhibitor Set 1	360	Profiled against 220 kinases at 0.1 µM and 1 µM
GSK Publish Kinase Inhibitor Set 2	523	Profiled against Kinome at 1 µM
In-House Commercial Profiled Kinase Inhibitors	66	K_d's of Kinome of 42/66 inhibitors and curated published data
Cayman Kinase Screening Library	154	Curated published data from ChEMBL
EMD Millipore InhibitorSelect Protein Kinase Inhibitor Library I	160	Curated published data from ChEMBL
Enzo Screen-Well Kinase Inhibitor Library	79	Curated published data from ChEMBL

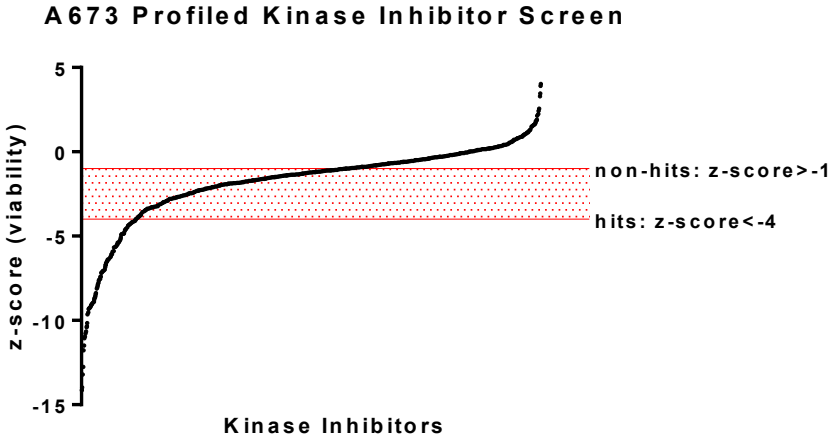

Figure 2.1: Representative sarcoma cell line screen with a profiled kinase inhibitor library. In this screen with the A674 Ewing's sarcoma cell line, viability (relative to vehicle) was converted to z-scores on a plate-per-plate basis and then averaged (n=2). Data was stratified into hits and non-hits using designated thresholds for subsequent analysis. Additional plots for other sarcoma cell line screens can be found in **Appendix A**.

Target Deconvolution using a Machine Learning-based Algorithm

Machine learning has emerged as a useful tool in cancer research.[30, 31] With the advent of large data sets that can be derived from a patient or group of patients, machine learning has proven useful to deconvolute and interpret these data in meaningful ways.[30] For example, machine learning has been used for prediction of cancer susceptibility, recurrence, and survival using proteomics and genomic sequencing.[30, 32-34] It is estimated that machine learning can improve cancer prediction accuracy by 15-25%.[31] Identification of predictive cancer biomarkers and targets has also benefited from machine learning.[35] Thus, machine learning has a well-established precedent for use in cancer research and will continue to be influential well into the future in this regard.

In light of this, I used a previously described machine learning-based algorithm to relate phenotypic (viability) data of screened compounds to their kinase inhibition profiles and identify kinase targets, i.e. kinases whose inhibition suppresses cellular proliferation.[5] Ultimately, the goal is to identify novel sarcoma subtype kinase targets that can be inhibited in order to suppress proliferation or viability. Towards that goal, I performed this analysis on the sarcoma cell line panel results.

Due to similarities in binding pocket architecture and inhibitor interactions of topologically similar kinases, a kinase can be identified as a target in the analysis even if it does not participate in the biological effect, provided the kinase is pharmacologically linked to one or more kinases that do participate. Therefore, kinases must first be scored as groups of pharmacologically linked members, and a second line of evidence is required to investigate which kinase(s) actually participate in the phenotypic readout.[†]

First, profiled kinases were organized into pharmacologically-linked groups (listed in **Table A.1**) as previously described.[5] Briefly, the algorithm then applies a rule-based feature selection scheme to identify the set of kinases whose inhibition is most relevant to the cellular outcome (**Max**imum **I**nformation **S**et, MAXIS).[5] Each group of kinases obtains a score that reflects overall frequency of appearance of its members in the MAXIS, earning a score of 1 for each appearance in 100 different test runs. Additionally, a metric devised by Al-Ali et al. was used to reflect whether a kinase is more frequently and/or strongly inhibited by hits or non-hits of a screen (stratified as described earlier).[5] This metric, B_k, is positive for a kinase whose inhibition directly correlates with hits

(suppressed proliferation), and negative when correlated with non-hits (minimal or increased proliferation) ($-2 \leq B_k \leq +2$).[5] Finally, kinase groups were prioritized using a score combining the group MAXIS scores and average group B_k. This is the Combined Score, with a higher Combined Score giving higher priority to a kinase group (Combined Score= Group MAXIS score * avg. group B_k).[5] A detailed list of MAXIS, B_k, and Combined Scores for each cell line can be found in **Table A.2**. Kinase groups were designated as targets using a cutoff of Combined Scores ≥ 50. These data are summarized in **Figure 2.2**. †

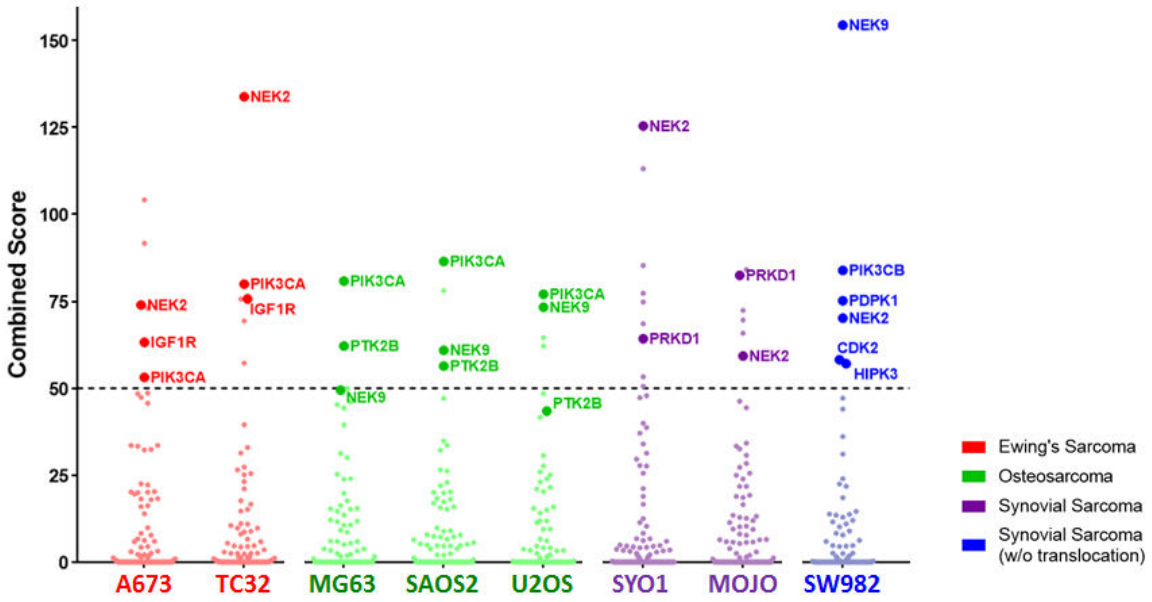

Figure 2.2: Combination scores of kinase groups across a sarcoma cell line panel. Kinase groups (circles) designated as targets (Combined Score > 50) in two cell lines within a sarcoma subtype are highlighted. All target kinase groups are highlighted in the SW982 cell line. The highlight kinase groups are labeled with a represented kinase. Only kinase groups with Combination Score ≥ 0 are shown.

Identification of Important Kinases in Sarcoma Cell Lines *in vitro*

I narrowed the list of highest scoring targets to kinase groups that were present in two cell lines within a sarcoma subtypes (with the exception of the SW982 cell line) (**Figure 2.2**). Gratifyingly, this method identified kinases in sarcoma subtypes that have been well established as targets. Inhibiting IGF1R has been well established to be efficacious in Ewing's sarcoma in preclinical studies.[23, 36, 37] However, it has had mixed results as a target with single agents at the clinical level.[36, 37] PIK3CA has also been found to regulate EWS-FL1 expression in Ewing's sarcoma cell lines.[38] In osteosarcoma,

PTK2B (FAK2 and by extension FAK) has recently been identified as a possible target.[39, 40] FAK inhibition or knockdown significantly lowered proliferation and invasion while increasing apoptosis in osteosarcoma cell lines.[40] Additionally, FAK was seen to be overexpressed in osteosarcoma and was a strong predictor of overall and metastasis-free survival.[40] PIK3CA and the PIK3/mTOR pathway have begun to emerge as vulnerabilities in osteosarcoma as well, with dual inhibitors of PIK3 and mTOR inducing apoptosis.[41] The NEK kinases were identified as targets across all subtypes. As regulators of cell mitosis, their identification as pan-sarcoma targets is not unexpected.[42] Identifying targets that range from the well-established to the emergent demonstrates that this approach can distinguish important kinases in sarcoma subtypes, at the very least *in vitro*.

Identification of PRKD as a Putative Novel Target in Synovial Sarcoma

The kinase group made up of the Protein Kinase Ds (PRKD1, PRKD2, PRKD3) was identified as a target in the synovial sarcoma cell lines and not in the other sarcoma subpanels. It is notable in that there is no literature evidence of PRKD as a target in synovial sarcoma, representing a potential novel discovery. These proteins have been implicated in disease progression of breast, pancreatic, prostate, and colorectal cancers.[43-46] Also, there has been multiple overlapping as well as distinct functions between the different PRKDs identified in cancer.[45, 47] I proceeded to pharmacologically confirm PRKD as a target(s) in synovial sarcoma cell lines. I obtained two commercially available inhibitors that were reported to inhibit PRKD, CRT0066101 and kb NB 142-70 (**Figure 2.3A**).[43, 46, 48, 49] These two inhibitors are structurally distinct and thus should have orthogonal off-targets. I then tested these inhibitors across the entire panel of sarcoma cell lines. In line with the previous finding of PRKD as a highly scored target only in the synovial sarcoma cell lines, I observed that both CRT0066101 and kb NB 142-70 displayed higher potency in the synovial sarcoma cell lines compared to the other sarcoma subtypes (**Figure 2.3B**). The activity of these inhibitors in these cell lines were comparable or better than the cell lines of cancers where PRKD has been implicated.[44, 46] To further confirm synovial sarcoma viability is dependent on PRKD and because there are no known small molecule inhibitors with selectivity to distinguish between PRKD1, PRKD2, and PRKD3, I examined the effect of siRNA knockdown of these genes in

SYO1 and MOJO synovial sarcoma cells.[‡] There was a significant ($p < 0.05$) reduction in cell proliferation upon knockdown of PRKD3 in each of the synovial sarcoma cell lines compared to non-targeting siRNA control (**Figure 2.4**). I also treated a cell line that had a low PRKD Combined Score with PRKD siRNA, MG63 osteosarcoma cell line (PRKD Combined Score= 0.0). No decrease in viability for this cell line was observed in any of the PRKD siRNA treatments. Thus, genetic knockdown is consistent with the pharmacological results. Of note, in data from siRNA screening studies of osteosarcoma and Ewing's sarcoma cell lines (including the ones used in this study), PRKD knockdown also did not result in significant decreases in viability.[50, 51] Together, these data indicate PRKD as a putative target specific to synovial sarcoma.

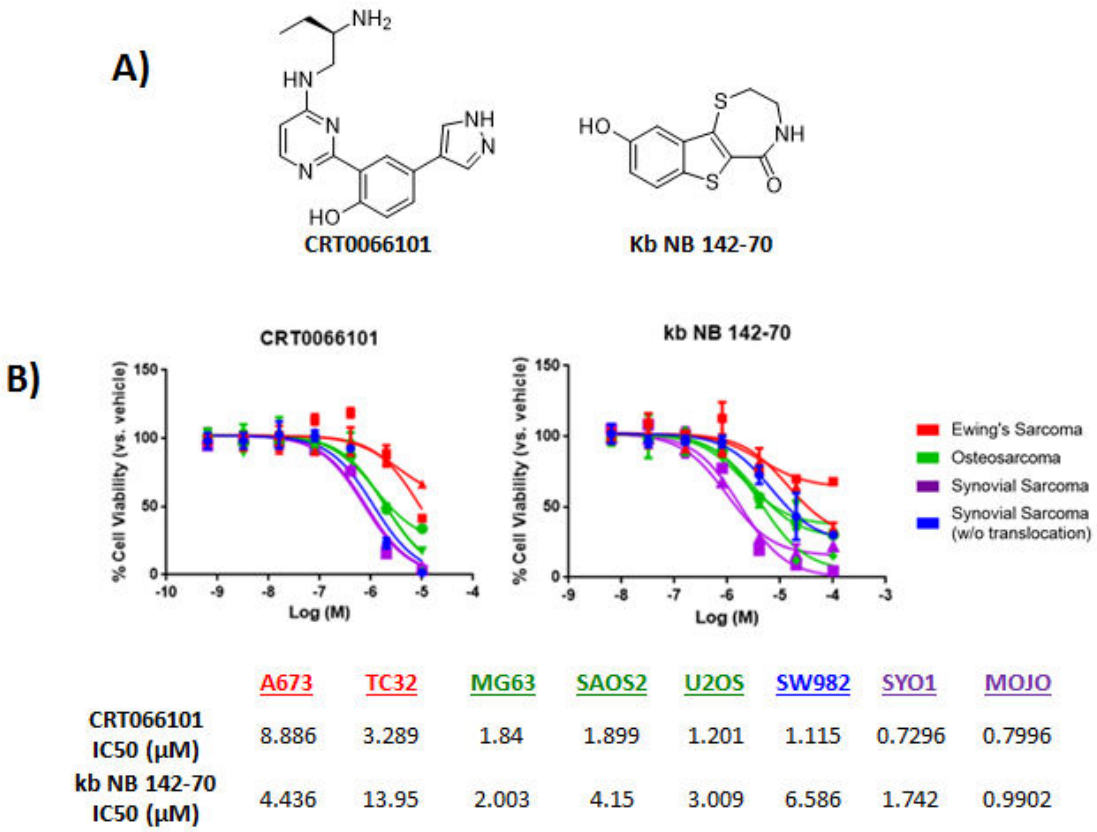

	A673	TC32	MG63	SAOS2	U2OS	SW982	SYO1	MOJO
CRT066101 IC50 (µM)	8.886	3.289	1.84	1.899	1.201	1.115	0.7296	0.7996
kb NB 142-70 IC50 (µM)	4.436	13.95	2.003	4.15	3.009	6.586	1.742	0.9902

Figure 2.3: PRKD inhibitor activity in a sarcoma cell line panel. **A)** Chemical structures of two structurally distinct PRKD inhibitors. **B)** Dose response curves of the sarcoma cell line panel with PRKD inhibitors after 72 hour compound exposure and calculated IC_{50}s (concentration at 50% maximum inhibition).

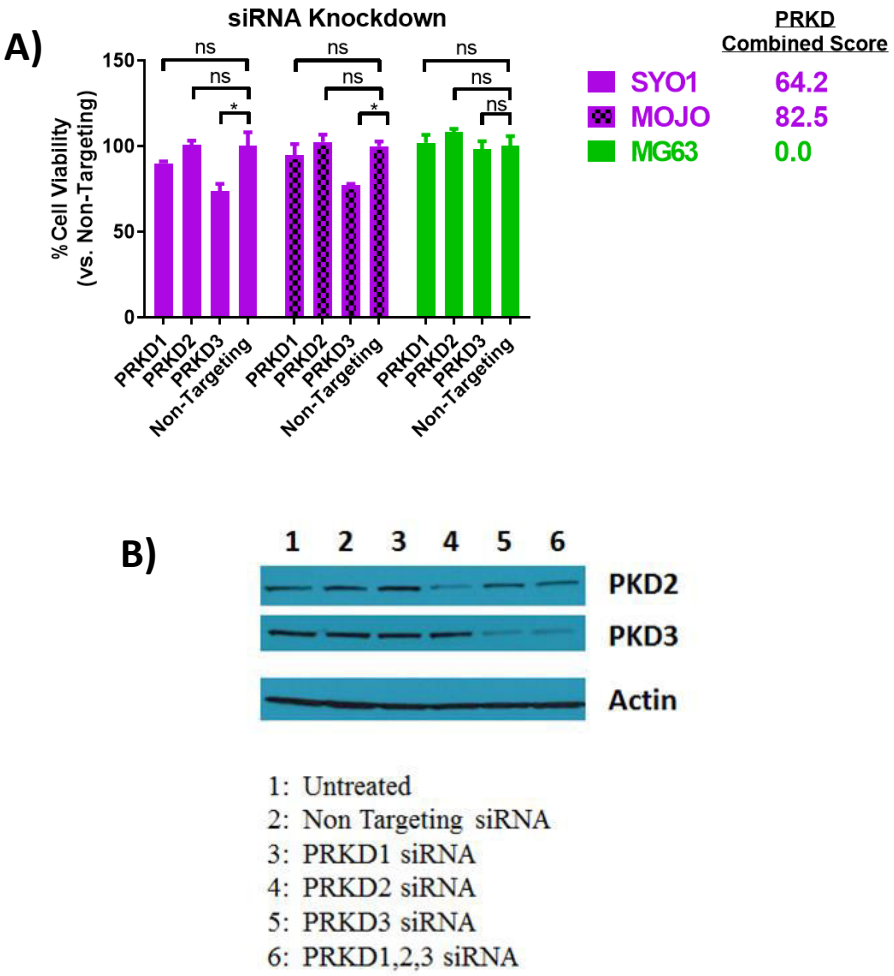

Figure 1.4: Sarcoma cell line viability after siRNA knockdown of PRKD. **A)** SYO1 and MOJO synovial sarcoma cell lines transfected with PRKD3 siRNA results in a significant decrease in viability relative to non-targeting siRNA (96 hours post transfection). No decrease in viability observed in MG63 osteosarcoma cell line.*p<0.05. **B)** Western blot confirming protein knockdown of PRKD. No high-quality PRKD1 antibody was available. Knockdown of all three PRKD proteins at the same time could not be achieved. ‡

Identifying Synergistic Drug Combinations through a Synergy Screen

Drug combination is a strategy in cancer treatment where increased therapeutic effect, dose reduction, toxicity reduction, and minimized resistance are desired.[52, 53] To these ends it is important to identify drug combinations in which the desired effect is synergistic, in other words greater than an additive effect of the drugs alone. I speculated that the profiled kinase inhibitor based target ID approach could be leveraged to identify novel synergistic drug combinations. For this aim, I repeated the phenotypic screen with the profiled kinase inhibitor collection against SYO1 cells in the presence of a PRKD

inhibitor, CRT0066101 (at 300 nM, IC_{30} concentration). From this "synergy screen" I again employed the machine learning target identification as described above. Strikingly, the top 15 scoring kinase groups were vastly different compared to the original screen as shown in **Table 2.2** (see **Table A.3** for a full comparison). These newly identified kinase groups, with their increased Combined Scores, thus have an amplified importance in SYO1 cell viability with concurrent of PRKD inhibition. Importantly, I observed a decrease in the Combined Score of PRKD in the screen with 300 nM CRT0066101, as would be expected.

Table 2.2: Top 15 target kinase groups of SYO screen and the SYO1 synergy screen with a PRKD inhibitor (300 nM CRT0066101). In the synergy screen, newly identified targets are bolded in green. In the original screen, targets no longer represented in the synergy screen list are bolded in red. Kinases listed are representative of their group.

Original Screen Top 15 Targets		
NEK2	**KIT**	**MAP4K4**
PRKX	**PRKD1**	PIK3CA
RPS6KB1	**PRKCH**	**DDR2**
PIM2	**MAPK11 (p38)**	**FGR**
PDGFRA	GSK3A	**AXL**

Synergy Screen Top 15 Targets		
PTK2B	PIK3CA	**ALK**
HIPK4	**BRSK2**	**CSF1R**
CDK4	GSK3A	**AKT1**
PDGFRA	**INSRR**	PRKX
ROS1	**FLT1**	**EPHA2**

I then moved to investigate if combinations of CRT0066101 and selective clinical inhibitors of the newly identified kinase targets would be synergistic. For this study I chose CDK4 and AKT, as selective clinical inhibitors for these kinases were readily available. Palbociclib is a selective inhibitor of CDK4/6 and is currently in Phase II/III clinical trials.[54] BAY1125976 and AZD5363 are selective inhibitors for AKT1/2/3 and are also currently in Phase II/III clinical trials.[55, 56] To assess if CRT0066101 is synergistic with these drugs I employed Chou-Talalay synergy analysis, which calculates a Combination Index (CI) at various effect levels of the combination.[52, 53, 57, 58] A CI< 1 denotes synergism, a CI=1 denotes additivity, and a CI>1 denotes antagonism of the drugs being assessed. I found that CRT0066101 was synergistic with all three inhibitors in SYO1 cells (**Table 2.3**). Combination Index plots, which relate CI across various effect levels, of each of the combinations demonstrated that synergy was present across a wide range of effect levels. The synergism found in the higher effect levels is an

important trait in combination treatments of cancer where high amounts of cancer cell death is desired.[52, 53] I also performed Chou-Talalay analysis of CRT0066101 with VX745, a highly selective p38 inhibitor, on the basis that the p38 kinase group (represented as MAPK11 in **Table 2.2**) dropped from in the target list.[59] This analysis revealed that these two agents range from additive to slightly antagonistic over similar effect levels as the previous combinations. I then repeated this Chou-Talalay synergy analysis with other PRKD inhibitor, kb NB 142-70. I observed the same trends, namely, synergy with the selective clinical CDK and AKT inhibitors and antagonism with the selective p38 inhibitor. These findings suggests that this methodology can distinguish synergistic combinations from ones that are not. I envision further use of this target ID synergy screen methodology to find new synergistic combinations for investigation in other diseases as well, and could be applied with established treatments.

Table 2.3: Combination Indexes (CI) of CRT0066101 and kb NB 142-70 with selective inhibitors at various effect levels (ED50, ED 75, ED, 90, and ED95). CI < 1 is synergism, CI=1 is additive, CI > 1 is antagonism. Newly identified targets are in green. Targets no longer represented in the synergy screen list are in red.

CRT0066101 (PRKD Inhibitor) +	Target	ED50 CI	ED75 CI	ED90 CI	ED95 CI
BAY1125976	AKT	0.435	0.308	0.257	0.235
AZD5363	AKT	0.626	0.515	0.443	0.406
Palbociclib	CDK	0.759	0.687	0.648	0.633
VX745	p38	1.11	1.11	1.12	1.13

kb NB 140-70 (PRKD Inhibitor) +	Target	ED50 CI	ED75 CI	ED90 CI	ED95 CI
BAY1125976	AKT	0.457	0.468	0.514	0.555
AZD5363	AKT	0.547	0.518	0.523	0.537
Palbociclib	CDK	0.483	0.534	0.687	0.831
VX745	p38	1.78	2.11	2.50	2.81

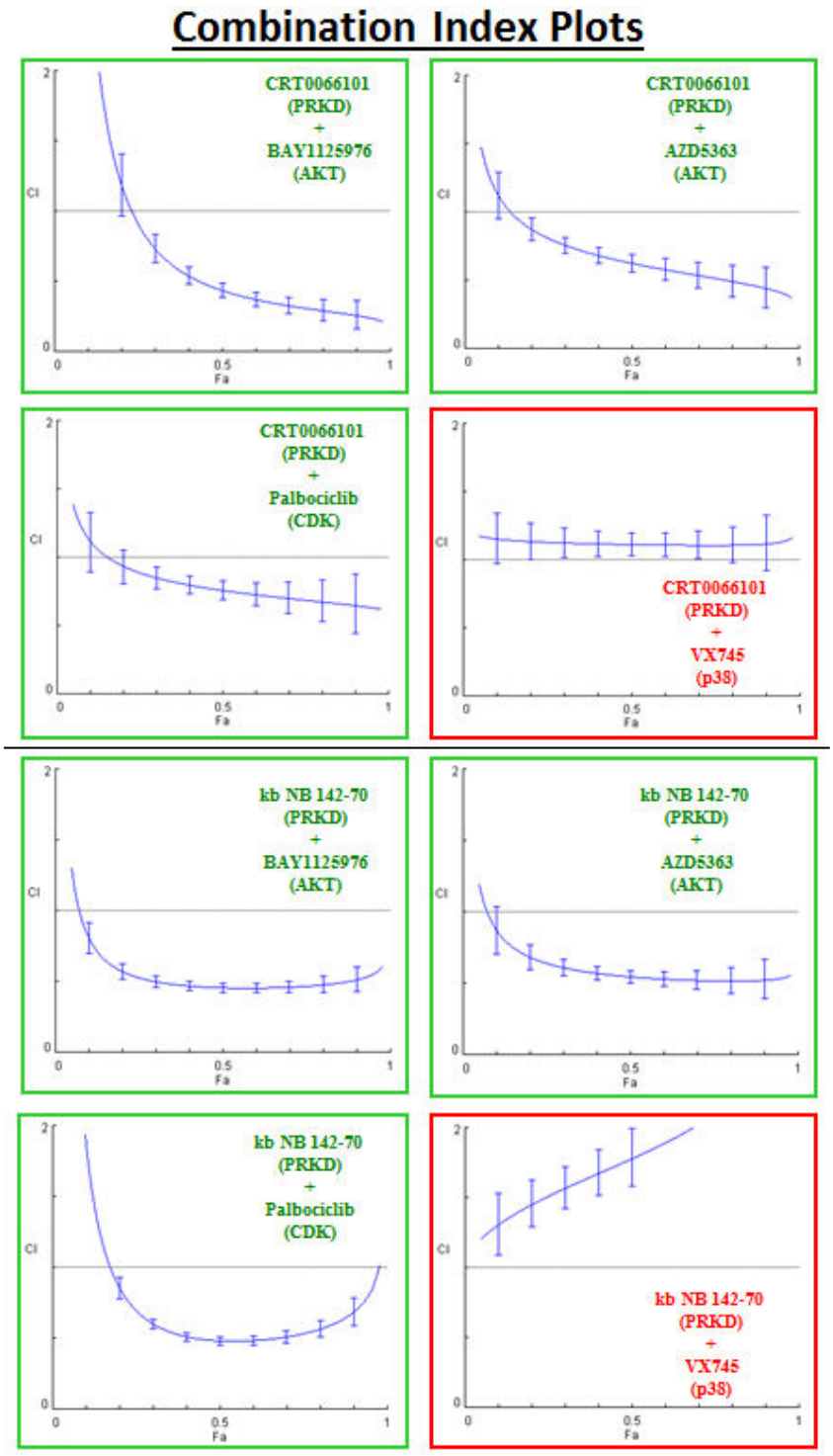

Figure 2.5: Combination Index Plots output by Compusyn showing continuous combination index (CI) values across fractional affect levels (Fa). The horizontal line shows CI=1. Error bars represent 95% confidence intervals calculated from serial deletion analysis.[52, 53] Plots are of combinations of CRT0066101or kb NB 142-40 with BAY1125976 (selective clinical AKT inhibitor), AZD5363 (selective clinical AKT inhibitor), Palbocicib (selective clinical CDK4/6 inhibitor), and VX745 (selective p38 inhibitor). Green and red are inhibitors whose targets appeared and did not appear in the synergy screen target list respectively. Full outputs from Compsyn can be found in **Appendix A**.

Conclusions

Progress toward developing targeted therapies against sarcomas has been slow due to the lack of defined and druggable molecular targets in these cancers. I have presented a strategy of combining phenotypic- and target-screening to overcome this obstacle. I identified various kinase targets in sarcomas using a profiled kinase inhibitor library made up of open source and commercial libraries. Of particular interest was the identification and confirmation of PRKD as a target in synovial sarcoma both due to its specificity in the panel and potential novelty in this disease. This success in target identification in the case of synovial sarcoma, a rare and understudied cancer, gives promise that targets may be identified in other more highly studied cancers such as that of the breast. Indeed, the progress of such studies is described in **Chapter III**. Further target confirmation in the other sarcoma subtypes tested in this chapter can also be carried out in the future, with studies currently being planned.

Expanding the scope of this work was the use of the machine-learning target deconvolution in scoring kinase targets as a means to identify novel combinational strategies. I performed an additional phenotypic screen of a synovial sarcoma cell line in the presence of a PRKD inhibitor. I discovered that scores of many kinases from the machine learning algorithm changed greatly, including CDK and AKT which increased. Using Chou-Talalay synergy analysis, I discovered that selective clinical inhibitors of these kinases synergistically decreased viability along with PRKD inhibition. This strategy could be reapplied with other cancers in the presence of any drug, kinase inhibitor or not, in which new combinational strategies are desired.

This work uses cancer cell lines and a simple cell viability readout to demonstrate the effectiveness of this methodology. However, as previously mentioned, more advanced sarcoma models and phenotypic readouts would be desirable to identify targets with higher clinical relevance. In the case of synovial sarcoma, a phenotypic screen which measures the disruption of the SS18-SSX fusion oncoprotein complex has been reported.[60] Combining the machine learning target identification approach with this assay in a high-throughput format would identify targets directly related to a key molecular event (oncoprotein complex disruption) shown to have a beneficial therapeutic effect.[60, 61] Demonstrating that this approach works using simple cancer cell viability data

positions it for use with higher relevant phenotypic outputs such as the one described above.

Materials and Methods

Cell Lines and General Cell Culture and Dosing Conditions

SYO1 synovial sarcoma cell, MOJO synovial sarcoma cells, TC32 Ewing's sarcoma cells, and SAOS2 osteosarcoma cells were maintained in 10% Fetal Bovine Serum (FBS) in RPMI 1640 media. SW982 sarcoma cells, A673 Ewing's Sarcoma cells, and MG63 osteosarcoma cells were maintained in 10% FBS in DMEM. U2OS osteosarcoma cells were maintained in 10% FBS in McCoy's 5A media. SYO1 and MOJO cell were kind gifts from Torsten Nielsen (University of British Colombia). A673, TC32, U2OS, and SAOS2 cells were kind gifts from Elizabeth Lawlor (University of Michigan). MG63 and SW982 cells were purchased from American Type Culture Collection (ATCC). A humidified incubator at 37 °C and 5 % CO_2 was used for storing all cell cultures.

General Cell Viability Assay Protocol

Cell lines were dispersed from 70-80% confluent monolayer cultures using 0.05% Trypsin-EDTA (Invitrogen) and plated in 96-well plates in 100 μL of appropriate cell culture media. Cells were seeded at concentrations of 3000 x 10^3 cells/well and were incubated overnight to adhere. Cells were then dosed with compounds to be tested by addition of 10 μL 1% DMSO stocks of 10x concentration in Cell Culture Media (0.1% DMSO final concentration). After the 72-hour dosing period was complete, plates were removed from the incubator and 11 μL of WST-1 reagent (Roche Applied Science) was added to each well. Plates were returned to the incubator until a sufficient color change developed (1-4 hr.). Plates were placed on a plate shaker for 60 s and read on a Synergy 4 plate reader (Biotek). The difference in the absorbance at wavelengths of 450 nM and 630 nM (A_{450}-A_{630}) was recorded for each well and then corrected by subtracting out the blank (no cell) readings. Cell viability was measured as percent viability with respect to vehicle. Dose-response growth curves were generated with measurements of triplicate wells with fitting performed using Graphpad Prism 7 (Graphpad Software). The equation Y = Bottom + (Top – Bottom)/(1 + 10^(X – LogIC_{50})), where X = log(concentration) and

Y = Response was used in the nonlinear regression. Plots summarizing this data for each screen can be found in **Appendix A**.

Phenotypic Screen with a Profiled Kinase Inhibitor Library

SYO1, MOJO, TC32, A673, MG63, SAO2, U2OS, and SW982 cells were subjected to a cell growth assay (detailed above) with a profiled kinase inhibitor library. A counter screen of SYO1 plus 300 nM CRT0066101 was also performed. This library was composed of the GSK PKIS1 and PKIS2 (obtained from GlaxoSmithKline), Enzo Screen-Well Kinase Inhibitor Library (#BML-2832-0100, Enzo), EMD Millipore InhibitorSelect Protein Kinase Inhibitor Library I (#539743, EMD Millipore), the Cayman Kinase Screening Library (#10505, Cayman Chemical), and an in-house collection of commercial profiled kinase inhibitors (purchased from various sources including SelleckChem and LC Labs). In the primary screen, 2 μL of the 1 mM (1000X) DMSO master stocks were diluted into 200 uL of cell culture media. From these daughter plates, 10 uL was added to each cell culture well to give 1 μM final compound concentrations (0.1% DMSO final concentration). The screen was performed in duplicate and the viabilities (measured as described above) were averaged and compared to vehicle. Viabilities were converted to z-scores (z-score = (x - vehicle)/(vehicle stdev.)).

Target Deconvolution by Machine Learning-based Algorithm

We excluded from this analysis compounds whose z-score fell between -4 and -1 (the SYO1 screen was the exception with compounds excluded between -6 and -1). This stratification accentuates differences between the hit and non-hit categories and improves selection of relevant kinases. The remaining compounds comprised the input for the analysis. For SYO1 (461 compounds; 256 stratified hits and 205 stratified non-hits), MOJO (606 compounds; 76 stratified hits and 530 stratified non-hits), A673 (452 compounds; 83 stratified hits and 369 stratified non-hits), TC32 (558 compounds; 118 stratified hits and 440 stratified non-hits), MG63 (661 compounds; 83 stratified hits and 578 stratified non-hits), SAOS2 (559 compounds; 85 stratified hits and 474 stratified non-hits), U2OS (540 compounds; 54 stratified hits and 486 stratified non-hits), and SW982 (605 compounds; 92 stratified hits and 513 stratified non-hits), and SYO1 plus

300 nM CRT0066101 (534 compounds; 92 stratified hits and 442 stratified non-hits) screens, compounds with profiling data against 237 wildtype kinases constituted the input for analysis. Generation of pharmacologically-linked kinase groups was done by pharmacological interaction strength (P_{ij}) (direct measure) and sequence similarity (indirect measure) as previously described.[5, 62] Any two kinases with a P_{ij} score ≥ 0.6 or kinase domain sequence similarity score ≥ 0.7 belonged to the same group. Calculation of group MAXIS scores, hit/non-hit inhibition bias (B_k), and Combined Scores within each phenotypic screen using a Support Vector Machine was performed by Hassan Al-Ali (University of Miami), as previously described.[5] †

Analysis of Combined Drug Effects

The effect of combining CRT0066101 or kb NB 142-70 with Palbociclib, BAY1125976, AZD5363, VX745 in SYO1 synovial sarcoma cells were analyzed using a median effect analysis as described by Chou and Talalay (2006). The fractional effect measured for the analysis was on cell viability after 72 hours (measured as described above). This analysis was performed using Compusyn software (ComboSyn).[58] Full outputs from Compusyn are given in **Appendix A**.

Western Blot Analysis

Plated cells were washed with ice cold PBS and lysed with radioimmunoprecipitation (RIPA) buffer containing freshly added protease (#1186145001) and phosphatase (#4906837001) inhibitors (Roche Applied Sciences). Lysed samples were sonicated and centrifuged at 14,000 rpm for 30 min at 4 °C. The supernatant was collected and the total amount of protein in the lysate was measured using the BCA kit. 40–50 μg of protein were separated in 8–12 % SDS polyacrylamide gel electrophoresis (SDS–PAGE). Resolved protein was transferred onto a polyvinylidene fluoride (PVDF) membrane (Bio-Rad Laboratories). The membrane was blocked using 5 % milk in PBS-Tween for 1h and then probed with specific mouse or rabbit primary antibody for PRKD2 (#8188S), PRKD3 (#5655S), β-actin (#3700S) overnight at 4 °C (Cell Signaling Technology). After washing the membrane in PBS-Tween, it was incubated with rabbit, mouse, or goat secondary antibody conjugated to

horseradish peroxidase for 1h at RT. The membrane was then washed three times in PBS-Tween and visualized with enhanced chemiluminescence reagent, following the manufacturer's instructions (Amersham ECL Western Blotting Analysis System, GE Healthcare). The blots shown were obtained with the help of Zhi Fen Wu.‡

siRNA Transfection

SYO1, MOJO, and MG63 cells were plated in a 24-well plate and allowed to adhere overnight. Cells were then transfected with pools of PRKD1, PRKD2, PRKD3, and non-targeting Accell siRNA (Dharmacon) (1 μM) using Accell delivery Media (Dhamacon) following manufacturer's instructions. After 96-hours post-transfection, cell viability was then measured as described above. The following siRNA pools used were: PRKD1 (GUUGUAAAUUUGGAGUGUA, CGAUCUUAUUGAAGUGGUC, CCAACUUGCACAGAGAUAU, CGGUCAGGUUUAACAUUUG), PRKD2 (CCCUUAUCAAUGGAGAUGU, GCGUGAUCAUGUACGUCAG, UCUUCUGCCUCAUCGUAUA, UGAAGAUGCGCAAACGCUA), PRKD3 (CUUGUGUGCUCCAUAGUUU, CGAUGUGCCUUCAAGAUUC, GCAUACAAGUUUCAUUUCUA, GCAACAGCUUCUAAGAUAA), non-targeting siRNA control (UGGUUUACAUGUCGACUAA, UGGUUUACAUGUUUUCUGA, UGGUUUACAUGUUUUCCUA, UGGUUUACAUGUUGUGUGA).

References

1. Al-Ali, H., The evolution of drug discovery: from phenotypes to targets, and back. *Med. Chem. Commun.* **2016,** *7*, 788-798.
2. Pemovska, T.; Kontro, M.; Yadav, B.; Edgren, H.; Eldfors, S.; Szwajda, A.; Almusa, H.; Bespalov, M. M.; Ellonen, P.; Elonen, E.; Gjertsen, B. T.; Karjalainen, R.; Kulesskiy, E.; Lagstrom, S.; Lehto, A.; Lepisto, M.; Lundan, T.; Majumder, M. M.; Marti, J. M.; Mattila, P.; Murumagi, A.; Mustjoki, S.; Palva, A.; Parsons, A.; Pirttinen, T.; Ramet, M. E.; Suvela, M.; Turunen, L.; Vastrik, I.; Wolf, M.; Knowles, J.; Aittokallio, T.; Heckman, C. A.; Porkka, K.; Kallioniemi, O.; Wennerberg, K., Individualized systems medicine strategy to tailor treatments for patients with chemorefractory acute myeloid leukemia. *Cancer Discov* **2013,** *3* (12), 1416-29.
3. Dranchak, P.; MacArthur, R.; Guha, R.; Zuercher, W. J.; Drewry, D. H.; Auld, D. S.; Inglese, J., Profile of the GSK published protein kinase inhibitor set across ATP-dependent and-independent luciferases: implications for reporter-gene assays. *PLoS One* **2013,** *8* (3), e57888.
4. Elkins, J. M.; Fedele, V.; Szklarz, M.; Abdul Azeez, K. R.; Salah, E.; Mikolajczyk, J.; Romanov, S.; Sepetov, N.; Huang, X. P.; Roth, B. L.; Al Haj Zen, A.; Fourches, D.; Muratov, E.; Tropsha, A.; Morris, J.; Teicher, B. A.; Kunkel, M.; Polley, E.; Lackey, K. E.; Atkinson, F. L.; Overington, J. P.; Bamborough, P.; Muller, S.; Price, D. J.; Willson, T. M.; Drewry, D. H.; Knapp, S.; Zuercher, W. J., Comprehensive characterization of the Published Kinase Inhibitor Set. *Nat Biotechnol* **2016,** *34* (1), 95-103.
5. Al-Ali, H.; Lee, D. H.; Danzi, M. C.; Nassif, H.; Gautam, P.; Wennerberg, K.; Zuercher, B.; Drewry, D. H.; Lee, J. K.; Lemmon, V. P.; Bixby, J. L., Rational Polypharmacology: Systematically Identifying and Engaging Multiple Drug Targets To Promote Axon Growth. *ACS Chem Biol* **2015,** *10* (8), 1939-51.
6. Borden, E. C.; Baker, L. H.; Bell, R. S.; Bramwell, V.; Demetri, G. D.; Eisenberg, B. L.; Fletcher, C. D.; Fletcher, J. A.; Ladanyi, M.; Meltzer, P.; O'Sullivan, B.; Parkinson, D. R.; Pisters, P. W.; Saxman, S.; Singer, S.; Sundaram, M.; van Oosterom, A. T.; Verweij, J.; Waalen, J.; Weiss, S. W.; Brennan, M. F., Soft tissue sarcomas of adults: state of the translational science. *Clin Cancer Res* **2003,** *9* (6), 1941-56.
7. Taylor, B. S.; Barretina, J.; Maki, R. G.; Antonescu, C. R.; Singer, S.; Ladanyi, M., Advances in sarcoma genomics and new therapeutic targets. *Nat Rev Cancer* **2011,** *11* (8), 541-57.
8. Nielsen, T. O.; West, R. B., Translating gene expression into clinical care: sarcomas as a paradigm. *J Clin Oncol* **2010,** *28* (10), 1796-805.
9. Burningham, Z.; Hashibe, M.; Spector, L.; Schiffman, J. D., The Epidemiology of Sarcoma. *Clinical Sarcoma Research* **2012,** *2* (1), 14.
10. Wunder, J. S.; Nielsen, T. O.; Maki, R. G.; O'Sullivan, B.; Alman, B. A., Opportunities for improving the therapeutic ratio for patients with sarcoma. *Lancet Oncol* **2007,** *8* (6), 513-24.
11. Zhang, J.; Yang, P. L.; Gray, N. S., Targeting cancer with small molecule kinase inhibitors. *Nature Reviews Cancer* **2009,** *9* (1), 28-39.
12. Bond, M.; Bernstein, M. L.; Pappo, A.; Schultz, K. R.; Krailo, M.; Blaney, S. M.; Adamson, P. C., A phase II study of imatinib mesylate in children with refractory or

relapsed solid tumors: a Children's Oncology Group study. *Pediatr Blood Cancer* **2008,** *50* (2), 254-8.
13. Maki, R. G.; D'Adamo, D. R.; Keohan, M. L.; Saulle, M.; Schuetze, S. M.; Undevia, S. D.; Livingston, M. B.; Cooney, M. M.; Hensley, M. L.; Mita, M. M.; Takimoto, C. H.; Kraft, A. S.; Elias, A. D.; Brockstein, B.; Blachere, N. E.; Edgar, M. A.; Schwartz, L. H.; Qin, L. X.; Antonescu, C. R.; Schwartz, G. K., Phase II study of sorafenib in patients with metastatic or recurrent sarcomas. *J Clin Oncol* **2009,** *27* (19), 3133-40.
14. Ray-Coquard, I.; Le Cesne, A.; Whelan, J. S.; Schoffski, P.; Bui, B. N.; Verweij, J.; Marreaud, S.; van Glabbeke, M.; Hogendoorn, P.; Blay, J. Y., A phase II study of gefitinib for patients with advanced HER-1 expressing synovial sarcoma refractory to doxorubicin-containing regimens. *Oncologist* **2008,** *13* (4), 467-73.
15. Michels, S.; Trautmann, M.; Sievers, E.; Kindler, D.; Huss, S.; Renner, M.; Friedrichs, N.; Kirfel, J.; Steiner, S.; Endl, E.; Wurst, P.; Heukamp, L.; Penzel, R.; Larsson, O.; Kawai, A.; Tanaka, S.; Sonobe, H.; Schirmacher, P.; Mechtersheimer, G.; Wardelmann, E.; Buttner, R.; Hartmann, W., SRC signaling is crucial in the growth of synovial sarcoma cells. *Cancer Res* **2013,** *73* (8), 2518-28.
16. Liberal, J. M.; Lagares-Tena, L.; Sáinz-Jaspeado, M.; Mateo-Lozano, M.; del Muro, X. G.; Tirado, O. M., Targeted therapies in sarcomas: challenging the challenge. *Sarcoma* **2012,** *2012*, Article ID 626094.
17. Dagher, R.; Cohen, M.; Williams, G.; Rothmann, M.; Gobburu, J.; Robbie, G.; Rahman, A.; Chen, G.; Staten, A.; Griebel, D.; Pazdur, R., Approval summary: imatinib mesylate in the treatment of metastatic and/or unresectable malignant gastrointestinal stromal tumors. *Clin Cancer Res* **2002,** *8* (10), 3034-8.
18. Druker, B. J.; Sawyers, C. L.; Kantarjian, H.; Resta, D. J.; Reese, S. F.; Ford, J. M.; Capdeville, R.; Talpaz, M., Activity of a specific inhibitor of the BCR-ABL tyrosine kinase in the blast crisis of chronic myeloid leukemia and acute lymphoblastic leukemia with the Philadelphia chromosome. *N Engl J Med* **2001,** *344* (14), 1038-42.
19. Andersson, J.; Sjogren, H.; Meis-Kindblom, J. M.; Stenman, G.; Aman, P.; Kindblom, L. G., The complexity of KIT gene mutations and chromosome rearrangements and their clinical correlation in gastrointestinal stromal (pacemaker cell) tumors. *Am J Pathol* **2002,** *160* (1), 15-22.
20. Martin, J. W.; Squire, J. A.; Zielenska, M., The Genetics of Osteosarcoma. *Sarcoma* **2011,** *2011*, Article ID 627254.
21. Herzog, C. E., Overview of sarcomas in the adolescent and young adult population. *J Pediatr Hematol Oncol* **2005,** *27* (4), 215-8.
22. Kansara, M.; Teng, M. W.; Smyth, M. J.; Thomas, D. M., Translational biology of osteosarcoma. *Nat Rev Cancer* **2014,** *14* (11), 722-35.
23. Lawlor, E. R.; Sorensen, P. H., Twenty Years on: What Do We Really Know about Ewing Sarcoma and What Is the Path Forward? *Crit Rev Oncog* **2015,** *20* (3-4), 155-71.
24. Womer, R. B.; West, D. C.; Krailo, M. D.; Dickman, P. S.; Pawel, B. R.; Grier, H. E.; Marcus, K.; Sailer, S.; Healey, J. H.; Dormans, J. P.; Weiss, A. R., Randomized controlled trial of interval-compressed chemotherapy for the treatment of localized Ewing sarcoma: a report from the Children's Oncology Group. *J Clin Oncol* **2012,** *30* (33), 4148-54.

25. Grier, H. E.; Krailo, M. D.; Tarbell, N. J.; Link, M. P.; Fryer, C. J.; Pritchard, D. J.; Gebhardt, M. C.; Dickman, P. S.; Perlman, E. J.; Meyers, P. A.; Donaldson, S. S.; Moore, S.; Rausen, A. R.; Vietti, T. J.; Miser, J. S., Addition of ifosfamide and etoposide to standard chemotherapy for Ewing's sarcoma and primitive neuroectodermal tumor of bone. *N Engl J Med* **2003,** *348* (8), 694-701.
26. Linch, M.; Miah, A. B.; Thway, K.; Judson, I. R.; Benson, C., Systemic treatment of soft-tissue sarcoma-gold standard and novel therapies. *Nat Rev Clin Oncol* **2014,** *11* (4), 187-202.
27. Al-Hussaini, H.; Hogg, D.; Blackstein, M. E.; O'Sullivan, B.; Catton, C. N.; Chung, P. W.; Griffin, A. M.; Hodgson, D.; Hopyan, S.; Kandel, R.; Ferguson, P. C.; Wunder, J. S.; Gupta, A. A., Clinical features, treatment, and outcome in 102 adult and pediatric patients with localized high-grade synovial sarcoma. *Sarcoma* **2011,** *2011*, Article ID 231789.
28. Spurrell, E. L.; Fisher, C.; Thomas, J. M.; Judson, I. R., Prognostic factors in advanced synovial sarcoma: an analysis of 104 patients treated at the Royal Marsden Hospital. *Ann Oncol* **2005,** *16* (3), 437-44.
29. Sultan, I.; Rodriguez-Galindo, C.; Saab, R.; Yasir, S.; Casanova, M.; Ferrari, A., Comparing children and adults with synovial sarcoma in the Surveillance, Epidemiology, and End Results program, 1983 to 2005: an analysis of 1268 patients. *Cancer* **2009,** *115* (15), 3537-47.
30. Kourou, K.; Exarchos, T. P.; Exarchos, K. P.; Karamouzis, M. V.; Fotiadis, D. I., Machine learning applications in cancer prognosis and prediction. *Comput Struct Biotechnol J* **2015,** *13*, 8-17.
31. Cruz, J. A.; Wishart, D. S., Applications of Machine Learning in Cancer Prediction and Prognosis. *Cancer Inform* **2006,** *2*, 59-77.
32. Abreu, P. H.; Santos, M. S.; Abreu, M. H.; Andrade, B.; Silva, D. C., Predicting Breast Cancer Recurrence Using Machine Learning Techniques: A Systematic Review. *ACM Computing Surveys (CSUR)* **2016,** *49* (3), Article No. 52.
33. Park, K.; Ali, A.; Kim, D.; An, Y.; Kim, M.; Shin, H., Robust predictive model for evaluating breast cancer survivability. *Engineering Applications of Artificial Intelligence* **2013,** *26* (9), 2194-2205.
34. Urbanowicz, R. J.; Andrew, A. S.; Karagas, M. R.; Moore, J. H., Role of genetic heterogeneity and epistasis in bladder cancer susceptibility and outcome: a learning classifier system approach. *J Am Med Inform Assoc* **2013,** *20* (4), 603-12.
35. Jeon, J.; Nim, S.; Teyra, J.; Datti, A.; Wrana, J. L.; Sidhu, S. S.; Moffat, J.; Kim, P. M., A systematic approach to identify novel cancer drug targets using machine learning, inhibitor design and high-throughput screening. *Genome Medicine* **2014,** *6* (7), 57.
36. Kelleher, F. C.; Thomas, D. M., Molecular pathogenesis and targeted therapeutics in Ewing sarcoma/primitive neuroectodermal tumours. *Clin Sarcoma Res* **2012,** *2*, 6.
37. Arnaldez, F. I.; Helman, L. J., New Strategies in Ewings Sarcoma: Lost in Translation? *Clin Cancer Res* **2014,** *20* (12), 3050-6.
38. Giorgi, C.; Boro, A.; Rechfeld, F.; Lopez-Garcia, L. A.; Gierisch, M. E.; Schafer, B. W.; Niggli, F. K., PI3K/AKT signaling modulates transcriptional expression of EWS/FLI1 through specificity protein 1. *Oncotarget* **2015,** *6* (30), 28895-910.

39. Ren, K.; Lu, X.; Yao, N.; Chen, Y.; Yang, A.; Chen, H.; Zhang, J.; Wu, S.; Shi, X.; Wang, C.; Sun, X., Focal adhesion kinase overexpression and its impact on human osteosarcoma. *Oncotarget* **2015,** *6* (31), 31085-103.
40. Hu, C.; Chen, X.; Wen, J.; Gong, L.; Liu, Z.; Wang, J.; Liang, J.; Hu, F.; Zhou, Q.; Wei, L.; Shen, Y.; Zhang, W., Antitumor effect of focal adhesion kinase inhibitor PF562271 against human osteosarcoma in vitro and in vivo. *Cancer Sci* **2017,** *108* (7), 1347-1356.
41. Bishop, M. W.; Janeway, K. A., Emerging concepts for PI3K/mTOR inhibition as a potential treatment for osteosarcoma. *F1000Res* **2016,** *5*.
42. Moniz, L.; Dutt, P.; Haider, N.; Stambolic, V., Nek family of kinases in cell cycle, checkpoint control and cancer. *Cell Div* **2011,** *6*, 18.
43. Lavalle, C. R.; Bravo-Altamirano, K.; Giridhar, K. V.; Chen, J.; Sharlow, E.; Lazo, J. S.; Wipf, P.; Wang, Q. J., Novel protein kinase D inhibitors cause potent arrest in prostate cancer cell growth and motility. *BMC Chem Biol* **2010,** *10*, 5.
44. Wei, N.; Chu, E.; Wipf, P.; Schmitz, J. C., Protein kinase d as a potential chemotherapeutic target for colorectal cancer. *Mol Cancer Ther* **2014,** *13* (5), 1130-41.
45. Durand, N.; Borges, S.; Storz, P., Functional and therapeutic significance of Protein Kinase D enzymes in invasive breast cancer. *Cell Mol Life Sci* **2015,** *72* (22), 4369-82.
46. Harikumar, K. B.; Kunnumakkara, A. B.; Ochi, N.; Tong, Z.; Deorukhkar, A.; Sung, B.; Kelland, L.; Jamieson, S.; Sutherland, R.; Raynham, T.; Charles, M.; Bagherzadeh, A.; Foxton, C.; Boakes, A.; Farooq, M.; Maru, D.; Diagaradjane, P.; Matsuo, Y.; Sinnett-Smith, J.; Gelovani, J.; Krishnan, S.; Aggarwal, B. B.; Rozengurt, E.; Ireson, C. R.; Guha, S., A novel small-molecule inhibitor of protein kinase D blocks pancreatic cancer growth in vitro and in vivo. *Mol Cancer Ther* **2010,** *9* (5), 1136-46.
47. Avriyanti, E.; Atik, N.; Kunii, M.; Furumoto, N.; Iwano, T.; Yoshimura, S.; Harada, R.; Harada, A., Functional redundancy of protein kinase D1 and protein kinase D2 in neuronal polarity. *Neurosci Res* **2015,** *95*, 12-20.
48. Bravo-Altamirano, K.; George, K. M.; Frantz, M. C.; Lavalle, C. R.; Tandon, M.; Leimgruber, S.; Sharlow, E. R.; Lazo, J. S.; Wang, Q. J.; Wipf, P., Synthesis and Structure-Activity Relationships of Benzothienothiazepinone Inhibitors of Protein Kinase D. *ACS Med Chem Lett* **2011,** *2* (2), 154-159.
49. Ni, Y.; Sinnett-Smith, J.; Young, S. H.; Rozengurt, E., PKD1 mediates negative feedback of PI3K/Akt activation in response to G protein-coupled receptors. *PLoS One* **2013,** *8* (9), e73149.
50. Campbell, J.; Ryan, C.; Brough, R.; Bajrami, I.; Pemberton, H.; Chong, I.; Costa-Cabral, S.; Frankum, J.; Gulati, A.; Holme, H.; Miller, R.; Postel-Vinay, S.; Rafiq, R.; Wei, W.; Williamson, C.; Quigley, D.; Tym, J.; Al-Lazikani, B.; Fenton, T.; Natrajan, R.; Strauss, S.; Ashworth, A.; Lord, C., Large-Scale Profiling of Kinase Dependencies in Cancer Cell Lines. In *Cell Rep*, 2016; Vol. 14, pp 2490-501.
51. Arora, S.; Gonzales, I. M.; Hagelstrom, R. T.; Beaudry, C.; Choudhary, A.; Sima, C.; Tibes, R.; Mousses, S.; Azorsa, D. O., RNAi phenotype profiling of kinases identifies potential therapeutic targets in Ewing's sarcoma. *Mol Cancer* **2010,** *9*, 218.
52. Chou, T. C., Drug combination studies and their synergy quantification using the Chou-Talalay method. *Cancer Res* **2010,** *70* (2), 440-6.

53. Chou, T.-C., Theoretical Basis, Experimental Design, and Computerized Simulation of Synergism and Antagonism in Drug Combination Studies. *Pharmacological Reviews* **2006,** *58* (3), 621–681.
54. Fry, D. W.; Harvey, P. J.; Keller, P. R.; Elliott, W. L.; Meade, M.; Trachet, E.; Albassam, M.; Zheng, X.; Leopold, W. R.; Pryer, N. K.; Toogood, P. L., Specific inhibition of cyclin-dependent kinase 4/6 by PD 0332991 and associated antitumor activity in human tumor xenografts. *Mol Cancer Ther* **2004,** *3* (11), 1427-38.
55. Politz, O.; Siegel, F.; Barfacker, L.; Bomer, U.; Hagebarth, A.; Scott, W. J.; Michels, M.; Ince, S.; Neuhaus, R.; Meyer, K.; Fernandez-Montalvan, A. E.; Liu, N.; von Nussbaum, F.; Mumberg, D.; Ziegelbauer, K., BAY 1125976, a selective allosteric AKT1/2 inhibitor, exhibits high efficacy on AKT signaling-dependent tumor growth in mouse models. *Int J Cancer* **2017,** *140* (2), 449-459.
56. Addie, M.; Ballard, P.; Buttar, D.; Crafter, C.; Currie, G.; Davies, B. R.; Debreczeni, J.; Dry, H.; Dudley, P.; Greenwood, R.; Johnson, P. D.; Kettle, J. G.; Lane, C.; Lamont, G.; Leach, A.; Luke, R. W.; Morris, J.; Ogilvie, D.; Page, K.; Pass, M.; Pearson, S.; Ruston, L., Discovery of 4-amino-N-[(1S)-1-(4-chlorophenyl)-3-hydroxypropyl]-1-(7H-pyrrolo[2,3-d]pyrimidin-4-yl)piperidine-4-carboxamide (AZD5363), an orally bioavailable, potent inhibitor of Akt kinases. *J Med Chem* **2013,** *56* (5), 2059-73.
57. Chou, T. C.; Talalay, P., Quantitative analysis of dose-effect relationships: the combined effects of multiple drugs or enzyme inhibitors. *Adv Enzyme Regul* **1984,** *22*, 27-55.
58. Chou; T.C.; N., M., CompuSyn for drug combinations: PC software and user's guide: a computer program for quantitation of synergism and antagonism in drug combinations, and the determination of IC50 and ED50 and LD50 values. ComboSyn (Paramus, NJ.) 2005.
59. Haddad, J. J., VX-745. Vertex Pharmaceuticals. *Curr Opin Investig Drugs* **2001,** *2* (8), 1070-6.
60. Laporte, A. N.; Ji, J. X.; Ma, L.; Nielsen, T. O.; Brodin, B. A., Identification of cytotoxic agents disrupting synovial sarcoma oncoprotein interactions by proximity ligation assay. *Oncotarget* **2016,** *7* (23), 34384-94.
61. Su, L.; Sampaio, A. V.; Jones, K. B.; Pacheco, M.; Goytain, A.; Lin, S.; Poulin, N.; Yi, L.; Rossi, F. M.; Kast, J.; Capecchi, M. R.; Underhill, T. M.; Nielsen, T. O., Deconstruction of the SS18-SSX Fusion Oncoprotein Complex: Insights into Disease Etiology and Therapeutics. *Cancer Cell* **2012,** *21* (3), 333-47.
62. Metz, J. T.; Johnson, E. F.; Soni, N. B.; Merta, P. J.; Kifle, L.; Hajduk, P. J., Navigating the kinome. *Nat Chem Biol* **2011,** *7* (4), 200-2.

CHAPTER III

Target Identification in Triple Negative Breast Cancer Patient Derived Xenograft Cell Cultures with a Profiled Kinase Inhibitor Library

Abstract

Triple negative breast cancer (TNBC) is a particularly aggressive subtype of breast cancer with poor prognosis and a lack of effective targeted therapies. Patient-derived xenografts (PDXs) are a promising avenue to improve the success of cancer drug development by better modeling patient tumors. In an effort to discover actionable molecular targets, I employ the profiled kinase inhibitor-based target identification platform from **Chapter II** in short-term *ex vivo* cell cultures of TNBC PDXs. I identify target kinases in ten established TNBC PDXs using this framework. Using kinase target scores to cluster these TNBC PDXs revealed heterogeneous sensitivity to kinase inhibition. Additionally, several kinases were identified as targets in at least half of the PDX screens, with some having little or early emergent evidence of importance in TNBC. This chapter highlights how higher cellular models can be leveraged when combining target- and phenotypic-based screening.[†] [‡]

Introduction

In drug discovery, cancer cell lines have been widely used in identifying disease targets, lead compounds, and biomarkers.[1-3] However, cancer cell lines have a variety of shortcomings which have hindered success in cancer drug development. These include: low heterogeneity as compared to patient tumors; clonal selection from long-term growth in cell culture conditions such that the cell lines may no longer behave like or embody the

[†]Tumor implantation, maintenance, and harvest of PDXs were performed by Xu Cheng and Rabia Gilani (University of Michigan).

[‡] Curation of inhibitor profiling data, kinase grouping, and kinase scoring using a machine learning algorithm was performed by Hassan Al-Ali (University of Miami).

parental cancer cells; and no longer representing the tumor microenvironment especially when grown on plastic.[4, 5] Several *in vitro* strategies to overcome these limitations have been implemented in cancer research. Co-cultures *in vitro*, where multiple cell types of a tumor are exposed to one another, help recreate the tumor environment.[6] Additionally, 3D cell cultures can be used to incorporate cell-cell and cell-extracellular matrix (ECM) interactions in *in vitro* models as well. Three-dimensional culture technologies, which range from spheroids or cells embedded in purified basement membrane extract, are regarded as a more stringent model that is better representative of the tumor environment compared to 2D models.[7] For example, 3D cultures are known to take into account diffusion limited nutrient supply in addition to the above mention cell-cell and cell-ECM contacts.[3, 7] Two-dimensional models are otherwise agnostic to these factors. Furthermore, advancements in these technologies have enabled their use in high-throughput studies.[3, 7, 8]

In *in vivo* studies, mouse xenografts of implanted cancer cell lines have widely been used in the evaluation of drug efficacy. However, it has been widely recognized that these models are poor predictors of success in clinical cancer trials. One reason is that the mice used are often immunocompromised to enable engraftment of human cancer cell lines. Thus, these models fail to take into account the immune system in the context of the progression of the tumor, which has been shown to be vital.[9, 10] In cases where the immune system must be taken into account, mice with humanized immune systems can be used.[10] Another key limitation of cancer cell line xenografts is that they lack the heterogeneity and molecular characteristics that are found in patient tumors, which is true of the cancer cell lines themselves.[3-5] Models that account for this heterogeneity and patient molecular features are positioned to be invaluable in cancer discovery.

Patient-derived xenografts (PDXs), where primary patient tumor material is explanted into immunocompromised mice, overcome these obstacles and thus have the potential to greatly improve success rates of cancer drug discovery studies.[11-14] These models are an improvement over traditional cancer cell line xenografts in that they are more likely to maintain the molecular characteristics and heterogeneity present in parental tumors.[4] Indeed, PDX response has been shown to accurately predict chemotherapeutic drug response in cancer patients.[13] Thus, PDX models have been

proposed has patient avatars to evaluate drug response for individual patients.[10] However, it is worth noting that PDXs share a limitation with cancer cell line xenografts, in that the immune system's role in tumor progression may not be fully taken into account.[9] Still, PDXs are widely regarded as highly clinically relevant models for cancer which, as described in **Chapter I**, are extremely valuable for phenotypic-based screening. A PDX-based phenotypic screen, such as the one described in **Chapter II**, would be extremely useful in identifying targets of clinical significance.

Triple negative breast cancer (TNBC) is an extremely aggressive breast cancer subtype that is highly lethal due to increased risks of metastasis and early reoccurrence.[15, 16] TNBCs are so named for their lack of expression of estrogen and progestogen receptors (ER and PR), and lack of overexpression of human epidermal growth factor receptor 2 (HER2). Thus, TNBC patients do not benefit from therapies targeting these receptors which have been successful in other breast cancer subtypes.[17, 18] The surprising heterogeneity and lack of predictive markers for patient response to targeted therapy have hindered the path to FDA-approved targeted drugs for TNBCs.[18, 19] With conventional cytotoxic chemotherapies as the current standard treatment, the benefits of effective molecular targeted therapies would be a boon for TNBC treatment.[19, 20] With this need in mind, I moved to apply the profiled kinase inhibitor-based target identification platform against an available panel of TNBC PDXs to discover actionable and clinically relevant targets. Herein, this ongoing effort is described.

A TNBC PDX Panel

Prof. Sofia Merajver and her group have acquired and developed a bank of over 30 TNBC PDXs. PDXs were maintained by passaging from mouse to mouse until the tumor burden became too high. To preserve the molecular characteristics of parental tumor, PDX tumor samples were saved and stored at low passages to be used as needed. In all experiments described herein, low passage tumors (<5) were used. Through collaboration with the Merajver group I have access to this extensive bank of TNBC PDXs.[†]

Short-term PDX Cell Cultures for High-Throughput Screening

High-throughput screening with PDXs is highly impractical due to size, cost, and technical limitations. For this reason, cell cultures that are derived from PDXs for use in *ex vivo* studies would be highly valuable for such screens. Such a use is directly analogous to the application of cancer cell lines in high-throughput screens (i.e. as described in **Chapter II**). Recently, Bruna et al. showed that short-term cell cultures derived from PDXs retain the molecular characteristics and heterogeneity of PDX tumors as well as the parental tumors from which they are derived.[4] It was also demonstrated that drug response in these *ex vivo* cultures matched the response of the PDX *in vivo*. I thus moved to establish short-term TNBC PDX-derived cell cultures through isolation of tumor cells.

I chose to use 3D cultures in this screening methodology which, as described above, have been shown to better mimic cell-cell and cell-ECM interaction as compared to 2D cultures. My 3D model of choice was suspension culture which promotes cell-cell adhesion in suspension culture. Through the Merajver Lab, I obtained isolated tumor cells from PDX mice following established preparations (outlined in **Figure 3.1** and materials and methods).[†] The resulting human tumor cells and tumor associated cells were plated in 384-well ultra-low attachment plates. The PDX-derived cell cultures resulted in spheroid formation over a span of 5 days. Presence of drug at the time of plating results in dose-dependent response after five days of culture with disrupted spheroid and cell aggregate formation (**Figure 3.1**). This dose response is also reflected in a high-lytic luminescence-based viability assay, amenable for high throughput screening (**Figure 3.1**).

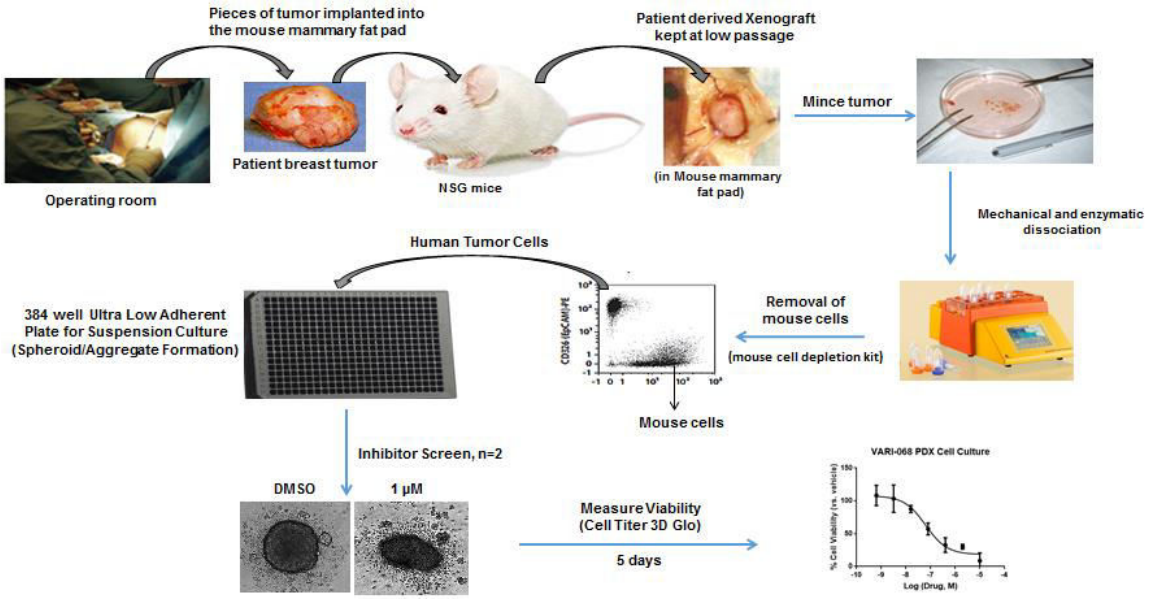

Figure 3.1: General workflow for preparation of assays using PDX derived cell cultures.

Satisfied that the short-term PDX-derived 3D cell cultures could be applied to a high-throughput format measuring drug response, I screened against the profiled kinase inhibitor library. The phenotypic screen was performed in duplicate at a concentration of 1 µM with viability measured after 5 days of compound exposure (dosing the same day as plating). With the acquired viability data, I applied the target identification methodology and scored kinase groups for each screen as described in **Chapter II**. In total, 10 PDX-derived cell cultures were screened. A full listing of the kinase group scores can be found in **Table B.1**.‡

Clustering TNBC PDXs using Kinase Group Target Scores

The heterogeneity of TNBC has proven to be an obstacle in establishing new treatments in clinical studies. Alternative ways to classify cancers that can complement more traditional methods such as RNAseq, IHC, and proteomic analysis would be valuable in improving the high attrition rate of drug discovery projects. Clustering PDXs based upon sensitivity to functional inhibition of proteins could provide a new layer of information that would aid in this end. Such a method also has the obvious benefit of relating its established subtypes directly to drug sensitivity. Thus, I subtyped the TNBC PDXs based on sensitivity to kinase inhibition. I employed unsupervised hierarchal

clustering using the combination scores of kinase groups. Consistent with what is known about TNBC, this subtyping returned a heterogeneous clustering result of the TNBC PDX screens (**Figure 3.2**). In other words, the PDX cell cultures overall were different in their sensitivities to specific kinase inhibition. Additional screening of other TNBC PDXs is currently underway and their kinase group target scores will be added to this analysis.

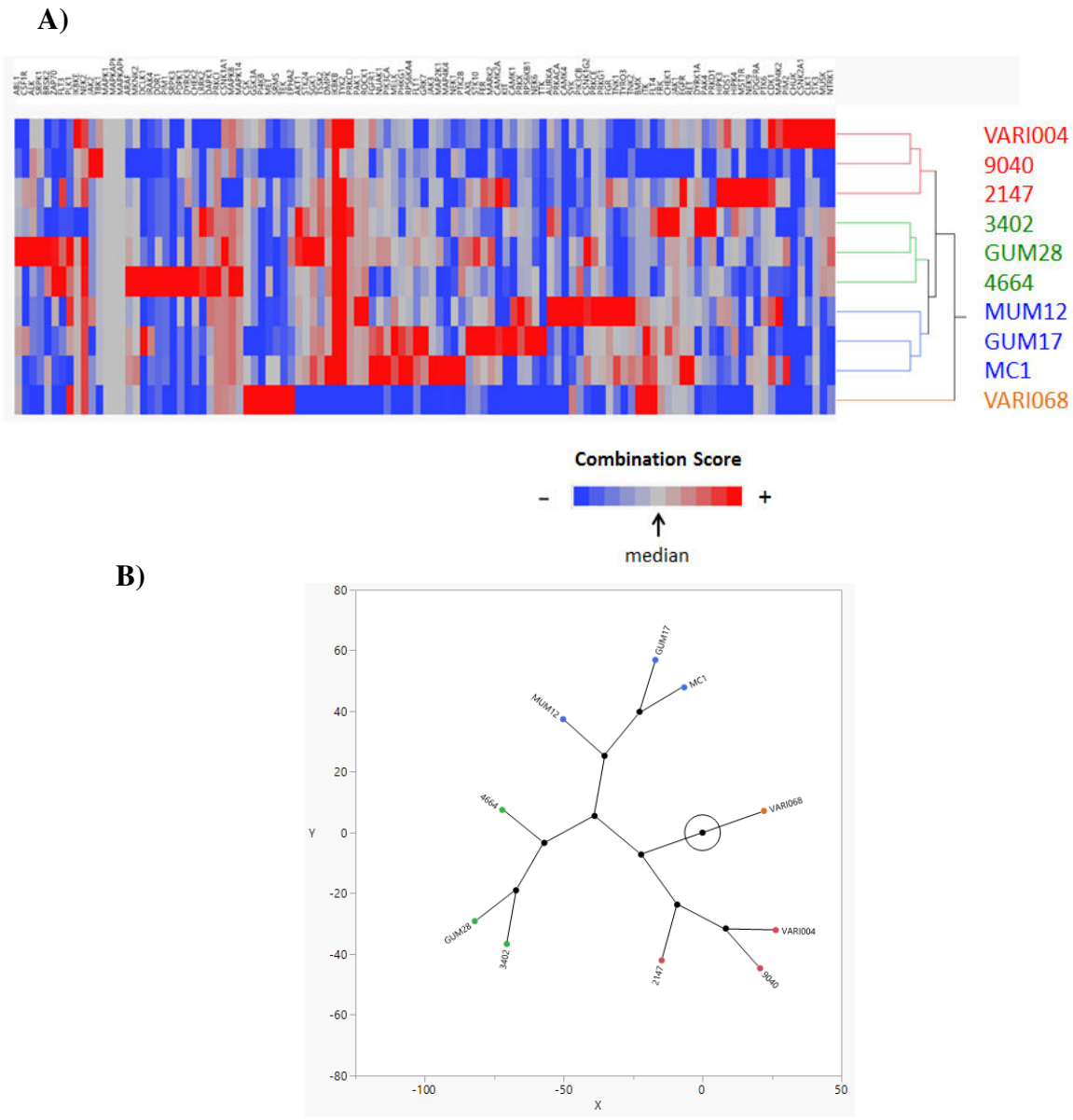

Figure 3.2: Unsupervised hierarchal clustering results of TNBC PDXs based on kinase inhibition sensitivity. Combination scores of kinase groups were used. **A)** Two-way clustering result of PDXs and kinase groups (one representative kinase for groups shown). **B)** Constellation plot of the PDX clusters. The circle represents the dendrogram tree stem.

Highly Scored Kinase Targets Identified Across TNBC PDX Screens

I identified the highest scoring target kinase groups (Top 15 by Combined Score) in each PDX screen to see if inhibition of any kinase was broadly effective in TNBC. Comparisons of these results revealed some common kinase groups present in at least half of the PDXs screened (**Table 3.1**). Several of these identified kinase groups have established and/or have emerging importance in TNBCs. PIK3CA was identified as a target in 9/10 PDX screens, and the PIK3/AKT pathway is commonly altered in TNBC.[21] The CDKs (5/10 screens) have proven to be promising targets in preclinical studies, and phase 2 trials with inhibitors of these kinases are underway. Downstream effectors of IGF1R (5/10 screens) signaling has been shown to be increased in malignant tissue in African American patients and IGF1R expression levels correlate with shorter survival.[22-24] Inhibitors of IGF1R and INSR have also shown efficacy in *in vivo* models.[25] Several papers have identified PLK1 (6/10 screens) as a potential therapeutic target in combination with conventional chemotherapy in TNBC.[26] High expression of PTK2B (FAK) (6/10 screens), has been shown to be associated with more invasive TNBC phenotypes.[27] Lastly, SRC (or SRC Family Kinases) was identified as a target in 5/10 screens. Recenlty it has be shown that inhibition of SRC can prevent tumor growth *in vivo*.[28] Together, these precedents in the literature demonstrate that this target identification methodology, when paired with clinically relevant PDX models, can distinguish kinase groups that are important in TNBC.

Table 3.1: Most frequent kinase target groups identified as targets in the PDX target identification screen. A kinase group was counted as a target if it was in the top 15 groups ranked by highest Combined Score. Those that were identified in in at least 5/10 screens are shown. Kinase groups listed in red are ones with novel or early emerging significance in TNBC.

# of PDXs	Kinase Targets Groups (one row = one group of pharmacologically-linked kinases)
9	PIK3CA
6	SIK2 SIK3 SIK1 MARK2 MARK1 MARK3 MARK4
6	PTK2B (FAK)
6	PLK1
5	FER FES
5	CDK1 CDK2 CDK3 CDK4 CDK6 CDK5
5	IGF1R TSSK1B TSSK2 INSR INSRR
5	SRC YES1 FGR HCK FYN BLK LCK LYN

Of greater interest are the kinase groups that were highly scored across PDX screens that are not established targets and/or have very early emerging importance in TNBC in the literature. The FES/FER kinase group was highly scored across 5 of the 10 PDX screens. I have not found literature where FES/FER was reliably proven to be targets in TNBC pharmacologically. This is due, in part, to the scarcity of selective inhibitors published for these kinases.[29] Despite this, there have been intriguing genomic results in some TNBC studies concerning FES/FER. RNAi of FER kinase results in decreased viable cell count compared to control in TNBC cell lines.[30, 31] Additionally, FER was found to contribute to pro-invasive features in TNBC cell lines, and knockdown of FER in MDA-MB-231 TNBC xenograft mice significantly abrogated tumor growth.[31] FES on the other hand was found to have pro-tumorigenic functions within the breast tumor niche in studies with knockout mice.[32] This role of FES has not been investigated in the TNBC subtype specifically. In light of this emerging genetic-based evidence of FER/FES importance in TNBC, syntheses of selective inhibitors for these kinases are currently being planned. Such inhibitors will further validate these kinases as targets pharmacologically.

There is less evidence in the literature of the MARK/SIK kinase group concerning TNBC. However, a recent study illustrated, again with primarily genetic experiments, that SIK2 is important in restricting autophagy in TNBC cells.[33] This was particularly true with TNBC cell lines of the claudin-low subtype.[33] In one example, genetic knockdown of SIK2 resulted in decreased tumor growth *in vivo* with the claudin-low TNBC cell line SUM159.[33] The finding that SIK2 kinase has more therapeutic importance in a subset of TNBC highlights that this subtype is itself heterogeneous, and that targets may be more important in one TNBC subtype than others. Like FER/FES, syntheses of selective inhibitors of these kinases are currently being planned to further validate them pharmacologically as targets.

Conclusions

PDXs have been positioned as one way to improve the success rate cancer drug development by better modeling patient tumor microenvironment and tumor heterogeneity. From the success in identifying new targets specific to cancer subtypes, I

combined the profiled kinase inhibitor target identification approach from **Chapter II** with PDX-derived models to discover clinically relevant and actionable drug targets in TNBC. I used short-term PDX-derived 3D cell culture model that has been previously shown to retain molecular characteristics of the PDX and parent primary tumors. I identified several kinase groups that scored highly as targets in at least half of the screens. Some of these have been well established as targets or possible targets in the literature, demonstrating that this method and PDX models can distinguish therapeutically relevant kinases. More importantly, I identified the FES/FER and MARK/SIK kinase groups as targets, which represent possible novel pharmacological findings in TNBC. Early evidence of these kinases as targets in TNBC has only been genetic in nature. In addition to supporting the emerging evidence of these kinases as TNBC targets, this pharmacological based approach indicates that these putative target kinases can be actionable. Studies to design and synthesize selective inhibitors for these kinases are being planned.

TNBC is itself a heterogeneous cancer which has, in part, resulted in a lack of FDA-approved targeted therapies. Alternative ways of subtyping this disease, as well as others, would aid in classifying patients as candidates who would respond to specific targeted therapies, thus improving outcome. To this end, I used the kinase target scores as a means of unsupervised hierarchal clustering of the PDXs screened. I observed heterogeneous clustering of the PDXs using this method. I plan to continue TNBC PDX screens and to use their results for further clustering.

The worked outlined in the chapter demonstrates how clinically relevant models can be leveraged for target discovery. While the use of PDXs in this chapter and in cancer research overall is noteworthy, it is important to appreciate that the PDXs fail to accurately model patient immune system. As mentioned above, this is because of the use of immunocompromised mice in their generation. Patient-derived mouse models with humanized immune systems will help to overcome this shortcoming.[10] Additionally, testing tumor samples taken directly from the patient with drug may also provide a way forward. Directly testing drugs on isolated patient cancer cells of blood-based cancers, such as leukemia, has steadily gained traction.[34, 35] However, directly testing cancer cells from solid tumors, such as breast cancer presents a challenge. Sample size, appropriate

culture conditions, time, and general experimental logistics are only a few considerations that need to be taken into account.[36-38] As our understanding progresses of what it takes for efficient and successful establishment of *ex vivo* cancer patient martial, we will be even closer in achieving personalized drug studies. Such studies, when combined with target identification methodologies like the one described in this chapter, will enable discovery of cancer targets on a patient-to-patient basis.

Materials and Methods

PDX Tumor Preparation

Tumor samples were obtained either directly from patient or from previous implantation from mouse for secondary implantation, or from frozen sample. If from frozen sample for implantation, sample was rapidly thawed in 37 °C water bath and put directly into sterile petri dish with a HBSS to wash. Tumor samples were cut into tiny pieces in sterile conditions, at least 2x2x2 mm^3. Tumor pieces were then implanted into the mammary fat pad in NSG mice. Fresh tumors were harvested once they reach to 0.8-1cm in diameter for organoid and spheroid culture. Freshly excised tumor tissue was washed with 1x pbs/HBBS in a 10 cm Petridish, cut into small pieces using scalpels while removing any obvious necrotic tissue. Tumor pieces were dissociated into single-cell suspensions by combining mechanical dissociation with enzymatic degradation using a tumor dissociation kit (MACS Miltenyi Biotec) following manufacturer's instructions. This work was primarily performed by Rabia Gilani and Xu Cheng (University of Michigan).[†]

Processing PDX Tumor Tissue into Suspension Culture for Drug Screening

Digested PDX tumor suspensions were subjected to a mouse cell depletion kit (MACS Miltenyi Biotec) following manufacturer's instructions. Eluted cells were pelleted by gentle centrifugation (5 min, 120 x g) and resuspended in suspension media (DMEM, 1X B-27 serum-free supplements, 1X insulin transferrin selenite ethanolamine, 1X non-essential amino acids, EGF (10 ng/mL), bFGF (10 ng/mL), Antibiotics). From this solution the concentration of viable cells was measured. Cells were then seeded into Costar Ultralow Attachment 384-well opaque-sided plates at a density of 7000 viable cells/well (if the total number of viable cells allowed). After seeding, the plates were briefly centrifuged (30 sec, 100 x g).

Phenotypic Screen with a Profiled Kinase Inhibitor Library

Cell cultures derived from ten PDXs (9040, VARI068, VARI004, GUM17, GUM28, 4664, 2147, 3402, MUM12, MC1) were treated the same day of plating with a

profiled kinase inhibitor library (see **Chapter II** for details). In the primary screen, 2 μL of the 1 mM (1000X) DMSO master stocks were diluted into 200 uL of suspension cell culture media. From these daughter plates, 5 μL was added to each cell culture well to give 1 μM final compound concentrations (0.1% DMSO final concentration). The screen was performed in duplicate and the viabilities measured after 5 days of compound incubation using a highly lytic luminescence-based assay (Cell Titer-Glo 3D Cell Viability Assay (Promega)) following manufacturer instructions. The viabilities were averaged and compared to vehicle. Viabilities were converted to z-scores on a per plate basis (z-score = (x - vehicle)/(vehicle stdev.)). Plots summarizing this data for each screen can be found in **Appendix B**.

Target Deconvolution by Machine Learning-based Algorithm

I used a similar method as described in **Chapter II** to score and identify target kinase groups. Briefly, I excluded from this analysis compounds whose z-score fell between -1 and 1. This stratification accentuates differences between the hit and non-hit categories and improves selection of relevant kinases. The remaining compounds comprised the input for the analysis. For VARI004 (486 compounds; 35 stratified hits and 435 stratified non-hits), 2147 (1036 compounds; 199 stratified hits and 837 stratified non-hits), 3402 (838 compounds; 137 stratified hits and 701 stratified non-hits), 4664 (1036 compounds; 394 stratified hits and 642 stratified non-hits), 9040 (534 compounds; 59 stratified hits and 475 stratified non-hits), MUM12 (1036 compounds; 232 stratified hits and 804 stratified non-hits), GUM17 (534 compounds; 105 stratified hits and 429 stratified non-hits), GUM28 (982 compounds; 263 stratified hits and 719 stratified non-hits), MC1 (534 compounds; 79 stratified hits and 455 stratified non-hits), and VARI068 (489 compounds; 101 stratified hits and 388 stratified non-hits) screens, compounds with profiling data against 237 wildtype kinases constituted the input for analysis. Generation of kinase groups and calculation of their MAXIS scores, hit/non-hit inhibition bias (B_k), and Combined Scores within each phenotypic screen using a Support Vector Machine was performed by Hassan Al-Ali (University of Miami) as previously described.[39] ‡

Hierarchal Clustering Analysis

I performed unsupervised hierarchal clustering using kinase group combination scores for each of the screens. I employed JMP 13 (SAS Institute Inc.) statistical software to perform the clustering analysis using the Average method of calculating cluster distances. The clustering history for both PDX screens and kinases can be found in **Table B.2**.

References

1. Heiser, L. M.; Sadanandam, A.; Kuo, W. L.; Benz, S. C.; Goldstein, T. C.; Ng, S.; Gibb, W. J.; Wang, N. J.; Ziyad, S.; Tong, F.; Bayani, N.; Hu, Z.; Billig, J. I.; Dueregger, A.; Lewis, S.; Jakkula, L.; Korkola, J. E.; Durinck, S.; Pepin, F.; Guan, Y.; Purdom, E.; Neuvial, P.; Bengtsson, H.; Wood, K. W.; Smith, P. G.; Vassilev, L. T.; Hennessy, B. T.; Greshock, J.; Bachman, K. E.; Hardwicke, M. A.; Park, J. W.; Marton, L. J.; Wolf, D. M.; Collisson, E. A.; Neve, R. M.; Mills, G. B.; Speed, T. P.; Feiler, H. S.; Wooster, R. F.; Haussler, D.; Stuart, J. M.; Gray, J. W.; Spellman, P. T., Subtype and pathway specific responses to anticancer compounds in breast cancer. *Proc Natl Acad Sci U S A* **2012,** *109* (8), 2724-9.
2. Weinstein, J. N., Integromic analysis of the NCI-60 cancer cell lines. *Breast Dis* **2004,** *19*, 11-22.
3. Moffat, J. G.; Rudolph, J.; Bailey, D., Phenotypic screening in cancer drug discovery [mdash] past, present and future. *Nature Reviews Drug Discovery* **2014,** *13*, 588-602.
4. Bruna, A.; Rueda, O.; Greenwood, W.; Batra, A.; Callari, M.; Batra, R.; Pogrebniak, K.; Sandoval, J.; Cassidy, J.; Tufegdzic-Vidakovic, A.; Sammut, S. J.; Jones, L.; Provenzano, E.; Baird, R.; Eirew, P.; Hadfield, J.; Eldridge, M.; McLaren-Douglas, A.; Barthorpe, A.; Lightfoot, H.; O'Connor, M.; Gray, J.; Cortes, J.; Baselga, J.; Marangoni, E.; Welm, A.; Aparicio, S.; Serra, V.; Garnett, M.; Caldas, C., A Biobank of Breast Cancer Explants with Preserved Intra-tumor Heterogeneity to Screen Anticancer Compounds. *Cell* **2016,** *167* (1), 260-274 e22.
5. Gillet, J. P.; Varma, S.; Gottesman, M. M., The Clinical Relevance of Cancer Cell Lines. *J Natl Cancer Inst* **2013,** *105* (7), 452-8.
6. Korff, T.; Augustin, H. G., Integration of endothelial cells in multicellular spheroids prevents apoptosis and induces differentiation. *J Cell Biol* **1998,** *143* (5), 1341-52.
7. Kimlin, L. C.; Casagrande, G.; Virador, V. M., In vitro three-dimensional (3D) models in cancer research: an update. *Mol Carcinog* **2013,** *52* (3), 167-82.
8. Li, Q.; Chen, C.; Kapadia, A.; Zhou, Q.; Harper, M. K.; Schaack, J.; LaBarbera, D. V., 3D models of epithelial-mesenchymal transition in breast cancer metastasis: high-throughput screening assay development, validation, and pilot screen. *J Biomol Screen* **2011,** *16* (2), 141-54.
9. Goodspeed, A.; Heiser, L. M.; Gray, J. W.; Costello, J. C., Tumor-Derived Cell Lines as Molecular Models of Cancer Pharmacogenomics. *Mol Cancer Res* **2016,** *14* (1), 3-13.
10. Lodhia, K. A.; Hadley, A. M.; Haluska, P.; Scott, C. L., Prioritizing therapeutic targets using patient-derived xenograft models. *Biochim Biophys Acta* **2015,** *1855* (2), 223-34.
11. Cassidy, J. W.; Caldas, C.; Bruna, A., Maintaining Tumor Heterogeneity in Patient-Derived Tumor Xenografts. *Cancer Res* **2015,** *75* (15), 2963-8.
12. Aparicio, S.; Hidalgo, M.; Kung, A. L., Examining the utility of patient-derived xenograft mouse models. *Nat Rev Cancer* **2015,** *15* (5), 311-6.
13. Gao, H.; Korn, J. M.; Ferretti, S.; Monahan, J. E.; Wang, Y.; Singh, M.; Zhang, C.; Schnell, C.; Yang, G.; Zhang, Y.; Balbin, O. A.; Barbe, S.; Cai, H.; Casey, F.;

Chatterjee, S.; Chiang, D. Y.; Chuai, S.; Cogan, S. M.; Collins, S. D.; Dammassa, E.; Ebel, N.; Embry, M.; Green, J.; Kauffmann, A.; Kowal, C.; Leary, R. J.; Lehar, J.; Liang, Y.; Loo, A.; Lorenzana, E.; Robert McDonald, E., 3rd; McLaughlin, M. E.; Merkin, J.; Meyer, R.; Naylor, T. L.; Patawaran, M.; Reddy, A.; Roelli, C.; Ruddy, D. A.; Salangsang, F.; Santacroce, F.; Singh, A. P.; Tang, Y.; Tinetto, W.; Tobler, S.; Velazquez, R.; Venkatesan, K.; Von Arx, F.; Wang, H. Q.; Wang, Z.; Wiesmann, M.; Wyss, D.; Xu, F.; Bitter, H.; Atadja, P.; Lees, E.; Hofmann, F.; Li, E.; Keen, N.; Cozens, R.; Jensen, M. R.; Pryer, N. K.; Williams, J. A.; Sellers, W. R., High-throughput screening using patient-derived tumor xenografts to predict clinical trial drug response. *Nat Med* **2015,** *21* (11), 1318-25.

14. Hidalgo, M.; Amant, F.; Biankin, A. V.; Budinska, E.; Byrne, A. T.; Caldas, C.; Clarke, R. B.; de Jong, S.; Jonkers, J.; Maelandsmo, G. M.; Roman-Roman, S.; Seoane, J.; Trusolino, L.; Villanueva, A., Patient-derived xenograft models: an emerging platform for translational cancer research. *Cancer Discov* **2014,** *4* (9), 998-1013.

15. Carey L , e. a., Triple-negative breast cancer: disease entity or title of convenience? *Nat Rev Clin Oncol.* **2010,** *7* (12), 683-692.

16. Anders, C. K.; Carey, L. A., Biology, Metastatic Patterns, and Treatment of Patients with Triple-Negative Breast Cancer. *Clin Breast Cancer.* **2009,** *9* (Supple 2), S73-S81.

17. Siegel, R. L.; Miller, K. D.; Jemal, A., Cancer statistics, 2015. *CA Cancer J Clin* **2015,** *65* (1), 5-29.

18. Bayraktar, S.; Gluck, S., Molecularly targeted therapies for metastatic triple-negative breast cancer. *Breast Cancer Res Treat* **2013,** *138* (1), 21-35.

19. Bianchini, G.; Balko, J. M.; Mayer, I. A.; Sanders, M. E.; Gianni, L., Triple-negative breast cancer: challenges and opportunities of a heterogeneous disease. *Nature Reviews Clinical Oncology* **2016,** *13*, 674-690.

20. Wahba, H. A.; El-Hadaad, H. A., Current approaches in treatment of triple-negative breast cancer. *Cancer Biol Med* **2015,** *12* (2), 106-16.

21. Cossu-Rocca, P.; Orru, S.; Muroni, M. R.; Sanges, F.; Sotgiu, G.; Ena, S.; Pira, G.; Murgia, L.; Manca, A.; Uras, M. G.; Sarobba, M. G.; Urru, S.; De Miglio, M. R., Analysis of PIK3CA Mutations and Activation Pathways in Triple Negative Breast Cancer. *PLoS One* **2015,** *10* (11), e0141763.

22. Farabaugh, S. M.; Boone, D. N.; Lee, A. V., Role of IGF1R in Breast Cancer Subtypes, Stemness, and Lineage Differentiation. *Front Endocrinol (Lausanne)* **2015,** *6*, 59.

23. Kalla Singh, S.; Tan, Q. W.; Brito, C.; De Leon, M.; De Leon, D., Insulin-like growth factors I and II receptors in the breast cancer survival disparity among African-American women. *Growth Horm IGF Res* **2010,** *20* (3), 245-54.

24. Nielsen, T. O.; Andrews, H. N.; Cheang, M.; Kucab, J. E.; Hsu, F. D.; Ragaz, J.; Gilks, C. B.; Makretsov, N.; Bajdik, C. D.; Brookes, C.; Neckers, L. M.; Evdokimova, V.; Huntsman, D. G.; Dunn, S. E., Expression of the insulin-like growth factor I receptor and urokinase plasminogen activator in breast cancer is associated with poor survival: potential for intervention with 17-allylamino geldanamycin. *Cancer Res* **2004,** *64* (1), 286-91.

25. Litzenburger, B. C.; Creighton, C. J.; Tsimelzon, A.; Chan, B. T.; Hilsenbeck, S. G.; Wang, T.; Carboni, J. M.; Gottardis, M. M.; Huang, F.; Chang, J. C.; Lewis, M. T.;

Rimawi, M. F.; Lee, A. V., High IGF-IR activity in triple-negative breast cancer cell lines and tumorgrafts correlates with sensitivity to anti-IGF-IR therapy. *Clin Cancer Res* **2011,** *17* (8), 2314-27.
26. Maire, V.; Nemati, F.; Richardson, M.; Vincent-Salomon, A.; Tesson, B.; Rigaill, G.; Gravier, E.; Marty-Prouvost, B.; De Koning, L.; Lang, G.; Gentien, D.; Dumont, A.; Barillot, E.; Marangoni, E.; Decaudin, D.; Roman-Roman, S.; Pierre, A.; Cruzalegui, F.; Depil, S.; Tucker, G. C.; Dubois, T., Polo-like kinase 1: a potential therapeutic option in combination with conventional chemotherapy for the management of patients with triple-negative breast cancer. *Cancer Res* **2013,** *73* (2), 813-23.
27. Golubovskaya, V. M.; Ylagan, L.; Miller, A.; Hughes, M.; Wilson, J.; Wang, D.; Brese, E.; Bshara, W.; Edge, S.; Morrison, C.; Cance, W. G., High focal adhesion kinase expression in breast carcinoma is associated with lymphovascular invasion and triple-negative phenotype. *BMC Cancer* **2014,** *14* (1), 769.
28. Gilani, R. A.; Phadke, S.; Bao, L. W.; Lachacz, E. J.; Dziubinski, M. L.; Brandvold, K. R.; Steffey, M. E.; Kwarcinski, F. E.; Graveel, C. R.; Kidwell, K. M.; Merajver, S. D.; Soellner, M. B., UM-164: A Potent c-Src/p38 Kinase Inhibitor with In Vivo Activity against Triple-Negative Breast Cancer. *Clin Cancer Res* **2016,** *22* (20), 5087-5096.
29. Hellwig, S.; Miduturu, C. V.; Kanda, S.; Zhang, J.; Filippakopoulos, P.; Salah, E.; Deng, X.; Choi, H. G.; Zhou, W.; Hur, W.; Knapp, S.; Gray, N. S.; Smithgall, T. E., Small Molecule Inhibitors of the c-Fes Protein-tyrosine Kinase. *Chem Biol* **2012,** *19* (4), 529-40.
30. Muellner, M. K.; Mair, B.; Ibrahim, Y.; Kerzendorfer, C.; Lechtermann, H.; Trefzer, C.; Klepsch, F.; Müller, A. C.; Leitner, E.; Macho-Maschler, S.; Superti-Furga, G.; Bennett, K. L.; Baselga, J.; Rix, U.; Kubicek, S.; Colinge, J.; Serra, V.; Nijman, S. M., Targeting a cell state common to triple-negative breast cancers. *Mol Syst Biol* **2015,** *11* (2), 789.
31. Ivanova, I. A.; Vermeulen, J. F.; Ercan, C.; Houthuijzen, J. M.; Saig, F. A.; Vlug, E. J.; van der Wall, E.; van Diest, P. J.; Vooijs, M.; Derksen, P. W. B., FER kinase promotes breast cancer metastasis by regulating α6- and β1-integrin-dependent cell adhesion and anoikis resistance. *Oncogene* **2013,** *32* (50), 5582-92.
32. Zhang, S.; Chitu, V.; Stanley, E. R.; Elliott, B. E.; Greer, P. A., Fes tyrosine kinase expression in the tumor niche correlates with enhanced tumor growth, angiogenesis, circulating tumor cells, metastasis and infiltrating macrophages. *Cancer Res* **2011,** *71* (4), 1465-73.
33. Maxfield, K. E.; Macion, J.; Vankayalapati, H.; Whitehurst, A. W., SIK2 Restricts Autophagic Flux To Support Triple-Negative Breast Cancer Survival. *Mol Cell Biol* **2016,** *36* (24), 3048-3057.
34. Gockeritz, E.; Kerwien, S.; Baumann, M.; Wigger, M.; Vondey, V.; Neumann, L.; Landwehr, T.; Wendtner, C. M.; Klein, C.; Liu, N.; Hallek, M.; Frenzel, L. P.; Krause, G., Efficacy of phosphatidylinositol-3 kinase inhibitors with diverse isoform selectivity profiles for inhibiting the survival of chronic lymphocytic leukemia cells. *Int J Cancer* **2015,** *137* (9), 2234-42.
35. Tina, E.; Prenkert, M.; Hoglund, M.; Paul, C.; Tidefelt, U., Topoisomerase IIalpha expression in acute myeloid leukaemia cells that survive after exposure to daunorubicin or ara-C. *Oncol Rep* **2009,** *22* (6), 1527-31.

36. Naipal, K. A. T.; Verkaik, N. S.; Sánchez, H.; van Deurzen, C. H. H.; den Bakker, M. A.; Hoeijmakers, J. H. J.; Kanaar, R.; Vreeswijk, M. P. G.; Jager, A.; van Gent, D. C., Tumor slice culture system to assess drug response of primary breast cancer. *BMC Cancer* **2016,** *16* (1), 78.
37. Corben, A. D.; Uddin, M. M.; Crawford, B.; Farooq, M.; Modi, S.; Gerecitano, J.; Chiosis, G.; Alpaugh, M. L., Ex Vivo Treatment Response of Primary Tumors and/or Associated Metastases for Preclinical and Clinical Development of Therapeutics. *J Vis Exp* **2014,** (92), 52157.
38. Dean, J. L.; McClendon, A. K.; Hickey, T. E.; Butler, L. M.; Tilley, W. D.; Witkiewicz, A. K.; Knudsen, E. S., Therapeutic response to CDK4/6 inhibition in breast cancer defined by ex vivo analyses of human tumors. *Cell Cycle* **2012,** *11* (14), 2756-61.
39. Al-Ali, H.; Lee, D. H.; Danzi, M. C.; Nassif, H.; Gautam, P.; Wennerberg, K.; Zuercher, B.; Drewry, D. H.; Lee, J. K.; Lemmon, V. P.; Bixby, J. L., Rational Polypharmacology: Systematically Identifying and Engaging Multiple Drug Targets To Promote Axon Growth. *ACS Chem Biol* **2015,** *10* (8), 1939-51.

CHAPTER IV

Development of a Turn-on No-Wash Fluorescent Probe for c-SRC in Live Cell Microscopy Studies

Abstract

The subcellular localization of kinases is an important regulator of their activation and function. Small molecule fluorescent probes for kinases offer complementary advantages to immunofluorescence and genetically encoded tag techniques. Through leveraging orthogonal selectivity filters of small molecule kinase inhibitors, I develop a highly selective and versatile fluorescent probe for the non-receptor tyrosine kinase c-SRC. This probe, which combines the kinase binding head group PP2 and a coumarin fluorophore, covalently binds through the non-conserved cysteine C280 of c-SRC through an electrophilic moiety within the linker. Covalent fluorophore labeling of this cysteine represents an alternative to previously utilized cysteines near the kinase ATP-binding site, expanding the scope of small molecule fluorophore strategies for kinases. This probe, PP2-Coumarin, displayed turn-on fluorescence and could be used in live-cell microscopy. This probe also enabled subcellular visualization of endogenous c-SRC, did not require washing, and was compatible with live-cell super-resolution stimulated emission depletion (STED) microscopy. I use PP2-Coumarin to profile differential c-SRC localization within a panel of Triple Negative Breast Cancer (TNBC) cell lines in which this kinase is therapeutically relevant. c-SRC localization in TNBC cells in response to drug treatment is also monitored using this probe. This chapter underscores how knowledge of chemical biology of kinases and their inhibitors can be utilized in designing small molecule probes to investigate therapeutically relevant kinase targets.[†]

[†] Kinases and kinase mutants were designed, prepared, and purified by Frank Kwarcinski and Christel Fox (University of Michigan).

Introduction

Modern cell biologists have long used fluorescence microscopy as a powerful tool to investigate protein localization in cells. However, there is a consistent need of new complementary strategies to existing techniques. Small molecule fluorescent probes have been positioned as a means to compensate the limitations of other microscopy methods such as immunofluorescence and genetically encoded tags.[1-3] Antibody-based immunofluorescence requires fixation (i.e. killing) and permeablization of the cell which prevents live-cell studies, can produce artifacts, and disrupts membrane archetecture.[4] For proteins which belong to families or classes with highly homologues members, antibodies can have limited use in immunofluorescent techniques due to nonspecificity.[5] Genetically encoded tags, such as GFP, enable studies of the dynamic changes in protein localization but can itself influence protein function and result in ectopic expression of the protein being studied.[4, 5] Additionally, such a technique is only possible in cellular systems highly amenable to genetic manipulation preventing its use with primary patient-derived cell lines. The aforementioned small molecule fluorescent probes, by virtue of being cell permeable, are capable of live-cell imaging and do not require genetic manipulation of the system being studied. Thus, they are thus highly complementary to the described commonly used methods.[6] While the use of such probes in the visualization of DNA, RNA, and specific cytoskeletal proteins has been well documented, their use in protein kinases has only recently been explored. [6, 7]

Kinases are involved in a myriad of cellular processes with localization and expression levels intimately tied to the dynamic cellular state (**Figure 4.1**).[8] Thus, native live-cell imaging enabled by small molecule fluorescent probes would greatly enhance kinase localization studies. This is especially true for investigations of therapeutically relevant kinases in specific disease states. In one of the first examples, the small molecule kinase inhibitor dasatinib was fluorescently tagged with BODIPY to enable fluorescent microscopy of c-SRC, the prototypical nonreceptor tyrosine kinase.[6] However, other homologous kinases (e.g. c-ABL, YES, LYN, etc.) were also fluorescently tagged as dasatinib itself is a relatively promiscuous kinase inhibitor.[6, 9] While this strategy of amending cell permeable fluorescent dyes with existing kinase inhibitors provides a robust basis for such probes, it can result in the staining of undesirable off-targets. This

is, in part, due to the highly conserved nature of the ATP-binding pocket where most kinase inhibitors bind.[10] Selectivity is very important for fluorescent probes in microcopy, as a signal that is not specific can confound results.

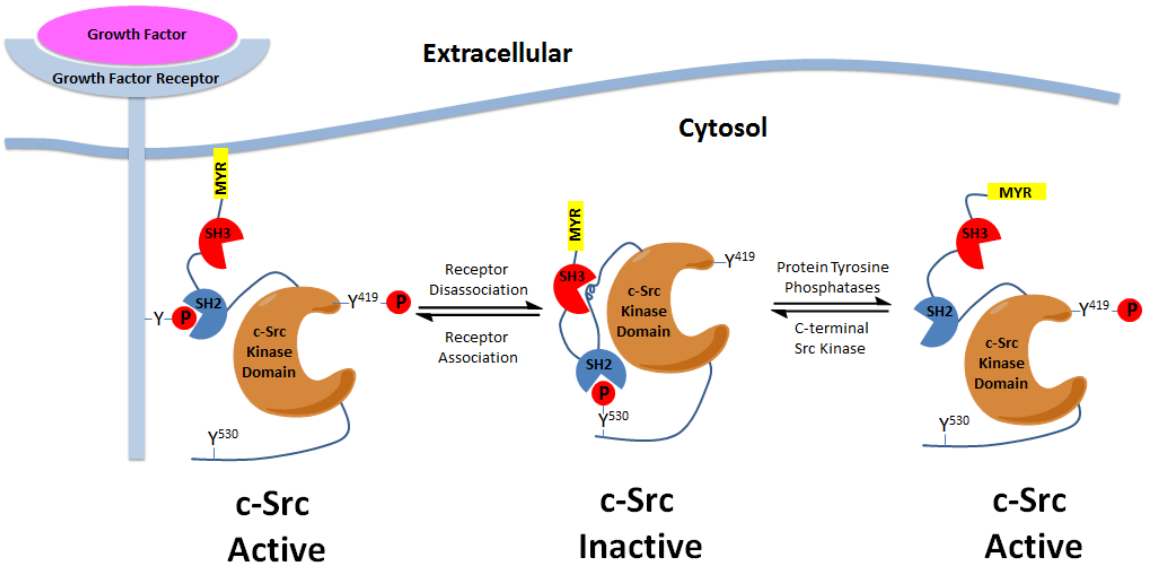

Figure 4.1: Generalized cartoon highlighting the dynamics of kinase localization and function with c-SRC as an example.

Irreversible fluorescent probes which target non-conserved cysteine residues help alleviate this shortcoming, as higher selectivity is obtained through combined reversible and covalent binding.[11] Lui et al. estimated that there are 18 cysteines that can theoretically be targeted by inhibitors that first bind reversibly to the ATP pocket, and then can react irreversibly (via an electrophilic moiety) to the non-conserved cysteine.[11] Thus, the binding of such probes are dependent on the ability to reversible bind *and* to be attacked by a cysteine (if present). With these cysteines present in 200 unique kinases, and well documented irreversible kinase inhibitor strategies present in the literature, there should be ample opportunity to leverage these probes for fluorescent microscopy against an array of kinases. Surprisingly, of these 18 cysteines I could find evidence of only one that has been utilized for fluorescence microscopy with irreversible probes (**Figure 4.2**).[12-15] This cysteine at C481 of BTK (and analogous positions) has been targeted successfully with a handful of fluorescent probes demonstrating that this approach is feasible.[12-15] Failure to utilize these other cysteines for irreversible fluorescent probes has severely limited the scope of live cell studies in kinases localization. As such, the full

potential of small molecule fluorescent probes for kinases, including therapeutically relevant kinases, remains unrealized.

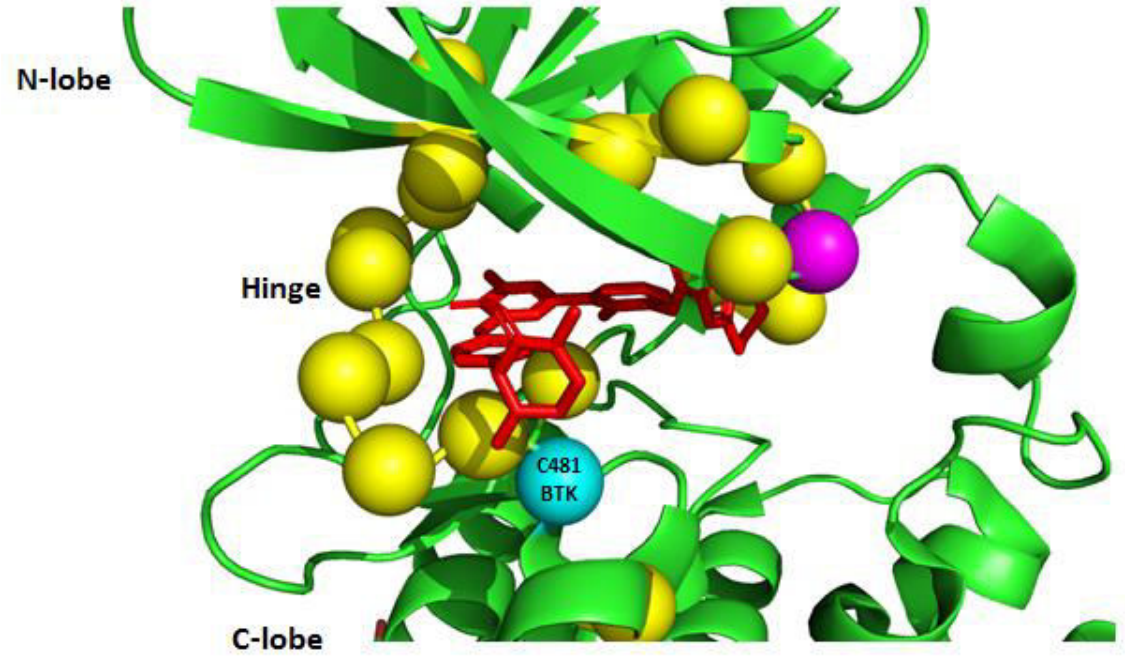

Figure 4.2: Representative kinase domain (with inhibitor bound, red) with accessible cysteines shown in representative positions. Locations where cysteines can sometimes be found are shown in yellow spheres. The cyan sphere is the cysteine found at C481 in BTK (and analogous position) that has been previously targeted for irreversible fluorescent probes in microscopy. In purple is a cysteine analogous to C280 of c-SRC, of which this work concerns. (PDB: 5P9F) [16]

Herein, I describe new strategies to confer selectivity to kinase fluorescent probes, using the kinase c-SRC as a model. This approach is two-fold: i) the incorporation of an electrophilic moiety into the probe that targets an alternative non-conserved cysteine found in c-SRC which have previously been shown to be readily amenable to covalent modification; ii) the addition of a fluorophore with turn-on characteristics upon covalent modification by this cysteine of c-SRC. I demonstrate the capabilities of this probe such as its turn-on, no-wash, optional-wash, live-cell microscopy, and stimulated emission depletion (STED) microscopy capability. In previous studies, c-SRC has been identified as a therapeutic target in TNBC.[17, 18] In **Chapter III**, I also identified c-SRC as a target in 5/10 PDX screens. I then utilize the c-SRC specificity of this probe to interrogate its

localization in live-triple negative breast cancer (TNBC) cell lines. I also use this fluorescent probe to show how different drugs can influence the localization of this therapeutically relevant kinase.

Design of a c-SRC Fluorescent Probe

High selectivity for the target kinase is an important feature for small molecule fluorescent probes for kinases to be fully realized.[3] Irreversible small molecule fluorescent probes with an electrophilic moiety targeting a non-conserved nucleophilic cysteine residue near the ATP-binding site have shown to be advantageous. Unbound probe may be subsequently washed away to give an increased signal to noise ratio. Probe that is bound reversibly to off-targets could also be washed away to help ensure a target specific signal. However, this strategy has been limited to the non-conserved C481 of BTK and analogous cysteines in other kinases. To increase the scope of this strategy, I employed a previously reported approach of covalent modification of an alternative non-conserved cysteine near the ATP binding site, using c-SRC as a model.[19] I began with a previously reported kinase-binding head group modeled after the pyrazole pyrimidine PP2, a classic ATP-competitive c-SRC inhibitor shown to be highly promiscuous across the kinome (**Figure 4.3B**, highlighted in pink).[20, 21] Strategically incorporating an electrophilic moiety within the probe would put it in close proximity to cysteine C280, a non-conserved residue in the P-loop (phosphate binding loop) in the kinase ATP-binding pocket of c-SRC (**Figure 4.3B**, highlighted in light blue).[19] This cysteine is found in only 9 of the 518 known protein kinases and was previously used to produce selective irreversible inhibitors of c-SRC.[19] The orthogonal selectivities of the kinase binding head group and the as-of-yet chosen electrophile would produce a highly selective fluorescent probe for c-SRC (**Figure 4.3B**). Only the SRC-family members YES and FGR are possible off target kinases with FGR only expressing in select cells. A detailed list of kinases bound by these selectivity filters can be found in **Figure C.1**.

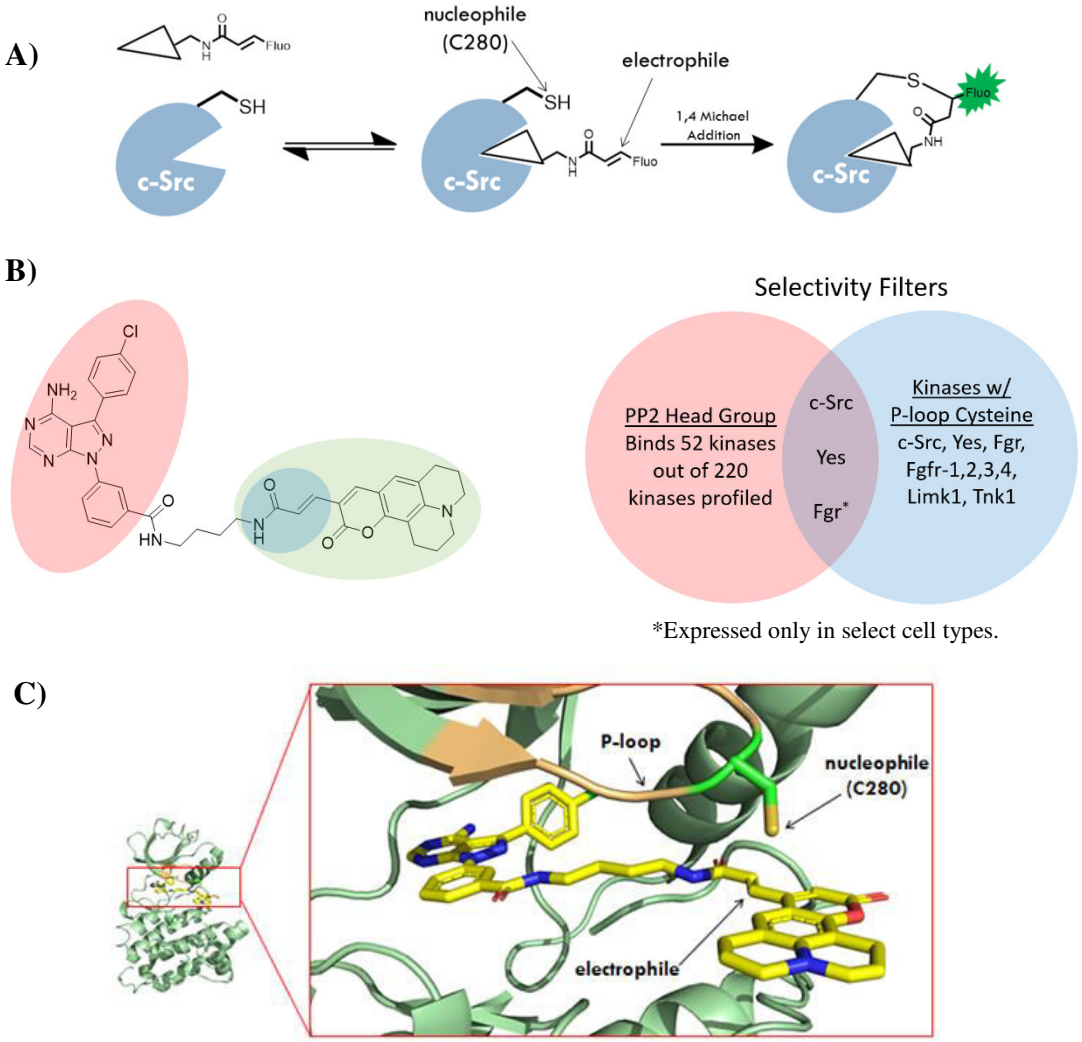

Figure 4.3: Design of PP2-Coumarin, an irreversible turn-on fluorescent probe selective for c-SRC. **A)** General strategy for an irreversible turn-on probe for c-SRC with a kinase binding head group and an electrophile. **B)** PP2-Coumarin and the selectivity filters for its various components. The kinase binding head group (pink) based off of the promiscuous c-SRC inhibitor PP2. The acrylamide electrophile (light blue) can undergo a 1,4 Michael addition with a non-conserved cysteine. The acrylamidecoumarin (green) increases in fluorescence intensity upon a 1,4-Michael addition with the acrylamide moiety. Venn diagram shows the selectivity filters of the various parts of the proposed fluorescent probe (full list in **Figure C.1**). **C)** Structure of PP2C built into a crystal structure of c-SRC bound to PP2 (PDB: 3GEQ). [22]

I chose the Michael acceptor-containing cyanoacrylamidecoumarin to serve as the basis of the fluorophore.[23] It has been shown that a 1,4-Michael addition across the cyanoacrylamide olefin moiety by thiols result in an increase in fluorescent intensity.[23, 24] Such a characteristic would further increase the S/N ratio of the probe and add versatility

for experiments where washing may be undesirable. For example, where real-time imaging immediately following addition of probe is desired, required repetitive washing would impair its use. To ensure c-SRC specific turn-on fluorescence, I chose to remove the cyano group which would decrease the reactivity of the electrophile with endogenous glutathione and other off-target cellular thiols. The cyano group also activates the retro 1,4-Michael addition reaction and its removal will ensure that any reaction with the electrophile is irreversible. Attachment of the kinase binding head group to the resultant acrylamidecoumarin (**Figure 4.3B**, highlighted in green) with an aliphatic linker produced the designed probe, PP2-Coumarin (PP2C). PP2C was found to have excitation and emission maxima at 450 and 510 nm respectively. These maxima correspond to commonly used filters used in fluorescent microscopy, specifically those used to visualize GFP.

PP2-Coumarin is a Turn-on Irreversible Fluorophore Specific for C280 of c-SRC

To determine if PP2C is an irreversible inhibitor of c-SRC, I employed a continuous fluorometric activity assay as a means to determine IC_{50} as a measure of potency.[25] Incubation with the kinase domain of c-SRC at varying time points showed that PP2C displayed a modest time-dependent increase in inhibition. Mutating C280 to a serine in c-SRC significantly abrogated this effect, giving no clear trend in the IC_{50} over time, a trait of irreversible inhibitors.[26] This indicates that this time-dependent characteristic of PP2C is dependent upon C280 of c-SRC.† These data, summarized in **Table 4.1**, is a trait of irreversible inhibitors. To expand upon these findings, I included the SRC-Family kinase HCK, which lacks a P-loop cysteine, in the evaluation of PP2C. As expected, PP2C exhibited no time-dependent increase in potency with wild-type HCK, but did so when a P-loop cysteine was added through mutagenesis (Q252C HCK) (**Table 4.1**).† This not only confirms that the presence of a P-loop cysteine is required for irreversible inhibition of PP2C, but also shows preliminary potential for its use with other kinases through chemical genetics. I can envision studies leveraging gene editing or transfecting P-Loop cysteine kinase mutants into cells for localization studies of other kinases.

Table 4.1: Time dependent IC_{50} values of PP2C with c-SRC and HCK and their mutants. Potency of PP2C increases with time for wild-type c-SRC and Q277C HCK. No clear time dependent increase in potency observed with C280S c-SRC and wild-type HCK. PP2C IC_{50} time-dependence is contingent on the presence of a cysteine in the P-loop of the kinase domain. * Denotes that no full dose response was achieved in any of the independent runs. Here, full dose response curves designated to have at least two points below IC_{50} enzyme activity.

	5 min	15 min	50 min	120 min	180 min	360 min
WT c-SRC Kinase Domain Avg. IC_{50} (μM)	1.88 ± 0.59	1.11 ± 0.09	0.763 ± 0.08	0.766 ± 0.08	0.603 ± 0.032	0.422 ± 0.076
C280S c-SRC Kinase Domain Avg. IC_{50} (μM)	4.29 ± 0.048	6.66 ± 4.93	4.17 ± 0.162	1.490 ± 0.632	1.91 ± 0.191	1.79 ± 0.42

	5 min	15 min	120 min
WT HCK Kinase Domain Avg. IC_{50} (μM)	*7.78 ± 4.20	*20.8 ± 0.30	*3.84 ± 0.453
Q272C HCK Kinase Domain Avg. IC_{50} (μM)	2.69 ± 0.24	1.61 ± 0.13	0.484 ± 0.064

In the presence of c-SRC kinase domain I measured a significant time dependent increase in the fluorescence intensity at 510 nm for PP2C (> 350% increase after 120 min) (**Figure 4.4**). This is consistent with the time-dependent inhibition of c-SRC by PP2C as measured above. Additionally, this increase in fluorescence intensity is significantly abrogated when the C280S c-SRC mutant is used instead.[†] This demonstrates that the turn-on fluorescence is dependent not only on c-SRC binding but also the presence C280 in the P-loop.

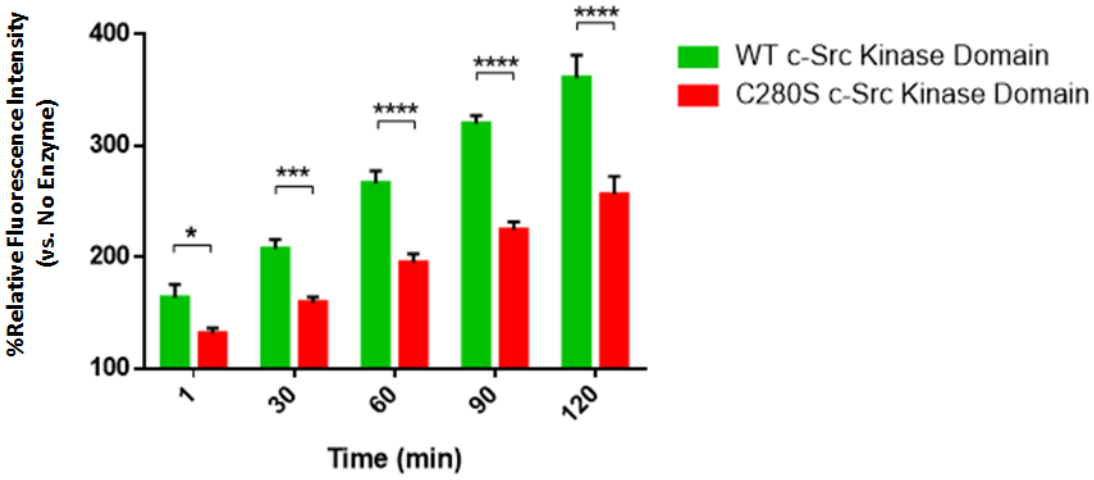

Figure 4.4: PP2C displays increased time-dependence turn-on fluorescence PP2C in the presence of C280 of c-SRC. PP2C (2 μM) was added to wells of buffer with no enzyme and wells with either wild-type or C280S c-SRC kinase domain (1 μM). Presence of the P-loop cysteine in c-SRC greatly enhances fluorescence intensity increase over time. Ex: 450 nm, Em: 510 nm * $p < 0.05$, *** $p < 0.001$, **** $p < 0.0001$.

In the cell, glutathione is present at high concentrations and could potentially react with PP2C. This would result in nonspecific turn-on fluorescence as well as prohibit wash out of non c-SRC bound probe. Average cellular glutathione concentration is approximately 5 mM.[27] Unlike c-SRC, the presence of increasing concentrations of glutathione of up to 20 mM resulted in no fluorescence intensity increase of PP2C. No increase in fluorescence intensity was measured at these glutathione concentrations over time as well. This data can be found in **Figure C.2**. This demonstrates the inertness of PP2C's turn-on fluorescence with glutathione biochemically.

PP2-Coumarin gives a c-SRC Specific Signal in Live-Cell Fluorescent Confocal Microscopy

I moved to see if fluorescent signal of PP2C is specific to c-SRC in fluorescent confocal microscopy. I utilized two cell lines, SYF mouse embryonic fibroblasts (MEF) (null for the ubiquitous SRC family kinases c-SRC, YES, and FYN) and SYF + c-SRC MEFs (SYF MEF cells in which c-SRC is stably transfected and overexpressed). Incubating 1 μM PP2C with SYF + c-SRC MEF cells for 4 hours resulted in strong PP2C staining upon examination with live-cell fluorescence confocal microscopy (**Figure 4.5**). This served in contrast to the lack of detectible signal with identical procedures and

microscope settings when performed with SYF MEF cells. This shows not only the no-wash capabilities of the probe but also demonstrates the c-SRC specific signal *in cellulo*.

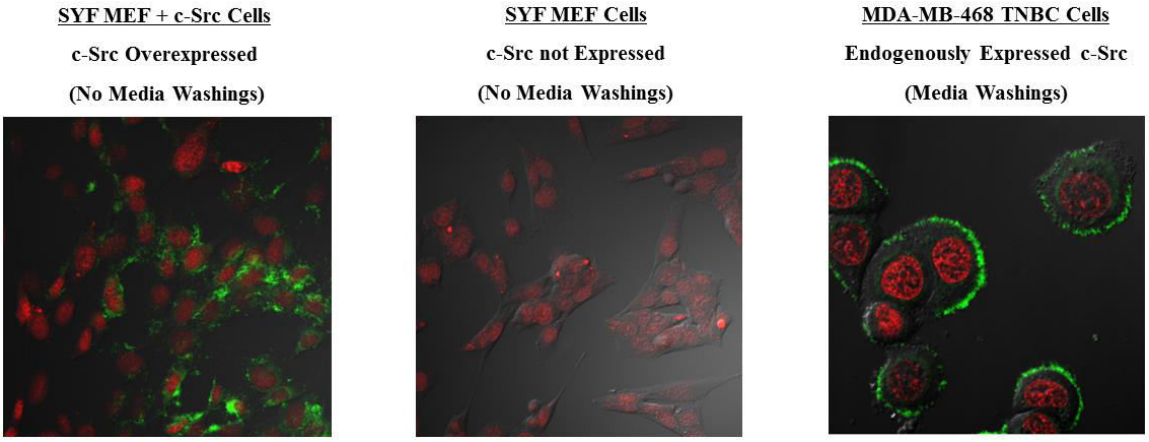

Figure 4.5: PP2-coumarin gives a c-SRC specific signal and can be used to in endogenous c-SRC expressing cells. SYF + c-SRC MEF and SYF MEF cell lines imaged 4 hours after PP2C (1 μM) treatment with no media renewal. MDA-MB-468 TNBC cells with endogenous c-SRC expression treated with PP2C as above, followed by multiple media washings. Image acquisition settings were identical between the left and center images. Green channel= PP2C, Red Channel= NucRed Live 647, and Grey channel= DIC.

The c-SRC expression levels in SYF + c-SRC MEF cells are not indicative of the endogenous levels of c-SRC in other cell lines where it would be lower. I thus moved to evaluate if PP2C can be used to detect c-SRC in cell lines that have not been genetically manipulated. To this end, I chose the TNBC cell line MDA-MB-468 and treated it with PP2C followed by probe-free washings. Upon imaging, a strong staining of the plasma membrane was observed, consistent with reports that c-SRC can sometimes be found on the plasma membrane of TNBC cells (**Figure 4.5**). To evaluate the endogenous c-SRC specificity of this observed signal I pre-incubated MDA-MB-468 TNBC cells with an irreversible analog of the c-SRC inhibitor dasatinib (Sprycel) before treatment with PP2C (structure in **Figure C.3**).[19] Irreversible dasatinib is highly selective for c-SRC and covalently modifies C280 of c-SRC and thus should occlude PP2C binding which can then be washed away.[19] This led to no observable signal in the irreversible dasatinib pre-incubated cells. Gratifyingly, this served in direct contrast to the strong plasma membrane staining observed in cells pre-incubated with DMSO vehicle and imaged under identical microscope settings (**Figure 4.6**). Such a result suggests that that the observed

fluorescent staining is a result of c-SRC specific binding of PP2C in this cell line. Thus, PP2C can be used in c-SRC localization studies in cells with endogenous levels of c-SRC and not just those in which it is overexpressed.

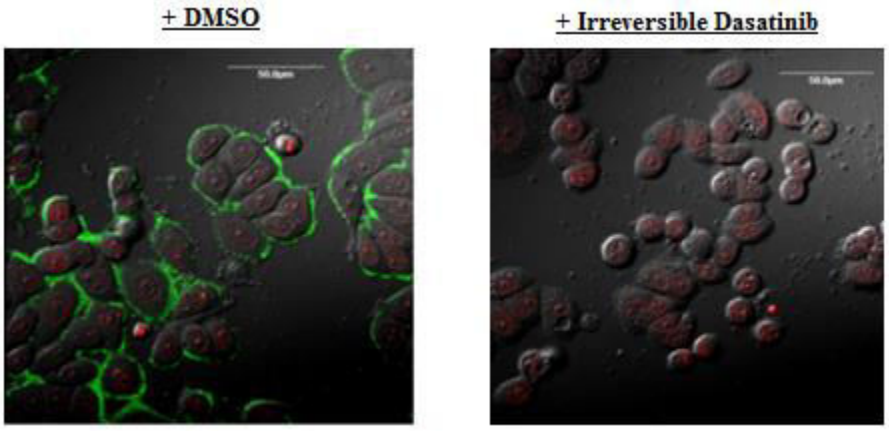

Figure 4.6: An irreversible analog of the c-SRC inhibitor dasatinib gives eliminates fluorescent signal in endogenous c-SRC expressing cells. MDA-MB-468 TNBC cells were pre-treated with DMSO vehicle or irreversible dasatinib analog for 2 hours followed by 1-hour incubation with PP2C, and then washings with probe-free media.. Image acquisition settings were identical. Green channel= PP2C, Red Channel= NucRed LiveGreen channel= PP2C, Red Channel= NucRed Live 647, and Grey channel= DIC.

PP2-Coumarin is Compatible with Live-Cell STED Super-Resolution Imaging

In traditional confocal microscopy resolution is restricted by the diffraction limit of the emitted light (~200 nm).[28] To distinguish features below the diffraction limit, Stimulated Emission Depletion (STED) microscopy has been used to obtain true super-resolution.[28, 29] In sum, employing a fluorescence excitation beam in combination with a surrounding doughnut-shaped STED beam has enabled microcopy to beat the diffraction limit.[28, 29] However, photobleaching from the high intensity STED laser has limited the fluorescent probes in live-cell STED microscopy.[29] I evaluated the probe's compatibility with live-cell STED microscopy in SYF + c-SRC MEF cells. At higher STED laser powers it was difficult to distinguish organized structure, likely in part due to movement of cellular components from localized heating by the STED laser. Decreasing the STED laser power remedied this (detailed settings listed in materials and methods). I was able to detect fine vesicle-like structures near the plasma membrane of many cells. The Full-Width at Half Maxima (FWHM) of these resolved structures were measured to be below

the diffraction limit while in conventional confocal microscopy were measured to be well above (**Figure 4.7**). Structures with detectible detail below the diffraction limit show that PP2C is compatible with live-cell STED microscopy. Such a feature is noteworthy as not all fluorophores are capable of withstanding the high power of the STED laser, quickly becoming photobleached in the process. Fewer fluorophores still have this capability with live-cells, which will lack strong antifade reagents typically present with fixed cells.

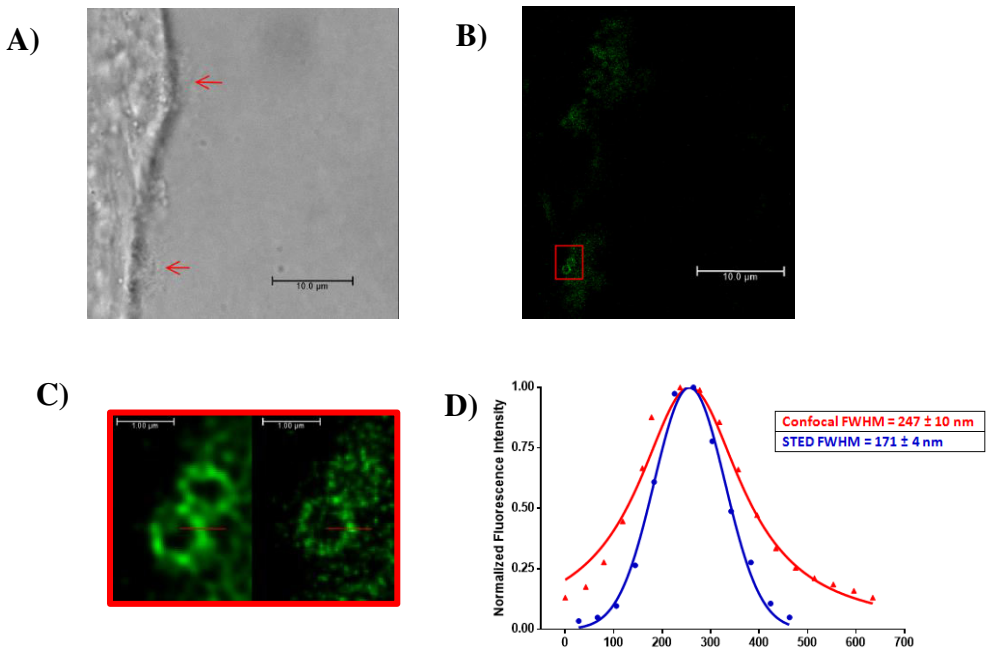

Figure 4.7: Live-Cell Stimulated Emission Depletion (STED) Super-Resolution Microscopy with PP2-Coumarin **A)** Bright field image of a portion of a SYF + c-SRC . Arrows indicate visible fine-structure on plasma membrane. **B)** STED image of the same cell. Visible vesicle-like structure can be seen in the within Region of Interest (ROI) (red box). **C)** A comparison of conventional confocal (left) and STED (right) images of the ROI. Images were taken sequentially and both were deconvoluted using Huygens Essential Package. **D)** Line intensity profiles along the red line in **C** were fitted to Gaussian or Lorentzian distributions. The Full Width at Half Maximum (FWHM) and associated standard deviation were calculated from the fits of each. The diffraction limit is ~200 nm.

Differential Localization of c-SRC in Triple Negative Breast Cancer Cell Lines

c-SRC has recently been identified as a target of interest in TNBC.[17, 30] As shown in **Chapter III**, c-SRC was also identified as a target in 5/10 TNBC PDX screens using the profiled kinase inhibitor approach. With c-SRC subcellular localization an important regulatory mechanism in its activation and function, c-SRC localization in TNBC cell lines is of particular interest.[31] c-SRC localization experiments in TNBC has previously relied upon immunofluorescence and immunohistochemistry despite their

disadvantages.[17, 18, 32] Thus I used PP2C as a means to interrogate c-SRC localization in TNBC cell lines using live-cell fluorescent microscopy. I treated live TNBC cells using PP2C and noted varying staining patters (**Figure 4.8**). As stated previously, MDA-MB-468 cells displayed primarily plasma membrane staining. Localization at the plasma membrane has been associated with a catalytically activated c-SRC.[31, 33] MDA-MB-231, SUM149, HCC1937, Hs57t, and Vari068 cells displayed either general cytosolic or perinuclear region staining, the latter of which is a common localization pattern of c-SRC. SUM159 cells showed a high population of cells (approximately 60%) with staining in both the cytosol and plasma membrane.

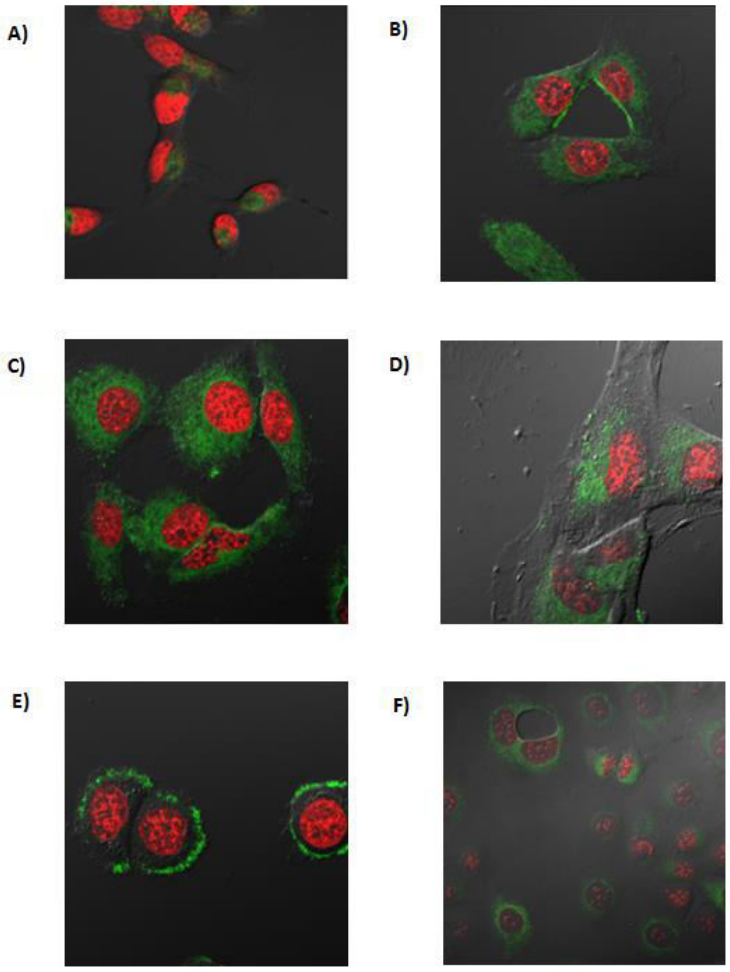

Figure 4.8: Representative live-cell confocal images of TNBC breast cancer cell lines imaged with PP2C. **A)** MDA-MB-231, **B)** SUM159 **C)** SUM149, **D)** Hs578t, **E)** MDA-MB-468, and **F)** HCC1937 TNBC Cell Line. Green channel= PP2C, Red Channel= NucRed Live 647, and Grey channel= DIC.

Recently, a promising lead compound for TNBC was identified, UM164.[30] The efficacy of this drug was attributed, in part, to inhibition of c-SRC through binding of an inactive kinase conformation.[30] The drug dasatinib, shares a very similar scaffold to UM164 but binds the active conformation of c-SRC but with diminished efficacy in TNBC.[30] It has been hypothesized that part of UM164's improved efficacy over dasatinib may be a result of it altering non-catalytic functions through binding of the different c-SRC conformation. To explore this hypothesis I imaged c-SRC using the PP2C probe in MDA-MB-468 cells treated with either UM164 or dasatinib (5 uM) for 4 hours before fixing of cells and washing away of drug. I observed a profound change in the localization of the c-SRC probe in the cells treated with UM164 but not dasatinib (**Figure 4.9**). The UM164 treated cells caused a distinct punctate staining as opposed to the nearly exclusive membrane staining found in cells treated with dasatinib and vehicle. This supports other published data that UM164s improved efficacy in TNBC could be, in part, the result of its induced changes in c-SRC localization. These experiments serve as examples of how PP2C is positioned as a valuable tool to continue live-cell investigations into the effects of c-SRC localization in TNBC.

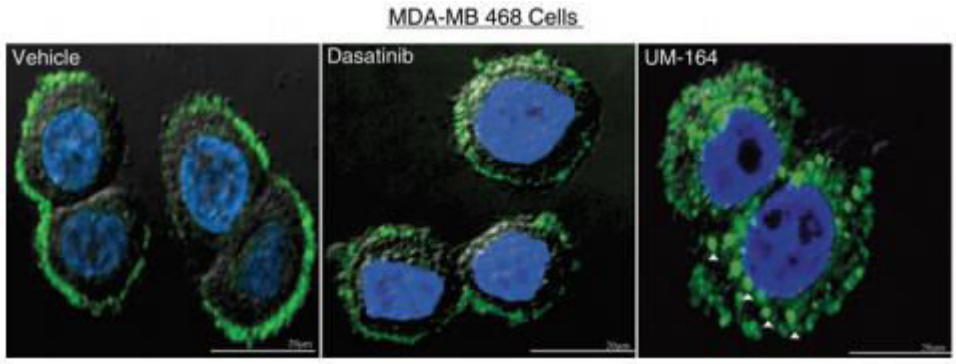

Figure 4.9: Altered localization of c-SRC when bound by UM-164. Representative fluorescence microscopy images of MDA-MB 468 cells treated with vehicle (DMSO), 5 uM dasatinib, or 5 uM UM-164 for 4 hours. In the vehicle-treated cells, c-SRC (green) is predominately localized to the cell membranes. UM-164–treated cells show cytoplasmic punctate structures indicated by the white triangles. Green channel= PP2-Coumarin, Red Channel= NucRed Live 647, and Grey channel= DIC.

Conclusions

I have developed a versatile small molecule fluorescent probe, PP2C, with turn-on, no-wash, and irreversible features with high selectivity for its target, c-SRC. The development of this probe expands the scope of small molecule irreversible fluorescent probes by demonstrating the use of an alternative non-conserved cysteine. I also demonstrated that incorporating a cysteine in the P-loop through mutagenesis can enable this probe's use in other kinases. This further expands its scope as either gene editing or transfecting P-Loop cysteine kinase mutants into cells will facilitate its use in other kinase localization studies. The probe also benefited from being compatible with live-cell STED microscopy techniques measuring structures below the diffraction limit. With this probe able to show localization of endogenous c-SRC, I used it in live-cell experiments with TNBC cell lines in which c-SRC has been shown to be a therapeutic target *in vivo*. I observed differential staining among the TNBC cell lines tested. Additionally, I used this fluorescent probe to show how an investigative drug can influence the localization of c-SRC in TNBC cell lines.

The capabilities of this or a similar probe would be useful for high-content analysis screens which interrogate changes in c-SRC localization. High-content analysis screens involve automated high-throughput fluorescent microscopy with automated image analysis. Such screens have been recognized as a means for their usefulness in phenotypic assays and can provide a strong mechanistic rationale for observed phenotypes (in this case c-SRC localization and cell viability).[34] This is important as strong mechanistic relationships between phenotype and disease states is integral for further advancing phenotypic-based screens, as discussed in **Chapter I**.[34]

This approach demonstrates how features of kinases and their inhibitors can be leveraged to design specific kinase fluorescent probes with varying uses. The applications of such specific and versatile probes, as described herein, demonstrate their value.

Materials and Methods

Cell Lines and General Cell Culture

SYF MEF and SYF + c-SRC MEF cell lines were purchased from American Type Culture Collection (ATCC). MDA-MB-468 and Hs578t TNBC breast cancer cell lines were purchased from ATCC. MDA-MB-231, HCC-1937, SUM-149, and SUM-159 TNBC breast cancer cell lines were kind gifts from Sofia Merajver. SYF MEF, SYF + c-SRC MEF, MDA-MB-231, and MDA-MB-468 were maintained in DMEM supplemented with 10% Fetal Bovine Serum (FBS). SUM149 and Sum 159 cell lines were maintained in 5% FBS in Ham's F-12 media supplemented with 5% FBS, 1 μg/mL hydrocortisone, and 5 μg/mL bovine insulin. Hs579t were maintained in DMEM supplemented with 10% FBS and 10 μg/mL insulin. HCC1937 cells were maintained in RPMI 1640 media supplemented with 10%. A humidified incubator at 37 °C and 5% CO_2 was used for storing all cell cultures with the exception of SUM149 and SUM159 cell lines which were grown at 10% CO_2.

Production of c-SRC, HCK, C280S c-SRC mutant, and Q272C HCK

Chicken c-SRC kinase domain and HCK kinase domain in pET28a plasmid with a TEV protease cleavable N-terminal 6X-His tags were provided by Markus Seeliger (SUNY, Stony Brook). The desired c-SRC mutation (C280S) was added to this plasmid using the Agilent QuikChange II kit. The desired HCK mutation (Q272C) was added to its plasmid using DpnI digent and transformation. The plasmids were transformed by electroporation into Bl21DE3 electrocompetent cells containing YopH expression vector in pCDFDuet-1. Cell growth and expression and protein purification were performed using modified literature protocols for expression of wild-type c-SRC kinase domain.[35] This work was performed by Frank Kwarcinski and Christel Fox.[†]

Determination of Biochemical IC_{50} Values

A continuous fluorescence assay was used to determine IC_{50} values.[25] Reaction volumes of 100 μL were used in 96-well black opaque plates. 85 μL of enzyme in buffer was added to each well. 2.5 μL of the appropriate inhibitor dilution was then added for

the various pre-incubation times. After the pre-incubation period, 2.5 µL of a c-SRC substrate peptide ("compound 3" as described in Wang et al)[4] solution (1.8 mM in DMSO) was added. The reaction was initiated with 10 µL of ATP (1 mM in water), and reaction progress was immediately monitored at 405 nm (ex. 340 nm) for 10 minutes using a Synergy 4 microplate reader (Biotek). Reactions had final concentrations of 45 µM c-SRC substrate peptide, 100 µM ATP, 100 µM TCEP, 100 µM Na_3VO_4, 100 mM Tris buffer (pH 8), 10 mM $MgCl_2$, 0.01% Triton X-100. Final enzyme concentrations were 30 nM for c-SRC Kinase Domain, 30 nM for C280S c-Sr Kinase Domain, 100 nM for HCK Kinase Domain, and Q272C HCK Kinase Domain. The initial rate data collected was used for determination of IC50 values for each time point. For IC_{50} determination, the kinetic values were obtained directly from nonlinear regression of substrate-velocity curves in the presence of various concentrations of the inhibitor. The equation Y = Bottom + (Top – Bottom)/(1 + 10^X – LogEC50), X = log(concentration) and Y = binding; was used in the nonlinear regression. Each inhibitor IC50 value was determined using at least two independent experiments; a representative inhibition curve for each condition is shown below. Representative dose response curves can be found in **Appendix C**.

Turn-on Fluorescence

In a 96 well plate, 2 µL of a 100 µM DMSO stock of PP2-Coumarin was added to a 98 uL of Buffer D (100 mM Tris buffer pH 8, 10 mM $MgCl_2$, 5% Glycerol, and 5 mM DTT) containing 1 µM enzyme (100 µL total reaction volume). Fluorescence intensity increase relative to no enzyme control at 510 nm (ex. 470 nm) was immediately recorded at the indicated time points with a Synergy 4 microplate reader (Biotek). The fluorescence intensities of the same wells were measured at each time point. Likewise, fluorescence increase in response to increasing concentrations of reduced glutathione at the indicated time points was also recorded under identical conditions (sans enzyme). All conditions were done in triplicate. Wells were re-read at each time point.

Live Cell Confocal Microscopy

Cells were trypsinized and allowed to adhere overnight on 4-well Lab-Tek II 1.5# chambered coverglass (Thermo Scientific). Unless otherwise specified, cells were then treated with PP2C at a final concentration of 1 μM for 4 hours, followed by three washings with complete media with 3 minute incubations in between. Cells typically grown with DMEM as a base media were washed and imaged with Flourobrite DMEM (Life Technologies) along with additional supplements to form complete medium. After the final wash the culture was treated with NucRed Live 647 nuclear stain (Life Technologies) (1 drop/500 μL culture media) and then incubated for 15 minutes. During image acquisition, cells were placed in a humidified enclosed stage with temperature and CO2 levels maintained at the growth conditions above for each cell cline by a regulator (Live Cell). Images were acquired with an Olympus FluoView 500 Laser Scanning Confocal Microscope with a 60X/1.4NA or 40X/1.2NA oil immersion objectives (Olympus). Samples were sequentially excited by Argon (488 nm), Helium-Neon Green (543 nm), and Helium-Neon Red (633 nm) lasers for coumarin fluorophores, m-Cherry-c-SRC, and NucRed Live 647 respectively. Emission signals were collected by barrier filters set to 505-525 nm for coumarin dyes, 610 nm NucRed Live 647. Differential Interference Contrast (DIC) images were also collected using the Argon laser channel. Images of 1024 x 1024 pixel dimensions were collected using the medium setting for scan speeds and Kalman filtering (averaging) of at least 4 scans. A zoom factor of two was also used when indicated. Unless otherwise stated the Z-resolution for each image was 0.5 μm. For each laser channel the laser intensity, detector PMT, and detector offset settings were adjusted to give sufficiently black background black backgrounds with minimal oversaturated pixels.

Stimulated Emission Depletion Microscopy

STED images were obtained using a Leica TCS SP8 Stimulated Emission Depletion Module (Leica Microsystems) equipped with a HCX PL APO 100X/1.40NA oil objective, White Light Laser, and an enclosed heated stage at 37 °C. SYF + c-SRC cells imaged were treated with PP2-Coumarin then washed as described above.

Excitation and depletion wavelengths were 488 nm and 594 nm respectively. For confocal imaging the 592 nm depletion laser was turned off. Signal detection was achieved using Leica Hybrid Detection System (HyD). For detection with bright field images a regular photomultiplier tube detector was used. The pinhole was set to 1.0 Airy Unit. For confocal and STED, Kalman filtering (averaging) of six scans at a speed of 600 Hz/scan and a zoom factor of three gave final images of 835 x 936 pixels with a pixel size of 38 nm. Bright field images of 1024 x 1024 pixels were likewise collected with an identical pixel size. Confocal and STED images were deconvoluted using Huygens Essentials package. A comprehensive list of acquisition parameters are given in **Table 4.2** below.

Table 4.2: Comprehensive list of parameters during STED image acquisition.

Image Size (Confocal, STED)	835 x 936 pixels, 31.63 µm x 36.61 µm, pixel size = 38 nm
Image Size (Bright Field)	1024 x 1024 pixels, 39.75 µm x 38.75 µm, pixel size = 38 nm
Scan Mode	xyz
Scan Direction X	Unidirectional
Objective Name	HCX PL APO 100x/1.40 OIL
Immersion	Oil
Numerical Aperture	1.4
Refraction Index	1.518
Zoom	3
Pinhole	151.6 µm
Pinhole Airy	1.00 AU
Emission Wavelength for Pinhole Airy Calculation	580.0 nm
Scan Speed	600 Hz
Frame Accumulation	6
Notch FW 2	NF 492
Polarization FW	NF 488
Attenuation MP	Min
External Detection FW	Mirror
Galvo Slider	Galvo X Normal
Multi-Function Port	Substrate

STED Beam Slider	SD 592
STED Phase Filter Beam 1	Vortex 600
Simple Beam Expander	No FRAP Booster
Target Slider	Target Park
X2 Lens Changer	CS2 UV Optics 1
White Light Laser	On
STED Output	1.2450 W
STED 1 (592 nm) Intensity	50%
Supercontinuum Visible (488 nm) Intensity	20%
Detector (Confocal, STED	HyD (493nm - 568nm), Gain=500, Offset= -0.1, Gate Start = 1.50 ns, Gate End = 6.00 ns, Reference Wavelength = 488.0 nm
Detector (Bright Field)	PMT, Gain = 329.5, Offset= 0

General Synthetic Methods

Unless otherwise noted, all reagents were obtained from commercial sources without further purification. ^{1}Hand ^{13}C NMR spectra were obtained using either a Varian Vnmrs500, Varian Vnmrs700, or Inova 500 spectrometer. Mass spectrometry (HRMS) was carried out by the University of Michigan Spectrometry Facility (J. Windak, director).

Synthetic Protocols

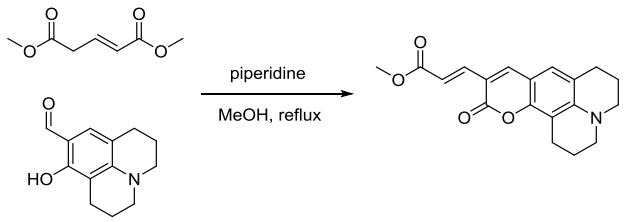

Scheme 4.1. Synthesis of compound **4.1**.

Synthesis of 4.1. 9-Formyl-8-hydroxyjulolidine (2.12 g, 9.76 mmol) (prepared as previously described)[36] and dissolved in anhydrous methanol in a flame dried flask. To this solution was added dimethyl 2-pentenedioate (1.62 g, 10.24 mmol) (prepared as previously described).[37] Three drops of piperidine that was distilled over KOH was added to the reaction mixture which was then heated to reflux under N2 overnight to form an orange precipitate. The reaction mixture was cooled on ice and the orange precipitate collected by vacuum filtration. The orange solid was further purified using silica chromatography to give compound **4.1** as an orange solid (0.692 g, 2.13 mmol, 21.8% yield). **Spectral Data:** ^{1}H NMR (500 MHz, $CDCl_3$) δ 7.59 (s, 1H), 7.54 (d, J = 15.7 Hz, 1H), 6.94 – 6.86 (m, 2H), 3.79 (s, 3H), 3.31 (q, J = 6.3 Hz, 4H), 2.88 (t, J = 6.5 Hz, 2H), 2.76 (t, J = 6.3 Hz, 2H), 1.97 (p, J = 6.2 Hz, 4H) ppm; ^{13}C NMR (126 MHz, $CDCl_3$) δ 168.33, 160.53, 151.58, 147.20, 144.58, 140.02, 125.87, 119.03, 118.12, 113.48, 108.48, 106.09, 77.18, 51.51, 50.16, 49.77, 27.45, 21.27, 20.32, 20.15; MS-ESI (m/z): $[M + Na]^+$ calcd for $C_{19}H_{19}NO_4$ 348.1206; found 348.1203.

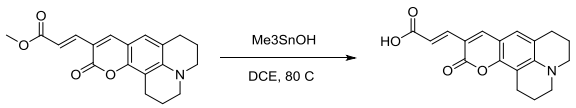

4.1 **4.2**

Scheme 4.2. Synthesis of compound **4.2**.

Synthesis of 4.2. In a flame dried flask compound **4.1** (40 mg, 0.123 mmol) was dissolved in 1,2-dichloroethane. Trimethyltinhydroxide (222 mg, 1.23 mmol) was then added and the reaction mixture heated at 80 C under N_2 for five days. Once the starting material was consumed as indicated by TLC, the reaction was diluted with 100 mL of ethyl acetate. The resulting mixture was then washed with 5% (w/w) HCl (5 x 25 mL), washed with brine (100 mL), dried over sodium sulfate. And then concentration *in vacuo* to give compound **4.2** as an orange solid (30 mg, 0.096 mmol, 78% yield). **Spectral Data:** ^{1}H NMR (500 MHz, DMSO-d_6) δ 8.05 (s, 1H), 7.38 (d, J = 15.7 Hz, 1H), 6.99 (s, 1H), 6.63 (d, J = 15.8 Hz, 1H), 3.23 – 3.09 (m, 4H), 2.68 (q, J = 6.7 Hz, 4H), 1.85 (td, J = 13.6, 11.6, 7.8 Hz, 4H) ppm; ^{13}C NMR (126 MHz, dmso) δ 168.56, 160.29, 151.47, 147.58, 145.59, 139.99, 126.61, 119.41, 118.29, 111.98, 108.24, 105.34, 49.91, 49.38, 27.20, 21.08, 20.14, 20.03 ppm; MS-ESI (m/z): $[M + H]^+$ calcd for $C_{18}H_{17}ClNO_4$ 312.1230; found 312.1230.

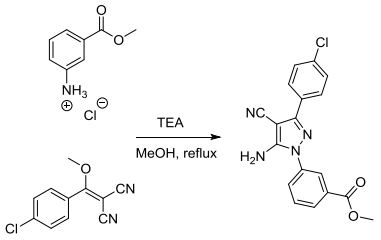

4.3

Scheme 4.3. Synthesis of compound **4.3**.

Synthesis of 4.3. 2-((4-chlorophenyl)(methoxy)methylene)malononitrile (5.00 g, 22.87 mmol) (prepared as previously described)[38] and added to a flame dried round bottom flask and dissolved in methanol. Triethylamine (5.79 g, 57.3 mmol) and methyl 3-hydrazinylbenzoate hydrochloride (4.63 g, 22.87 mmol) (prepared as previously described)[39] were then added and the reaction mixture was heated to reflux for 1 hour.

Reaction mixture was then cooled to room temperature and an orange precipitate was formed. Approximately half the solvent volume was removed and 100 mL of water was added. The precipitate was collected by vacuum filtration and washed with water and then dried to give compound **4.3** as an orange solid (6.29 g, 17.6 mmol, 77% yield). **Spectra Data:** ^{1}H NMR (401 MHz, DMSO-d_6) δ 8.07 (s, 1H), 7.98 (d, J = 7.8 Hz, 1H), 7.91 – 7.81 (m, 3H), 7.67 (t, J = 7.9 Hz, 1H), 7.54 (d, J = 8.2 Hz, 2H), 6.99 (s, 2H), 3.86 (s, 3H). ^{13}C NMR (101 MHz, DMSO-d_6) δ 165.86, 153.70, 149.89, 138.01, 134.29, 131.32, 130.60, 130.28, 129.40, 129.29, 128.94, 128.11, 125.15, 115.68, 71.87, 52.91. MS-ESI (m/z): $[M + H]^+$ calcd for $C_{18}H_{13}ClN_4O_2$ 353.0800; found 353.0797.

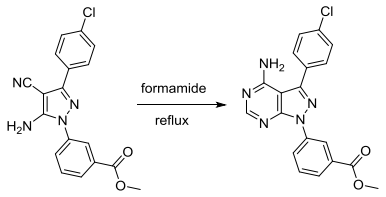

4.3 **4.4**

Scheme 4.4. Synthesis of compound **4.4**.

Synthesis of 4.4. In a flame dried round bottom flask compound **4.3** (3.00 mg, 8.5 mmol) was dissolved in formamide. The reaction mixture was gently heated to reflux for 2.5 hours. The reaction mixture was cooled on ice and water added to form a tan precipitate that was collected by vacuum filtration and washed with water followed by hexanes then dried. The tan solid was further purified by silica chromatography to give compound **4.4** as a white solid (100 mg, 0.272 mmol, 3.1% yield) (note: increase yields were observed by only heating to 160 C in subsequent analogous reactions). **Spectral Data:** ^{1}H NMR (700 MHz, DMSO-d_6) δ 8.83 (t, J = 2.0 Hz, 1H), 8.55 (ddt, J = 8.1, 2.0, 0.8 Hz, 1H), 8.40 (s, 1H), 7.91 (ddt, J = 7.8, 1.7, 0.8 Hz, 1H), 7.79 – 7.75 (m, 2H), 7.71 (t, J = 7.9 Hz, 1H), 7.65 – 7.61 (m, 2H), 3.89 (s, 3H). ^{13}C NMR (176 MHz, dmso) δ 166.19, 158.85, 157.25, 155.20, 145.46, 139.41, 134.48, 131.30, 131.07, 130.74, 130.27, 129.68, 127.16, 125.61, 121.40, 99.30, 52.91. MS-ESI (m/z): $[M + H]^+$ calcd for $C_{19}H_{14}ClN_5O_2$ 380.0909; found 380.0906.

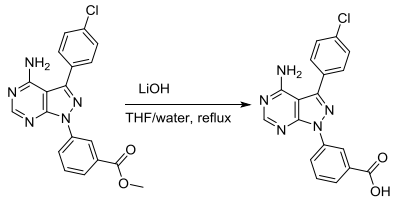

4.4 **4.5**

Scheme 4.5. Synthesis of compound **4.5**.

Synthesis of 4.5. In round bottom flask compound **4.4** (100 mg, 0.263 mmol) was dissolved in THF/H_2O (3:1). LiOH was then added and dissolved and resulting mixture was heated to reflux for until starting material was consumed as indicated by TLC. The reaction mixture was cooled and the THF was removed *in vacuo* and then acidified with addition of aq. HCl to form a white precipitate. The mixture was vacuum filtered and the collected precipitate washed with water to give compound **4.5** as a white solid (45 mg, 0.123 mmol, 46.7%). **Spectral Data:** ^{1}H NMR (500 MHz, DMSO-d_6) δ 8.84 (s, 1H), 8.51 (d, J = 8.2 Hz, 1H), 8.44 (s, 1H), 7.93 (d, J = 7.7 Hz, 1H), 7.79 (d, J = 8.1 Hz, 2H), 7.70 (t, J = 8.0 Hz, 1H), 7.65 (d, J = 8.1 Hz, 2H). ^{13}C NMR (176 MHz, dmso) δ 167.21, 158.28, 156.47, 154.90, 145.54, 139.17, 134.53, 132.29, 131.19, 130.75, 130.10, 129.71, 127.49, 125.39, 121.84, 99.28. MS-ESI (m/z): $[M + H]^+$ calcd for $C_{18}H_{12}ClN_5O_2$ 366.0752; found 366.0751.

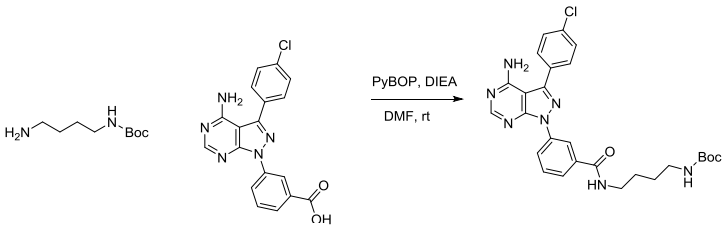

4.5 **4.6**

Scheme 4.6. Synthesis of compound **4.6**.

Synthesis of 4.6. To a flame dried flask compound **4.5** (45 mg, 0.123 mmol) was dissolved in dry DMF followed by addition of DIEA (47.7 mg, 0.369 mmol) and PyBOP (70 mg, 0.135 mmol). The solution was stirred under N2 at room temperature for 10 minutes. *tert*-butyl (4-aminobutyl)carbamate (26 mg, 0.135 mmol) (prepared as previously described)[40] dissolved in dry DMF was then added and the resultant reaction mixture was stirred for 2 hrs. Upon consumption of the starting material as determined

by TLC, water was added to give a precipitate that was collected by vacuum filtration then washed with water which resulted in compound **4.6** as a tan brown solid (58 mg, 0.108 mmol, 88% yield). Spectral Data: ^{1}H NMR (500 MHz, DMSO-d_6) δ 8.68 – 8.59 (m, 2H), 8.46 – 8.35 (m, 2H), 7.82 (d, *J* = 7.9 Hz, 1H), 7.80 – 7.75 (m, 2H), 7.69 – 7.59 (m, 3H), 6.80 (t, *J* = 5.8 Hz, 1H), 3.27 (q, *J* = 6.4, 5.8 Hz, 2H), 2.93 (q, *J* = 6.5 Hz, 2H), 1.51 (p, *J* = 7.8, 7.4 Hz, 2H), 1.42 (t, *J* = 7.7 Hz, 2H), 1.36 (d, *J* = 1.8 Hz, 9H). ^{13}C NMR (176 MHz, DMSO-d_6) δ 165.96, 158.84, 157.15, 156.02, 155.08, 145.18, 139.06, 136.32, 134.39, 131.42, 130.74, 129.67, 129.54, 125.21, 123.90, 120.49, 109.99, 99.16, 77.77, 39.87, 28.71, 27.55, 26.96. MS-ESI (m/z): $[M + Na]^+$ calcd for $C_{27}H_{30}ClN_7O_3$ 558.1991; found 558.1990.

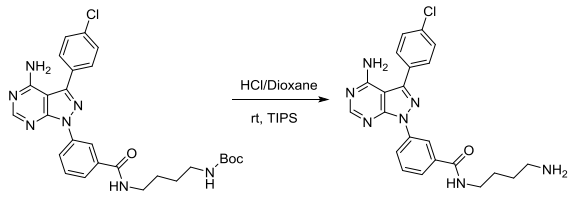

4.6 **4.7**

Scheme 4.7. Synthesis of compound **4.7**.

Synthesis of 4.7. In a round bottom flask, compound **4.6** (58 mg, 0.108 mmol) was dissolved in 4 M HCl in Dioxane and stirred at room temperature for 3 hours. The solvent was removed under reduced pressure to give a white residue. The residue was suspended in 1 M NaOH and the suspension was vacuum filtered. The collected solid was washed with water to give compound **4.7** as a brown tan solid (32 mg, 0.073 mmol 67.8% yield). **Spectral Data:** ^{1}H NMR (500 MHz, DMSO-d_6) δ 8.68 (t, *J* = 5.7 Hz, 1H), 8.60 (m, 1H), 8.38 (m, 2H), 7.78 (m, 4H), 7.66 – 7.53 (m, 4H), 3.27 (m, 2H), 2.62 (t, *J* = 7.0 Hz, 2H), 1.60 – 1.45 (m, 4H) ppm; ^{13}C NMR (126 MHz, dmso) δ 165.95, 158.85, 157.14, 155.08, 145.18, 139.08, 136.32, 134.40, 131.42, 130.73, 129.66, 129.54, 125.18, 123.91, 120.47, 99.18, 40.99, 29.40, 26.94 ppm; MS-ESI (m/z): $[M + H]^+$ calcd for $C_{22}H_{22}ClN_7O$ 436.1647; found 436.1645.

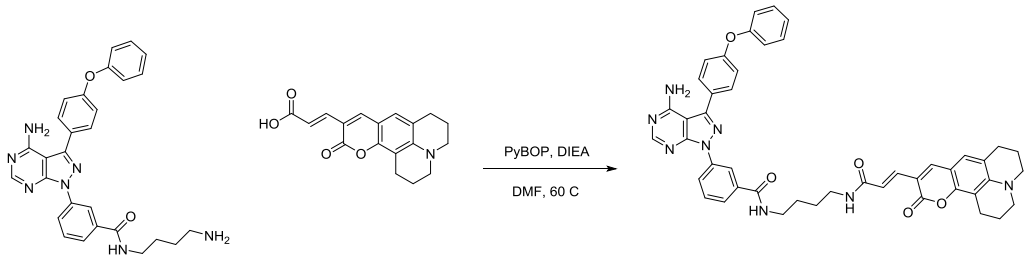

4.7 **4.2** **PP2-Coumarin**

Scheme 4.8. Synthesis of compound **PP2-Coumarin**.

Synthesis of PP2-Coumarin. In a flame dried flask compound **4.2** (30 mg, 0.096 mmol) was dissolved in dry DMF followed by addition of DIEA (51.9 mg, 0.401 mmol) and PyBOP (50 mg, 0.096 mmol). The solution was stirred under N2 at room temperature for 10 minutes. Compound **4.7** (35 mg, 0.080 mmol) dissolved in dry DMF was then added and the resultant reaction mixture was stirred under N2 at 60 C overnight. When progress of the reaction was halted as determined by TLC, water was added. This mixture was then extracted with ethyl acetate (3 X 20 mL), the combined organics washed with water (5 x 10 mL) to remove DMF, washed with Brine, dried over sodium sulphate, and concentrated to give a crude orange solid. The orange solid was further purified using a reverse phase HPLC to give **PP2-Coumarin** as a orange yellow solid (7 mg, 0.0096 mmol, 11% yield). **Spectral Data:** ^{1}H NMR (500 MHz, DMSO-d_6) δ 8.64 (d, J = 6.0 Hz, 2H), 8.44 – 8.38 (m, 2H), 8.15 (t, J = 5.7 Hz, 1H), 7.95 (s, 1H), 7.80 (dd, J = 17.4, 7.9 Hz, 4H), 7.68 – 7.61 (m, 4H), 7.23 (d, J = 15.4 Hz, 1H), 7.03 (s, 1H), 6.92 (d, J = 15.5 Hz, 1H), 3.19 (q, J = 6.5, 5.9 Hz, 2H), 2.72 (dt, J = 13.2, 6.3 Hz, 4H), 2.54 (s, 2H), 1.87 (dp, J = 12.3, 6.0 Hz, 4H), 1.63 – 1.53 (m, 6H), 1.23 (s, 2H) ppm; ^{13}C NMR 165.56, 159.85, 158.42, 156.72, 154.65, 150.68, 146.64, 144.75, 144.58, 138.65, 135.87, 134.42, 133.98, 130.99, 130.32, 129.25, 129.13, 125.84, 124.78, 123.48, 122.06, 120.05, 118.77, 112.73, 107.89, 104.95, 98.75, 49.43, 48.91, 40.43, 38.48, 31.33, 26.80, 26.66, 20.76, 19.85, 19.72 ppm; MS-ESI (m/z): $[M + Na]^+$ calcd for $C_{40}H_{37}ClN_8O_4$ 751.2519; found 751.2509.

Spectral Data for Compounds

^{1}H and ^{13}C NMR spectra for compounds **4.1-4.7** and **PP2-Coumarin** are shown in **Appendix C**.

References

1. Chalfie, M.; Tu, Y.; Euskirchen, G.; Ward, W. W.; Prasher, D. C., Green fluorescent protein as a marker for gene expression. *Science* **1994,** *263* (5148), 802-5.
2. Stadler, C.; Rexhepaj, E.; Singan, V. R.; Murphy, R. F.; Pepperkok, R.; Uhlen, M.; Simpson, J. C.; Lundberg, E., Immunofluorescence and fluorescent-protein tagging show high correlation for protein localization in mammalian cells. *Nat Methods* **2013,** *10* (4), 315-23.
3. Chan, J.; Dodani, S. C.; Chang, C. J., Reaction-based small-molecule fluorescent probes for chemoselective bioimaging. *Nat Chem* **2012,** *4* (12), 973-84.
4. Schnell, U.; Dijk, F.; Sjollema, K. A.; Giepmans, B. N., Immunolabeling artifacts and the need for live-cell imaging. *Nat Methods* **2012,** *9* (2), 152-8.
5. Crivat, G.; Taraska, J. W., Imaging proteins inside cells with fluorescent tags. *Trends Biotechnol* **2012,** *30* (1), 8-16.
6. Vetter, M. L.; Zhang, Z.; Liu, S.; Wang, J.; Cho, H.; Zhang, J.; Zhang, W.; Gray, N. S.; Yang, P. L., Fluorescent visualization of Src by using dasatinib-BODIPY. *Chembiochem* **2014,** *15* (9), 1317-24.
7. Zhang, Z.; Kwiatkowski, N.; Zeng, H.; Lim, S. M.; Gray, N. S.; Zhang, W.; Yang, P. L., Leveraging kinase inhibitors to develop small molecule tools for imaging kinases by fluorescence microscopy. *Mol Biosyst* **2012,** *8* (10), 2523-6.
8. Kholodenko, B. N., Cell signaling dynamics in time and space. *Nat Rev Mol Cell Biol* **2006,** *7* (3), 165-76.
9. Davis, M. I.; Hunt, J. P.; Herrgard, S.; Ciceri, P.; Wodicka, L. M.; Pallares, G.; Hocker, M.; Treiber, D. K.; Zarrinkar, P. P., Comprehensive analysis of kinase inhibitor selectivity. *Nat Biotechnol* **2011,** *29* (11), 1046-51.
10. Knight, Z. A.; Shokat, K. M., Features of selective kinase inhibitors. *Chem Biol* **2005,** *12* (6), 621-37.
11. Liu, Q.; Sabnis, Y.; Zhao, Z.; Zhang, T.; Buhrlage, S. J.; Jones, L. H.; Gray, N. S., Developing irreversible inhibitors of the protein kinase cysteinome. *Chem Biol* **2013,** *20* (2), 146-59.
12. Turetsky, A.; Kim, E.; Kohler, R. H.; Miller, M. A.; Weissleder, R., Single cell imaging of Bruton's tyrosine kinase using an irreversible inhibitor. *Sci Rep* **2014,** *4*, 4782.
13. Zhang, Q.; Liu, H.; Pan, Z., A general approach for the development of fluorogenic probes suitable for no-wash imaging of kinases in live cells. *Chem Commun (Camb)* **2014,** *50* (97), 15319-22.
14. Zuo, Y.; Shi, Y.; Li, X.; Teng, Y.; Pan, Z., A novel 2,5-diaminopyrimidine-based affinity probe for Bruton's tyrosine kinase. *Scientific Reports* **2015,** *5*, Article number: 4782.
15. Honigberg, L. A.; Smith, A. M.; Sirisawad, M.; Verner, E.; Loury, D.; Chang, B.; Li, S.; Pan, Z.; Thamm, D. H.; Miller, R. A.; Buggy, J. J., The Bruton tyrosine kinase inhibitor PCI-32765 blocks B-cell activation and is efficacious in models of autoimmune disease and B-cell malignancy. *Proc Natl Acad Sci U S A* **2010,** *107* (29), 13075-80.
16. Bender, A. T.; Gardberg, A.; Pereira, A.; Johnson, T.; Wu, Y.; Grenningloh, R.; Head, J.; Morandi, F.; Haselmayer, P.; Liu-Bujalski, L., Ability of Bruton's Tyrosine Kinase Inhibitors to Sequester Y551 and Prevent Phosphorylation Determines Potency

for Inhibition of Fc Receptor but not B-Cell Receptor Signaling. *Mol Pharmacol* **2017,** *91* (3), 208-219.
17. Tryfonopoulos, D.; Walsh, S.; Collins, D. M.; Flanagan, L.; Quinn, C.; Corkery, B.; McDermott, E. W.; Evoy, D.; Pierce, A.; O'Donovan, N.; Crown, J.; Duffy, M. J., Src: a potential target for the treatment of triple-negative breast cancer. *Annals of Oncology* **2011,** *22* (10), 2234-2240.
18. Anbalagan, M.; Moroz, K.; Ali, A.; Carrier, L.; Glodowski, S.; Rowan, B. G., Subcellular Localization of Total and Activated Src Kinase in African American and Caucasian Breast Cancer. *PLoS One* **2012,** *7* (3).
19. Kwarcinski, F. E.; Fox, C. C.; Steffey, M. E.; Soellner, M. B., Irreversible inhibitors of c-Src kinase that target a nonconserved cysteine. *ACS Chem Biol* **2012,** *7* (11), 1910-7.
20. Brandvold, K. R.; Steffey, M. E.; Fox, C. C.; Soellner, M. B., Development of a highly selective c-Src kinase inhibitor. *ACS Chem Biol* **2012,** *7* (8), 1393-8.
21. Brandvold, K. R.; Santos, S. M.; Breen, M. E.; Lachacz, E. J.; Steffey, M. E.; Soellner, M. B., Exquisitely specific bisubstrate inhibitors of c-Src kinase. *ACS Chem Biol* **2015,** *10* (6), 1387-91.
22. Muratore, K. E.; Seeliger, M. A.; Wang, Z.; Fomina, D.; Neiswinger, J.; Havranek, J. J.; Baker, D.; Kuriyan, J.; Cole, P. A., Comparative analysis of mutant tyrosine kinase chemical rescue. *Biochemistry* **2009,** *48* (15), 3378-86.
23. Cho, A. Y.; University, K.; Choi, K.; Chemistry, D. o., A coumarin-based fluorescence sensor for the reversible detection of thiols. *Chemistry Letters* **2017,** *41* (12), 1611-1612.
24. Jung, H. S.; Ko, K. C.; Kim, G. H.; Lee, A. R.; Na, Y. C.; Kang, C.; Lee, J. Y.; Kim, J. S., Coumarin-Based Thiol Chemosensor: Synthesis, Turn-On Mechanism, and Its Biological Application. *Org. Lett.* **2011,** *13* (6), 1498–1501.
25. Wang, Q.; Cahill, S. M.; Blumenstein, M.; Lawrence, D. S., Self-reporting fluorescent substrates of protein tyrosine kinases. *J Am Chem Soc* **2006,** *128* (6), 1808-9.
26. Barf, T.; Kaptein, A., Irreversible Protein Kinase Inhibitors: Balancing the Benefits and Risks. *J. Med. Chem.* **2012,** *55* (14), 6243–6262.
27. Lushchak, V. I., Glutathione Homeostasis and Functions: Potential Targets for Medical Interventions. *Journal of Amino Acids* **2012** *2012*, Article ID 736837.
28. Klar, T. A.; Jakobs, S.; Dyba, M.; Egner, A.; Hell, S. W., Fluorescence microscopy with diffraction resolution barrier broken by stimulated emission. *Proc Natl Acad Sci U S A* **2000,** *97* (15), 8206-10.
29. Fernandez-Suarez, M.; Ting, A. Y., Fluorescent probes for super-resolution imaging in living cells. *Nat Rev Mol Cell Biol* **2008,** *9* (12), 929-43.
30. Gilani, R. A.; Phadke, S.; Bao, L. W.; Lachacz, E. J.; Dziubinski, M. L.; Brandvold, K. R.; Steffey, M. E.; Kwarcinski, F. E.; Graveel, C. R.; Kidwell, K. M.; Merajver, S. D.; Soellner, M. B., UM-164: A Potent c-Src/p38 Kinase Inhibitor with In Vivo Activity against Triple-Negative Breast Cancer. *Clin Cancer Res* **2016,** *22* (20), 5087-5096.
31. Bjorge, J. D.; Jakymiw, A.; Fujita, D. J., Selected glimpses into the activation and function of Src kinase. *Oncogene* **2000,** *19* (49), 5620-35.

32. Irwin, M. E.; Bohin, N.; Boerner, J. L., Src family kinases mediate epidermal growth factor receptor signaling from lipid rafts in breast cancer cells. *Cancer Biol Ther* **2011,** *12* (8), 718-26.
33. Frame, M. C., Src in cancer: deregulation and consequences for cell behaviour. *Biochim Biophys Acta* **2002,** *1602* (2), 114-30.
34. Moffat, J. G.; Rudolph, J.; Bailey, D., Phenotypic screening in cancer drug discovery - past, present and future. *Nature Reviews Drug Discovery* **2014,** *13*, 588-602.
35. Seeliger, M. A.; Young, M.; Henderson, M. N.; Pellicena, P.; King, D. S.; Falick, A. M.; Kuriyan, J., High yield bacterial expression of active c-Abl and c-Src tyrosine kinases. *Protein Sci* **2005,** *14* (12), 3135-9.
36. Gompel, J. V.; Schuster, G. B., Chemiluminescence of organic peroxides: intramolecular electron-exchange luminescence from a secondary perester. *J. Org. Chem.* **1987,** *52* (8), 1465–1468.
37. Poldy, J.; Peakall, R.; Barrow, R. A., Identification of the First Alkenyl Chiloglottone Congener. *European Journal of Organic Chemistry* **2012,** *2012* (29), 5818-5827.
38. Hanefeld, U.; Rees, C. W.; White, A. J. P.; Williams, D. J., One-pot synthesis of tetrasubstituted pyrazoles—proof of regiochemistry. *J. Chem. Soc. Perk. T. 1* **1996,** *1* (13), 1545–1552.
39. Bowers, E. M.; Yan, G.; Mukherjee, C.; Orry, A.; Wang, L.; Holbert, M. A.; Crump, N. T.; Hazzalin, C. A.; Liszczak, G.; Yuan, H.; Larocca, C.; Saldanha, S. A.; Abagyan, R.; Sun, Y.; Meyers, D. J.; Marmorstein, R.; Mahadevan, L. C.; Alani, R. M.; Cole, P. A., Virtual ligand screening of the p300/CBP histone acetyltransferase: identification of a selective small molecule inhibitor. *Chem Biol* **2010,** *17* (5), 471-82.
40. Caumes, C.; Hjelmgaard, T.; Roy, O.; Reynaud, M.; Servent, D.; Taillefumier, C.; Faure, S., Synthesis and binding affinities for sst receptors of cyclic peptoid SRIF-mimetics. *MedChemComm* **2012,** *3* (12), 1531–1535.

CHAPTER V
Conclusions

Abstract

Combining target screening with phenotypic assays has driven the discovery of approved drugs with novel mechanisms of action. The exception is kinase inhibitor drug discovery, which is still primarily target-based due to limitations of many phenotypic models. My approach, which employed machine learning data deconvolution, combined kinase target data of compounds with phenotypic results. This work provided a framework that enables kinase inhibitors to be used for the discovery of novel kinase targets and new lead compounds using cancer models such as cell lines and more advanced models like patient-derived xenografts. Interrogating newly identified kinase targets can be done through design of versatile chemical probes as described herein. In this chapter, I summarize my findings from these approaches.

Small Molecule Kinase Inhibitors in Target- and Phenotypic-Based Cancer Drug Discovery

Kinases are attractive drug targets in cancer due to their role in cellular signaling.[1-3] Target-based drug discovery has driven the approval of kinase inhibitors in cancer.[4, 5] However, only one kinase inhibitor has been approved whose lead was discovered in a phenotypic screen.[4, 6, 7] This is in sharp contrast to other cancer drug classes which have recently seen an increase in approved drugs with phenotypic-based origins.[5] This is important because drugs discovered through phenotypic approaches can possibly exert their effect through novel mechanisms of action. Kinase inhibitor drug discovery will need to take advantage of phenotypic screening if it is to benefit from potential novel mechanisms of action.

One reason kinase inhibitors have lagged behind in phenotypic-based lead discovery is a flaw inherent to phenotypic screening itself. Cancer cell lines are often

used as models in these approaches and do not recapitulate cells found in tumors.[5] This is especially true of cell lines grown on 2D plastic. Cellular signaling, and by extension kinases, is extremely sensitive to the context of the cellular environment. Therefore, if success is to be had with kinase inhibitors in phenotypic screening, appropriate models and readouts will need to be utilized. Phenotypes that are mechanistically related to the progression of a specific cancer subtype, if appropriately modeled, will enable phenotypic screening to identify more clinically relevant targets. Furthermore, recently approved drugs and those in clinical trials have been discovered by combining target-based and phenotypic-based approaches.[5, 8, 9] Strategically combining kinase-target data with clinically relevant cancer phenotype models would aid in identifying novel targets and lead compounds for this drug class.

Once novel kinase cancer targets are discovered, kinase chemical probes will need to be utilized to understand their role. These probes, which can inhibit and/or bind to a specific kinase, or combination of kinases, will need to be carefully designed to answer the desired questions. New approaches in the design of such tool, like fluorescent probes, will expand their versatility in both kinases and overall techniques. A clear understanding of individual kinase chemical biology as well as the kinome at large will be valuable in continuing kinase inhibitors as an important class of cancer therapeutics.

Target Identification in Sarcomas using Machine Learning and a Profiled Kinase Inhibitor Library

Sarcomas are a rare class of cancers with no highly effective targeted therapies against most subtypes.[10-13] Progress toward developing targeted therapies for these cancers has been slow due to the lack of defined and druggable molecular targets in these cancers. I have presented a strategy that combines phenotypic- and target-screening to efficiently overcome this obstacle. Combining kinase target data from a profiled kinase inhibitor library with a phenotypic screen enabled us to identify various kinase targets in sarcoma subtypes via a machine learning approach. Of particular interest was the identification of PRKD as a possible target in synovial sarcoma both due to its specificity in the panel and potential novelty in this disease. This success in target identification in synovial sarcoma, a rare and understudied cancer, gives promise that targets may be

identified in other cancers. In this study I screened for kinase importance in viability to demonstrate this approach, but other phenotypes, such as motility and metastasis, could also be interrogated using the presented framework. Phenotypes directly related to a cancer subtype, like disruption of the SS18-SSX fusion oncoprotein complex in synovial sarcoma for example, could also be used with this methodology.[14] Clinically relevant phenotypic readouts such as this, when combined with this target ID approach, would enable the discovery of highly relevant cancer targets.

We also used of this machine-learning target deconvolution as a means to identify novel combinational strategies. I performed a synergy screen of a synovial sarcoma cell line in the presence of a PRKD inhibitor. I discovered that scores of many kinases from the machine learning algorithm changed greatly, including CDK and AKT which increased. Using Chou-Talalay synergy analysis, I discovered that selective clinical inhibitors of these kinases synergistically decreased viability along with PRKD inhibition. This strategy could also be used in the presence of any drug, kinase inhibitor or not, in which new combinational strategies are desired. I envision that this strategy could be reapplied with other cancers to find novel combination of approved treatments. This could be highly impactful for approved treatments with toxicity or resistance concerns. This work shows how combining kinase profiling data with phenotypic screening can be used to advance kinase target identification and drug discovery.

Target Identification in Triple Negative Breast Cancer Patient Derived Xenograft Cell Cultures with a Profiled Kinase Inhibitor Library

Our previous framework of discovering kinase targets using a profiled kinase inhibitor library will need to be used with higher-level cancer models to discover clinically relevant targets. Patient-derived xenografts (PDXs) have been positioned as one way to improve the success rate of cancer drug development by better modeling patient tumor microenvironment and tumor heterogeneity.[15-19] I combined short-term triple negative breast cancer (TNBC) PDX-derived 3D cell cultures with the profiled kinase inhibitor target ID framework.[19] I identified several kinase groups that scored highly as targets in at least half of the screens. Some of these kinases have been well established as possible TNBC targets in the literature. This demonstrates that this method with PDX

models can identify therapeutically important kinases. More importantly, I identified the FES/FER and MARK/SIK kinase groups as targets, which represent possible novel pharmacological findings in TNBC.[20-22] Early evidence of these kinases as targets in TNBC has only been genetic in nature. In addition to supporting the emerging evidence of these kinases as TNBC targets, this pharmacological based approach indicates that these putative target kinases can be actionable. Synthesis of selective inhibitors of these kinases for further studies is currently planned.

TNBC is itself a heterogeneous cancer which has, in part, resulted in a lack of FDA-approved targeted therapies.[23, 24] Alternative ways of subtyping this disease, as well as others, would aid in classifying patients as candidates who would respond to specific targeted therapies, thus improving outcome. Subtyping based on sensitivity to protein inhibition (such as kinases) would directly classify patients based on inhibitor sensitivity. To this end, I used the kinase target scores as a means of unsupervised hierarchal clustering of the PDXs screened. I observed a heterogeneous clustering of the PDXs using this method. I plan to continue TNBC PDX screens and to add the results to this target clustering.

The use of PDXs in this work demonstrates that this target identification methodology can be applied to higher level phenotypic models. Models which take into account the immune systems role in tumor progression will be needed as most PDXs are generated in immunocompetent mice. Mice with humanized immune systems would fill this role and are positioned to impact the *in vivo* cancer studies.[25] Another way to account for the immune systems role is through *ex vivo* cultures derived from solid tumor samples taken directly from the patient.[5] Such models will also be important in the future of cancer drug discovery. With further advances in this technique, we will be able to treat these patient cancer cells directly with drug and predict patient drug response. It is easy to envision using this target identification approach with either of these two approaches that take into account the role of the immune system. With regards to *ex viv*o solid tumor patient samples, we could use the described approach for target identification on a patient-to-patient basis. This will further help the goal of personalized medicine come closer to reality.

Development of a Turn-on No-Wash Fluorescent Probe for c-SRC in Live Cell Microscopy Studies

Versatile small molecule probes will be needed to investigate kinase targets identified from the previously described approaches. For example, c-SRC, which has been identified as a target in TNBC in previous studies as well as in a handful PDX screens in **Chapter III**.[26, 27] To this end, I developed a versatile small molecule fluorescent probe, PP2-Coumarin, with turn-on, no-wash, and irreversible features with high selectivity for its target, c-SRC. The development of this probe also expands the scope of small molecule irreversible fluorescent probes through the use of an alternative non-conserved cysteine. I also demonstrated that incorporating a cysteine in the P-loop through mutagenesis can enable this probe's use in other kinases. Thus, by using gene editing or transfecting P-Loop cysteine kinase mutants into cells, localization of other kinases can be investigated. The probe also benefited from being compatible with live-cell super resolution stimulated emission depletion (STED) microscopy techniques, measuring structures below the diffraction limit.

With the probe able to show localization of endogenous c-SRC, I used it in live-cell experiments with TNBC cell lines. I observed differential staining among the TNBC cell lines tested. Additionally, I used this fluorescent probe to show how drug treatment can influence the localization of c-SRC in TNBC cell lines. The capabilities of this or a similar probe would be useful for high-content screens which interrogate changes in c-SRC localization. Such screens, which involve automated high-throughput fluorescent microscopy with automated image analysis, have been recognized as means for their usefulness in phenotypic assays.[5] They can provide a strong mechanistic rationale for observed phenotypes in the screen performed (in this case c-SRC localization and cell viability). This is important as strong mechanistic relationships between phenotype and disease states are integral for further advancing phenotypic-based screens.

My approach demonstrates how features of kinases and their inhibitors can be leveraged to design specific kinase fluorescent probes with a variety of uses. This work also highlights that understanding kinase chemical biology on the molecular level, will be needed to continue investigating these *bona fide* cancer targets.

References

1. Manning, G.; Whyte, D. B.; Martinez, R.; Hunter, T.; Sudarsanam, S., The protein kinase complement of the human genome. *Science* **2002,** *298* (5600), 1912-34.
2. Marshall, C. J., Specificity of receptor tyrosine kinase signaling: transient versus sustained extracellular signal-regulated kinase activation. *Cell* **1995,** *80* (2), 179-85.
3. Zhang, J.; Yang, P. L.; Gray, N. S., Targeting cancer with small molecule kinase inhibitors. *Nature Reviews Cancer* **2009,** *9* (1), 28-39.
4. Wu, P.; Nielsen, T. E.; Clausen, M. H., Small-molecule kinase inhibitors: an analysis of FDA-approved drugs. *Drug Discov Today* **2016,** *21* (1), 5-10.
5. Moffat, J. G.; Rudolph, J.; Bailey, D., Phenotypic screening in cancer drug discovery - past, present and future. *Nature Reviews Drug Discovery* **2014,** *13*, 588-602.
6. Yoshida, T.; Kakegawa, J.; Yamaguchi, T.; Hantani, Y.; Okajima, N.; Sakai, T.; Watanabe, Y.; Nakamura, M., Identification and characterization of a novel chemotype MEK inhibitor able to alter the phosphorylation state of MEK1/2. *Oncotarget* **2012,** *3* (12), 1533-45.
7. Yamaguchi, T.; Yoshida, T.; Kurachi, R.; Kakegawa, J.; Hori, Y.; Nanayama, T.; Hayakawa, K.; Abe, H.; Takagi, K.; Matsuzaki, Y.; Koyama, M.; Yogosawa, S.; Sowa, Y.; Yamori, T.; Tajima, N.; Sakai, T., Identification of JTP-70902, a p15(INK4b)-inductive compound, as a novel MEK1/2 inhibitor. *Cancer Sci* **2007,** *98* (11), 1809-16.
8. Al-Ali, H.; Lee, D. H.; Danzi, M. C.; Nassif, H.; Gautam, P.; Wennerberg, K.; Zuercher, B.; Drewry, D. H.; Lee, J. K.; Lemmon, V. P.; Bixby, J. L., Rational Polypharmacology: Systematically Identifying and Engaging Multiple Drug Targets To Promote Axon Growth. *ACS Chem Biol* **2015,** *10* (8), 1939-51.
9. Al-Ali, H., The evolution of drug discovery: from phenotypes to targets, and back. *Med. Chem. Commun.* **2016,** *7*, 788-798.
10. Nielsen, T. O.; West, R. B., Translating gene expression into clinical care: sarcomas as a paradigm. *J Clin Oncol* **2010,** *28* (10), 1796-805.
11. Burningham, Z.; Hashibe, M.; Spector, L.; Schiffman, J. D., The Epidemiology of Sarcoma. *Clinical Sarcoma Research* **2012,** *2* (1), 14.
12. Borden, E. C.; Baker, L. H.; Bell, R. S.; Bramwell, V.; Demetri, G. D.; Eisenberg, B. L.; Fletcher, C. D.; Fletcher, J. A.; Ladanyi, M.; Meltzer, P.; O'Sullivan, B.; Parkinson, D. R.; Pisters, P. W.; Saxman, S.; Singer, S.; Sundaram, M.; van Oosterom, A. T.; Verweij, J.; Waalen, J.; Weiss, S. W.; Brennan, M. F., Soft tissue sarcomas of adults: state of the translational science. *Clin Cancer Res* **2003,** *9* (6), 1941-56.
13. Taylor, B. S.; Barretina, J.; Maki, R. G.; Antonescu, C. R.; Singer, S.; Ladanyi, M., Advances in sarcoma genomics and new therapeutic targets. *Nat Rev Cancer* **2011,** *11* (8), 541-57.
14. Laporte, A. N.; Ji, J. X.; Ma, L.; Nielsen, T. O.; Brodin, B. A., Identification of cytotoxic agents disrupting synovial sarcoma oncoprotein interactions by proximity ligation assay. *Oncotarget* **2016,** *7* (23), 34384-94.
15. Cassidy, J. W.; Caldas, C.; Bruna, A., Maintaining Tumor Heterogeneity in Patient-Derived Tumor Xenografts. *Cancer Res* **2015,** *75* (15), 2963-8.
16. Aparicio, S.; Hidalgo, M.; Kung, A. L., Examining the utility of patient-derived xenograft mouse models. *Nat Rev Cancer* **2015,** *15* (5), 311-6.

17. Gao, H.; Korn, J. M.; Ferretti, S.; Monahan, J. E.; Wang, Y.; Singh, M.; Zhang, C.; Schnell, C.; Yang, G.; Zhang, Y.; Balbin, O. A.; Barbe, S.; Cai, H.; Casey, F.; Chatterjee, S.; Chiang, D. Y.; Chuai, S.; Cogan, S. M.; Collins, S. D.; Dammassa, E.; Ebel, N.; Embry, M.; Green, J.; Kauffmann, A.; Kowal, C.; Leary, R. J.; Lehar, J.; Liang, Y.; Loo, A.; Lorenzana, E.; Robert McDonald, E., 3rd; McLaughlin, M. E.; Merkin, J.; Meyer, R.; Naylor, T. L.; Patawaran, M.; Reddy, A.; Roelli, C.; Ruddy, D. A.; Salangsang, F.; Santacroce, F.; Singh, A. P.; Tang, Y.; Tinetto, W.; Tobler, S.; Velazquez, R.; Venkatesan, K.; Von Arx, F.; Wang, H. Q.; Wang, Z.; Wiesmann, M.; Wyss, D.; Xu, F.; Bitter, H.; Atadja, P.; Lees, E.; Hofmann, F.; Li, E.; Keen, N.; Cozens, R.; Jensen, M. R.; Pryer, N. K.; Williams, J. A.; Sellers, W. R., High-throughput screening using patient-derived tumor xenografts to predict clinical trial drug response. *Nat Med* **2015,** *21* (11), 1318-25.
18. Hidalgo, M.; Amant, F.; Biankin, A. V.; Budinska, E.; Byrne, A. T.; Caldas, C.; Clarke, R. B.; de Jong, S.; Jonkers, J.; Maelandsmo, G. M.; Roman-Roman, S.; Seoane, J.; Trusolino, L.; Villanueva, A., Patient-derived xenograft models: an emerging platform for translational cancer research. *Cancer Discov* **2014,** *4* (9), 998-1013.
19. Bruna, A.; Rueda, O.; Greenwood, W.; Batra, A.; Callari, M.; Batra, R.; Pogrebniak, K.; Sandoval, J.; Cassidy, J.; Tufegdzic-Vidakovic, A.; Sammut, S. J.; Jones, L.; Provenzano, E.; Baird, R.; Eirew, P.; Hadfield, J.; Eldridge, M.; McLaren-Douglas, A.; Barthorpe, A.; Lightfoot, H.; O'Connor, M.; Gray, J.; Cortes, J.; Baselga, J.; Marangoni, E.; Welm, A.; Aparicio, S.; Serra, V.; Garnett, M.; Caldas, C., A Biobank of Breast Cancer Explants with Preserved Intra-tumor Heterogeneity to Screen Anticancer Compounds. *Cell* **2016,** *167* (1), 260-274 e22.
20. Ivanova, I. A.; Vermeulen, J. F.; Ercan, C.; Houthuijzen, J. M.; Saig, F. A.; Vlug, E. J.; van der Wall, E.; van Diest, P. J.; Vooijs, M.; Derksen, P. W. B., FER kinase promotes breast cancer metastasis by regulating α6- and β1-integrin-dependent cell adhesion and anoikis resistance. *Oncogene* **2013,** *32* (50), 5582-92.
21. Zhang, S.; Chitu, V.; Stanley, E. R.; Elliott, B. E.; Greer, P. A., Fes tyrosine kinase expression in the tumor niche correlates with enhanced tumor growth, angiogenesis, circulating tumor cells, metastasis and infiltrating macrophages. *Cancer Res* **2011,** *71* (4), 1465-73.
22. Maxfield, K. E.; Macion, J.; Vankayalapati, H.; Whitehurst, A. W., SIK2 Restricts Autophagic Flux To Support Triple-Negative Breast Cancer Survival. *Mol Cell Biol* **2016,** *36* (24), 3048-3057.
23. Bayraktar, S.; Gluck, S., Molecularly targeted therapies for metastatic triple-negative breast cancer. *Breast Cancer Res Treat* **2013,** *138* (1), 21-35.
24. Bianchini, G.; Balko, J. M.; Mayer, I. A.; Sanders, M. E.; Gianni, L., Triple-negative breast cancer: challenges and opportunities of a heterogeneous disease. *Nature Reviews Clinical Oncology* **2016,** *13*, 674-690.
25. Lodhia, K. A.; Hadley, A. M.; Haluska, P.; Scott, C. L., Prioritizing therapeutic targets using patient-derived xenograft models. *Biochim Biophys Acta* **2015,** *1855* (2), 223-34.
26. Tryfonopoulos, D.; Walsh, S.; Collins, D. M.; Flanagan, L.; Quinn, C.; Corkery, B.; McDermott, E. W.; Evoy, D.; Pierce, A.; O'Donovan, N.; Crown, J.; Duffy, M. J., Src: a potential target for the treatment of triple-negative breast cancer. *Annals of Oncology* **2011,** *22* (10), 2234-2240.

27. Gilani, R. A.; Phadke, S.; Bao, L. W.; Lachacz, E. J.; Dziubinski, M. L.; Brandvold, K. R.; Steffey, M. E.; Kwarcinski, F. E.; Graveel, C. R.; Kidwell, K. M.; Merajver, S. D.; Soellner, M. B., UM-164: A Potent c-Src/p38 Kinase Inhibitor with In Vivo Activity against Triple-Negative Breast Cancer. *Clin Cancer Res* **2016,** *22* (20), 5087-5096.

APPENDIX A

Supplemental Information for Chapter II

Supplemental Tables

Table A.1: Pharmacologically linked kinase groups. Kinases on the same row represent one group. Kinases were grouped by pharmacological interaction strength (P_{ij}) (direct measure) and sequence similarity (indirect measure) as previously described. Any two kinases with a P_{ij} score ≥ 0.6 or kinase domain sequence similarity score ≥ 0.7 belonged to the same group.[1, 2]

AAK1, BMP2K	CIT	IRAK1	MLTK	PRKAA1, PRKAA2	STK10, SLK
AATK	CLK1, CLK2, CLK3, CLK4	IRAK2	MOS	PRKACA, PRKACB, PRKACG	STK11
ABL1, ABL2	CSF1R	IRAK3	MST1R	PRKCA, PRKCB, PRKCG	STK16
ACVR1, ACVRL1	CSK	IRAK4	MTOR	PRKCD, PRKCQ	STK17B, STK17A
ACVR1B, BMPR1A, BMPR1B, TGFBR1, ACVR1C	CSNK1A1, CSNK1D, CSNK1E	ITK, TEC, TXK	MUSK	PRKCE, PRKCH	STK24, STK25, STK26
ADCK1	CSNK1G2, CSNK1G3, CSNK1G1	JAK1	MYLK	PRKCI, PRKCZ	STK3, STK4
ADCK2	CSNK2A1, CSNK2A2	JAK2	MYLK2	PRKD1, PRKD2, PRKD3	STK31
ADCK3	DAPK1, DAPK3, DAPK2	JAK3	MYLK3, MYLK4	PRKDC	STK32B, STK32A, STK32C
ADCK4	DCLK1, DCLK2	KALRN	MYO3A, MYO3B	PRKG1, PRKG2	STK33
ADCK5	DCLK3	KIT	NEK1, NEK5	PRKX, PRKY	STK35
ADRBK1, ADRBK2	DDR1, DDR2	KSR1, KSR2	NEK10	PRPF4B	STK38, STK38L
AKT1, AKT2, AKT3	DMPK, CDC42BPA, CDC42BPB, CDC42BPG	LATS1, LATS2	NEK11	PSKH1, PSKH2	STK40
ALK, LTK	DSTYK	LIMK1, LIMK2	NEK2	PTK2	STYK1
AMHR2	DYRK1A, DYRK1B	LMTK2	NEK3	PTK2B	SYK
ANKK1	DYRK3, DYRK2	LMTK3	NEK4	PTK6	TAOK2, TAOK3, TAOK1
ARAF, BRAF, RAF1	DYRK4	LRRK1	NEK6, NEK7	PTK7	TBCK
ATM	EEF2K	LRRK2	NEK8	RAGE	TBK1
ATR	EGFR, ERBB2, ERBB4	MAK, ICK	NEK9	RET	TEK, TIE1
AURKA, AURKC, AURKB	EIF2AK1	MAP2K1, MAP2K2	NIM1	RIOK1	TESK1
AXL, MERTK	EIF2AK2	MAP2K3, MAP2K6	NLK	RIOK2	TESK2
BCKDK	EIF2AK3	MAP2K4	NPR1, NPR2	RIOK3	TEX14
BMPR2	EIF2AK4	MAP2K5	NRBP1	RIPK1	TGFBR2
BMX, BTK	EPHA1	MAP2K7	NRBP2	RIPK2	TLK1, TLK2
BRSK2, BRSK1	EPHA10	MAP3K1	NRK	RIPK3	TNK1
BUB1	EPHA2, EPHA3, EPHA4, EPHA5, EPHA7, EPHA8, EPHB1, EPHB2, EPHB3, EPHB4	MAP3K12, MAP3K13	NTRK1, NTRK2, NTRK3	RIPK4	TNK2
BUB1B	EPHA6	MAP3K14	NUAK1, NUAK2	RNASEL	TP53RK
CAMK1, CAMK1D, CAMK1G, PNCK	EPHB6	MAP3K19	OBSCN	ROCK1, ROCK2	TRIB1, TRIB2
CAMK2A, CAMK2B, CAMK2D, CAMK2G	ERBB3	MAP3K3, MAP3K2	OXSR1	ROR1	TRIB3
CAMK4	ERN1	MAP3K4	PAK1, PAK2, PAK3	ROR2	TRIO
CAMKK1	ERN2	MAP3K5, MAP3K6, MAP3K15	PAK4, PAK6, PAK7	ROS1	TRPM7, TRPM6

CAMKK2	FER, FES	MAP3K7	PASK	RPS6KA4, RPS6KA5, RPS6KA2, RPS6KA1, RPS6KA3, RPS6KA6	TSSK2, TSSK1B, IGF1R, INSR, INSRR
CAMKV	FGFR1, FGFR3, FGFR2, FGFR4	MAP3K8	PBK	RPS6KB1, RPS6KB2	TSSK3
CASK	FGR, FYN, SRC, YES1, HCK, BLK, LCK, LYN	MAP3K9, MAP3K10, MAP3K11, MLK4	PDGFRA, PDGFRB	RYK	TSSK4
CDC7	FLT1, KDR	MAP4K2, MAP4K5, MAP4K1	PDIK1L	SBK1	TSSK6
CDK1, CDK2, CDK3, CDK4, CDK6, CDK5	FLT3	MAP4K4, TNIK, MINK1	PDK1, PDK2, PDK3, PDK4	SBK2	TTBK1, TTBK2
CDK10	FLT4	MAPK1, MAPK3	PDPK1	SCYL1	TTK
CDK11A	FRK	MAPK14, MAPK11, MAPK13, MAPK12	PEAK1	SCYL2	TTN
CDK13, CDK12	GAK	MAPK15	PHKG1, PHKG2	SCYL3	TYK2
CDK14, CDK15	GRK1	MAPK4, MAPK6	PI4KB	SGK071	TYRO3
CDK16, CDK17, CDK18	GRK4, GRK5, GRK6	MAPK7	PIK3CA	SGK1, SGK2, SGK3	UHMK1
CDK20	GRK7	MAPK8, MAPK9, MAPK10	PIK3CB, PIK3CD	SGK110	ULK1, ULK2
CDK7	GSG2	MAPKAPK3, MAPKAPK2	PIK3CG	SGK196	ULK3
CDK8, CDK19	GSK3A, GSK3B	MAPKAPK5	PIM1, PIM3	SGK223	ULK4
CDK9	GUCY2D	MARK2, MARK1, MARK3, MARK4, SIK2, SIK3, SIK1	PIM2	SGK494	VRK1
CDKL1, CDKL4	GUCY2F	MAST1, MAST3, MAST2, MAST4	PINK1	SMG1	VRK2
CDKL2	HIPK3, HIPK2, HIPK1	MASTL	PKDCC	SNRK	VRK3
CDKL3	HIPK4	MATK	PKMYT1	SPEG	WEE1
CDKL5	HUNK	MELK	PKN1, PKN2, PKN3	SRMS	WEE2
CHEK1	IKBKB	MET	PLK1	SRPK1	WNK1, WNK4, WNK3, WNK2
CHEK2	IKBKE	MKNK2, MKNK1	PLK3, PLK2	SRPK2	ZAP70
CHUK	ILK	MLKL	PLK4	SRPK3	

Table A.2: Complete MAXIS, B_k, and Combination Scores for kinase groups for each sarcoma screen performed. One representative of kinase groups is shown.

A673

Cluster MAXIS Rank	Cluster MAXIS score	Cluster Mean Bk	Combined Score	Kinase Group
39	15	0.285029	4.275442	ABL1
50	5	0.366382	1.831909	AKT1
30	25	0.888609	22.21521	ALK
292	0	-0.31528	0	ARAF
11	61	0.369814	22.55866	AURKA
40	15	0.399117	5.98675	AXL
3	75	0.648396	48.62973	BMX
16	49	0.661184	32.39803	BRSK2
99	0	0	0	CAMK1
4	73	1.4275	104.2075	CAMK2A
98	0	0	0	CAMK4
13	60	0.537511	32.25063	CDK1
101	0	0	0	CHEK1
123	0	-0.0394	0	CHEK2
173	0	0	0	CHUK
27	27	0.672984	18.17056	CLK1
49	6	0.429612	2.577672	CSF1R
253	0	0.257508	0	CSK
134	0	-0.09141	0	CSNK1A1
12	60	-0.7608	-45.6477	CSNK1G2
152	0	0.242105	0	CSNK2A1
110	0	-0.15867	0	DAPK1
112	0	0	0	DCLK1
255	0	-0.05318	0	DDR1
23	31	0.654125	20.27787	DMPK
15	52	0.645512	33.56664	DYRK1A
153	0	-0.23831	0	DYRK3
25	29	-0.61347	-17.7908	EGFR
48	6	0.246613	1.479679	EPHA2
22	34	0.981461	33.36969	FER
262	0	0.258727	0	FGFR1
29	27	0.287568	7.764339	FGR
278	0	0.068228	0	FLT1
114	0	0	0	MAPKAPK3
115	0	0	0	MAPKAPK5
60	2	0.262868	0.525735	MARK2
42	11	0.567735	6.245086	MELK
268	0	0.245139	0	MET
24	31	-0.12706	-3.9388	MKNK2
14	54	0.877171	47.36723	MST1R
21	35	0.521902	18.26656	MUSK
183	0	0.391939	0	NEK1
17	49	1.509259	73.95369	NEK2
188	0	0	0	NEK6
38	15	1.064055	15.96082	NEK9
54	5	0.247269	1.236346	NTRK1
9	69	0.661788	45.66336	NUAK1
239	0	0.060841	0	PAK1
240	0	-0.07867	0	PAK4
41	15	0.392368	5.885524	PDGFRA
71	0	0	0	PDPK1
46	8	0.563568	4.508548	PHKG1
62	1	0.404439	0.404439	PI4KB
8	72	0.738437	53.16744	PIK3CA
31	25	0.556972	13.92429	PIK3CB
120	0	0.186258	0	PIM1
121	0	-0.25157	0	PIM2
1	95	0.965582	91.73028	PLK1
72	0	0.089451	0	PRKACA
75	0	0.199512	0	PRKCD
57	3	0.443606	1.330819	PRKCE
76	0	0	0	PRKCI
2	81	0.598393	48.46981	PRKD1
58	3	0.315364	0.946092	PRKG1
73	0	-0.01642	0	PRKX
6	72	1.014537	73.04669	PTK2B

269	0	0.180533	0	FLT3
59	3	0.254333	0.762999	FLT4
273	0	-0.14945	0	FRK
37	15	0.552743	8.29115	GRK7
44	10	0.31998	3.199803	GSK3A
32	24	0.839199	20.14077	HIPK3
36	16	0.617624	9.881983	HIPK4
174	0	0	0	IKBKB
33	23	0.779173	17.92099	IKBKE
55	5	-1.51733	-7.58667	IRAK4
56	4	0.196942	0.787769	ITK
263	0	0	0	JAK1
7	72	-1.55268	-111.793	JAK2
26	29	-0.68164	-19.7676	JAK3
45	9	0.241	2.168998	KIT
19	37	0.529439	19.58925	LRRK2
243	0	-0.18172	0	MAP2K1
235	0	0.049282	0	MAP4K2
236	0	-0.01016	0	MAP4K4
156	0	0	0	MAPK1
35	20	-0.53337	-10.6674	MAPK14
61	1	-0.44091	-0.44091	MAPK8

274	0	-0.14032	0	PTK6
47	8	0.242517	1.940137	RET
43	10	0.226154	2.261543	ROCK1
18	38	0.882808	33.54669	ROS1
51	5	0.109048	0.54524	RPS6KA4
5	72	0.280631	20.2054	RPS6KB1
79	0	0.160845	0	SGK1
305	0	-0.29879	0	SRMS
163	0	0.474665	0	SRPK1
165	0	-0.29808	0	SRPK3
28	27	0.600537	16.21449	STK10
242	0	-0.03472	0	STK24
52	5	0.002802	0.014011	STK3
275	0	0.116398	0	SYK
175	0	-0.00972	0	TBK1
34	22	0.304127	6.690789	TEK
53	5	0.607175	3.035874	TNK1
250	0	-0.01044	0	TNK2
10	61	1.036474	63.22494	TSSK2
20	35	0.570427	19.96495	TTK
264	0	-0.47866	0	TYK2
251	0	0.171951	0	TYRO3
276	0	0	0	ZAP70

TC32

Cluster MAXIS Rank	Cluster MAXIS score	Cluster Mean Bk	Combined Score	Kinase Group
60	2	0.230314	0.460627	ABL1
31	17	0.522048	8.874818	AKT1
28	20	0.832483	16.64966	ALK
12	63	-0.54371	-34.2537	ARAF
48	5	0.170406	0.852029	AURKA
255	0	0.341658	0	AXL
24	25	0.607231	15.18078	BMX
41	7	0.366793	2.567553	BRSK2
102	0	0	0	CAMK1
63	1	0.482061	0.482061	CAMK2A
101	0	0	0	CAMK4
6	80	0.314138	25.13107	CDK1
104	0	0.301775	0	CHEK1
127	0	0.112105	0	CHEK2
178	0	0	0	CHUK
26	21	0.465435	9.774142	CLK1
57	3	0.466382	1.399145	CSF1R
258	0	0.305525	0	CSK
66	1	0.151423	0.151423	CSNK1A1
138	0	-0.12947	0	CSNK1G2
156	0	0.15085	0	CSNK2A1
35	12	0.392199	4.706387	DAPK1
115	0	0	0	DCLK1
50	4	0.305508	1.222032	DDR1
54	3	0.523986	1.571959	DMPK
43	6	0.398413	2.390478	DYRK1A
15	56	-0.7998	-44.7889	DYRK3
39	9	-0.32638	-2.93739	EGFR
27	21	0.500452	10.5095	EPHA2
21	29	0.914852	26.53071	FER
51	4	0.335558	1.342231	FGFR1
9	78	0.350235	27.31831	FGR
16	52	0.490206	25.49073	FLT1
270	0	0.197513	0	FLT3
45	6	0.481589	2.889534	FLT4
274	0	0.106278	0	FRK

Cluster MAXIS Rank	Cluster MAXIS score	Cluster Mean Bk	Combined Score	Kinase Group
117	0	0	0	MAPKAPK3
118	0	0	0	MAPKAPK5
23	25	0.322514	8.062852	MARK2
107	0	0.272199	0	MELK
56	3	0.378866	1.136597	MET
119	0	0.002132	0	MKNK2
37	10	0.464881	4.64881	MST1R
8	78	0.733805	57.23676	MUSK
188	0	0.167279	0	NEK1
4	89	1.503703	133.8296	NEK2
193	0	0	0	NEK6
5	83	0.911231	75.63219	NEK9
53	4	0.207226	0.828903	NTRK1
64	1	0.351628	0.351628	NUAK1
244	0	-0.10423	0	PAK1
245	0	0.201775	0	PAK4
25	24	0.407739	9.785733	PDGFRA
13	60	0.523213	31.39281	PDPK1
124	0	0.465016	0	PHKG1
305	0	0.306775	0	PI4KB
3	96	0.833324	79.99907	PIK3CA
46	6	0.422727	2.536363	PIK3CB
65	1	0.221206	0.221206	PIM1
125	0	-0.05067	0	PIM2
38	9	0.655662	5.900956	PLK1
77	0	0.282496	0	PRKACA
62	1	0.335627	0.335627	PRKCD
40	7	0.504655	3.532582	PRKCE
80	0	0	0	PRKCI
1	100	0.693563	69.3563	PRKD1
58	2	0.369058	0.738116	PRKG1
78	0	0.235743	0	PRKX
18	33	0.99908	32.96965	PTK2B
275	0	0.162474	0	PTK6
44	6	0.255882	1.535294	RET
69	0	0.11601	0	ROCK1

36	11	0.497061	5.46767	GRK7
159	0	0.021901	0	GSK3A
22	27	0.654839	17.68065	HIPK3
17	33	0.639048	21.08859	HIPK4
179	0	-0.27789	0	IKBKB
19	31	0.474395	14.70625	IKBKE
67	1	-1.475	-1.475	IRAK4
52	4	0.035526	0.142105	ITK
266	0	0	0	JAK1
10	71	-0.87889	-62.4015	JAK2
61	2	-0.47828	-0.95656	JAK3
29	19	0.349361	6.637851	KIT
30	18	0.251646	4.529622	LRRK2
247	0	0.057846	0	MAP2K1
240	0	-0.0869	0	MAP4K2
241	0	-0.04746	0	MAP4K4
160	0	0	0	MAPK1
2	98	0.236492	23.17619	MAPK14
164	0	-0.10198	0	MAPK8

33	14	0.792306	11.09229	ROS1
20	29	0.377931	10.95999	RPS6KA4
7	79	0.500493	39.53891	RPS6KB1
47	5	0.50166	2.508301	SGK1
304	0	-0.05069	0	SRMS
168	0	0.442923	0	SRPK1
170	0	-0.45856	0	SRPK3
32	17	0.511051	8.687868	STK10
55	3	0.479048	1.437143	STK24
14	60	-0.2944	-17.6637	STK3
276	0	-0.1212	0	SYK
180	0	-0.43291	0	TBK1
42	7	0.62345	4.364149	TEK
49	4	0.624509	2.498038	TNK1
254	0	0.087576	0	TNK2
11	70	1.08115	75.68048	TSSK2
59	2	0.488756	0.977512	TTK
34	13	-1.5	-19.5	TYK2
256	0	0	0	TYRO3
277	0	0	0	ZAP70

MG63

Cluster MAXIS Rank	Cluster MAXIS score	Cluster Mean Bk	Combined Score	Kinase Groups
250	0	0.250132	0	ABL1
22	27	0.502368	13.56393	AKT1
36	15	0.786955	11.80432	ALK
292	0	-0.19004	0	ARAF
58	1	-0.0323	-0.0323	AURKA
252	0	0.352027	0	AXL
50	8	0.479285	3.834277	BMX
40	12	0.495858	5.950298	BRSK2
99	0	0	0	CAMK1
51	6	0.284007	1.704043	CAMK2A
98	0	0	0	CAMK4
5	67	0.675922	45.28677	CDK1
101	0	0.37033	0	CHEK1
126	0	-0.04903	0	CHEK2
174	0	-1.56667	0	CHUK
18	31	0.6397	19.83071	CLK1
41	12	0.503243	6.038912	CSF1R
255	0	-0.01482	0	CSK
45	10	-0.53076	-5.30762	CSNK1A1
26	22	-1.4875	-32.725	CSNK1G2
154	0	-0.02049	0	CSNK2A1
111	0	-0.15259	0	DAPK1
113	0	0	0	DCLK1
59	1	0.343245	0.343245	DDR1
23	25	0.465686	11.64216	DMPK
3	70	0.633744	44.36205	DYRK1A
16	36	-0.38804	-13.9693	DYRK3
27	21	-0.58301	-12.2432	EGFR
38	14	0.425992	5.963881	EPHA2
20	28	1.072757	30.03721	FER
42	11	-0.21996	-2.41959	FGFR1
56	4	0.126379	0.505515	FGR
14	47	0.511597	24.04505	FLT1
43	11	0.342621	3.768835	FLT3
34	18	0.59254	10.66572	FLT4
272	0	-0.43209	0	FRK

Cluster MAXIS Rank	Cluster MAXIS score	Cluster Mean Bk	Combined Score	Kinase Groups
115	0	0	0	MAPKAPK3
116	0	0	0	MAPKAPK5
12	52	0.486746	25.31078	MARK2
104	0	0.272263	0	MELK
267	0	-0.13799	0	MET
117	0	-0.02804	0	MKNK2
268	0	0.471674	0	MST1R
39	14	0.654393	9.161506	MUSK
183	0	-0.22549	0	NEK1
8	58	0.794085	46.05695	NEK2
188	0	0	0	NEK6
11	53	0.933221	49.46071	NEK9
54	5	0.342885	1.714427	NTRK1
13	47	0.508175	23.88424	NUAK1
240	0	-0.59275	0	PAK1
241	0	0.181031	0	PAK4
2	71	0.440582	31.28131	PDGFRA
69	0	-1.58333	0	PDPK1
122	0	-0.00903	0	PHKG1
305	0	0.435323	0	PI4KB
1	84	0.961929	80.80201	PIK3CA
32	19	0.800948	15.21801	PIK3CB
44	10	0.249405	2.494045	PIM1
123	0	-0.36487	0	PIM2
10	54	0.925011	49.95057	PLK1
70	0	0.005745	0	PRKACA
73	0	0.129899	0	PRKCD
52	5	0.383232	1.916159	PRKCE
74	0	0	0	PRKCI
124	0	0.308789	0	PRKD1
75	0	0.243631	0	PRKG1
71	0	0.276639	0	PRKX
4	70	0.888169	62.17182	PTK2B
37	15	-0.36584	-5.48764	PTK6
49	9	0.358515	3.226634	RET
61	0	0.023334	0	ROCK1

47	9	0.378272	3.404446	GRK7
17	34	0.431283	14.66362	GSK3A
25	23	0.768521	17.67599	HIPK3
30	19	0.638808	12.13735	HIPK4
53	5	-1.54213	-7.71065	IKBKB
24	25	0.61317	15.32925	IKBKE
281	0	-1.484	0	IRAK4
275	0	-0.59954	0	ITK
263	0	-1.57778	0	JAK1
28	21	-0.76952	-16.16	JAK2
9	55	-1.57917	-86.8542	JAK3
33	18	0.302911	5.452392	KIT
21	28	0.553599	15.50077	LRRK2
243	0	-0.12198	0	MAP2K1
235	0	0.134817	0	MAP4K2
236	0	0.027998	0	MAP4K4
157	0	0	0	MAPK1
7	60	-1.299	-77.9401	MAPK14
48	9	-0.68586	-6.17276	MAPK8

29	20	0.81425	16.285	ROS1
19	29	0.297617	8.630896	RPS6KA4
77	0	0.305195	0	RPS6KB1
79	0	0.38283	0	SGK1
6	62	-1.55667	-96.5133	SRMS
164	0	0.608774	0	SRPK1
166	0	-0.09424	0	SRPK3
46	10	0.51111	5.111095	STK10
35	16	0.668885	10.70216	STK24
238	0	-0.03272	0	STK3
273	0	0	0	SYK
175	0	-0.15049	0	TBK1
276	0	0.211128	0	TEK
55	4	0.570942	2.283766	TNK1
251	0	0.05631	0	TNK2
15	45	0.878149	39.5167	TSSK2
57	2	0.495424	0.990848	TTK
31	19	-1.53168	-29.1018	TYK2
253	0	0.27033	0	TYRO3
274	0	0	0	ZAP70

SAOS2

Cluster MAXIS Rank	Cluster MAXIS score	Cluster Mean Bk	Combined Score	Kinase Groups
12	39	0.462225	18.02678	ABL1
16	33	0.667329	22.02185	AKT1
20	27	0.678128	18.30946	ALK
293	0	-0.10704	0	ARAF
24	24	0.306564	7.357544	AURKA
249	0	0.1283	0	AXL
42	11	0.596814	6.564949	BMX
39	11	0.430383	4.734212	BRSK2
94	0	0	0	CAMK1
95	0	0.133745	0	CAMK2A
93	0	0	0	CAMK4
18	30	0.530657	15.9197	CDK1
97	0	0.254505	0	CHEK1
121	0	-0.52734	0	CHEK2
173	0	0	0	CHUK
13	37	0.541599	20.03916	CLK1
37	12	0.427494	5.129925	CSF1R
252	0	0.385383	0	CSK
132	0	0.003615	0	CSNK1A1
6	66	-1.50364	-99.2404	CSNK1G2
150	0	0.191683	0	CSNK2A1
107	0	-0.23462	0	DAPK1
109	0	0	0	DCLK1
254	0	0.286125	0	DDR1
21	26	0.765219	19.89568	DMPK
9	60	0.536732	32.20392	DYRK1A
40	11	-0.38344	-4.21782	DYRK3
4	74	-0.94007	-69.5649	EGFR
49	7	0.302317	2.116221	EPHA2
23	25	0.918508	22.96271	FER
261	0	0.46237	0	FGFR1
10	51	0.33228	16.94626	FGR
29	19	0.41076	7.804448	FLT1
267	0	0.171872	0	FLT3
43	11	0.450395	4.954342	FLT4
272	0	0.364724	0	FRK

Cluster MAXIS Rank	Cluster MAXIS score	Cluster Mean Bk	Combined Score	Kinase Groups
111	0	0	0	MAPKAPK3
112	0	0	0	MAPKAPK5
31	16	0.329027	5.264427	MARK2
100	0	0.315592	0	MELK
266	0	0.342078	0	MET
113	0	-0.16951	0	MKNK2
56	2	0.617727	1.235453	MST1R
51	7	0.5472	3.830402	MUSK
182	0	0.320918	0	NEK1
8	64	0.736351	47.12647	NEK2
187	0	0	0	NEK6
5	67	0.909397	60.92963	NEK9
61	1	0.151763	0.151763	NTRK1
53	5	0.401723	2.008614	NUAK1
239	0	-0.68644	0	PAK1
240	0	0.093061	0	PAK4
26	23	0.38641	8.887441	PDGFRA
54	3	-1.55	-4.65	PDPK1
118	0	-0.36203	0	PHKG1
52	6	0.642727	3.856359	PI4KB
2	92	0.93974	86.45609	PIK3CA
35	15	0.601739	9.026084	PIK3CB
55	3	0.241624	0.724873	PIM1
119	0	-0.11297	0	PIM2
15	34	0.771363	26.22634	PLK1
44	9	0.510246	4.59221	PRKACA
33	15	0.482698	7.240467	PRKCD
25	23	0.680446	15.65025	PRKCE
71	0	0	0	PRKCI
1	100	0.781029	78.10288	PRKD1
17	33	0.526339	17.36917	PRKG1
45	9	0.521128	4.690148	PRKX
7	66	0.854602	56.40376	PTK2B
273	0	-0.15886	0	PTK6
268	0	0.093012	0	RET
22	26	0.378164	9.83227	ROCK1

38	11	0.510079	5.610874	GRK7
153	0	0.246448	0	GSK3A
27	21	0.726279	15.25185	HIPK3
19	29	0.696394	20.19542	HIPK4
34	15	-1.54531	-23.1797	IKBKB
32	16	0.465492	7.447864	IKBKE
281	0	-1.475	0	IRAK4
57	2	0.354769	0.709537	ITK
262	0	-1.53778	0	JAK1
50	7	-0.7352	-5.14642	JAK2
60	1	-0.5706	-0.5706	JAK3
46	9	0.26672	2.400478	KIT
286	0	0.289619	0	LRRK2
58	1	-1.5246	-1.5246	MAP2K1
235	0	-0.1892	0	MAP4K2
236	0	-0.14261	0	MAP4K4
154	0	0	0	MAPK1
160	0	-0.05172	0	MAPK14
158	0	-0.4233	0	MAPK8

14	36	0.736399	26.51035	ROS1
3	78	0.446706	34.84304	RPS6KA4
73	0	0.307432	0	RPS6KB1
36	13	0.371863	4.834218	SGK1
47	9	-0.47718	-4.29464	SRMS
163	0	0.243061	0	SRPK1
165	0	-0.12748	0	SRPK3
30	18	0.438923	7.90062	STK10
242	0	0.267078	0	STK24
48	8	-0.3462	-2.76963	STK3
274	0	0.078509	0	SYK
174	0	-0.14492	0	TBK1
276	0	0.142603	0	TEK
41	11	0.590794	6.498735	TNK1
59	1	0.207525	0.207525	TNK2
11	41	0.818838	33.57235	TSSK2
218	0	0.192604	0	TTK
28	19	-1.52789	-29.03	TYK2
250	0	0	0	TYRO3
275	0	0	0	ZAP70

U2OS

Cluster MAXIS Rank	Cluster MAXIS score	Cluster Mean Bk	Combined Score	Kinase Groups
14	39	0.614956	23.98328	ABL1
59	0	0.13992	0	AKT1
31	22	0.430553	9.472167	ALK
28	24	-0.79118	-18.9884	ARAF
38	12	0.280355	3.364258	AURKA
25	28	0.566018	15.8485	AXL
11	48	0.57643	27.66863	BMX
21	31	0.743642	23.05291	BRSK2
99	0	0	0	CAMK1
100	0	0	0	CAMK2A
98	0	0	0	CAMK4
5	74	0.840164	62.17217	CDK1
102	0	0.484615	0	CHEK1
126	0	-0.14488	0	CHEK2
176	0	0	0	CHUK
17	36	0.720776	25.94794	CLK1
47	6	0.414145	2.484868	CSF1R
254	0	-0.10963	0	CSK
55	1	-0.64005	-0.64005	CSNK1A1
137	0	-1.4996	0	CSNK1G2
155	0	-0.20584	0	CSNK2A1
112	0	0.017857	0	DAPK1
114	0	0	0	DCLK1
256	0	0.383049	0	DDR1
61	0	0.325714	0	DMPK
22	30	0.716735	21.50206	DYRK1A
156	0	-0.05595	0	DYRK3
42	8	-0.27197	-2.17576	EGFR
24	29	-0.71764	-20.8115	EPHA2
52	2	0.595833	1.191667	FER
15	39	0.095159	3.711196	FGFR1
1	94	0.443484	41.6875	FGR
279	0	0.102425	0	FLT1
57	1	0.326223	0.326223	FLT3
43	8	0.411059	3.288473	FLT4
272	0	0.229947	0	FRK

Cluster MAXIS Rank	Cluster MAXIS score	Cluster Mean Bk	Combined Score	Kinase Groups
116	0	0	0	MAPKAPK3
117	0	0	0	MAPKAPK5
16	36	0.584904	21.05656	MARK2
105	0	0.058824	0	MELK
267	0	0.045833	0	MET
118	0	-0.01712	0	MKNK2
268	0	0.459615	0	MST1R
35	18	0.66311	11.93598	MUSK
187	0	0.172115	0	NEK1
10	58	0.836403	48.51138	NEK2
192	0	0	0	NEK6
4	78	0.939696	73.29628	NEK9
278	0	0.261259	0	NTRK1
33	18	0.782762	14.08971	NUAK1
49	5	-0.49015	-2.45075	PAK1
242	0	-0.06667	0	PAK4
29	23	0.493929	11.36037	PDGFRA
3	80	0.807215	64.57721	PDPK1
123	0	0.021324	0	PHKG1
30	23	0.652778	15.01389	PI4KB
2	90	0.855998	77.03982	PIK3CA
46	7	0.481094	3.367656	PIK3CB
44	7	0.29726	2.080817	PIM1
124	0	-0.19015	0	PIM2
23	29	0.866185	25.11938	PLK1
70	0	0.120803	0	PRKACA
73	0	-0.18425	0	PRKCD
74	0	-0.08052	0	PRKCE
75	0	0	0	PRKCI
54	1	-0.03564	-0.03564	PRKD1
76	0	0.03037	0	PRKG1
71	0	0.185521	0	PRKX
8	61	0.712025	43.43355	PTK2B
273	0	-0.29299	0	PTK6
58	1	0.200603	0.200603	RET
12	47	-1.59504	-74.967	ROCK1

65	0	0.284615	0	GRK7
20	32	0.634356	20.29939	GSK3A
18	34	0.901475	30.65014	HIPK3
40	10	0.666383	6.663829	HIPK4
177	0	-1.54213	0	IKBKB
178	0	0.182039	0	IKBKE
283	0	-1.48667	0	IRAK4
51	3	-0.86797	-2.6039	ITK
263	0	0.512394	0	JAK1
26	28	-1.5615	-43.722	JAK2
13	46	-1.56316	-71.9053	JAK3
37	16	0.383351	6.133611	KIT
9	60	-1.49643	-89.7857	LRRK2
244	0	0.365743	0	MAP2K1
34	18	0.658242	11.84835	MAP4K2
39	11	0.374453	4.118983	MAP4K4
159	0	0	0	MAPK1
7	62	-1.53812	-95.3637	MAPK14
19	34	-1.53021	-52.0271	MAPK8

48	6	0.767742	4.60645	ROS1
27	24	-1.28265	-30.7835	RPS6KA4
53	1	-1.47989	-1.47989	RPS6KB1
79	0	0.522115	0	SGK1
6	71	-1.56154	-110.869	SRMS
166	0	0.560217	0	SRPK1
168	0	0.110714	0	SRPK3
36	16	0.594816	9.517057	STK10
32	21	0.737619	15.49	STK24
56	1	0.233988	0.233988	STK3
274	0	0.298505	0	SYK
179	0	0.046429	0	TBK1
276	0	-0.19369	0	TEK
251	0	0.32524	0	TNK1
41	10	0.411716	4.11716	TNK2
50	4	0.396813	1.587254	TSSK2
223	0	0.019868	0	TTK
45	7	-1.55057	-10.854	TYK2
252	0	0	0	TYRO3
275	0	0	0	ZAP70

SYO1

Cluster MAXIS Rank	Cluster MAXIS score	Cluster Mean Bk	Combined Score	Kinase Groups
37	6	0.791189	4.747134	ABL1
25	15	1.260228	18.90342	AKT1
28	12	0.560921	6.73105	ALK
291	0	0.328345	0	ARAF
31	9	0.411208	3.70087	AURKA
15	42	0.809304	33.99076	AXL
39	6	0.825952	4.955711	BMX
43	4	0.386188	1.544754	BRSK2
93	0	0	0	CAMK1
94	0	0	0	CAMK2A
92	0	0	0	CAMK4
17	35	0.731052	25.58681	CDK1
96	0	0.21217	0	CHEK1
44	4	1.502778	6.01111	CHEK2
171	0	0	0	CHUK
33	7	0.960073	6.720511	CLK1
52	2	0.812507	1.625014	CSF1R
252	0	-0.00861	0	CSK
46	3	0.473437	1.420312	CSNK1A1
129	0	0.228555	0	CSNK1G2
147	0	0.109804	0	CSNK2A1
106	0	0.024726	0	DAPK1
108	0	0	0	DCLK1
14	43	0.899528	38.67972	DDR1
57	0	0.630451	0	DMPK
148	0	0.456146	0	DYRK1A
149	0	0.117038	0	DYRK3
254	0	-0.31452	0	EGFR
21	27	1.161113	31.35004	EPHA2
23	26	1.068332	27.77663	FER
27	15	0.689197	10.33795	FGFR1
10	62	0.597895	37.06949	FGR
30	11	1.037298	11.41027	FLT1
49	3	0.71876	2.15628	FLT3
51	3	1.037384	3.112153	FLT4
42	5	0.883621	4.418107	FRK

Cluster MAXIS Rank	Cluster MAXIS score	Cluster Mean Bk	Combined Score	Kinase Groups
110	0	0	0	MAPKAPK3
111	0	0	0	MAPKAPK5
22	26	0.641437	16.67737	MARK2
99	0	0.399164	0	MELK
48	3	0.83964	2.51892	MET
112	0	0.139911	0	MKNK2
267	0	0.118731	0	MST1R
29	11	0.753299	8.286291	MUSK
181	0	0.528837	0	NEK1
6	83	1.511111	125.4222	NEK2
186	0	0	0	NEK6
41	5	0.698708	3.493539	NEK9
34	7	0.487506	3.41254	NTRK1
32	7	0.883954	6.187675	NUAK1
238	0	-0.21063	0	PAK1
239	0	0.143335	0	PAK4
4	96	0.779259	74.80882	PDGFRA
66	0	0.181234	0	PDPK1
117	0	0.50958	0	PHKG1
305	0	0.167141	0	PI4KB
13	51	0.782638	39.91451	PIK3CA
53	2	0.472796	0.945592	PIK3CB
24	17	0.736418	12.5191	PIM1
12	53	1.458333	77.29167	PIM2
206	0	0.297519	0	PLK1
67	0	0.574063	0	PRKACA
69	0	0.369789	0	PRKCD
18	33	1.615152	53.30001	PRKCE
70	0	0	0	PRKCI
9	66	0.973469	64.24899	PRKD1
40	5	0.580125	2.900626	PRKG1
8	73	1.55	113.15	PRKX
16	42	0.705006	29.61024	PTK2B
271	0	0.516016	0	PTK6
45	4	0.816088	3.264353	RET
54	1	0.434039	0.434039	ROCK1

61	0	0.164565	0	GRK7
7	77	0.621543	47.85883	GSK3A
151	0	0.569245	0	HIPK3
36	6	0.717314	4.303884	HIPK4
26	15	-1.52083	-22.8125	IKBKB
172	0	0.804366	0	IKBKE
279	0	-0.51862	0	IRAK4
274	0	0.366099	0	ITK
261	0	0	0	JAK1
2	100	-0.96648	-96.6485	JAK2
262	0	-0.26286	0	JAK3
3	99	0.69279	68.58621	KIT
284	0	0.59192	0	LRRK2
242	0	-0.2671	0	MAP2K1
235	0	0.406866	0	MAP4K2
5	89	0.531018	47.26056	MAP4K4
153	0	0	0	MAPK1
1	100	0.506079	50.60786	MAPK14
157	0	0.437406	0	MAPK8

20	28	0.987268	27.6435	ROS1
35	6	0.758916	4.553498	RPS6KA4
11	58	1.47037	85.28146	RPS6KB1
73	0	0.470312	0	SGK1
304	0	-0.22454	0	SRMS
161	0	0.041079	0	SRPK1
163	0	-0.46567	0	SRPK3
47	3	0.587673	1.763018	STK10
241	0	0.452118	0	STK24
55	1	0.314243	0.314243	STK3
272	0	0	0	SYK
173	0	0.345503	0	TBK1
50	3	1.533611	4.600833	TEK
249	0	0.383105	0	TNK1
38	6	0.691863	4.151181	TNK2
19	33	0.640581	21.13918	TSSK2
218	0	0.592401	0	TTK
263	0	-0.77862	0	TYK2
250	0	0	0	TYRO3
273	0	0	0	ZAP70

MOJO

Cluster MAXIS Rank	Cluster MAXIS score	Cluster Mean Bk	Combined Score	Kinase Groups
243	0	-0.15336	0	ABL1
21	29	0.750595	21.76724	AKT1
39	13	0.492891	6.407584	ALK
12	43	-0.85614	-36.8142	ARAF
24	27	0.421685	11.3855	AURKA
56	2	0.433369	0.866738	AXL
52	6	0.329983	1.979899	BMX
10	46	0.725763	33.38511	BRSK2
91	0	0	0	CAMK1
92	0	0.338483	0	CAMK2A
90	0	0	0	CAMK4
20	32	0.680589	21.77886	CDK1
33	18	0.715842	12.88515	CHEK1
117	0	0.153089	0	CHEK2
167	0	0	0	CHUK
25	26	0.726704	18.89431	CLK1
43	12	0.477112	5.725347	CSF1R
246	0	0.021717	0	CSK
58	1	-0.54895	-0.54895	CSNK1A1
128	0	-0.31666	0	CSNK1G2
146	0	0.204314	0	CSNK2A1
102	0	-0.2213	0	DAPK1
104	0	0	0	DCLK1
248	0	0.274222	0	DDR1
49	7	0.828697	5.80088	DMPK
15	40	0.709784	28.39137	DYRK1A
147	0	0.178599	0	DYRK3
249	0	-0.07233	0	EGFR
251	0	-0.1074	0	EPHA2
23	28	0.853342	23.89356	FER
257	0	0.294182	0	FGFR1
271	0	0.147909	0	FGR
4	87	0.510267	44.39321	FLT1
57	2	0.357844	0.715689	FLT3
44	12	0.542758	6.513099	FLT4
270	0	-0.02766	0	FRK

Cluster MAXIS Rank	Cluster MAXIS score	Cluster Mean Bk	Combined Score	Kinase Groups
106	0	0	0	MAPKAPK3
107	0	0	0	MAPKAPK5
54	3	0.443463	1.330389	MARK2
51	6	0.650649	3.903896	MELK
264	0	-0.22688	0	MET
108	0	-0.27715	0	MKNK2
265	0	0.461312	0	MST1R
42	12	0.645797	7.749562	MUSK
177	0	0.340084	0	NEK1
7	73	0.812031	59.27826	NEK2
182	0	0	0	NEK6
5	74	0.978317	72.39545	NEK9
53	4	0.366804	1.467215	NTRK1
18	37	0.674658	24.96235	NUAK1
234	0	0.352222	0	PAK1
235	0	-0.0876	0	PAK4
28	23	0.413713	9.515402	PDGFRA
3	88	0.791198	69.62543	PDPK1
113	0	0.289671	0	PHKG1
305	0	0.459371	0	PI4KB
38	14	0.944016	13.21622	PIK3CA
2	97	0.867344	84.13236	PIK3CB
114	0	0.159976	0	PIM1
115	0	-0.11525	0	PIM2
35	16	0.747002	11.95202	PLK1
30	20	0.506752	10.13503	PRKACA
36	14	0.404043	5.656606	PRKCD
31	19	0.709837	13.48689	PRKCE
69	0	0	0	PRKCI
1	100	0.825058	82.50585	PRKD1
13	42	0.649283	27.2699	PRKG1
55	2	0.595711	1.191421	PRKX
27	23	0.80916	18.61067	PTK2B
16	39	-0.72263	-28.1827	PTK6
266	0	0.332263	0	RET
8	68	0.680744	46.29062	ROCK1

47	9	0.594265	5.348384	GRK7
45	10	0.298612	2.986118	GSK3A
6	73	0.901677	65.82245	HIPK3
19	33	0.774876	25.5709	HIPK4
168	0	-1.55417	0	IKBKB
37	14	0.670794	9.391119	IKBKE
280	0	0.167501	0	IRAK4
274	0	0.407143	0	ITK
258	0	-1.63472	0	JAK1
259	0	-0.36109	0	JAK2
260	0	-0.52485	0	JAK3
50	7	0.362761	2.539325	KIT
285	0	0.15197	0	LRRK2
46	10	0.64592	6.459197	MAP2K1
229	0	0.074659	0	MAP4K2
230	0	0.081754	0	MAP4K4
150	0	0	0	MAPK1
11	45	-1.28519	-57.8337	MAPK14
48	9	-0.66035	-5.94313	MAPK8

26	25	0.768358	19.20895	ROS1
9	59	0.52101	30.73958	RPS6KA4
22	29	0.571873	16.58432	RPS6KB1
41	12	0.489267	5.871206	SGK1
304	0	-0.16574	0	SRMS
157	0	0.570919	0	SRPK1
159	0	-0.14908	0	SRPK3
34	17	0.474396	8.064724	STK10
17	38	0.900783	34.22976	STK24
232	0	0.242388	0	STK3
272	0	0	0	SYK
169	0	0.074835	0	TBK1
275	0	0.130549	0	TEK
32	19	0.663015	12.59728	TNK1
244	0	-0.04743	0	TNK2
14	40	0.81433	32.5732	TSSK2
59	1	0.557867	0.557867	TTK
29	21	-1.52789	-32.0857	TYK2
40	13	0.792153	10.29799	TYRO3
273	0	0	0	ZAP70

SW982

Cluster MAXIS Rank	Cluster MAXIS score	Cluster Mean Bk	Combined Score	Kinase Groups
38	10	0.259689	2.596887	ABL1
56	1	0.11247	0.11247	AKT1
30	14	0.637092	8.919286	ALK
60	1	-0.33548	-0.33548	ARAF
163	0	0.132652	0	AURKA
248	0	0.295219	0	AXL
10	66	0.547418	36.12958	BMX
20	23	0.602043	13.847	BRSK2
98	0	0	0	CAMK1
52	2	-1.6	-3.2	CAMK2A
97	0	0	0	CAMK4
5	87	0.669049	58.20725	CDK1
100	0	0.254471	0	CHEK1
6	85	-1.52144	-129.322	CHEK2
171	0	0.097918	0	CHUK
15	41	0.585555	24.00775	CLK1
265	0	0.251826	0	CSF1R
251	0	0.205836	0	CSK
132	0	0.039209	0	CSNK1A1
133	0	0.161688	0	CSNK1G2
54	2	0.582981	1.165963	CSNK2A1
110	0	-0.09495	0	DAPK1
112	0	0	0	DCLK1
253	0	-0.28286	0	DDR1
9	66	0.470848	31.07599	DMPK
24	20	0.676791	13.53582	DYRK1A
49	3	0.20419	0.612569	DYRK3
31	14	-0.34444	-4.8221	EGFR
29	16	0.280189	4.483021	EPHA2
12	47	0.936977	44.03791	FER
55	2	0.237641	0.475281	FGFR1
18	35	0.289539	10.13388	FGR
278	0	-0.0382	0	FLT1
58	1	0.183924	0.183924	FLT3
279	0	0.212222	0	FLT4
271	0	-0.18534	0	FRK

Cluster MAXIS Rank	Cluster MAXIS score	Cluster Mean Bk	Combined Score	Kinase Groups
114	0	0	0	MAPKAPK3
115	0	0	0	MAPKAPK5
40	8	0.322982	2.583854	MARK2
103	0	0.189514	0	MELK
36	11	0.572023	6.292253	MET
53	2	0.108334	0.216669	MKNK2
26	19	0.579201	11.00482	MST1R
264	0	0.188454	0	MUSK
46	4	0.409523	1.638092	NEK1
7	82	0.855845	70.17932	NEK2
185	0	0	0	NEK6
2	99	1.56	154.44	NEK9
43	6	0.005473	0.032839	NTRK1
16	38	0.574688	21.83814	NUAK1
236	0	0.014586	0	PAK1
237	0	-0.10884	0	PAK4
45	5	0.202232	1.01116	PDGFRA
3	97	0.775035	75.17842	PDPK1
120	0	0.258714	0	PHKG1
305	0	0.280854	0	PI4KB
39	9	0.922061	8.29855	PIK3CA
1	100	0.839345	83.93448	PIK3CB
28	16	0.489452	7.831232	PIM1
41	7	0.355054	2.48538	PIM2
42	6	0.766689	4.600135	PLK1
70	0	-0.09694	0	PRKACA
57	1	0.316931	0.316931	PRKCD
73	0	0.231058	0	PRKCE
74	0	0	0	PRKCI
4	87	0.541922	47.14722	PRKD1
75	0	0.31258	0	PRKG1
71	0	0.172398	0	PRKX
27	18	0.809292	14.56725	PTK2B
272	0	-0.18569	0	PTK6
267	0	-0.18173	0	RET
62	0	0.113887	0	ROCK1

34	11	0.538629	5.924917	GRK7
17	35	0.529129	18.5195	GSK3A
8	67	0.851775	57.06896	HIPK3
37	10	0.475825	4.758252	HIPK4
32	13	-1.54464	-20.0803	IKBKB
172	0	0.237801	0	IKBKE
59	1	-1.52167	-1.52167	IRAK4
275	0	0.262079	0	ITK
51	3	-1.57778	-4.73333	JAK1
22	21	-0.70106	-14.7224	JAK2
260	0	0.101138	0	JAK3
266	0	0.065631	0	KIT
48	4	0.370062	1.480247	LRRK2
239	0	-0.18462	0	MAP2K1
232	0	0.189417	0	MAP4K2
233	0	0.070284	0	MAP4K4
153	0	0	0	MAPK1
33	12	-0.09734	-1.16812	MAPK14
21	22	-0.45775	-10.0704	MAPK8

23	21	0.615482	12.92511	ROS1
13	41	0.29363	12.03881	RPS6KA4
14	41	0.335119	13.73989	RPS6KB1
78	0	0.347604	0	SGK1
44	6	-0.49466	-2.96795	SRMS
160	0	0.459523	0	SRPK1
162	0	-0.20667	0	SRPK3
35	11	0.435856	4.794411	STK10
19	29	0.774553	22.46204	STK24
50	3	0.236699	0.710097	STK3
273	0	0	0	SYK
173	0	0.345888	0	TBK1
276	0	-0.1538	0	TEK
247	0	0.240762	0	TNK1
246	0	0.09262	0	TNK2
25	19	0.610861	11.60636	TSSK2
47	4	0.459722	1.838887	TTK
11	51	-1.49712	-76.3532	TYK2
249	0	0.147918	0	TYRO3
274	0	0	0	ZAP70

SYO1 (synergy screen with 300 nM CRT0066101)

Cluster MAXIS Rank	Cluster MAXIS score	Cluster Mean Bk	Combined Score	Kinase Groups
31	16	0.533594	8.537507	ABL1
19	35	0.880709	30.8248	AKT1
17	37	0.88285	32.66545	ALK
290	0	0.085512	0	ARAF
27	25	0.544029	13.60072	AURKA
40	10	0.448906	4.48906	AXL
55	5	0.573409	2.867043	BMX
6	71	0.695603	49.38781	BRSK2
97	0	0	0	CAMK1
98	0	0	0	CAMK2A
96	0	0	0	CAMK4
2	79	0.705954	55.7704	CDK1
100	0	0.437141	0	CHEK1
122	0	0.352038	0	CHEK2
173	0	0.164531	0	CHUK
29	21	0.531725	11.16623	CLK1
10	48	0.664934	31.91685	CSF1R
254	0	0.040044	0	CSK
58	2	0.421079	0.842158	CSNK1A1
133	0	0.319842	0	CSNK1G2
151	0	0.334016	0	CSNK2A1
109	0	0.320474	0	DAPK1
111	0	0	0	DCLK1
33	15	0.598678	8.980177	DDR1
42	8	0.713253	5.706024	DMPK
48	6	0.538941	3.233646	DYRK1A
152	0	0.431073	0	DYRK3
256	0	-0.2623	0	EGFR
13	44	0.646182	28.43201	EPHA2
25	27	1.036152	27.9761	FER
21	33	0.693671	22.89115	FGFR1
35	14	0.400778	5.610885	FGR
9	49	0.71552	35.06049	FLT1
22	29	0.50852	14.74708	FLT3
24	28	0.745448	20.87255	FLT4
16	38	0.743225	28.24256	FRK

Cluster MAXIS Rank	Cluster MAXIS score	Cluster Mean Bk	Combined Score	Kinase Groups
113	0	0	0	MAPKAPK3
114	0	0	0	MAPKAPK5
44	7	0.456015	3.192105	MARK2
57	3	0.479693	1.43908	MELK
43	8	0.753348	6.026786	MET
115	0	0.400627	0	MKNK2
269	0	0.54308	0	MST1R
41	9	0.691013	6.219113	MUSK
184	0	0.295476	0	NEK1
49	6	0.655431	3.932584	NEK2
189	0	0	0	NEK6
30	20	0.730431	14.60861	NEK9
61	1	0.286263	0.286263	NTRK1
18	36	0.616518	22.19466	NUAK1
240	0	0.195476	0	PAK1
241	0	0.378806	0	PAK4
1	94	0.546102	51.33363	PDGFRA
71	0	0.376031	0	PDPK1
45	7	0.794808	5.563655	PHKG1
305	0	0.099377	0	PI4KB
7	59	0.846075	49.91844	PIK3CA
302	0	0.233697	0	PIK3CB
120	0	0.464853	0	PIM1
46	7	0.741707	5.191951	PIM2
36	12	0.547218	6.566621	PLK1
47	6	0.612101	3.672608	PRKACA
39	10	0.629507	6.295074	PRKCD
38	11	0.660609	7.266699	PRKCE
73	0	0	0	PRKCI
11	47	0.602404	28.31298	PRKD1
20	33	0.617553	20.37926	PRKG1
15	39	0.769422	30.00748	PRKX
4	78	0.934916	72.92345	PTK2B
54	5	0.509355	2.546773	PTK6
28	23	0.498226	11.4592	RET
63	0	0.243046	0	ROCK1

32	15	0.588764	8.831461	GRK7
3	79	0.544697	43.03109	GSK3A
52	5	0.656643	3.283214	HIPK3
5	74	0.831282	61.5149	HIPK4
174	0	-1.5474	0	IKBKB
175	0	0.534048	0	IKBKE
279	0	0.062714	0	IRAK4
60	1	0.465541	0.465541	ITK
263	0	-1.55972	0	JAK1
264	0	-0.33564	0	JAK2
265	0	0.172213	0	JAK3
37	12	0.399084	4.789003	KIT
26	26	0.739574	19.22891	LRRK2
244	0	-0.1811	0	MAP2K1
236	0	0.240173	0	MAP4K2
59	1	0.414497	0.414497	MAP4K4
155	0	0	0	MAPK1
12	47	0.466013	21.90261	MAPK14
159	0	0.385289	0	MAPK8

8	49	1.037943	50.85919	ROS1
75	0	-0.18461	0	RPS6KA4
76	0	0.506599	0	RPS6KB1
56	4	0.97024	3.880959	SGK1
304	0	0.053858	0	SRMS
163	0	0.235364	0	SRPK1
165	0	0.103858	0	SRPK3
34	14	0.502394	7.033515	STK10
243	0	0.530431	0	STK24
238	0	-0.24539	0	STK3
273	0	0	0	SYK
176	0	0.016358	0	TBK1
51	6	0.571351	3.428104	TEK
50	6	0.668121	4.008726	TNK1
251	0	0.138091	0	TNK2
14	40	0.977866	39.11464	TSSK2
53	5	0.684597	3.422986	TTK
23	28	-1.5236	-42.6608	TYK2
252	0	0.297868	0	TYRO3
274	0	0	0	ZAP70

Table A.3: Comparison of Combined Scores between original SYO1 screen and SYO1 counter screen with 300 nM CRT0066101. One representative of kinase groups is shown.

Kinase Groups	SYO1 Combined Score Difference (w/ CRT0066101 - Original Screen)
ABL1	3.790373
AKT1	11.92138
ALK	25.9344
ARAF	0
AURKA	9.899848
AXL	-29.5017
BMX	-2.08867
BRSK2	47.84306
CAMK1	0
CAMK2A	0
CAMK4	0
CDK1	30.1836
CHEK1	0
CHEK2	-6.01111
CHUK	0
CLK1	4.445722
CSF1R	30.29184
CSK	0
CSNK1A1	-0.57815
CSNK1G2	0
CSNK2A1	0
DAPK1	0
DCLK1	0
DDR1	-29.6995
DMPK	5.706024
DYRK1A	3.233646
DYRK3	0
EGFR	0

Kinase Groups	SYO1 Combined Score Difference (w/ CRT0066101 - Original Screen)
EPHA2	-2.91803
FER	0.199469
FGFR1	12.5532
FGR	-31.4586
FLT1	23.65022
FLT3	12.5908
FLT4	17.7604
FRK	23.82445
GRK7	8.831461
GSK3A	-4.82775
HIPK3	3.283214
HIPK4	57.21101
IKBKB	22.81251
IKBKE	0
IRAK4	0
ITK	0.465541
JAK1	0
JAK2	96.64846
JAK3	0
KIT	-63.7972
LRRK2	19.22891
MAP2K1	0
MAP4K2	0
MAP4K4	-46.8461
MAPK1	0
MAPK14	-28.7053
MAPK8	0
MAPKAPK3	0

Kinase Groups	SYO1 Combined Score Difference (w/ CRT0066101 - Original Screen)
MAPKAPK5	0
MARK2	-13.4853
MELK	1.43908
MET	3.507866
MKNK2	0
MST1R	0
MUSK	-2.06718
NEK1	0
NEK2	-121.49
NEK6	0
NEK9	11.11508
NTRK1	-3.12628
NUAK1	16.00698
PAK1	0
PAK4	0
PDGFRA	-23.4752
PDPK1	0
PHKG1	5.563655
PI4KB	0
PIK3CA	10.00393
PIK3CB	-0.94559
PIM1	-12.5191
PIM2	-72.0997
PLK1	6.566621
PRKACA	3.672608
PRKCD	6.295074
PRKCE	-46.0333
PRKCI	0

Kinase Groups	SYO1 Combined Score Difference (w/ CRT0066101 - Original Screen)
PRKD1	-35.936
PRKG1	17.47863
PRKX	-83.1425
PTK2B	43.3132
PTK6	2.546773
RET	8.194847
ROCK1	-0.43404
ROS1	23.21569
RPS6KA4	-4.5535
RPS6KB1	-85.2815
SGK1	3.880959
SRMS	0
SRPK1	0
SRPK3	0
STK10	5.270497
STK24	0
STK3	-0.31424
SYK	0
TBK1	0
TEK	-1.17273
TNK1	4.008726
TNK2	-4.15118
TSSK2	17.97546
TTK	3.422986
TYK2	-42.6608
TYRO3	0
ZAP70	0

Compusyn Outputs for Median-Effect Plots of Single Agents

Fa=Fraction affected, Fu=fraction unaffected, m=slope, D=Dose, Dm= median-effect dose, r=goodness of fit.

CRT0066101

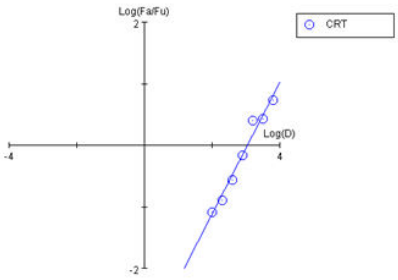

Data for Drug: CRT [nM]

Dose	Effect
6400.0	0.84665
3200.0	0.73248
1600.0	0.72141
800.0	0.40788
400.0	0.21619
200.0	0.11480
100.0	0.07561

7 data points entered.
X-int: 3.04888
Y-int: -3.2951 +/- 0.24040
m: 1.08075 +/- 0.08108
Dm: 1119.13
r: 0.98622

kb NB 142-40

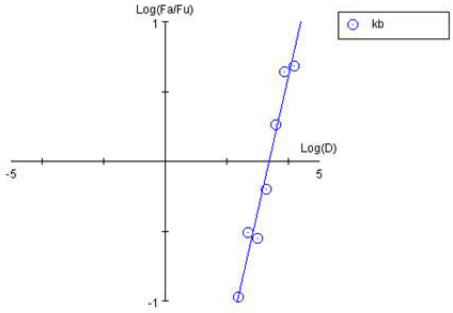

Data for Drug: kb [nM]

Dose	Effect
16000.0	0.82962
8000.0	0.81622
4000.0	0.64776
2000.0	0.38933
1000.0	0.22087
500.0	0.23810
250.0	0.09643

7 data points entered.
X-int: 3.39330
Y-int: -3.2589 +/- 0.30381
m: 0.96039 +/- 0.09054
Dm: 2473.41
r: 0.97849

BAY1125976

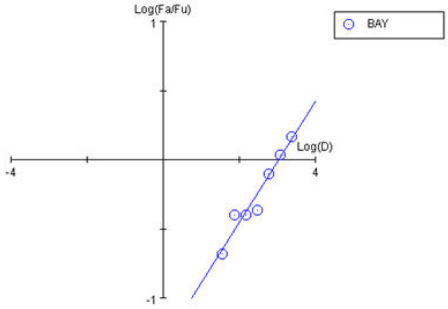

Data for Drug: BAY [nM]

Dose	Effect
2400.0	0.59679
1200.0	0.52348
600.0	0.44101
300.0	0.30355
150.0	0.28653
75.0	0.28653
37.5	0.17395

7 data points entered.
X-int: 3.03616
Y-int: -1.3356 +/- 0.12119
m: 0.43991 +/- 0.04754
Dm: 1086.82
r: 0.97202

AZD5363

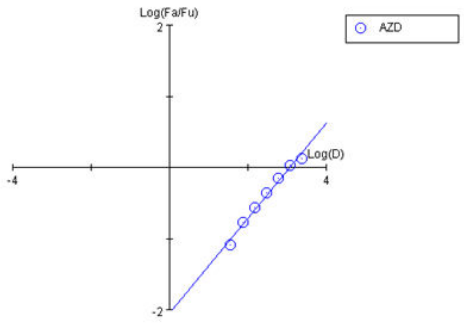

Data for Drug: AZD [nM]

Dose	Effect
2400.0	0.57447
1200.0	0.52199
600.0	0.41844
300.0	0.30638
150.0	0.21560
75.0	0.14752
37.5	0.07660

7 data points entered.
X-int: 3.05934
Y-int: -2.0517 +/- 0.10234
m: 0.67063 +/- 0.04015
Dm: 1146.42
r: 0.99116

Palbociclib

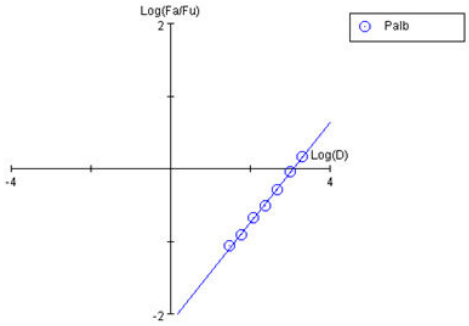

Data for Drug: Palb [nM]

Dose	Effect
2000.0	0.59702
1000.0	0.48115
500.0	0.34483
250.0	0.23749
125.0	0.17529
62.5	0.10969
31.25	0.08158

7 data points entered.
X-int: 3.07747
Y-int: -2.1226 +/- 0.04768
m: 0.68972 +/- 0.01929
Dm: 1195.27
r: 0.99805

VX745

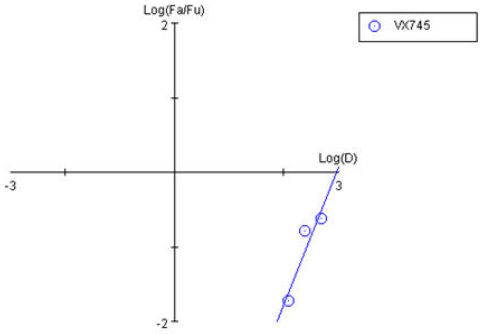

Data for Drug: VX745 [nM]

Dose	Effect
500.0	0.19679
250.0	0.14090
125.0	0.01873

3 data points entered.
X-int: 2.96197
Y-int: -5.4530 +/- 1.75635
m: 1.84101 +/- 0.72862
Dm: 916.166
r: 0.92983

Compusyn Outputs for Median-Effect Plots of Combinations and Experimental Combination Index Values

Fa=Fraction affected, Fu=fraction unaffected, m=slope, D=Dose, Dm= median-effect dose, r=goodness of fit, CI= Combination Index.

CRT0066101 + BAY1125976 Combination (6400:2400 Dose Ratio)

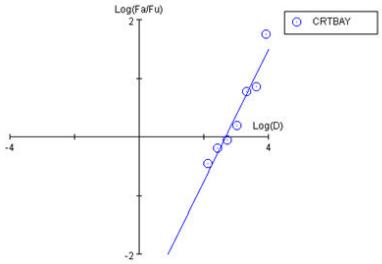

Data for Drug Combo: CR-BAY (CRTlat+BAY [6400:2400])

Dose A	Effect
6400.0+	0.98298
3200.0+	0.87825
1600.0+	0.85600
800.0+	0.61119
400.0+	0.47112
200.0+	0.39257
100.0+	0.26297

7 data points entered.
X-int: 2.67527
Y-int: -3.0303 +/- 0.44131
m: 1.13271 +/- 0.14234
Dm: 473.451
r: 0.96272

CI values for actual experimental points:

Total Dose	Fa	CI Value
8800.0	0.98298	0.10770
4400.0	0.87825	0.43085
2200.0	0.85600	0.26286
1100.0	0.61119	0.56912
550.0	0.47112	0.59143
275.0	0.39257	0.46880
137.5	0.26297	0.61315

CRT0066101 + AZD5363 Combination (6400:2400 Dose Ratio)

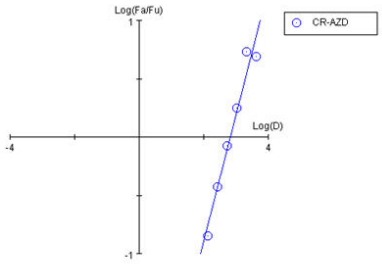

Data for Drug Combo: CR-AZD (CRTlat+AZD [6400:2400])

Dose A	Effect
3200.0+	0.83121
1600.0+	0.84397
800.0+	0.64255
400.0+	0.45674
200.0+	0.27376
100.0+	0.12482

6 data points entered.
X-int: 2.83964
Y-int: -3.0971 +/- 0.32373
m: 1.09067 +/- 0.11025
Dm: 691.254
r: 0.98017

CI values for actual experimental points:

Total Dose	Fa	CI Value
4400.0	0.83121	0.70704
2200.0	0.84397	0.32020
1100.0	0.64255	0.52123
550.0	0.45674	0.60557
275.0	0.27376	0.76137
137.5	0.12482	1.22448

CRT0066101 + Palbociclib Combination (6400:2000 Dose Ratio)

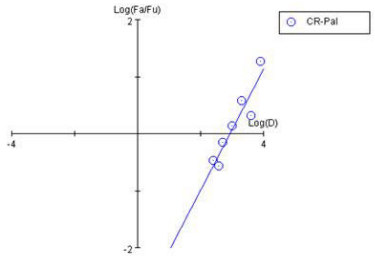

Data for Drug Combo: CR-Pal (CRT+Palb [3.2:1])

Dose A	Effect
6400.0+	0.94973
1600.0+	0.79553
800.0+	0.57913
400.0+	0.41470
200.0+	0.25708
300.0+	0.21448
3200.0+	0.67966

7 data points entered.
X-int: 2.93553
Y-int: -3.1552 +/- 0.56388
m: 1.07485 +/- 0.18002
Dm: 862.036
r: 0.93648

CI values for actual experimental points:

Total Dose	Fa	CI Value
8400.0	0.94973	0.40060
2100.0	0.79553	0.46508
1050.0	0.57913	0.66371
525.0	0.41470	0.66399
262.5	0.25708	0.72063
393.75	0.21448	1.40609
4200.0	0.67966	1.70672

CRT0066101 + VX745 Combination (6400:500 Dose Ratio)

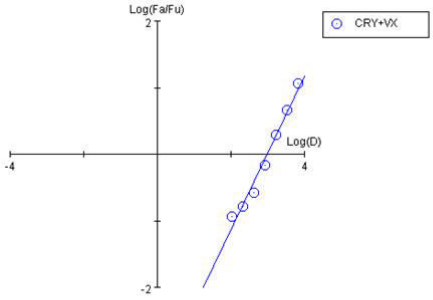

Data for Drug Combo: CRY+VX (CRT+VX745 [6400:500])

Dose A	Effect
6400.0+	0.92202
3200.0+	0.82324
1600.0+	0.66728
800.0+	0.41254
400.0+	0.21109
200.0+	0.14350
100.000+	0.10451

7 data points entered.
X-int: 2.98399
Y-int: -3.4623 +/- 0.22958
m: 1.16028 +/- 0.07661
Dm: 963.810
r: 0.98928

CI values for actual experimental points:

Total Dose	Fa	CI Value
6900.0	0.92202	0.95617
3450.0	0.82324	1.05491
1725.0	0.66728	1.08916
862.5	0.41254	1.35643
431.25	0.21109	1.58066
215.625	0.14350	1.19368
107.813	0.10451	0.82126

kb NB 142-40 + BAY1125976 Combination (16000:2400 Dose Ratio)

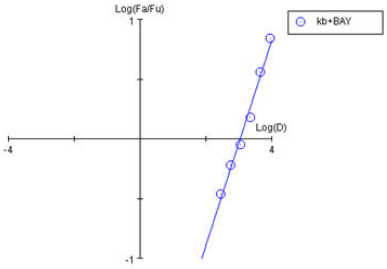

Data for Drug Combo: kb+BAY (kb+Bay [16000:2400])

Dose A	Effect
8000.0+	0.87557
4000.0+	0.78368
2000.0+	0.60182
1000.0+	0.47356
500.0+	0.37784
250.0+	0.25724

6 data points entered.
X-int: 3.04459
Y-int: -2.6272 +/- 0.17778
m: 0.86291 +/- 0.05467
Dm: 1108.12
r: 0.99207

CI values for actual experimental points:

Total Dose	Fa	CI Value
9200.0	0.87557	0.43396
4600.0	0.78368	0.44280
2300.0	0.60182	0.58563
1150.0	0.47356	0.53890
575.0	0.37784	0.43854
287.5	0.25724	0.46311

kb NB 142-40 + AZD5363 Combination (16000:2400 Dose Ratio)

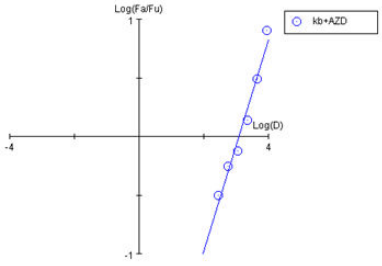

Data for Drug Combo: kb+AZD (kb+AZD [16000:2400])

Dose A	Effect
8000.0+	0.88961
4000.0+	0.75679
2000.0+	0.57913
1000.0+	0.42906
500.0+	0.35834
250.0+	0.23933

6 data points entered.
X-int: 3.09002
Y-int: -2.7988 +/- 0.26431
m: 0.90575 +/- 0.08127
Dm: 1230.33
r: 0.98428

CI values for actual experimental points:

Total Dose	Fa	CI Value
9200.0	0.88961	0.38952
4600.0	0.75679	0.55322
2300.0	0.57913	0.70135
1150.0	0.42906	0.72145
575.0	0.35834	0.52054
287.5	0.23933	0.54373

kb NB 142-40 + Palbociclib Combination (16000:2000 Dose Ratio)

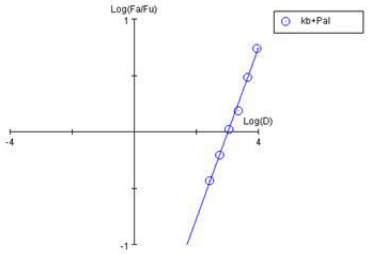

Data for Drug Combo: kb+Pal (kb+Palb [16000:2000])

Dose A	Effect
8000.0+	0.84593
4000.0+	0.75450
2000.0+	0.60720
1000.0+	0.51407
500.0+	0.38540
250.0+	0.27196

6 data points entered.
X-int: 3.02535
Y-int: -2.3178 +/- 0.08971
m: 0.76612 +/- 0.02767
Dm: 1060.11
r: 0.99740

CI values for actual experimental points:

Total Dose	Fa	CI Value
9000.0	0.84593	0.55991
4500.0	0.75450	0.52637
2250.0	0.60720	0.58406
1125.0	0.51407	0.47456
562.5	0.38540	0.50791
281.25	0.27196	0.62192

kb NB 142-40 + VX745 Combination (16000:5000 Dose Ratio)

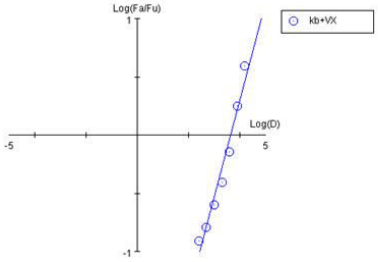

Data for Drug Combo: kb+VX (kb+VX [16000:500])

Dose A	Effect
16000.0+	0.79702
8000.0+	0.64207
4000.0+	0.41894
2000.0+	0.28259
1000.0+	0.20201
500.0+	0.14003
250.000+	0.11059

7 data points entered.
X-int: 3.65477
Y-int: -3.0511 +/- 0.24015
m: 0.83484 +/- 0.07129
Dm: 4516.17
r: 0.98225

CI values for actual experimental points:

Total Dose	Fa	CI Value
16500.0	0.79702	1.55906
8250.0	0.64207	1.76489
4125.0	0.41894	2.28846
2062.5	0.28259	2.15869
1031.25	0.20201	1.72126
515.625	0.14003	1.37589
257.813	0.11059	0.91859

Primary Phenotypic Screens of a Profiled Kinase Inhibitor Library against Sarcoma Cell Lines with Stratification of Hits and Non-hits Shown

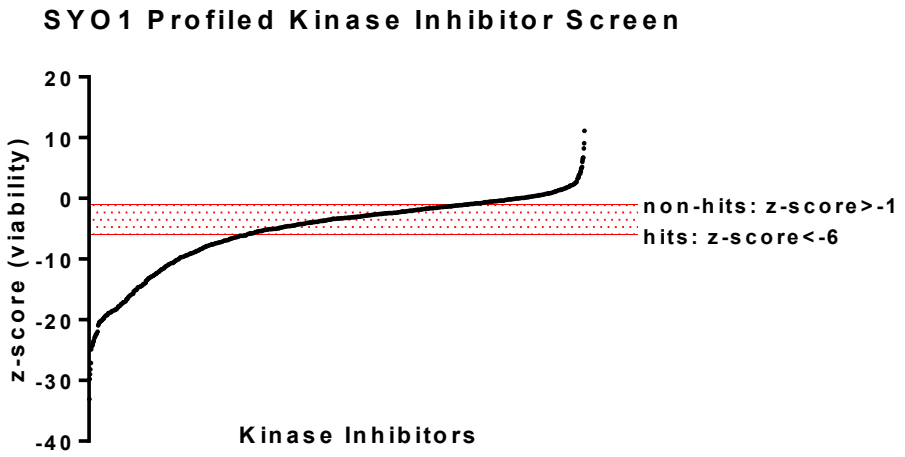

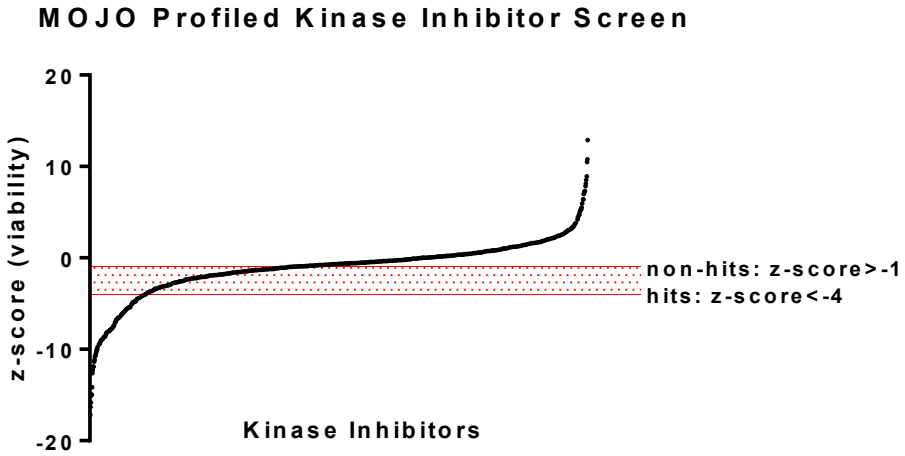

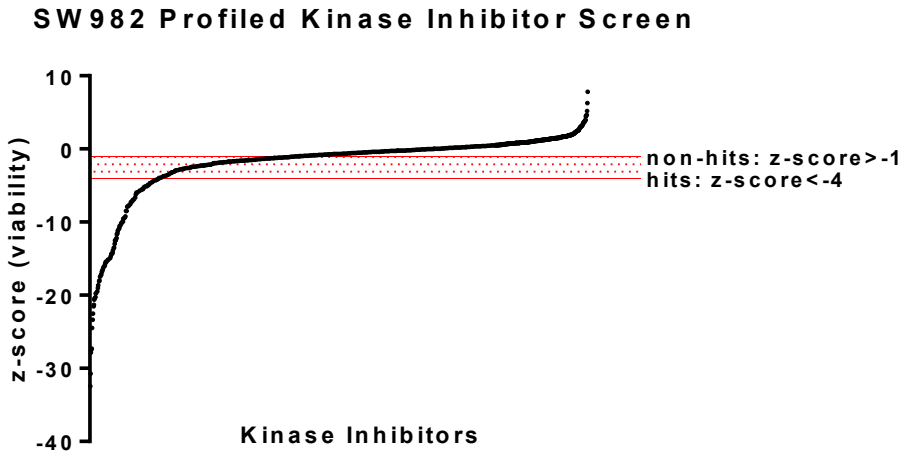

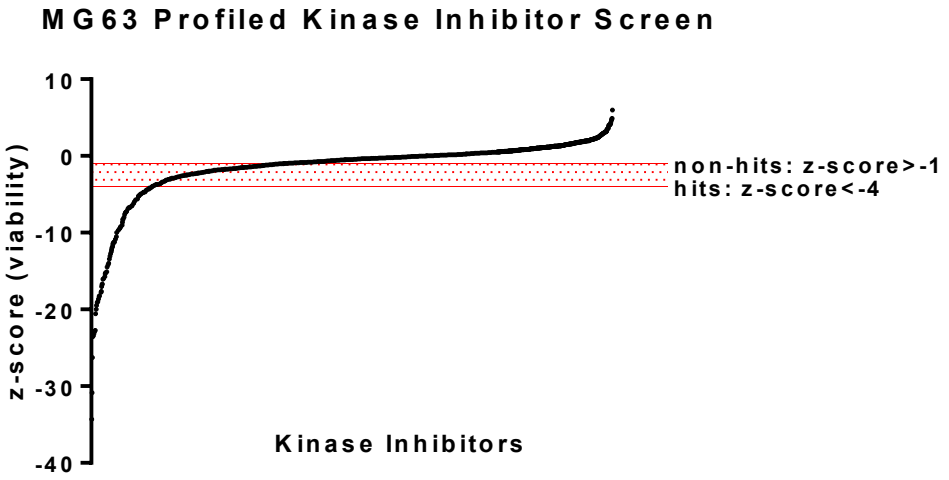
MG63 Profiled Kinase Inhibitor Screen
10
0
-10
-20
-30
-40
z-score (viability)
non-hits: z-score>-1
hits: z-score<-4
Kinase Inhibitors

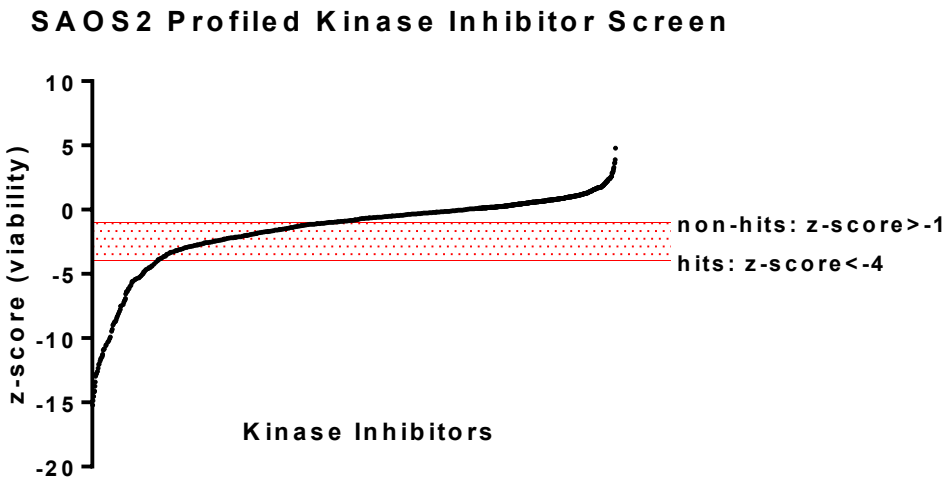
SAOS2 Profiled Kinase Inhibitor Screen
10
5
0
-5
-10
-15
-20
z-score (viability)
non-hits: z-score>-1
hits: z-score<-4
Kinase Inhibitors

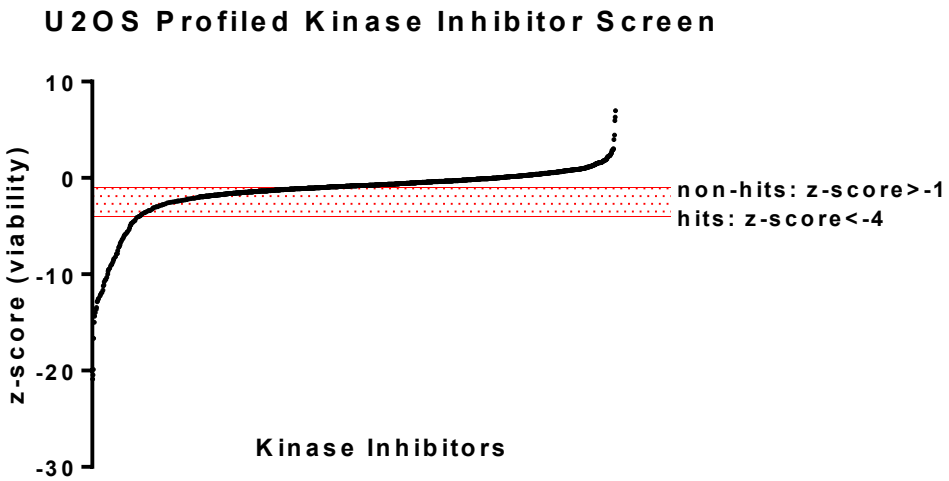
U2OS Profiled Kinase Inhibitor Screen
10
0
-10
-20
-30
z-score (viability)
non-hits: z-score>-1
hits: z-score<-4
Kinase Inhibitors

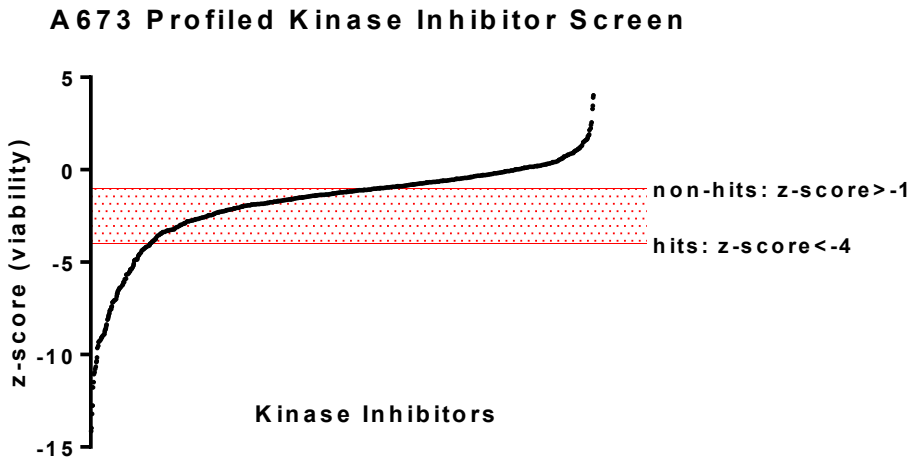
A673 Profiled Kinase Inhibitor Screen
5
0
-5
-10
-15
z-score (viability)
non-hits: z-score>-1
hits: z-score<-4
Kinase Inhibitors

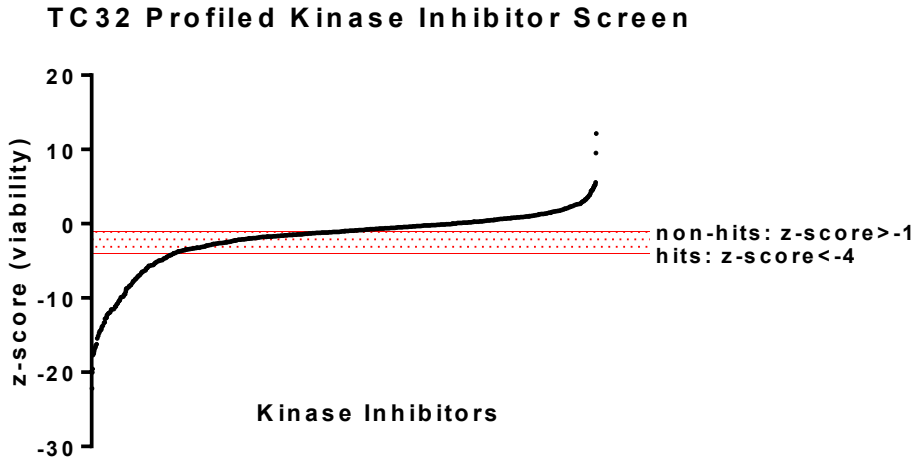
TC32 Profiled Kinase Inhibitor Screen
20
10
0
-10
-20
-30
z-score (viability)
non-hits: z-score>-1
hits: z-score<-4
Kinase Inhibitors

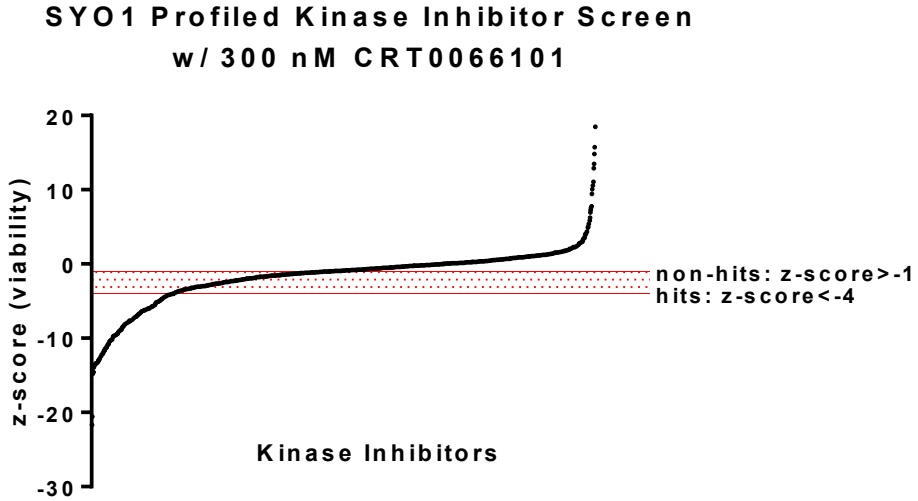
SYO1 Profiled Kinase Inhibitor Screen
w/ 300 nM CRT0066101
20
10
0
-10
-20
-30
z-score (viability)
non-hits: z-score>-1
hits: z-score<-4
Kinase Inhibitors

References

1. Al-Ali, H.; Lee, D. H.; Danzi, M. C.; Nassif, H.; Gautam, P.; Wennerberg, K.; Zuercher, B.; Drewry, D. H.; Lee, J. K.; Lemmon, V. P.; Bixby, J. L., Rational Polypharmacology: Systematically Identifying and Engaging Multiple Drug Targets To Promote Axon Growth. *ACS Chem Biol* **2015,** *10* (8), 1939-51.
2. Metz, J. T.; Johnson, E. F.; Soni, N. B.; Merta, P. J.; Kifle, L.; Hajduk, P. J., Navigating the kinome. *Nat Chem Biol* **2011,** *7* (4), 200-2.

APPENDIX B

Supplemental Information for Chapter III

Supplemental Tables

Table B.1: Complete MAXIS, B_k, and Combination Scores for kinase groups for each PDX screen performed. One representative of kinase groups is shown.

9040PDX

Cluster MAXIS Rank	Cluster MAXIS score	Cluster Mean Bk	Combined Score	Kinase Groups
6	65	-0.09648	-6.27103	ABL1
27	26	-0.29822	-7.75371	AKT1
14	51	0.21501	10.96551	ALK
9	60	-0.3775	-22.6503	ARAF
34	20	0.209496	4.189928	AURKA
19	42	-0.19497	-8.18891	AXL
22	40	-0.32885	-13.1538	BMX
44	12	0.286061	3.43273	BRSK2
106	0	-0.13075	0	CAMK1
66	1	0.468258	0.468258	CAMK2A
105	0	0	0	CAMK4
21	40	0.104557	4.182289	CDK1
17	45	-1.55625	-70.0313	CHEK1
128	0	-0.19501	0	CHEK2
177	0	0.087265	0	CHUK
10	58	0.201657	11.69609	CLK1
266	0	-0.07375	0	CSF1R
51	9	-0.55282	-4.97539	CSK
26	29	-0.25358	-7.35384	CSNK1A1
56	7	-0.21911	-1.53374	CSNK1G2
157	0	0.244561	0	CSNK2A1
117	0	0.038653	0	DAPK1
119	0	0	0	DCLK1
58	6	-0.24447	-1.46683	DDR1
36	18	-0.43405	-7.81289	DMPK
23	37	0.400433	14.81602	DYRK1A
60	4	0.2057	0.8228	DYRK3
1	98	-0.65636	-64.3234	EGFR
7	64	-0.14156	-9.05952	EPHA2
55	8	-0.014	-0.11203	FER
262	0	-0.00252	0	FGFR1

Cluster MAXIS Rank	Cluster MAXIS score	Cluster Mean Bk	Combined Score	Kinase Groups
121	0	0	0	MAPKAPK3
122	0	0	0	MAPKAPK5
5	66	0.219249	14.47042	MARK2
110	0	0.046022	0	MELK
68	1	-0.20399	-0.20399	MET
20	41	-0.2581	-10.5821	MKNK2
42	15	0.241537	3.623054	MST1R
69	1	-0.23536	-0.23536	MUSK
18	44	0.360864	15.878	NEK1
50	9	-0.13451	-1.21061	NEK2
53	8	0.156274	1.250193	NEK6
191	0	0.062048	0	NEK9
275	0	-0.02018	0	NTRK1
38	17	0.209086	3.554461	NUAK1
54	8	-0.32132	-2.57056	PAK1
41	15	-0.56602	-8.49024	PAK4
269	0	-0.03347	0	PDGFRA
37	18	0.653749	11.76747	PDPK1
45	12	0.326442	3.917301	PHKG1
305	0	0.11853	0	PI4KB
8	63	0.779338	49.09832	PIK3CA
13	52	0.332768	17.30394	PIK3CB
57	6	-0.15539	-0.93237	PIM1
49	10	0.229029	2.290291	PIM2
35	19	0.517545	9.833363	PLK1
80	0	-0.18299	0	PRKACA
39	16	-0.23811	-3.80971	PRKCD
83	0	-0.18738	0	PRKCE
84	0	0	0	PRKCI
48	11	-0.17293	-1.90224	PRKD1
52	8	0.031362	0.250899	PRKG1

4	70	-0.12454	-8.71779	FGR
276	0	-0.10505	0	FLT1
267	0	0.008958	0	FLT3
277	0	0.0507	0	FLT4
46	12	-0.23208	-2.78496	FRK
47	11	0.306312	3.369427	GRK7
64	2	-0.01526	-0.03053	GSK3A
24	36	0.145153	5.225512	HIPK3
159	0	0.030855	0	HIPK4
178	0	-0.07161	0	IKBKB
179	0	0.147559	0	IKBKE
71	1	-0.2092	-0.2092	IRAK4
30	23	-0.3753	-8.63187	ITK
3	80	-0.44441	-35.5529	JAK1
25	34	0.146214	4.971265	JAK2
61	4	-0.14825	-0.59298	JAK3
268	0	-0.01459	0	KIT
285	0	0.282451	0	LRRK2
244	0	-0.2342	0	MAP2K1
239	0	0.02001	0	MAP4K2
67	1	-0.04033	-0.04033	MAP4K4
161	0	0	0	MAPK1
2	92	-0.42342	-38.9544	MAPK14
62	3	-0.11743	-0.35229	MAPK8

81	0	-0.10644	0	PRKX
11	57	0.465758	26.54822	PTK2B
32	22	-0.39611	-8.71432	PTK6
12	53	-0.19114	-10.1303	RET
33	20	-0.19474	-3.89487	ROCK1
29	25	0.449452	11.23631	ROS1
15	49	-0.04977	-2.43893	RPS6KA4
59	4	-0.37747	-1.50988	RPS6KB1
28	26	-0.68411	-17.7868	SGK1
304	0	-0.12814	0	SRMS
40	15	0.240016	3.600244	SRPK1
169	0	0.075936	0	SRPK3
31	22	-0.2199	-4.83782	STK10
243	0	-0.13158	0	STK24
16	46	-0.06664	-3.06532	STK3
273	0	-0.01878	0	SYK
43	13	0.520532	6.766914	TBK1
63	3	-0.19553	-0.5866	TEK
252	0	-0.03239	0	TNK1
251	0	0.002525	0	TNK2
136	0	-0.068	0	TSSK2
222	0	-0.20634	0	TTK
65	2	-0.16291	-0.32582	TYK2
253	0	-0.22582	0	TYRO3
70	1	-0.18059	-0.18059	ZAP70

MUM12PDX

Cluster MAXIS Rank	Cluster MAXIS score	Cluster Mean Bk	Combined Score	Kinase Groups
60	2	0.37788	0.755759	ABL1
18	25	0.793645	19.84113	AKT1
51	6	0.438013	2.628079	ALK
292	0	0.426473	0	ARAF
8	51	0.607084	30.96131	AURKA
56	4	0.489126	1.956503	AXL
25	20	0.764438	15.28875	BMX
99	0	0.292129	0	BRSK2
41	9	0.790266	7.112396	CAMK1
97	0	0.465399	0	CAMK2A
55	4	1.415	5.66	CAMK4
7	54	0.55004	29.70219	CDK1
62	1	0.771881	0.771881	CHEK1
46	8	0.708227	5.665813	CHEK2
172	0	0.329342	0	CHUK
49	6	0.437408	2.62445	CLK1
267	0	0.347374	0	CSF1R
249	0	0.583267	0	CSK
131	0	0.455795	0	CSNK1A1
9	41	0.659606	27.04385	CSNK1G2
43	9	0.81542	7.338776	CSNK2A1
52	5	0.650451	3.252253	DAPK1
109	0	0	0	DCLK1
251	0	0.271099	0	DDR1
65	0	0.512882	0	DMPK
15	28	0.508402	14.23525	DYRK1A
149	0	0.515041	0	DYRK3
252	0	0.02175	0	EGFR
30	16	0.645268	10.32428	EPHA2
12	30	1.09832	32.9496	FER
35	11	0.512114	5.633249	FGFR1
2	99	0.67278	66.60524	FGR
276	0	0.332255	0	FLT1
268	0	0.278587	0	FLT3
40	10	0.481747	4.817475	FLT4
28	18	0.541338	9.744075	FRK

Cluster MAXIS Rank	Cluster MAXIS score	Cluster Mean Bk	Combined Score	Kinase Groups
111	0	0	0	MAPKAPK3
112	0	0	0	MAPKAPK5
13	29	0.913247	26.48416	MARK2
31	13	0.676409	8.793314	MELK
264	0	0.102444	0	MET
113	0	0.327501	0	MKNK2
265	0	0.575602	0	MST1R
266	0	0.476935	0	MUSK
32	13	0.730791	9.50028	NEK1
186	0	0.585316	0	NEK2
23	21	1.44375	30.31875	NEK6
37	10	0.800227	8.002271	NEK9
57	4	0.404436	1.617746	NTRK1
42	9	0.734649	6.611841	NUAK1
24	20	0.94466	18.8932	PAK1
239	0	0.670086	0	PAK4
270	0	0.26716	0	PDGFRA
29	17	0.812602	13.81423	PDPK1
14	29	0.650896	18.87599	PHKG1
305	0	0.344281	0	PI4KB
26	19	1.6205	30.7895	PIK3CA
3	99	0.946098	93.66369	PIK3CB
118	0	0.498544	0	PIM1
119	0	0.345503	0	PIM2
1	99	0.775768	76.80098	PLK1
10	40	0.700365	28.01459	PRKACA
74	0	0.350993	0	PRKCD
20	23	0.591819	13.61183	PRKCE
75	0	0.546628	0	PRKCI
53	5	0.503174	2.515868	PRKD1
6	66	0.755241	49.84592	PRKG1
4	74	0.887095	65.645	PRKX
27	18	0.658647	11.85565	PTK2B
38	10	0.600931	6.009308	PTK6
61	2	0.46455	0.929101	RET
11	31	0.562867	17.44887	ROCK1

45	8	0.799045	6.392357	GRK7
152	0	-0.15625	0	GSK3A
22	21	0.602357	12.64949	HIPK3
44	9	0.580084	5.220759	HIPK4
173	0	0.504682	0	IKBKB
174	0	0.525267	0	IKBKE
280	0	0.270461	0	IRAK4
48	8	0.609364	4.874915	ITK
58	3	0.679243	2.037729	JAK1
54	5	0.526861	2.634303	JAK2
259	0	0.33445	0	JAK3
269	0	0.243189	0	KIT
285	0	0.489715	0	LRRK2
50	6	0.58353	3.50118	MAP2K1
5	68	0.860374	58.50546	MAP4K2
235	0	0.172175	0	MAP4K4
153	0	0	0	MAPK1
159	0	0.29749	0	MAPK14
157	0	0.184294	0	MAPK8

16	28	0.835294	23.38825	ROS1
59	2	0.441987	0.883974	RPS6KA4
36	10	0.69793	6.979299	RPS6KB1
78	0	0.580206	0	SGK1
63	1	0.632538	0.632538	SRMS
162	0	0.464946	0	SRPK1
164	0	0.400518	0	SRPK3
47	8	0.42233	3.378636	STK10
241	0	0.205498	0	STK24
237	0	0.243143	0	STK3
17	28	0.893489	25.0177	SYK
175	0	0.529248	0	TBK1
274	0	0.269638	0	TEK
19	24	0.696123	16.70695	TNK1
21	22	0.811942	17.86272	TNK2
33	11	0.596588	6.562472	TSSK2
218	0	0.234759	0	TTK
260	0	0.320497	0	TYK2
34	11	0.847801	9.325814	TYRO3
39	10	1.433333	14.33333	ZAP70

GUM17PDX

Cluster MAXIS Rank	Cluster MAXIS score	Cluster Mean Bk	Combined Score	Kinase Groups
30	28	0.213887	5.988842	ABL1
40	12	0.265626	3.187506	AKT1
45	10	0.274962	2.749624	ALK
9	69	0.233433	16.10691	ARAF
49	7	0.252119	1.764836	AURKA
4	93	0.327473	30.45502	AXL
275	0	0.148792	0	BMX
103	0	0.135266	0	BRSK2
35	16	0.546108	8.737728	CAMK1
42	11	0.946103	10.40713	CAMK2A
101	0	0	0	CAMK4
62	1	0.120333	0.120333	CDK1
19	41	1.45625	59.70625	CHEK1
125	0	0.030451	0	CHEK2
179	0	0.05754	0	CHUK
155	0	0.094745	0	CLK1
20	41	0.429415	17.606	CSF1R
8	71	-0.2436	-17.2955	CSK
136	0	-0.12056	0	CSNK1A1
32	27	0.451213	12.18274	CSNK1G2
154	0	0.139255	0	CSNK2A1
112	0	-0.13328	0	DAPK1
38	13	1.482143	19.26785	DCLK1
256	0	0.134896	0	DDR1
66	0	0.078153	0	DMPK
156	0	-0.03702	0	DYRK1A
157	0	-0.21894	0	DYRK3
28	30	0.285195	8.555852	EGFR
258	0	0.141382	0	EPHA2
6	77	1.181045	90.94044	FER
7	76	0.486036	36.93876	FGFR1
1	97	0.33848	32.83256	FGR
18	42	0.382677	16.07241	FLT1
51	6	0.293763	1.76258	FLT3
31	28	0.306616	8.585251	FLT4
25	32	0.352866	11.29172	FRK

Cluster MAXIS Rank	Cluster MAXIS score	Cluster Mean Bk	Combined Score	Kinase Groups
115	0	0	0	MAPKAPK3
116	0	0	0	MAPKAPK5
14	51	0.820613	41.85124	MARK2
17	48	0.34676	16.64448	MELK
269	0	0.277348	0	MET
117	0	0.015824	0	MKNK2
270	0	0.283352	0	MST1R
271	0	0.315759	0	MUSK
190	0	0.270283	0	NEK1
194	0	0.253977	0	NEK2
2	95	1.485714	141.1429	NEK6
59	2	0.361931	0.723861	NEK9
278	0	0.035544	0	NTRK1
26	31	0.423147	13.11754	NUAK1
244	0	0.175182	0	PAK1
245	0	-0.10488	0	PAK4
16	50	0.282901	14.14507	PDGFRA
75	0	0.269828	0	PDPK1
11	65	0.814189	52.92226	PHKG1
305	0	-0.04191	0	PI4KB
5	81	0.837088	67.80415	PIK3CA
303	0	-0.08895	0	PIK3CB
122	0	0.043595	0	PIM1
123	0	-0.25173	0	PIM2
3	93	0.529705	49.26258	PLK1
76	0	0.224375	0	PRKACA
78	0	-0.01596	0	PRKCD
79	0	0.25176	0	PRKCE
80	0	0	0	PRKCI
58	2	-0.0912	-0.18241	PRKD1
33	25	0.41389	10.34725	PRKG1
10	65	0.728335	47.34178	PRKX
22	35	0.821711	28.75987	PTK2B
56	3	0.242868	0.728605	PTK6
37	14	0.314485	4.402786	RET
67	0	0.232654	0	ROCK1

27	30	0.608368	18.25105	GRK7
21	39	-0.42188	-16.4535	GSK3A
159	0	-0.08789	0	HIPK3
29	29	0.504059	14.6177	HIPK4
180	0	-0.07386	0	IKBKB
181	0	0.424234	0	IKBKE
47	9	0.552713	4.97442	IRAK4
23	35	0.267495	9.362325	ITK
61	2	0.28318	0.56636	JAK1
54	5	-0.15864	-0.79321	JAK2
264	0	0.02034	0	JAK3
15	50	0.341228	17.06141	KIT
64	1	0.369019	0.369019	LRRK2
34	20	0.5082	10.164	MAP2K1
48	8	0.387005	3.096037	MAP4K2
60	2	0.240215	0.48043	MAP4K4
161	0	0	0	MAPK1
63	1	-0.0506	-0.0506	MAPK14
165	0	-0.16323	0	MAPK8

39	13	0.521684	6.781887	ROS1
12	55	0.467248	25.69863	RPS6KA4
36	15	0.711523	10.67284	RPS6KB1
41	11	0.403913	4.443038	SGK1
52	6	0.424022	2.544131	SRMS
169	0	0.121299	0	SRPK1
171	0	0.008088	0	SRPK3
24	32	0.410573	13.13832	STK10
247	0	-0.12126	0	STK24
50	7	0.191848	1.342936	STK3
46	9	0.21625	1.946251	SYK
182	0	0.158716	0	TBK1
276	0	0.134548	0	TEK
44	11	0.365797	4.023763	TNK1
43	11	0.51529	5.668193	TNK2
13	52	0.694191	36.09792	TSSK2
55	3	0.329658	0.988975	TTK
265	0	-0.22732	0	TYK2
53	5	0.333955	1.669773	TYRO3
57	3	0.630838	1.892515	ZAP70

GUM28

Cluster MAXIS Rank	Cluster MAXIS score	Cluster Mean Bk	Combined Score	Kinase Groups
14	39	0.5083	19.82369	ABL1
6	61	0.742574	45.29701	AKT1
24	25	0.72841	18.21025	ALK
8	51	0.302854	15.44557	ARAF
28	22	0.495517	10.90137	AURKA
11	47	0.401956	18.89192	AXL
274	0	0.187839	0	BMX
4	71	1.125407	79.90391	BRSK2
100	0	0.435788	0	CAMK1
101	0	0.472049	0	CAMK2A
99	0	0.031779	0	CAMK4
13	40	0.451929	18.07718	CDK1
35	16	1.527206	24.43529	CHEK1
43	12	0.723092	8.677106	CHEK2
174	0	0.126564	0	CHUK
150	0	0.370603	0	CLK1
5	69	0.498962	34.42835	CSF1R
252	0	-0.34975	0	CSK
49	7	0.465993	3.26195	CSNK1A1
17	33	0.893082	29.47172	CSNK1G2
53	6	0.657444	3.944662	CSNK2A1
111	0	0.48909	0	DAPK1
57	1	1.532143	1.532143	DCLK1
41	14	0.47659	6.672254	DDR1
65	0	0.324181	0	DMPK
58	1	0.394093	0.394093	DYRK1A
151	0	0.36506	0	DYRK3
254	0	-0.16281	0	EGFR
2	81	0.841359	68.15006	EPHA2
21	29	1.524544	44.21178	FER
18	32	0.707036	22.62515	FGFR1
63	1	0.295405	0.295405	FGR
37	16	0.47164	7.546234	FLT1
32	20	0.506285	10.12571	FLT3
50	7	0.516527	3.615689	FLT4
272	0	0.325564	0	FRK

Cluster MAXIS Rank	Cluster MAXIS score	Cluster Mean Bk	Combined Score	Kinase Groups
114	0	0	0	MAPKAPK3
115	0	0	0	MAPKAPK5
16	35	1.003215	35.11252	MARK2
52	6	0.537054	3.222326	MELK
268	0	0.445581	0	MET
116	0	0.395716	0	MKNK2
55	4	0.61955	2.478201	MST1R
46	10	0.865179	8.651793	MUSK
184	0	0.449923	0	NEK1
60	1	0.691641	0.691641	NEK2
189	0	0.239759	0	NEK6
61	1	0.467091	0.467091	NEK9
33	20	0.485414	9.708271	NTRK1
42	12	0.809664	9.715974	NUAK1
62	1	0.287295	0.287295	PAK1
240	0	0.387465	0	PAK4
44	12	0.396061	4.752729	PDGFRA
19	30	0.60366	18.1098	PDPK1
30	21	0.762613	16.01488	PHKG1
305	0	0.039167	0	PI4KB
3	76	0.960987	73.03504	PIK3CA
20	30	0.541717	16.25152	PIK3CB
121	0	0.370335	0	PIM1
38	15	0.67422	10.1133	PIM2
1	99	0.852243	84.37203	PLK1
74	0	0.519296	0	PRKACA
76	0	0.409609	0	PRKCD
26	23	0.340851	7.839581	PRKCE
77	0	0.589922	0	PRKCI
9	49	0.500865	24.54239	PRKD1
27	23	0.40831	9.391126	PRKG1
51	6	0.461966	2.771798	PRKX
10	48	1.521545	73.03417	PTK2B
273	0	0.097869	0	PTK6
40	15	0.514247	7.713698	RET
66	0	0.21752	0	ROCK1

47	8	0.762248	6.097985	GRK7
155	0	0.079905	0	GSK3A
153	0	0.514231	0	HIPK3
39	15	0.594538	8.918072	HIPK4
175	0	-0.19499	0	IKBKB
59	1	0.466798	0.466798	IKBKE
281	0	0.528494	0	IRAK4
275	0	0.121886	0	ITK
261	0	0.629978	0	JAK1
262	0	0.390578	0	JAK2
263	0	0.232953	0	JAK3
48	8	0.33134	2.650717	KIT
54	6	0.719869	4.319215	LRRK2
12	43	0.691025	29.71407	MAP2K1
31	21	0.718568	15.08992	MAP4K2
56	2	0.324635	0.64927	MAP4K4
156	0	0	0	MAPK1
162	0	0.220044	0	MAPK14
160	0	0.215336	0	MAPK8

36	16	0.825343	13.20549	ROS1
15	35	0.32746	11.46109	RPS6KA4
79	0	0.289423	0	RPS6KB1
29	21	1.003343	21.0702	SGK1
304	0	-0.16126	0	SRMS
25	24	0.557197	13.37273	SRPK1
166	0	0.203058	0	SRPK3
22	26	0.450253	11.70658	STK10
34	18	0.877118	15.78812	STK24
238	0	0.189765	0	STK3
45	11	0.694515	7.639667	SYK
176	0	0.711578	0	TBK1
276	0	0.394037	0	TEK
249	0	0.292584	0	TNK1
248	0	0.132374	0	TNK2
7	57	0.938767	53.5097	TSSK2
220	0	0.235089	0	TTK
264	0	0.280503	0	TYK2
250	0	-0.03338	0	TYRO3
23	26	1.425	37.05	ZAP70

MC1PDX

Cluster MAXIS Rank	Cluster MAXIS score	Cluster Mean Bk	Combined Score	Kinase Groups
252	0	0.211608	0	ABL1
14	48	0.379391	18.21078	AKT1
57	4	0.228154	0.912614	ALK
10	72	0.277521	19.98153	ARAF
43	15	0.192524	2.887863	AURKA
60	3	0.248459	0.745377	AXL
24	34	0.423192	14.38852	BMX
16	46	0.708177	32.57616	BRSK2
105	0	0.273149	0	CAMK1
52	7	0.538945	3.772612	CAMK2A
104	0	0	0	CAMK4
12	64	0.50368	32.2355	CDK1
53	7	0.718216	5.027513	CHEK1
125	0	0.420913	0	CHEK2
177	0	0.168414	0	CHUK
47	10	0.37178	3.7178	CLK1
66	1	0.202406	0.202406	CSF1R
254	0	0.157589	0	CSK
136	0	0.063592	0	CSNK1A1
17	46	0.416686	19.16756	CSNK1G2
154	0	0.439961	0	CSNK2A1
54	5	0.284406	1.422032	DAPK1
116	0	0	0	DCLK1
256	0	0.233855	0	DDR1
26	30	0.492677	14.78031	DMPK
23	34	0.526632	17.90549	DYRK1A
155	0	0.171542	0	DYRK3
1	100	0.487751	48.77513	EGFR
40	20	0.238675	4.77349	EPHA2
25	31	1.05962	32.84821	FER
6	78	0.630625	49.18873	FGFR1
5	80	0.382478	30.59821	FGR
20	41	0.273217	11.20189	FLT1
67	1	0.274217	0.274217	FLT3
31	28	0.39091	10.94547	FLT4
35	24	0.417611	10.02266	FRK

Cluster MAXIS Rank	Cluster MAXIS score	Cluster Mean Bk	Combined Score	Kinase Groups
118	0	0	0	MAPKAPK3
119	0	0	0	MAPKAPK5
19	41	0.630983	25.87031	MARK2
22	36	0.347184	12.49863	MELK
55	5	0.418234	2.091169	MET
46	12	0.337482	4.04979	MKNK2
269	0	0.101255	0	MST1R
270	0	-0.16467	0	MUSK
4	80	0.60005	48.004	NEK1
191	0	-0.11764	0	NEK2
62	2	0.563945	1.127889	NEK6
36	23	0.607591	13.9746	NEK9
278	0	0.04046	0	NTRK1
29	28	0.531929	14.89402	NUAK1
243	0	0.38157	0	PAK1
244	0	0.25603	0	PAK4
15	47	0.267208	12.55877	PDGFRA
78	0	-0.09262	0	PDPK1
8	76	0.804911	61.17327	PHKG1
305	0	0.352461	0	PI4KB
9	74	1.632143	120.7786	PIK3CA
32	28	0.591429	16.56001	PIK3CB
64	1	0.30955	0.30955	PIM1
34	24	0.618032	14.83277	PIM2
212	0	0.095645	0	PLK1
51	7	0.297125	2.079878	PRKACA
80	0	0.135352	0	PRKCD
81	0	0.13366	0	PRKCE
82	0	0	0	PRKCI
39	20	0.27486	5.497207	PRKD1
27	30	0.474007	14.22021	PRKG1
58	3	0.434306	1.302917	PRKX
7	77	1.499811	115.4855	PTK2B
275	0	0.232959	0	PTK6
18	43	0.420678	18.08915	RET
70	0	0.126682	0	ROCK1

38	20	0.525197	10.50394	GRK7
65	1	0.211202	0.211202	GSK3A
56	4	0.297068	1.188271	HIPK3
45	13	0.367282	4.774662	HIPK4
178	0	0.131747	0	IKBKB
179	0	0.198863	0	IKBKE
68	1	0.431629	0.431629	IRAK4
30	28	0.282692	7.91537	ITK
263	0	0.439961	0	JAK1
264	0	0.129413	0	JAK2
28	30	0.435608	13.06824	JAK3
271	0	0.163645	0	KIT
286	0	0.073581	0	LRRK2
2	82	0.912565	74.83036	MAP2K1
44	15	0.610208	9.153115	MAP4K2
13	52	0.507679	26.39932	MAP4K4
158	0	0	0	MAPK1
164	0	0.037335	0	MAPK14
162	0	0.005248	0	MAPK8

49	9	0.455338	4.09804	ROS1
3	81	0.504018	40.82547	RPS6KA4
84	0	0.328828	0	RPS6KB1
37	21	0.657634	13.81031	SGK1
33	25	0.398565	9.964125	SRMS
167	0	0.020833	0	SRPK1
169	0	-0.13412	0	SRPK3
42	16	0.349376	5.590024	STK10
50	8	0.63793	5.103441	STK24
59	3	0.25243	0.757289	STK3
61	3	0.31196	0.93588	SYK
180	0	-0.07964	0	TBK1
276	0	0.100208	0	TEK
21	37	0.364961	13.50357	TNK1
41	18	0.574763	10.34574	TNK2
11	64	0.521196	33.35653	TSSK2
224	0	0.221746	0	TTK
265	0	0.081124	0	TYK2
48	9	0.463192	4.16873	TYRO3
63	2	0.547278	1.094556	ZAP70

VARI068PDX

Cluster MAXIS Rank	Cluster MAXIS score	Cluster Mean Bk	Combined Score	Kinase Groups
38	10	0.429114	4.291143	ABL1
9	55	-0.54683	-30.0755	AKT1
249	0	0.016447	0	ALK
293	0	0.144979	0	ARAF
163	0	-0.07684	0	AURKA
58	1	-0.04019	-0.04019	AXL
21	22	1.46875	32.3125	BMX
35	11	1.42	15.62	BRSK2
93	0	-0.36504	0	CAMK1
94	0	-0.23171	0	CAMK2A
92	0	0	0	CAMK4
29	16	0.696996	11.15194	CDK1
42	9	-0.60574	-5.45164	CHEK1
45	8	-0.45786	-3.66289	CHEK2
171	0	-0.34912	0	CHUK
147	0	-0.1396	0	CLK1
55	2	0.253188	0.506375	CSF1R
26	19	1.488889	28.28889	CSK
57	1	-0.31307	-0.31307	CSNK1A1
54	2	-0.23594	-0.47189	CSNK1G2
146	0	-0.20962	0	CSNK2A1
104	0	0.074071	0	DAPK1
106	0	0	0	DCLK1
253	0	0.183049	0	DDR1
3	86	-0.57289	-49.2685	DMPK
148	0	-0.04398	0	DYRK1A
149	0	-0.33756	0	DYRK3
59	1	-0.18018	-0.18018	EGFR
4	77	1.524832	117.4121	EPHA2
49	6	1.45	8.7	FER
261	0	0.145904	0	FGFR1
12	47	0.3682	17.30541	FGR
277	0	0.068072	0	FLT1
268	0	0.147011	0	FLT3
27	18	0.756066	13.60919	FLT4
17	32	0.585423	18.73352	FRK

Cluster MAXIS Rank	Cluster MAXIS score	Cluster Mean Bk	Combined Score	Kinase Groups
108	0	0	0	MAPKAPK3
109	0	0	0	MAPKAPK5
24	19	-0.17242	-3.27607	MARK2
25	19	-0.52408	-9.95746	MELK
39	10	1.444444	14.44444	MET
110	0	0.00656	0	MKNK2
266	0	0.381226	0	MST1R
267	0	0.436571	0	MUSK
180	0	0.039417	0	NEK1
184	0	-0.04189	0	NEK2
33	12	-0.29948	-3.59374	NEK6
186	0	0.12567	0	NEK9
47	7	0.286461	2.005228	NTRK1
56	1	-0.24462	-0.24462	NUAK1
2	91	-0.64446	-58.6455	PAK1
36	11	-0.63074	-6.93811	PAK4
15	40	0.268717	10.74868	PDGFRA
69	0	-0.29189	0	PDPK1
115	0	-0.19837	0	PHKG1
19	24	1.52	36.48	PI4KB
37	11	1.625	17.875	PIK3CA
44	9	1.503703	13.53333	PIK3CB
48	6	-0.35345	-2.12068	PIM1
116	0	-0.20856	0	PIM2
10	48	1.663889	79.86666	PLK1
41	9	-0.5923	-5.33071	PRKACA
22	21	-0.52509	-11.0268	PRKCD
20	22	-0.61194	-13.4626	PRKCE
71	0	0	0	PRKCI
117	0	-0.15073	0	PRKD1
16	39	-0.60771	-23.7007	PRKG1
11	47	-0.67131	-31.5515	PRKX
259	0	0	0	PTK2B
274	0	0.168819	0	PTK6
52	4	-0.13797	-0.55187	RET
1	97	-0.72765	-70.5817	ROCK1

64	0	-0.49196	0	GRK7
6	64	1.512468	96.79792	GSK3A
151	0	-0.25671	0	HIPK3
152	0	-0.12827	0	HIPK4
13	43	-0.71574	-30.7767	IKBKB
172	0	-0.09189	0	IKBKE
281	0	0	0	IRAK4
30	16	0.580603	9.289656	ITK
34	12	-0.41863	-5.02353	JAK1
262	0	0.060484	0	JAK2
28	17	-0.33974	-5.77551	JAK3
269	0	0.075269	0	KIT
286	0	0.303448	0	LRRK2
241	0	-0.08118	0	MAP2K1
234	0	-0.43759	0	MAP4K2
235	0	-0.10069	0	MAP4K4
154	0	0	0	MAPK1
8	56	-0.26736	-14.9723	MAPK14
50	5	-0.23212	-1.16058	MAPK8

273	0	0.112429	0	ROS1
7	59	-0.50286	-29.6686	RPS6KA4
32	13	-0.39635	-5.15252	RPS6KB1
5	71	-0.90883	-64.5271	SGK1
14	41	1.5375	63.0375	SRMS
51	5	-0.18827	-0.94136	SRPK1
162	0	-0.18635	0	SRPK3
239	0	0.104211	0	STK10
18	31	-0.67037	-20.7815	STK24
237	0	0.228463	0	STK3
40	10	1.47	14.7	SYK
43	9	-0.51259	-4.61329	TBK1
23	21	1.552565	32.60387	TEK
53	3	0.536816	1.610448	TNK1
248	0	0.119659	0	TNK2
31	15	-0.43759	-6.56381	TSSK2
217	0	0.010132	0	TTK
46	7	-0.43592	-3.05143	TYK2
250	0	0.249071	0	TYRO3
275	0	-0.41259	0	ZAP70

VARI004PDX

Cluster MAXIS Rank	Cluster MAXIS score	Cluster Mean Bk	Combined Score	Kinase Groups
8	65	-0.13585	-8.83055	ABL1
20	33	0.325977	10.75724	AKT1
44	13	0.528937	6.876178	ALK
28	28	-0.23156	-6.48355	ARAF
11	52	0.246245	12.80472	AURKA
250	0	0.149718	0	AXL
13	49	-0.11549	-5.65889	BMX
109	0	-0.00049	0	BRSK2
64	3	0.287473	0.862418	CAMK1
107	0	0	0	CAMK2A
106	0	0	0	CAMK4
4	77	0.469553	36.15555	CDK1
110	0	0.055899	0	CHEK1
55	10	-0.39411	-3.94111	CHEK2
51	12	0.40375	4.844995	CHUK
1	90	0.547152	49.24368	CLK1
268	0	0.095289	0	CSF1R
62	4	-0.323	-1.292	CSK
142	0	0.152327	0	CSNK1A1
19	35	0.253562	8.874665	CSNK1G2
3	79	0.513634	40.57706	CSNK2A1
48	12	-0.29735	-3.56818	DAPK1
121	0	0	0	DCLK1
254	0	-0.18269	0	DDR1
38	20	0.288678	5.773562	DMPK
16	43	0.438889	18.87221	DYRK1A
67	2	0.331954	0.663908	DYRK3
37	21	-0.14261	-2.99487	EGFR
34	24	0.153376	3.681024	EPHA2
261	0	0	0	FER
10	60	0.508441	30.50648	FGFR1
14	48	-0.02822	-1.35469	FGR
23	31	-0.10488	-3.25125	FLT1
269	0	0.034665	0	FLT3
277	0	-0.03524	0	FLT4
65	3	0.242025	0.726076	FRK

Cluster MAXIS Rank	Cluster MAXIS score	Cluster Mean Bk	Combined Score	Kinase Groups
123	0	0	0	MAPKAPK3
124	0	0	0	MAPKAPK5
22	31	0.164469	5.098545	MARK2
113	0	0.088023	0	MELK
71	1	0.223466	0.223466	MET
125	0	0.165152	0	MKNK2
53	11	0.406289	4.469182	MST1R
12	52	0.437638	22.75717	MUSK
68	2	0.364623	0.729245	NEK1
189	0	0.045153	0	NEK2
36	22	0.510971	11.24135	NEK6
61	4	0.418488	1.67395	NEK9
9	61	0.218904	13.35314	NTRK1
43	14	0.350733	4.910257	NUAK1
7	69	-0.03933	-2.71357	PAK1
56	9	-0.45633	-4.107	PAK4
72	1	0.118555	0.118555	PDGFRA
21	31	-0.21818	-6.76361	PDPK1
29	27	0.605615	16.3516	PHKG1
32	26	0.475593	12.36543	PI4KB
35	23	0.808914	18.60502	PIK3CA
54	11	0.523884	5.762725	PIK3CB
49	12	0.2528	3.033602	PIM1
30	27	0.582296	15.722	PIM2
33	24	0.478843	11.49223	PLK1
82	0	0.017566	0	PRKACA
46	12	0.187473	2.249673	PRKCD
84	0	0.072675	0	PRKCE
41	17	-1.45	-24.65	PRKCI
39	20	0.249479	4.989584	PRKD1
47	12	0.251739	3.020873	PRKG1
26	28	0.31629	8.85611	PRKX
45	13	0.543488	7.065338	PTK2B
274	0	-0.01308	0	PTK6
270	0	-0.05367	0	RET
5	75	-0.11719	-8.78928	ROCK1

77	0	0.190132	0	GRK7
17	43	0.30827	13.25563	GSK3A
25	29	0.429124	12.44458	HIPK3
42	16	0.466578	7.465256	HIPK4
178	0	0.007355	0	IKBKB
57	8	0.513634	4.109069	IKBKE
281	0	-0.06791	0	IRAK4
275	0	0.104432	0	ITK
70	1	-0.11377	-0.11377	JAK1
262	0	0.049098	0	JAK2
263	0	0.068356	0	JAK3
27	28	0.117558	3.291611	KIT
286	0	0.059438	0	LRRK2
31	27	0.389623	10.51981	MAP2K1
6	72	0.633478	45.61043	MAP4K2
60	6	0.218307	1.30984	MAP4K4
162	0	0	0	MAPK1
50	12	-0.03661	-0.43931	MAPK14
69	1	-0.17139	-0.17139	MAPK8

15	46	0.72952	33.55791	ROS1
24	29	0.134241	3.892994	RPS6KA4
86	0	0.303511	0	RPS6KB1
2	83	-0.29291	-24.3114	SGK1
305	0	0.199798	0	SRMS
52	11	0.194951	2.144458	SRPK1
170	0	0.158884	0	SRPK3
240	0	0.088239	0	STK10
242	0	0.055899	0	STK24
18	42	0.190527	8.002119	STK3
40	18	0.310807	5.594522	SYK
59	6	0.393488	2.360925	TBK1
66	3	0.173778	0.521334	TEK
249	0	-0.12824	0	TNK1
58	8	-0.28044	-2.24348	TNK2
138	0	0.083131	0	TSSK2
221	0	0.059438	0	TTK
264	0	-0.11535	0	TYK2
251	0	0.119592	0	TYRO3
63	4	0.460154	1.840617	ZAP70

2147PDX

Cluster MAXIS Rank	Cluster MAXIS score	Cluster Mean Bk	Combined Score	Kinase Groups
52	2	0.354477	0.708954	ABL1
54	0	0.132651	0	AKT1
28	22	0.471415	10.37113	ALK
293	0	-0.04887	0	ARAF
42	7	0.324936	2.274549	AURKA
24	27	0.476381	12.8623	AXL
274	0	0.391093	0	BMX
21	31	0.651512	20.19687	BRSK2
96	0	0.003275	0	CAMK1
34	16	0.734042	11.74467	CAMK2A
95	0	-0.09568	0	CAMK4
11	53	0.616842	32.69264	CDK1
98	0	0.416373	0	CHEK1
122	0	0.422963	0	CHEK2
171	0	0.311671	0	CHUK
31	17	0.387604	6.589268	CLK1
19	35	0.413625	14.47688	CSF1R
51	3	0.54846	1.645381	CSK
14	49	-0.42375	-20.7637	CSNK1A1
133	0	0.210175	0	CSNK1G2
151	0	0.469498	0	CSNK2A1
108	0	0.23289	0	DAPK1
110	0	0.734052	0	DCLK1
252	0	-0.16562	0	DDR1
56	0	0.017765	0	DMPK
15	42	0.610062	25.62262	DYRK1A
50	3	0.417158	1.251475	DYRK3
1	100	0.485647	48.56472	EGFR
254	0	-0.11396	0	EPHA2
6	65	1.095937	71.2359	FER
25	24	0.564914	13.55794	FGFR1
3	94	0.525117	49.36096	FGR
48	5	0.3386	1.692999	FLT1
20	33	0.378214	12.48105	FLT3
49	4	0.443945	1.775778	FLT4
45	6	0.457862	2.747174	FRK

Cluster MAXIS Rank	Cluster MAXIS score	Cluster Mean Bk	Combined Score	Kinase Groups
112	0	0	0	MAPKAPK3
113	0	0	0	MAPKAPK5
8	59	0.515762	30.42993	MARK2
101	0	0.380075	0	MELK
267	0	0.435474	0	MET
114	0	0.290164	0	MKNK2
26	24	0.629467	15.10722	MST1R
268	0	0.285926	0	MUSK
181	0	0.17607	0	NEK1
185	0	0.462152	0	NEK2
187	0	0.729529	0	NEK6
10	57	0.767238	43.73255	NEK9
277	0	0.057411	0	NTRK1
30	17	0.474238	8.06205	NUAK1
239	0	0.096649	0	PAK1
240	0	-0.426	0	PAK4
4	92	0.450961	41.48837	PDGFRA
66	0	0.125681	0	PDPK1
35	15	0.55918	8.387702	PHKG1
39	11	0.405168	4.45685	PI4KB
13	52	0.889529	46.25549	PIK3CA
27	24	0.453501	10.88402	PIK3CB
119	0	0.360243	0	PIM1
41	8	0.719759	5.758072	PIM2
38	11	0.660961	7.270567	PLK1
67	0	0.007825	0	PRKACA
70	0	0.046033	0	PRKCD
71	0	-0.08975	0	PRKCE
72	0	0	0	PRKCI
120	0	0.16418	0	PRKD1
73	0	0.160391	0	PRKG1
68	0	0.044234	0	PRKX
36	13	0.568096	7.385251	PTK2B
29	21	0.649646	13.64257	PTK6
40	9	0.329866	2.968796	RET
57	0	0.030438	0	ROCK1

61	0	0.20382	0	GRK7
5	83	0.518326	43.02103	GSK3A
18	36	0.713943	25.70196	HIPK3
16	41	0.584153	23.95029	HIPK4
172	0	0.124126	0	IKBKB
53	1	0.282505	0.282505	IKBKE
281	0	-0.00357	0	IRAK4
43	7	0.437571	3.063	ITK
260	0	-0.22204	0	JAK1
261	0	0.233766	0	JAK2
262	0	0.264702	0	JAK3
17	37	0.390446	14.44651	KIT
286	0	0.27571	0	LRRK2
32	17	0.744027	12.64846	MAP2K1
22	31	0.557039	17.26821	MAP4K2
235	0	0.23297	0	MAP4K4
154	0	0	0	MAPK1
2	97	-0.46533	-45.1367	MAPK14
12	53	-0.50887	-26.97	MAPK8

9	59	0.704588	41.57071	ROS1
23	28	-0.00807	-0.22602	RPS6KA4
75	0	-0.13481	0	RPS6KB1
46	5	0.243075	1.215373	SGK1
33	17	0.788867	13.41074	SRMS
161	0	0.204477	0	SRPK1
163	0	0.206734	0	SRPK3
44	6	0.42276	2.536563	STK10
242	0	0.09507	0	STK24
237	0	0.141491	0	STK3
272	0	0.518365	0	SYK
173	0	0.07077	0	TBK1
275	0	0.099396	0	TEK
37	12	0.547494	6.569929	TNK1
249	0	0.425328	0	TNK2
7	62	0.645294	40.00826	TSSK2
218	0	0.379974	0	TTK
263	0	0.169834	0	TYK2
47	5	0.602306	3.01153	TYRO3
273	0	0.485123	0	ZAP70

3402PDX

Cluster MAXIS Rank	Cluster MAXIS score	Cluster Mean Bk	Combined Score	Kinase Groups
253	0	0.086507	0	ABL1
4	74	0.681428	50.42564	AKT1
29	21	0.431257	9.056388	ALK
16	34	0.291339	9.90552	ARAF
5	73	0.362349	26.45149	AURKA
43	13	0.331613	4.310969	AXL
62	4	0.184626	0.738503	BMX
108	0	-0.15625	0	BRSK2
53	8	0.428876	3.43101	CAMK1
106	0	0	0	CAMK2A
105	0	0	0	CAMK4
14	37	0.530805	19.6398	CDK1
9	52	1.485714	77.25714	CHEK1
36	15	0.559885	8.398274	CHEK2
179	0	0.194343	0	CHUK
17	31	0.43323	13.43013	CLK1
39	15	0.332419	4.98629	CSF1R
256	0	0.23133	0	CSK
140	0	0.292096	0	CSNK1A1
59	5	0.279241	1.396207	CSNK1G2
60	5	0.421303	2.106515	CSNK2A1
50	9	0.487895	4.391052	DAPK1
118	0	0	0	DCLK1
258	0	0.236205	0	DDR1
55	7	0.340257	2.381798	DMPK
2	93	0.546653	50.8387	DYRK1A
158	0	0.052073	0	DYRK3
12	46	0.224936	10.34705	EGFR
10	52	0.300578	15.63005	EPHA2
41	14	0.468275	6.555852	FER
19	30	0.564015	16.92046	FGFR1
56	7	0.171603	1.20122	FGR
24	25	0.193167	4.829168	FLT1
67	2	0.237217	0.474434	FLT3
27	24	0.4259	10.2216	FLT4
7	69	0.572173	39.47995	FRK

Cluster MAXIS Rank	Cluster MAXIS score	Cluster Mean Bk	Combined Score	Kinase Groups
120	0	0	0	MAPKAPK3
121	0	0	0	MAPKAPK5
48	11	0.183848	2.022329	MARK2
63	3	0.425728	1.277184	MELK
271	0	0.039644	0	MET
122	0	0.182948	0	MKNK2
28	22	0.272844	6.002576	MST1R
23	26	0.37314	9.701652	MUSK
21	27	0.682317	18.42256	NEK1
8	57	-0.37384	-21.3087	NEK2
46	12	0.400899	4.81079	NEK6
31	18	0.351462	6.32632	NEK9
26	24	0.276268	6.630444	NTRK1
45	12	0.479008	5.7481	NUAK1
49	11	0.028217	0.310382	PAK1
3	86	0.632734	54.41509	PAK4
33	16	0.233373	3.73396	PDGFRA
81	0	0.119461	0	PDPK1
69	1	0.437302	0.437302	PHKG1
305	0	0.200867	0	PI4KB
11	51	0.894481	45.61855	PIK3CA
52	9	0.304032	2.736288	PIK3CB
127	0	0.043117	0	PIM1
128	0	0.107536	0	PIM2
42	13	0.33524	4.358118	PLK1
20	27	0.489378	13.21321	PRKACA
58	6	0.323778	1.94267	PRKCD
47	11	0.175489	1.930383	PRKCE
83	0	0	0	PRKCI
1	98	0.586365	57.46376	PRKD1
30	20	0.41619	8.323799	PRKG1
35	15	0.314165	4.712477	PRKX
18	30	0.771736	23.15208	PTK2B
71	1	0.232166	0.232166	PTK6
61	4	0.339366	1.357466	RET
73	0	-0.03444	0	ROCK1

34	15	0.537633	8.064495	GRK7
65	2	0.145325	0.290649	GSK3A
37	15	0.509533	7.642997	HIPK3
22	26	0.662257	17.21869	HIPK4
180	0	-0.10155	0	IKBKB
15	36	-0.27405	-9.86595	IKBKE
282	0	-0.09121	0	IRAK4
276	0	0.184048	0	ITK
44	13	0.746547	9.70511	JAK1
265	0	0.130415	0	JAK2
266	0	0.247679	0	JAK3
40	15	0.268825	4.032379	KIT
32	18	0.431241	7.76233	LRRK2
66	2	0.335799	0.671599	MAP2K1
240	0	0.280536	0	MAP4K2
241	0	0.083959	0	MAP4K4
161	0	0	0	MAPK1
54	8	0.222061	1.776489	MAPK14
165	0	0.253608	0	MAPK8

51	9	0.617885	5.560966	ROS1
68	1	0.074009	0.074009	RPS6KA4
85	0	0.057558	0	RPS6KB1
13	37	-0.02814	-1.04133	SGK1
25	25	0.331724	8.293092	SRMS
169	0	0.153629	0	SRPK1
171	0	0.10342	0	SRPK3
245	0	0.205959	0	STK10
38	15	0.61565	9.234756	STK24
243	0	-0.0056	0	STK3
57	7	0.393677	2.755738	SYK
181	0	0.099462	0	TBK1
277	0	0.122796	0	TEK
254	0	0.042895	0	TNK1
64	3	0.359062	1.077185	TNK2
6	69	0.600582	41.44018	TSSK2
223	0	0.240295	0	TTK
267	0	0.106129	0	TYK2
70	1	0.38049	0.38049	TYRO3
275	0	-0.12595	0	ZAP70

4664PDX

Cluster MAXIS Rank	Cluster MAXIS score	Cluster Mean Bk	Combined Score	Kinase Groups
45	7	0.223399	1.563791	ABL1
11	34	0.464899	15.80656	AKT1
39	10	0.424465	4.244655	ALK
5	90	0.495835	44.62518	ARAF
13	32	0.353114	11.29964	AURKA
37	11	0.427667	4.704342	AXL
273	0	0.108096	0	BMX
6	87	0.551568	47.98638	BRSK2
101	0	0.19304	0	CAMK1
102	0	0.230361	0	CAMK2A
100	0	0.08048	0	CAMK4
34	13	0.255359	3.319668	CDK1
35	12	0.706346	8.476148	CHEK1
17	27	0.751203	20.28249	CHEK2
169	0	0.145857	0	CHUK
149	0	0.329851	0	CLK1
267	0	0.264425	0	CSF1R
249	0	0.141962	0	CSK
131	0	0.336266	0	CSNK1A1
54	4	0.44646	1.785841	CSNK1G2
27	18	0.601642	10.82955	CSNK2A1
42	9	0.603481	5.431331	DAPK1
33	13	1.505714	19.57428	DCLK1
7	81	0.425983	34.50464	DDR1
44	8	0.603478	4.82782	DMPK
36	12	0.345981	4.151772	DYRK1A
48	6	0.477992	2.867952	DYRK3
251	0	-0.15601	0	EGFR
20	26	0.437296	11.36969	EPHA2
18	27	0.439001	11.85302	FER
258	0	0.152365	0	FGFR1
24	21	0.267145	5.610037	FGR
277	0	0.118597	0	FLT1
12	34	0.433861	14.75129	FLT3
278	0	0.111736	0	FLT4
272	0	0.174236	0	FRK

Cluster MAXIS Rank	Cluster MAXIS score	Cluster Mean Bk	Combined Score	Kinase Groups
114	0	0	0	MAPKAPK3
115	0	0	0	MAPKAPK5
23	23	0.542148	12.4694	MARK2
61	2	0.272192	0.544385	MELK
46	7	0.55448	3.881358	MET
21	25	0.350629	8.765716	MKNK2
266	0	0.107301	0	MST1R
14	32	0.333978	10.6873	MUSK
57	3	0.413272	1.239816	NEK1
65	1	0.543356	0.543356	NEK2
31	16	1.475	23.6	NEK6
55	4	0.615414	2.461658	NEK9
29	17	0.372192	6.327265	NTRK1
51	5	0.348477	1.742385	NUAK1
58	3	0.502831	1.508492	PAK1
235	0	0.364637	0	PAK4
63	2	0.227361	0.454721	PDGFRA
4	96	0.709689	68.13019	PDPK1
15	31	0.542895	16.82976	PHKG1
305	0	0.107073	0	PI4KB
50	6	0.763163	4.578976	PIK3CA
3	100	0.670158	67.01583	PIK3CB
9	73	0.658096	48.04101	PIM1
64	1	0.494112	0.494112	PIM2
2	100	0.625991	62.5991	PLK1
75	0	0.356467	0	PRKACA
77	0	0.303034	0	PRKCD
78	0	0.278536	0	PRKCE
60	2	1.495833	2.991665	PRKCI
16	29	0.456758	13.24597	PRKD1
10	38	0.494408	18.7875	PRKG1
59	2	0.461004	0.922009	PRKX
8	81	0.855685	69.31053	PTK2B
66	1	0.239723	0.239723	PTK6
268	0	0.229626	0	RET
38	10	0.457824	4.578242	ROCK1

47	6	0.627022	3.762134	GRK7
152	0	-0.04402	0	GSK3A
30	16	0.502798	8.044761	HIPK3
56	3	0.423161	1.269483	HIPK4
170	0	-0.16376	0	IKBKB
171	0	0.382984	0	IKBKE
32	16	0.616599	9.865589	IRAK4
274	0	0.194084	0	ITK
259	0	-0.15999	0	JAK1
260	0	0.210494	0	JAK2
261	0	0.104421	0	JAK3
62	2	0.257644	0.515288	KIT
40	10	0.666811	6.668105	LRRK2
238	0	0.386017	0	MAP2K1
49	6	0.460006	2.760033	MAP4K2
231	0	0.156194	0	MAP4K4
153	0	-0.05517	0	MAPK1
1	100	0.217025	21.70247	MAPK14
52	5	0.441218	2.206092	MAPK8

22	25	0.325334	8.133346	ROS1
26	18	0.449758	8.095639	RPS6KA4
80	0	0.448246	0	RPS6KB1
41	9	0.358645	3.227808	SGK1
304	0	-0.0245	0	SRMS
160	0	0.423553	0	SRPK1
28	18	0.643278	11.57901	SRPK3
53	5	0.245398	1.226991	STK10
237	0	0.037841	0	STK24
233	0	0.010985	0	STK3
43	9	0.48135	4.33215	SYK
172	0	0.086758	0	TBK1
275	0	0.213202	0	TEK
246	0	0.299519	0	TNK1
245	0	0.036806	0	TNK2
25	19	0.450657	8.562483	TSSK2
214	0	0.116911	0	TTK
262	0	0.0183	0	TYK2
247	0	-0.10492	0	TYRO3
19	27	1.422222	38.4	ZAP70

Table B.2: Clustering history of PDXs and kinase groups.

PDX Clustering History

Number of Clusters	Distance	Leader	Joiner
9	8.75297218	3402	GUM28
8	8.76696068	VARI004	9040
7	8.77513789	GUM17	MC1
6	9.41529839	3402	4664
5	9.95002835	VARI004	2147
4	9.96036614	MUM12	GUM17
3	10.91785391	3402	MUM12
2	11.78114869	VARI004	3402
1	14.02383804	VARI004	VARI068

Kinase Group Clustering History

Number of Clusters	Distance	Leader	Joiner
110	0.00000000	MAPK1	MAPKAPK3
109	0.00000000	MAPK1	MAPKAPK5
108	0.17783690	PIM1	SRPK3
107	0.21998936	PAK1	ROCK1
106	0.22682724	IKBKB	TYK2
105	0.50047695	DDR1	PIM1
104	0.54560248	NEK6	TTK
103	0.54776426	SRMS	TEK
102	0.63960051	CHUK	CSNK2A1
101	0.64909602	TNK1	TYRO3
100	0.67233483	MUSK	NTRK1
99	0.74644931	DCLK1	IRAK4
98	0.75406424	DMPK	IKBKB
97	0.78433492	IKBKE	NEK2
96	0.78572243	MET	SRMS
95	0.79442605	PRKX	RPS6KB1
94	0.80616964	MAP2K1	MAP4K4
93	0.81438201	CSNK1A1	MAPK8
92	0.85737404	PAK4	PRKD1
91	0.87816795	TNK1	TNK2
90	0.88211354	GSK3A	PI4KB
89	0.90266215	DDR1	PDPK1
88	0.90412644	DMPK	PRKCD
87	0.91657160	JAK3	MAP2K1
86	0.92878525	CAMK2A	KIT
85	0.95060185	FLT1	GRK7
84	0.97765138	ARAF	MKNK2
83	0.98262564	AKT1	STK24
82	0.98989218	CHUK	CLK1

Number of Clusters	Distance	Leader	Joiner
81	1.00676925	AURKA	PRKACA
80	1.01549212	AXL	STK10
79	1.01872422	PHKG1	RPS6KA4
78	1.04594231	PRKCE	PRKG1
77	1.05588337	NUAK1	PIK3CA
76	1.05596017	HIPK3	ROS1
75	1.05795709	NEK9	PDGFRA
74	1.07255218	CAMK1	PRKX
73	1.09740573	FER	MARK2
72	1.12461954	CSK	GSK3A
71	1.14241370	MELK	PHKG1
70	1.20397288	DMPK	PAK1
69	1.22353959	CHEK1	JAK1
68	1.22605419	ABL1	CSF1R
67	1.23891388	CHUK	STK3
66	1.24012719	CAMK4	SYK
65	1.25141125	CSK	MET
64	1.26507791	CHEK2	LRRK2
63	1.27342010	ALK	SRPK1
62	1.34396902	EGFR	RET
61	1.37188008	BRSK2	ZAP70
60	1.40107727	FGFR1	NUAK1
59	1.40267054	FGR	TNK1
58	1.40884681	AKT1	SGK1
57	1.44542668	JAK3	NEK1
56	1.44797686	DDR1	DYRK3
55	1.47570503	BMX	ITK
54	1.49919180	HIPK4	MST1R
53	1.50881899	FLT4	FRK
52	1.53269524	NEK9	PTK6
51	1.61476887	CHEK2	DAPK1
50	1.62390055	CSNK1A1	MAPK14
49	1.63092761	CSK	EPHA2
48	1.63214948	AXL	FER
47	1.64153523	CAMK4	PIK3CB
46	1.66535376	JAK2	TBK1
45	1.71972027	CDK1	MAP4K2
44	1.76337924	JAK3	PTK2B
43	1.77171141	AKT1	TSSK2
42	1.77744029	DYRK1A	PAK4
41	1.78127794	BRSK2	FLT3
40	1.86334114	FGFR1	MELK
39	1.90948192	CSNK1G2	PRKCE
38	2.00840923	HIPK4	NEK9
37	2.11139675	FGFR1	FLT1
36	2.22218410	CHUK	MUSK
35	2.29708700	CDK1	PIM2
34	2.31979300	AURKA	CAMK4
33	2.32319309	CAMK1	NEK6
32	2.36701186	ABL1	ALK
31	2.42548784	ARAF	DCLK1
30	2.44529966	BMX	FLT4

Number of Clusters	Distance	Leader	Joiner
29	2.47046006	HIPK3	HIPK4
28	2.47519953	AXL	CAMK2A
27	2.48148636	CHEK2	PRKCI
26	2.48399978	CHEK1	EGFR
25	2.56116247	BRSK2	PLK1
24	2.79437405	AURKA	CSNK1G2
23	2.82442886	ARAF	DDR1
22	2.95792332	AKT1	DMPK
21	3.02257475	JAK2	MAPK1
20	3.15050455	ABL1	BRSK2
19	3.34941738	BMX	CHEK1
18	3.40585723	CDK1	CHUK
17	3.40730431	AURKA	FGR
16	3.64926286	ARAF	CHEK2
15	3.66447689	IKBKE	JAK2
14	3.69259273	AXL	CAMK1
13	3.70517239	FGFR1	JAK3
12	4.43395441	BMX	DYRK1A
11	4.65867277	ARAF	CSNK1A1
10	4.98392424	ABL1	IKBKE
9	6.04681516	AKT1	FGFR1
8	6.25123285	BMX	HIPK3
7	6.43179366	ABL1	ARAF
6	6.67528178	AKT1	AXL
5	7.07170622	BMX	CDK1
4	7.58240146	AURKA	BMX
3	8.14171009	ABL1	CSK
2	8.53924352	AKT1	AURKA
1	10.10631691	ABL1	AKT1

Primary Phenotypic Screens of a Profiled kinase Inhibitor Library against Short-term PDX Cell Cultures with Stratification of Hits and Non-hits Shown

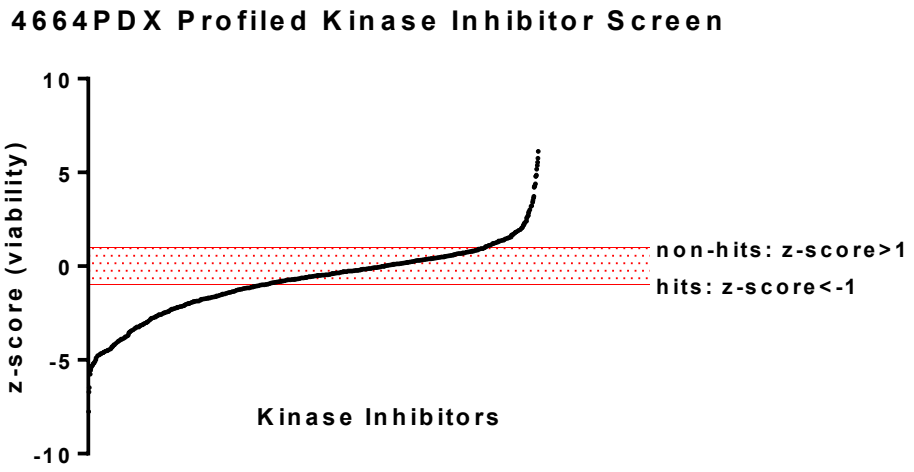

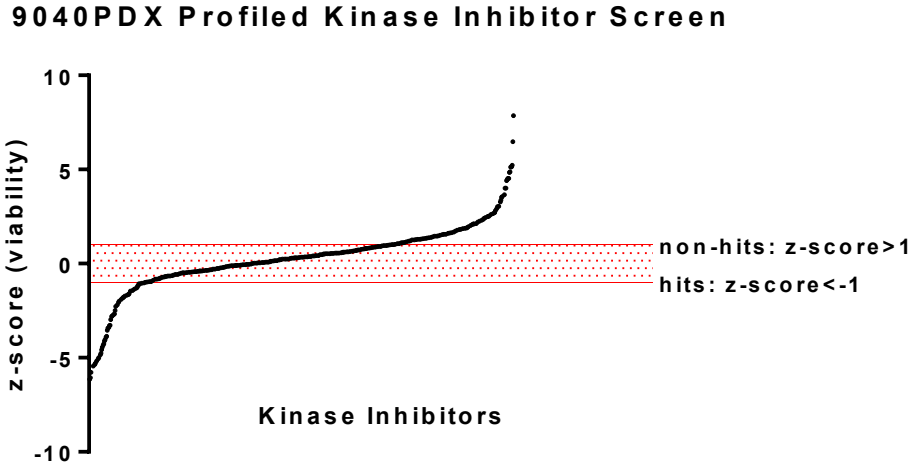

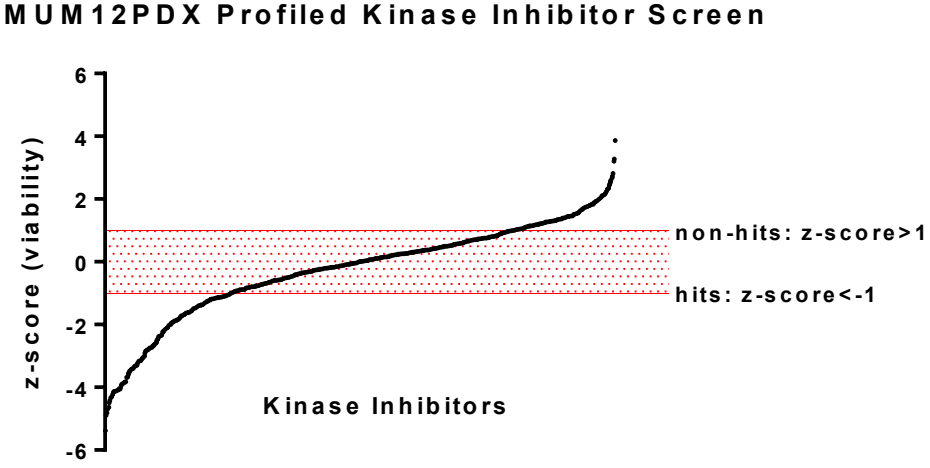

VARI004PDX Profiled Kinase Inhibitor Screen

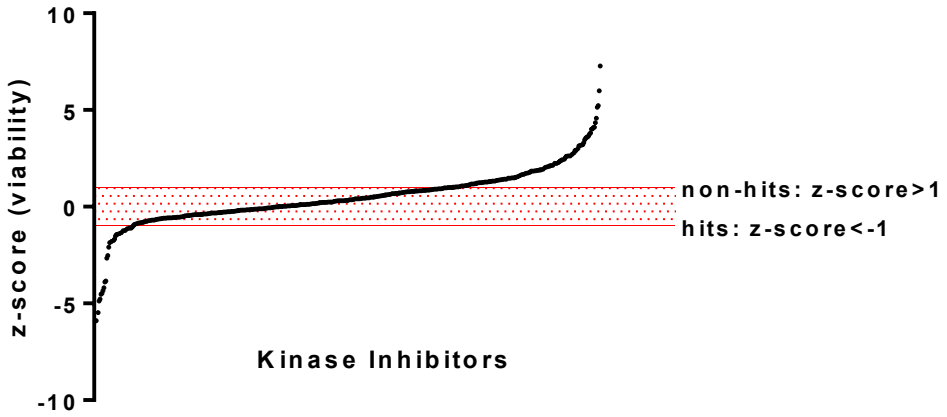

2147PDX Profiled Kinase Inhibitor Screen

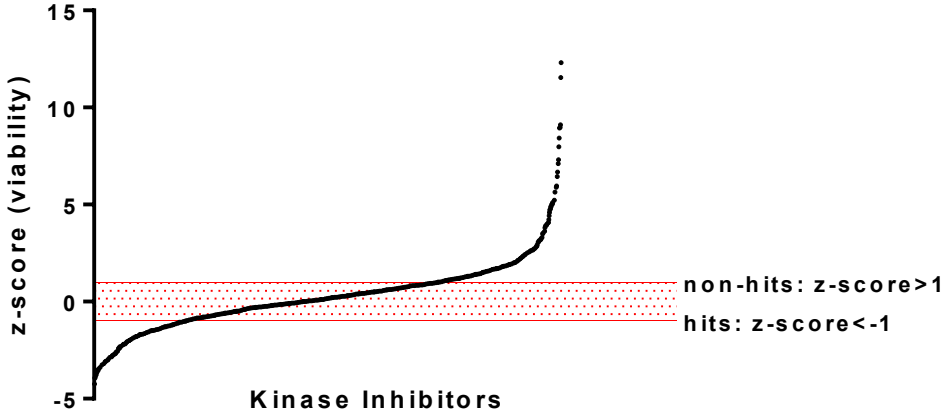

3402PDX Profiled Kinase Inhibitor Screen

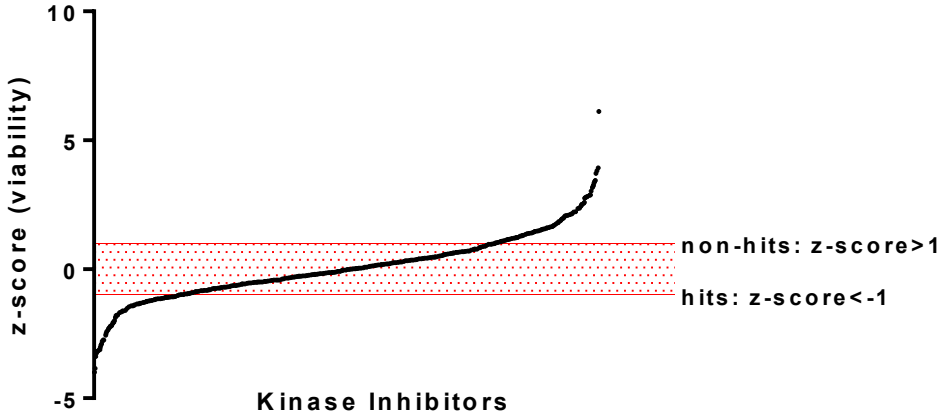

GUM17PDX Profiled Kinase Inhibitor Screen

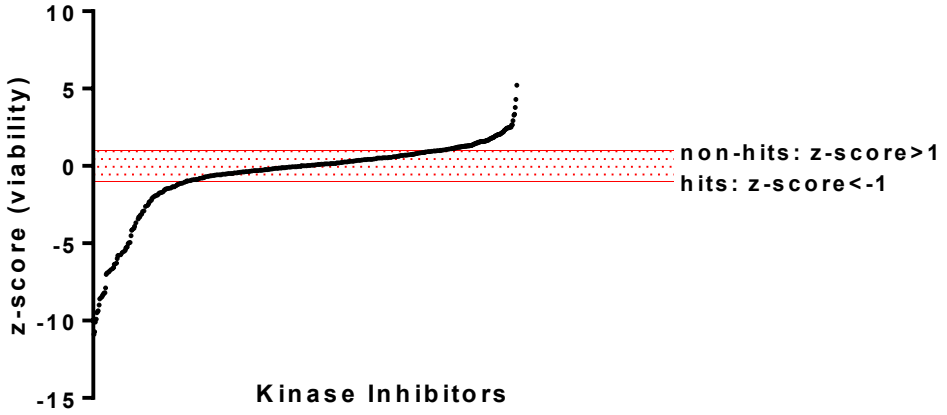

GUM28PDX Profiled Kinase Inhibitor Screen

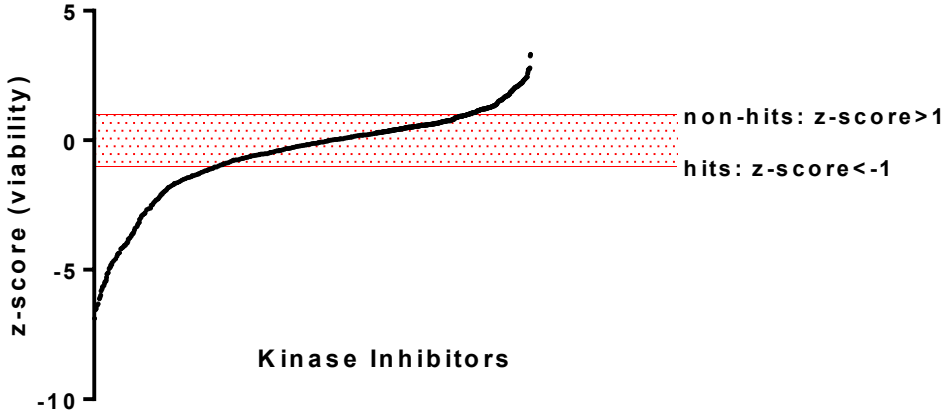

MC1PDX Profiled Kinase Inhibitor Screen

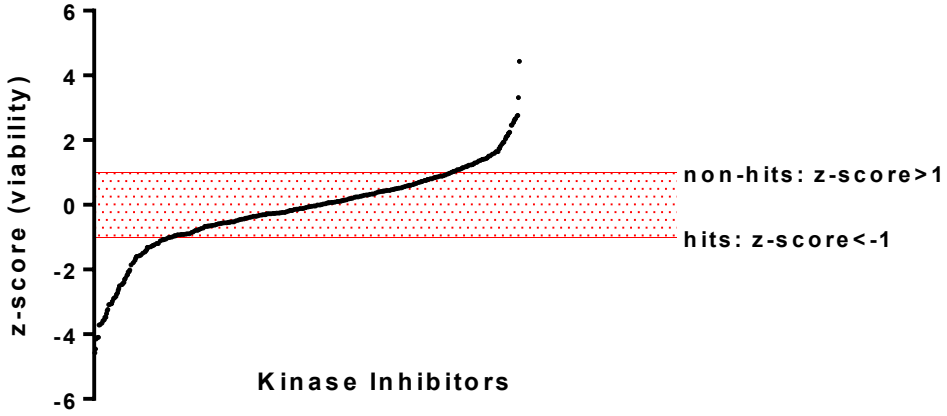

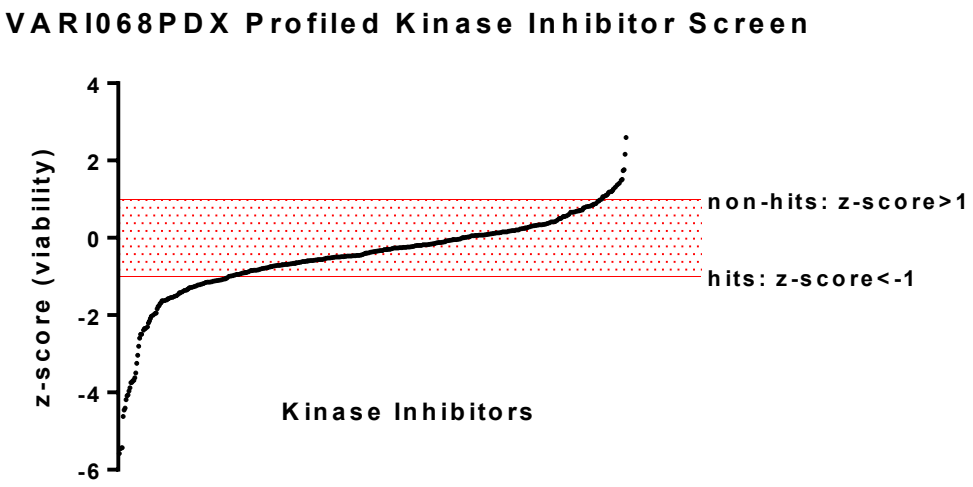
VARI068PDX Profiled Kinase Inhibitor Screen
z-score (viability)
4
2
0
-2
-4
-6
non-hits: z-score>1
hits: z-score<-1
Kinase Inhibitors

APPENDIX C

Supplemental Information for Chapter IV

Supplemental Tables and Figures

Profiled Kinases that PP2-Coumarin

ABL1(H396P)-nonphosphorylated	FRK
ABL2	FYN
ACVR1	GAK
ACVR2B	HCK
ACVRL1	KIT
BLK	KIT(D816V
BRAF	KIT(L576P
BRAF(V600E)	KIT(V559D)
CSNK1E	LCK
DDR1	LYN
DMPK2	MEK5
DMPK2	NLK
EGFR	PDGFRB
EGFR(E746-A750del)	PFCDPK1(P.falciparum)
EGFR(G719C	PIK3CG
EGFR(G719S)	RAF1
EGFR(L747-E749del, A750P)	RET
EGFR(L747-S752del, P753S)	RET(M918T)
EGFR(L747-T751del,Sins)	RIPK2
EGFR(L858R)	SIK
EGFR(L861Q)	SIK2
EGFR(S752-I759del)	SRC
EPHA1	TESK1
EPHA8	TGFBR2
EPHB3	TXK
FGR	YES

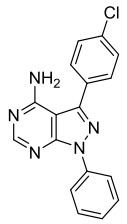

PP2-Coumarin Precursor

Kinases with P-loop

SRC	FGFR4
FGR	LIMK1
FGFR1	TNK1
FGFR2	YES
FGFR3	

Kinases with P-loop Cysteines that Bind PP2-Coumarin Precursor

SRC

FGR

YES

Figure C.1: Selectivity filter information for PP2-Coumarin. *Selectivity Filter #1:* PP2-Coumarin Precursor was previously profiled against a panel of 200 diverse kinases by KINOMEscan (DiscoveRx) at a concentration of 10 μM. Kinases which bound >35% are listed (52/200). Previously reported.[1] ***Selectivity Filter #2:*** Kinases with P-loops containing cysteines.[2] Kinases that pass both selectivity filters are also listed.

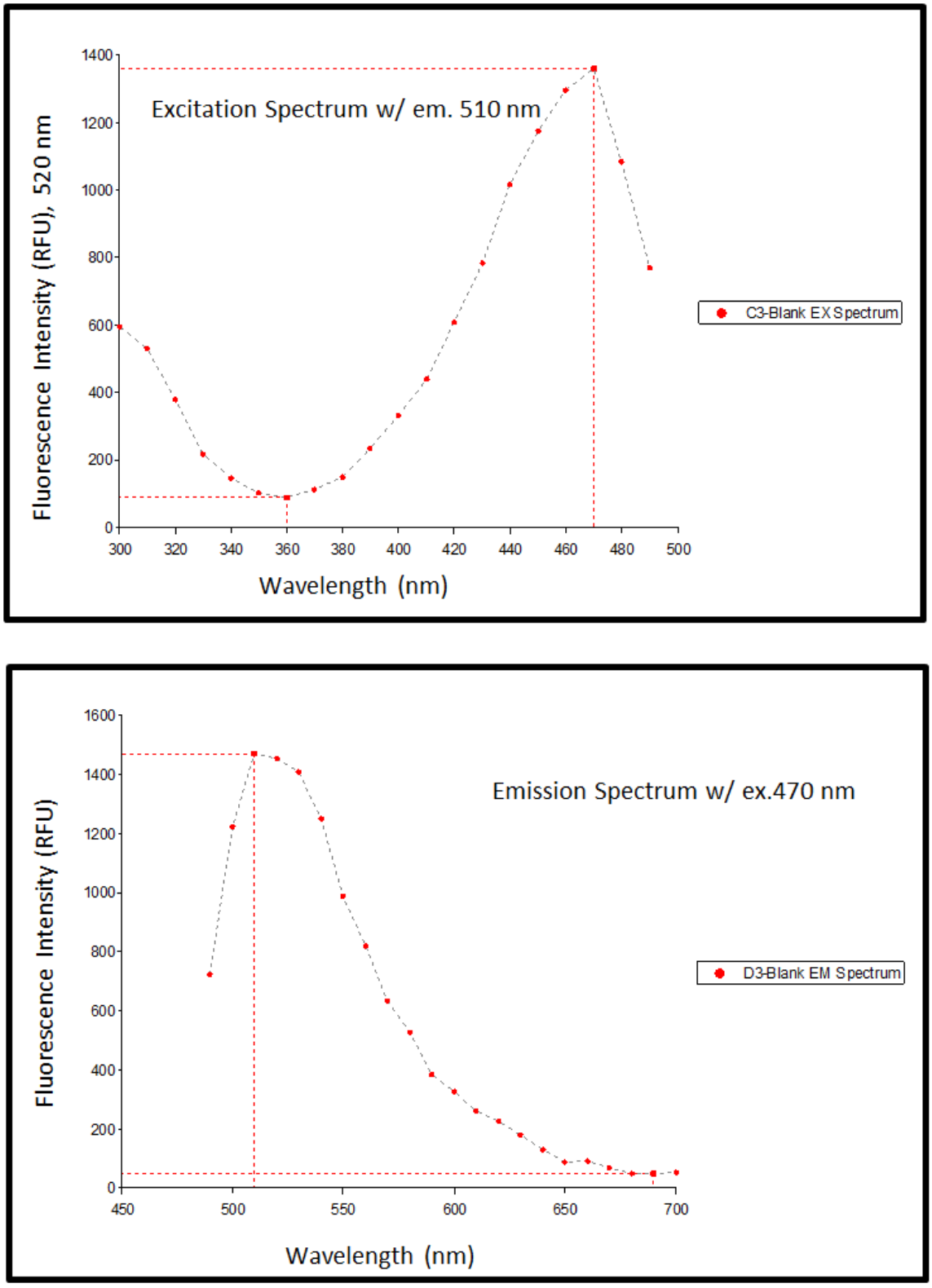

Figure C.2: Representative excitation and emission spectra of PP2-Coumarin.

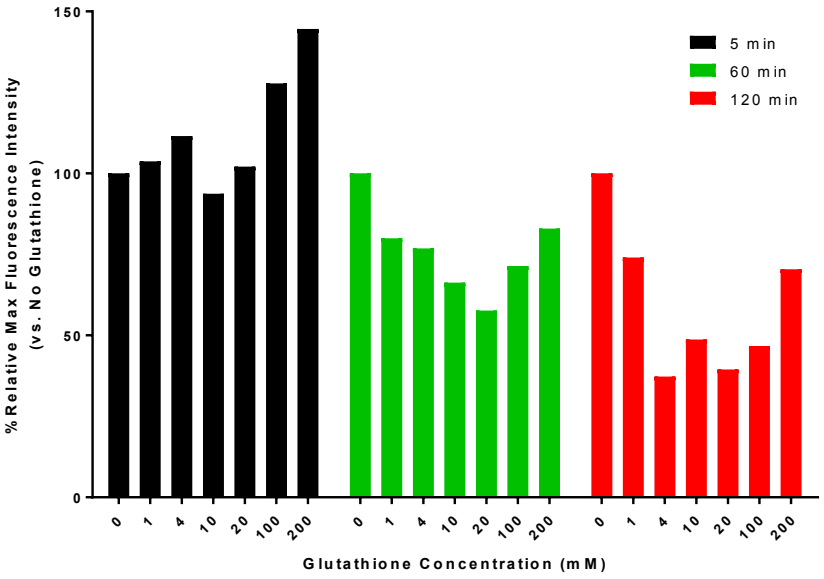

Figure C.3: PP2-Coumarin max fluorescence intensity after reduced glutathione (GSH) addition. PP2-Coumarin (2 μM) was added to concentrations of GSH. The change in the max Fluorescence Intensity of an emission spectra (ex. 450 nm) for each condition compared to no GSH wells were determined at multiple time points. No clear treads over time were observed.

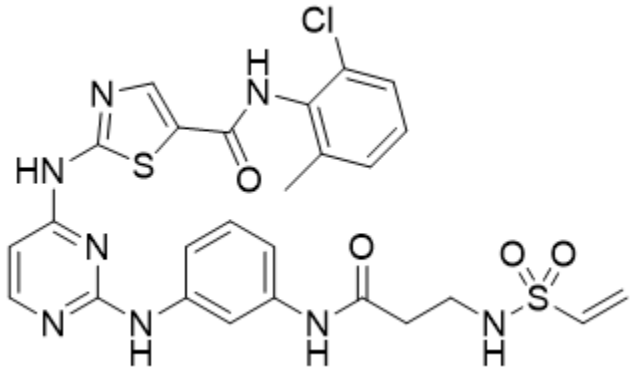

Irreversible Dasatinib Analog

Figure C.4: Structure of a previously reported irreversible dasatinib analog.[2]

Spectral Data for Compounds 4.1-4.7 and PP2-Coumarin

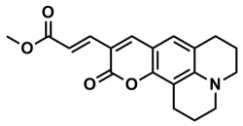

4.1

4.1 ^{1}H:

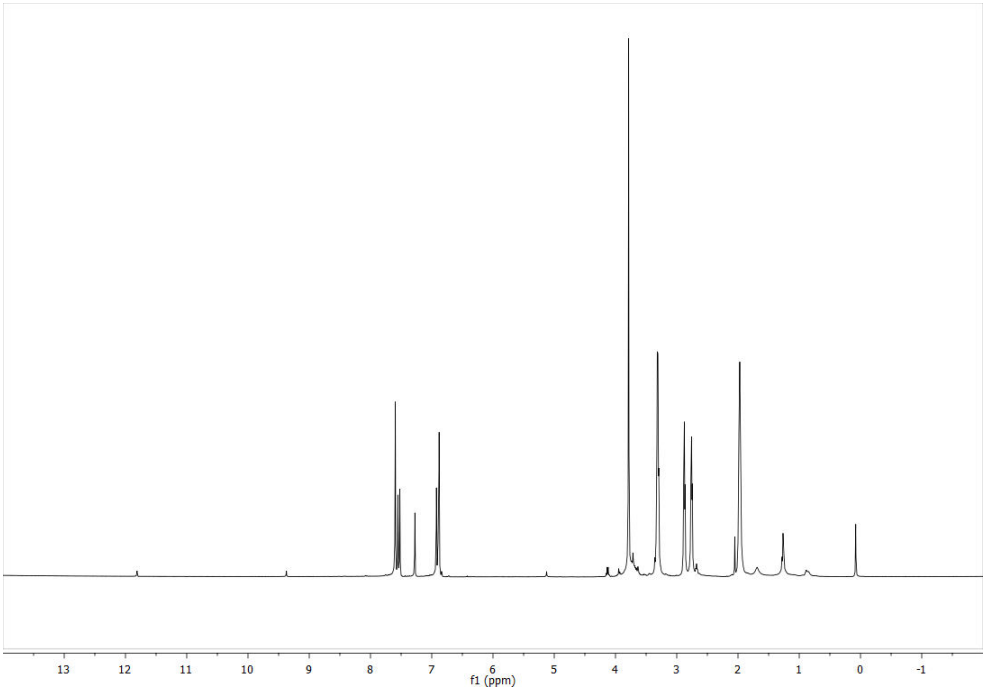

4.1 ^{13}C:

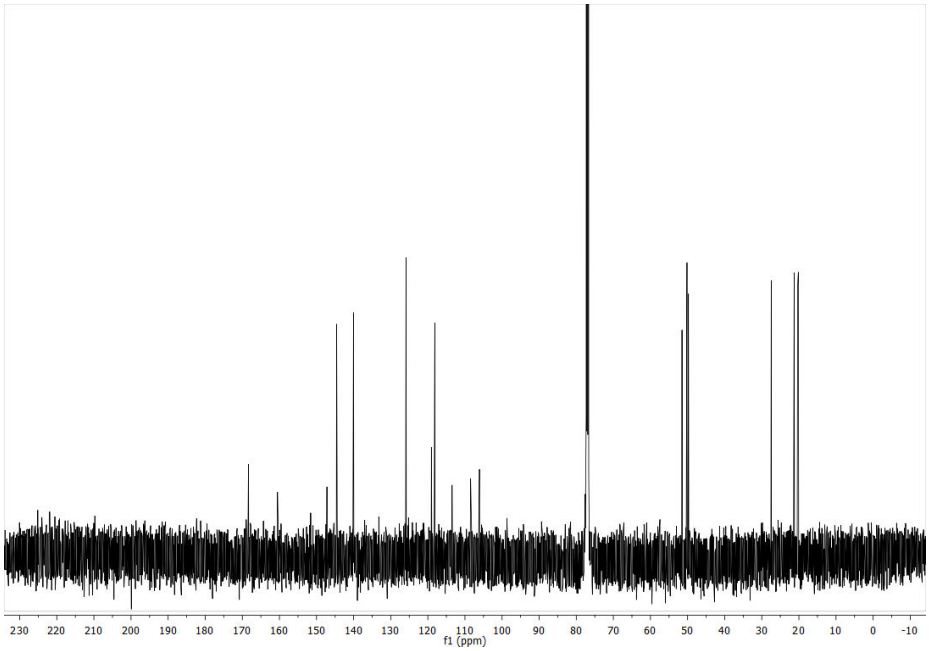

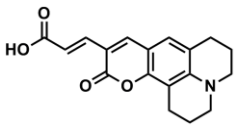

4.2

4.2 ^{1}H:

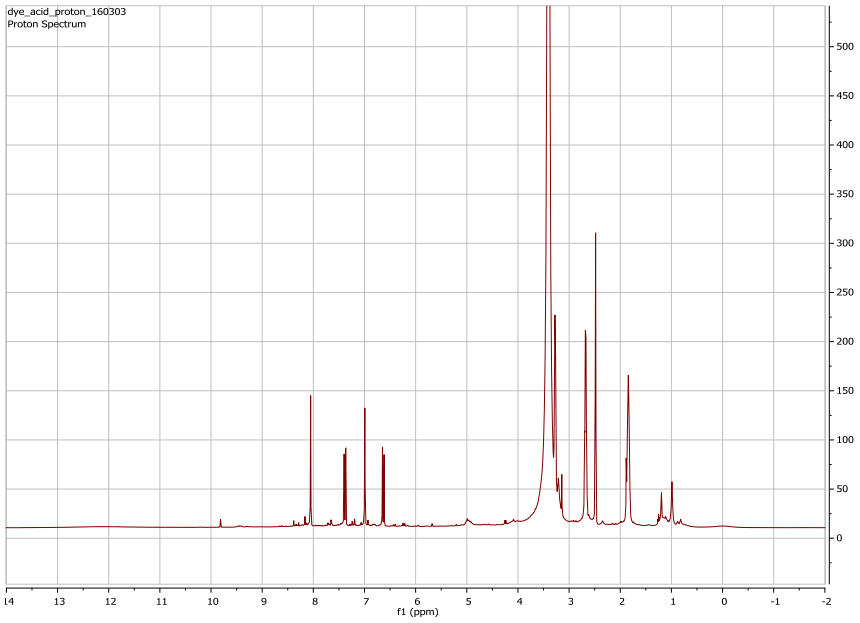

4.1 ^{13}C:

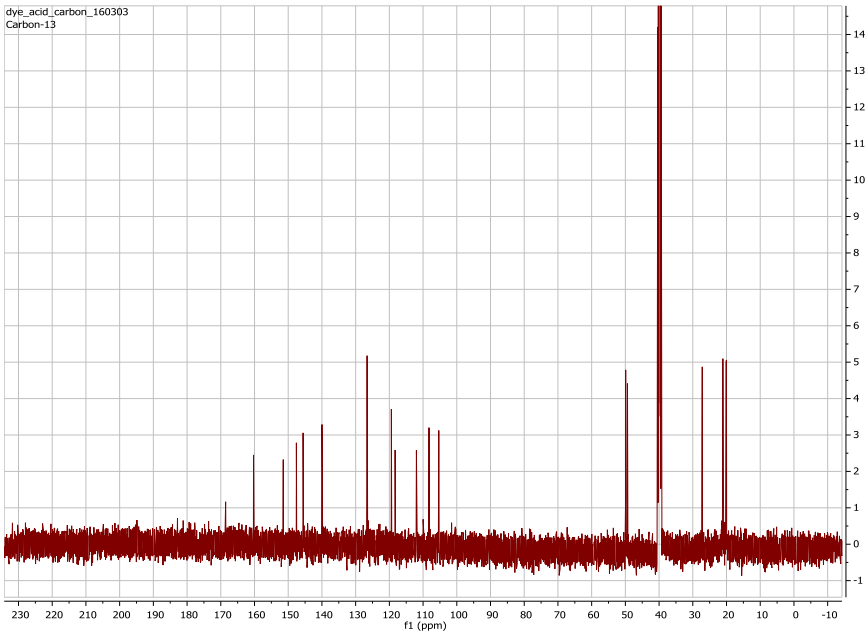

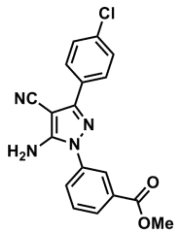

4.3

4.3 ^{1}H:

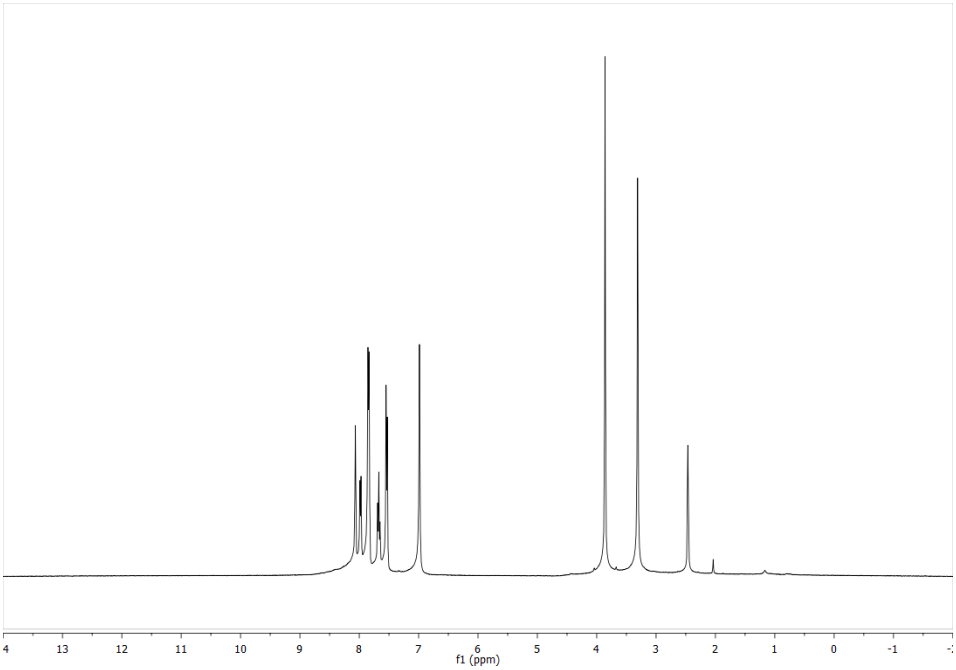

4.3 ^{13}C:

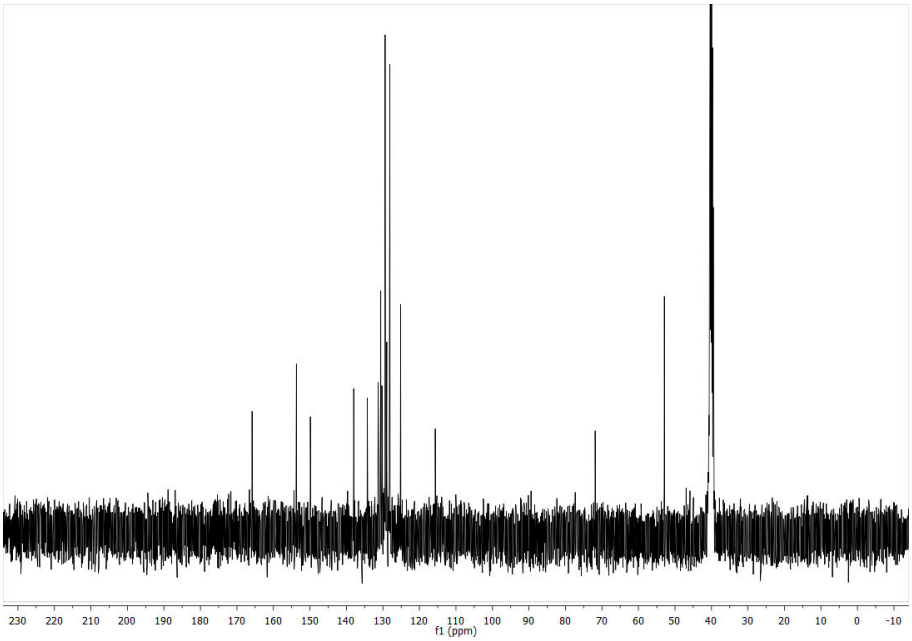

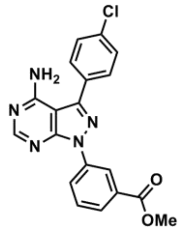

4.4

4.4 ^{1}H:

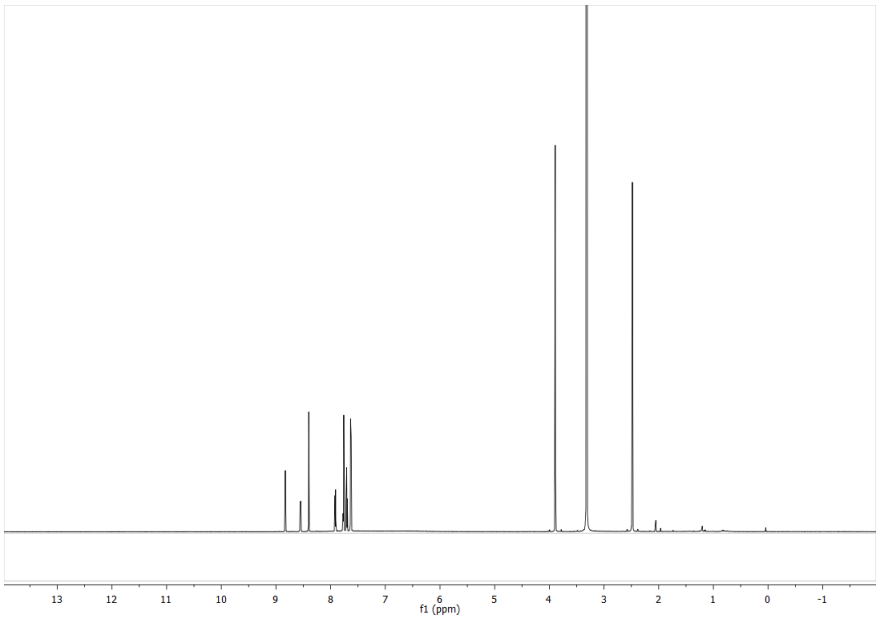

4.4 ^{13}C:

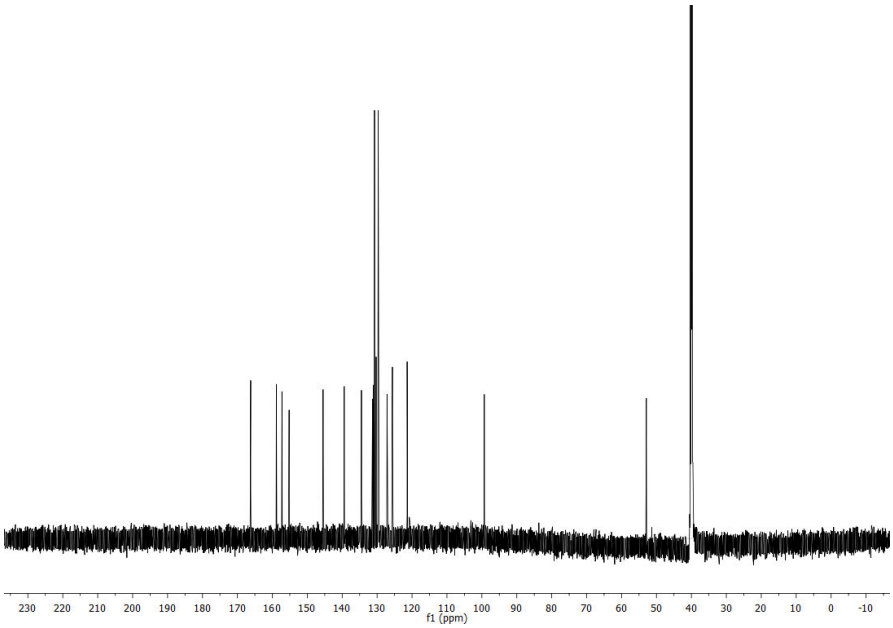

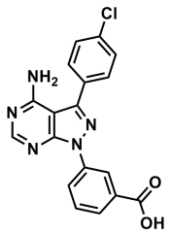

4.5

4.5 ^{1}H:

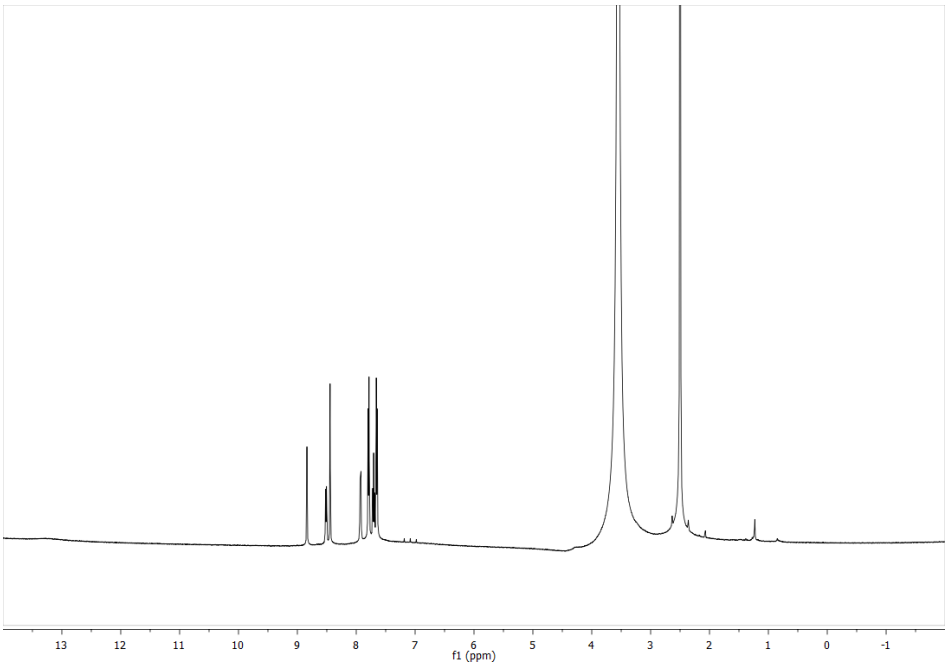

4.5 ^{13}C:

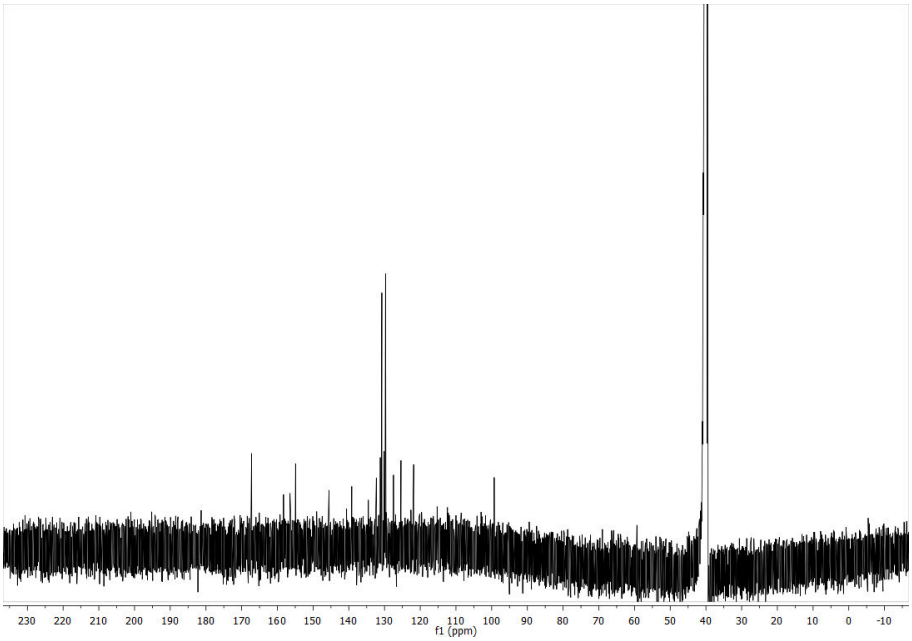

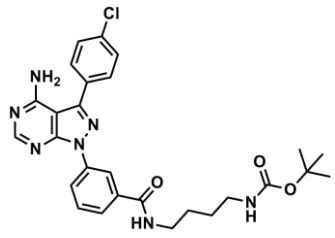

4.6

4.6 ^{1}H:

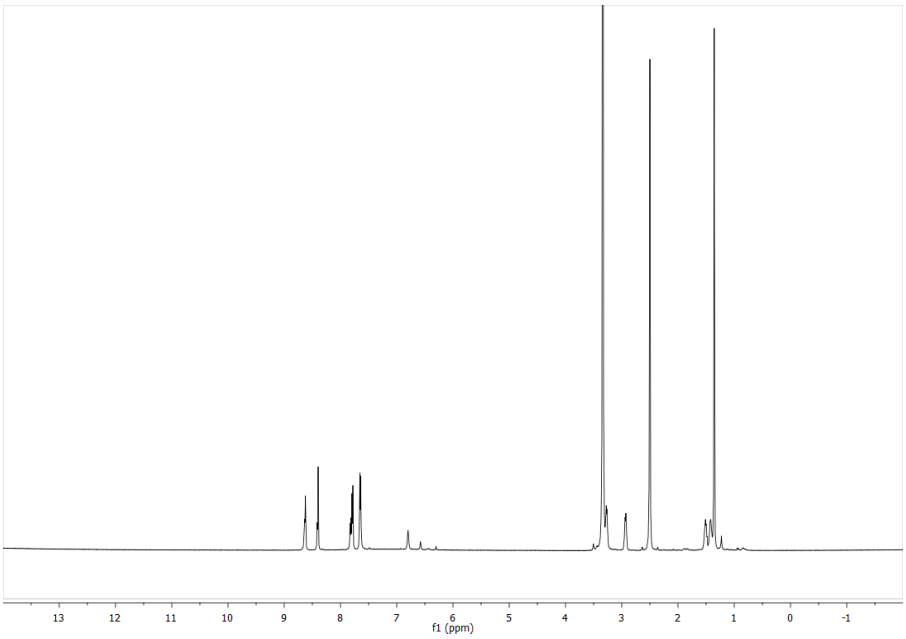

4.6 ^{13}C:

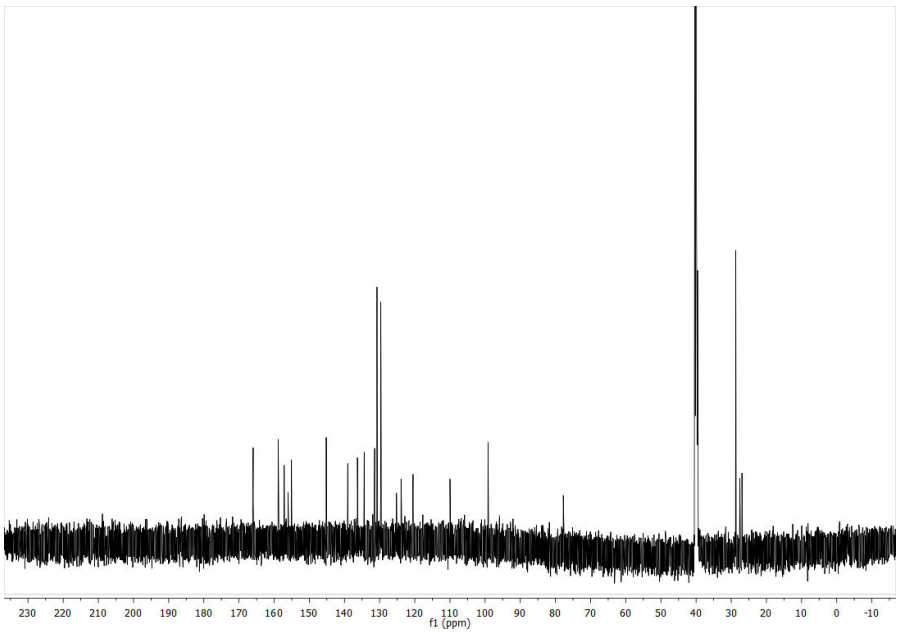

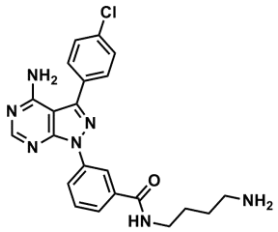

4.7

4.7 ^{1}H:

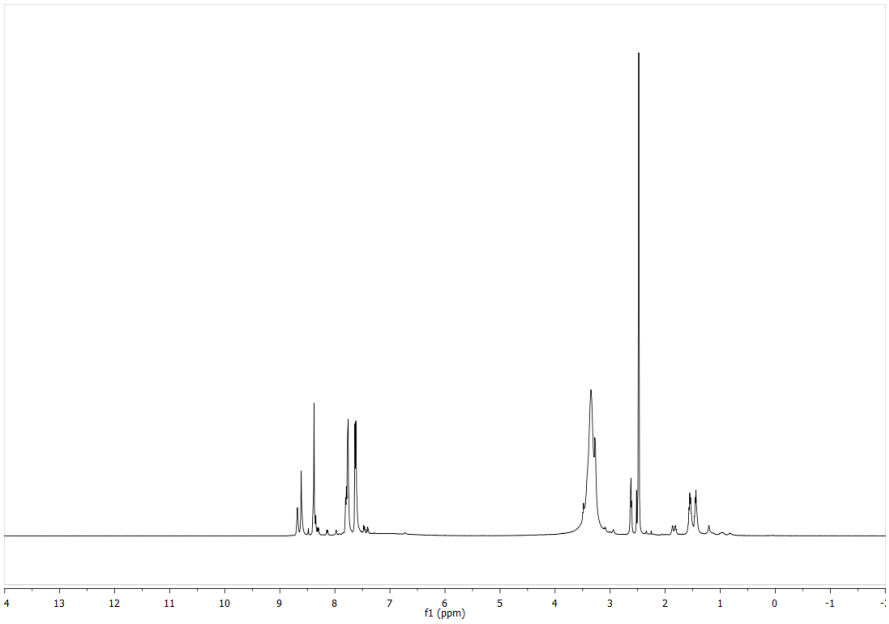

4.7 ^{13}C:

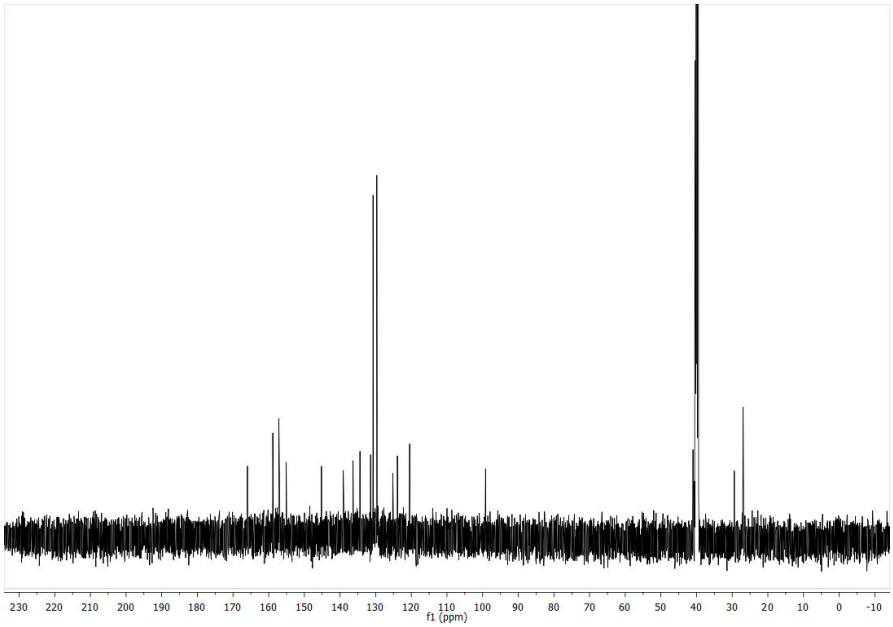

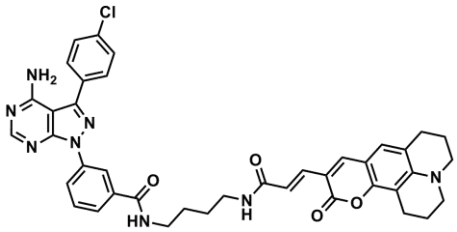

PP2-Coumarin

PP2-Coumarin ^{1}H:

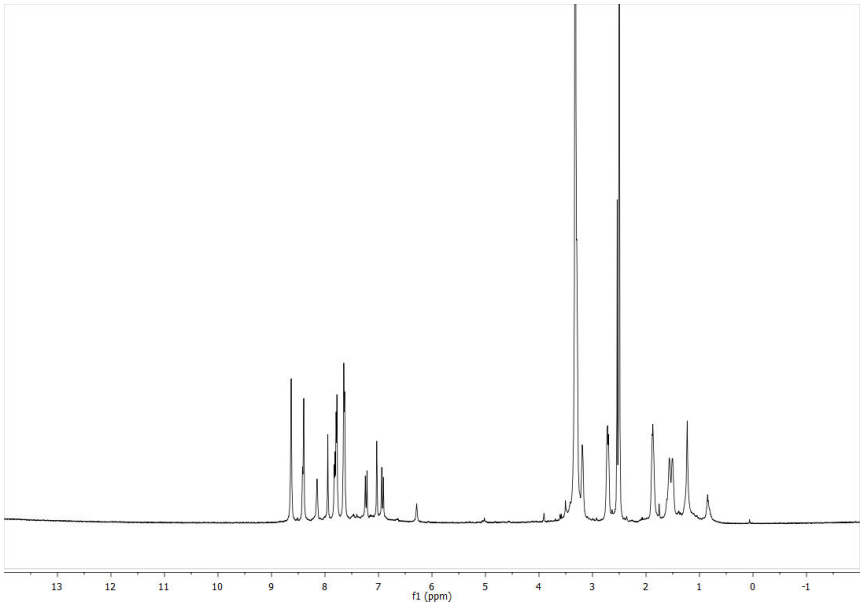

PP2-Coumarin ^{13}C:

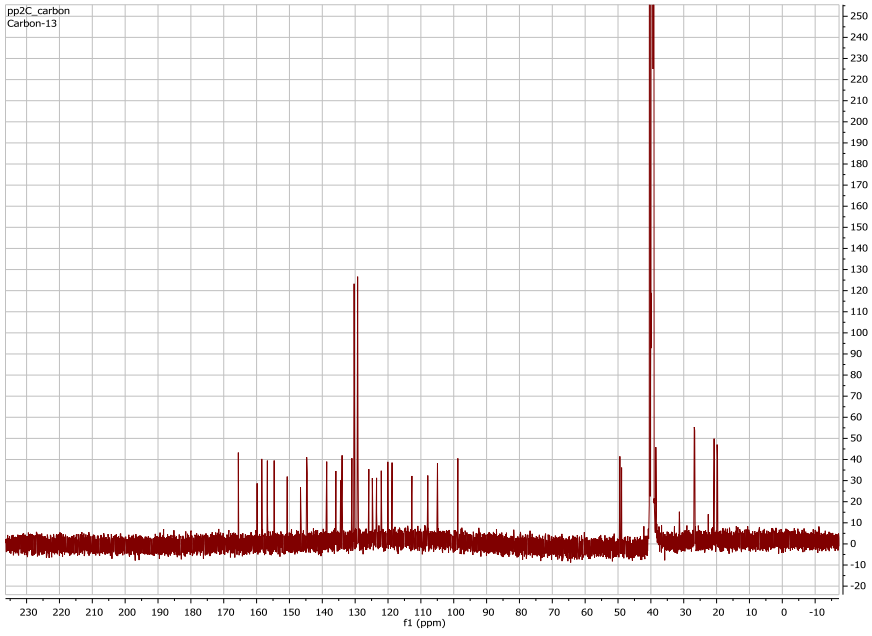

Representative Time Dependent IC_{50} Curves of PP2-Coumarin in Kinase activity Assays

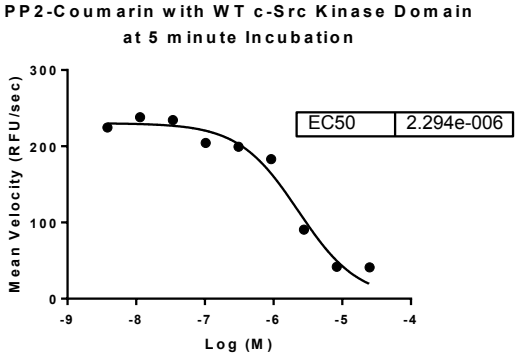

Avg 5 min IC_{50} Value = 1.88 ± 0.59 µM

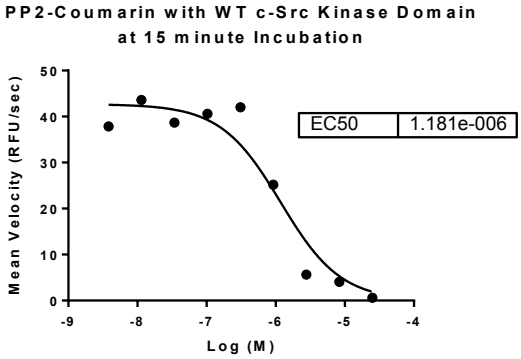

Avg 15 min IC_{50} Value = 1.11 ± 0.09 µM

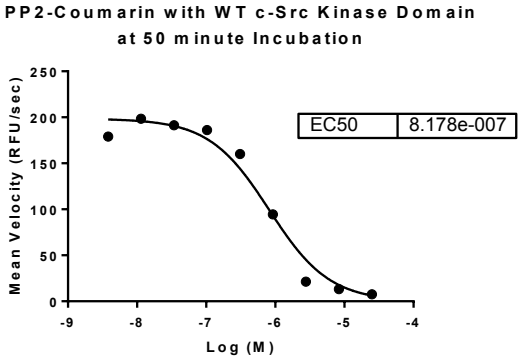

Avg 50 min IC_{50} Value = 0.763 ± 0.08 µM

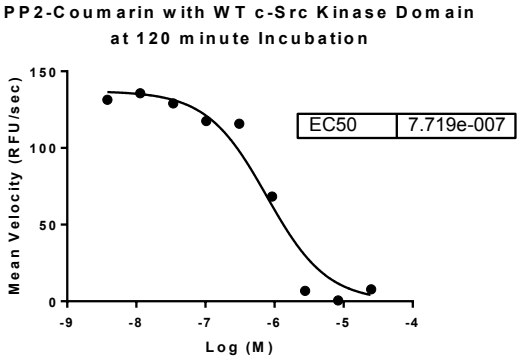

Avg 120 min IC_{50} Value = 0.766 ± 0.08 µM

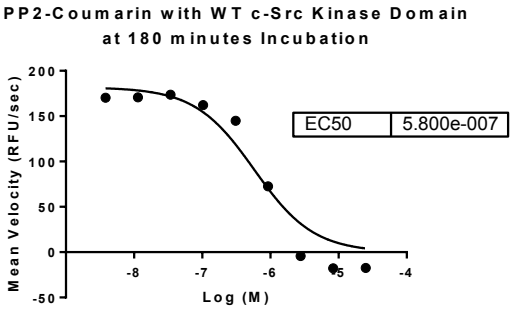

Avg 180 min IC_{50} Value = 0.603 ± 0.032 µM

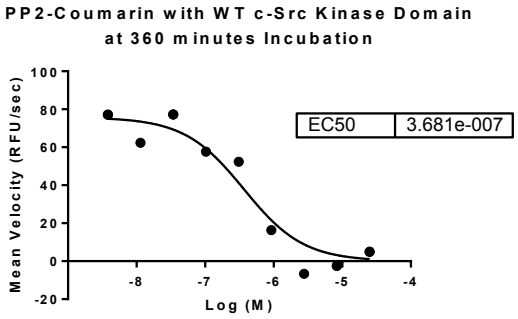

Avg 360 min IC_{50} Value = 0.422 ± 0.076 µM

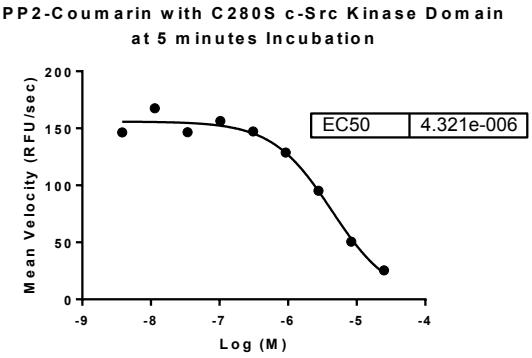

Avg 5 min IC_{50} Value = 4.29 ± 0.048 µM

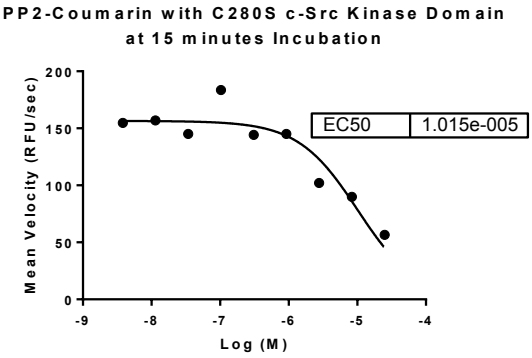

Avg 15 min IC_{50} Value = 6.66 ± 4.93 µM

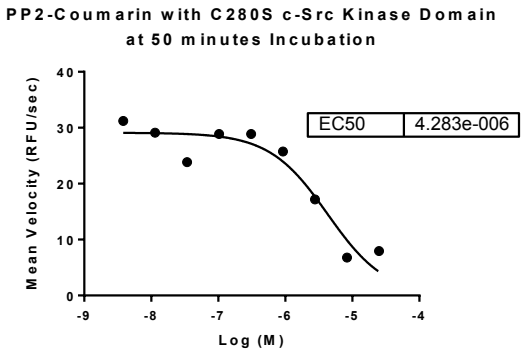

Avg 50 min IC_{50} Value = 4.17 ± 0.162 µM

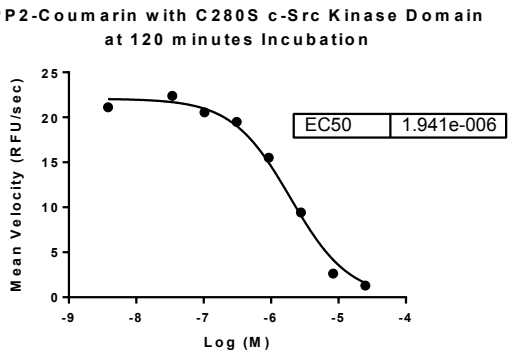

Avg 120 min IC_{50} Value = 1.490 ± 0.632 µM

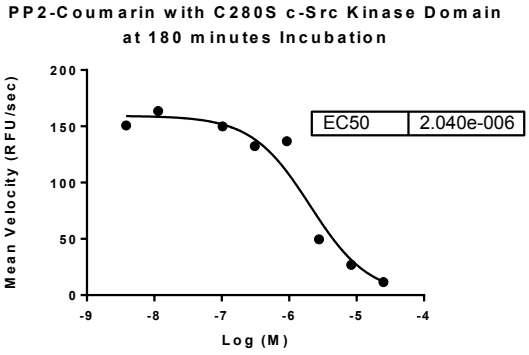

Avg 180 min IC_{50} Value = 1.91 ± 0.191 µM

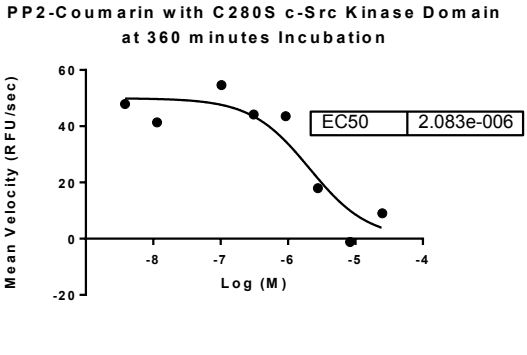

Avg 360 min IC_{50} Value = 1.79 ± 0.42 µM

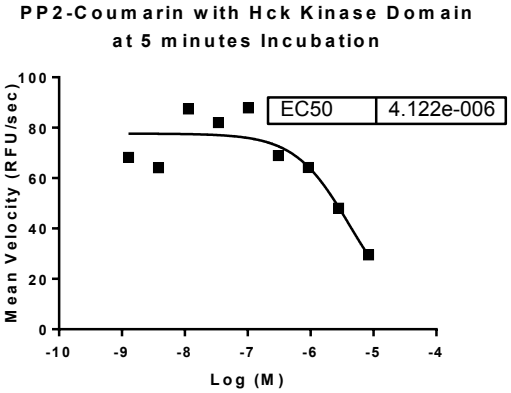

Avg 5 min IC_{50} Value = 7.78 ± 4.20 µM

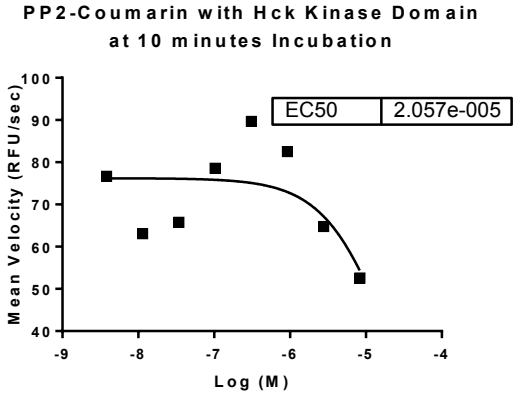

Avg 10 min IC_{50} Value = 20.8 ± 0.30 µM

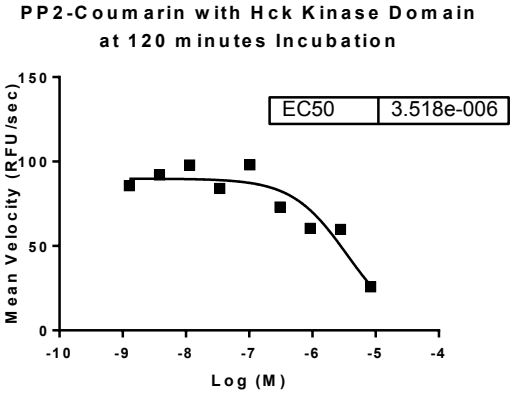

Avg 120 min IC_{50} Value = 3.84 ± 0.453 µM

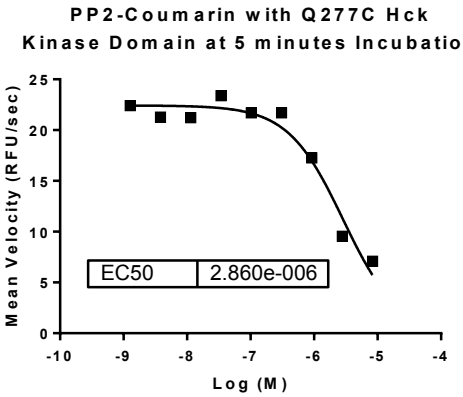

Avg 5 min IC_{50} Value = 2.69 ± 0.24 μM

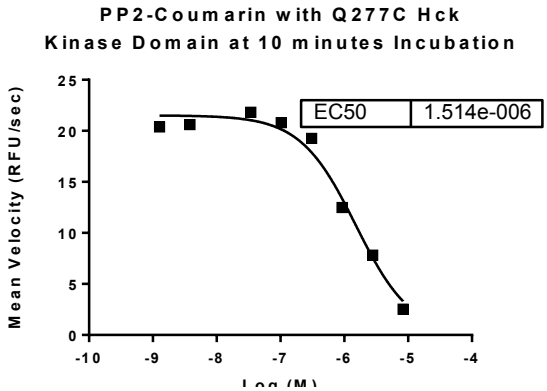

Avg 10 min IC_{50} Value = 1.61 ± 0.13 μM

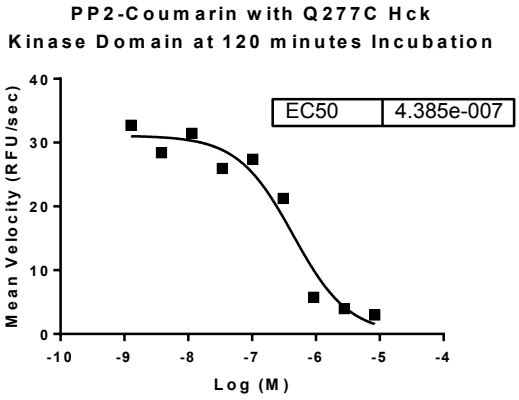

Avg 120 min IC_{50} Value = 0.484 ± 0.064 μM

References

1. Brandvold, K. R.; Santos, S. M.; Breen, M. E.; Lachacz, E. J.; Steffey, M. E.; Soellner, M. B., Exquisitely specific bisubstrate inhibitors of c-Src kinase. *ACS Chem Biol* **2015,** *10* (6), 1387-91.
2. Kwarcinski, F. E.; Fox, C. C.; Steffey, M. E.; Soellner, M. B., Irreversible inhibitors of c-Src kinase that target a nonconserved cysteine. *ACS Chem Biol* **2012,** *7* (11), 1910-7.